I am submitting here with a dissertation written by Ifeyinwa Jane Iwuchukwu entitled "Protein engineering for the Enhanced Photo-production of Hydrogen by Cyanobacterial Photosystem I." I have examined the final electronic copy of this thesis for form and content and recommend that it be accepted in partial fulfillment of the requirements for the degree of Doctor of Philosophy, with a major in Chemical Engineering.

Paul D. Frymier, Major Professor

We have read this dissertation

and recommend its acceptance:

Barry Bruce

Hugh O'Neill

Eric Boder

Accepted for the Council:

Carolyn R. Hodges

Vice President and Dean of the Graduate School

Protein engineering for the Enhanced Photo-production of Hydrogen by Cyanobacterial Photosystem I

A Dissertation Presented for the

Doctor of Philosophy

Degree

The University of Tennessee, Knoxville

Ifeyinwa Jane Iwuchukwu

May 2011

Copyright © 2010 by Ifeyinwa Jane Iwuchukwu

All rights reserved.

DEDICATION

This thesis is dedicated to my husband, Ernest Iwuchukwu, my kids, Oge and Ife, and my entire family whose faith and confidence in me never faltered.

ACKNOWLEDGEMENTS

I am deeply indebted to many people for their support and encouragement during my academic career at the UT Knoxville. First of all, I would like to thank my major advisor, Dr. Paul Frymier for his patience, enthusiastic guidance, encouragement and helpful criticisms throughout the course of this work. Special thanks also go to Dr. Barry Bruce for his guidance and help throughout my work, and for serving as a member of the committee. I would like to express my appreciation to Dr. Hugh O'Neill for his contributions and for serving as a member of the committee. My gratitude goes to Dr Eric Boder for his insightful contributions and for serving as a member of my committee.

I commend the contributions of Rosemary Le, Khoa Dang, Prakitchai Chotewotmuntri, Richard Simmerman, Michael Vaughn, Danielle Williams and the entire Bruce Lab members, towards the success of this work.

To all my friends at UT, Jessica, Sabina, Seyi, Nelson, Irene, Susan, the Navigators and the catholic community at John the 23rd, thank you for creating an enjoyable environment.

I am also indebted to my husband, Ernest and my kids, Oge and Ife. Too often they were without a wife and a mother, but they did so without a single complaint. I will also like to express my appreciation to my parents, Joseph and Bridget Oranugo, for all their support.

Lastly, my profound gratitude goes to the Almighty God, my Creator and Sustainer for his guidance and inspiration throughout the course of this work.

ABSTRACT

Photosystem I (PSI) from plants, algae, and cyanobacteria can mediate H_2 evolution *in vivo* and *in vitro*. A simple, self-platinization procedure that permits stable PSI-mediated H_2 evolution *in vitro* has been developed. The H_2 evolution capabilities of PSI from *Thermosynechococcus elongatus* have been characterized. This organism utilizes cytochrome c_6 (cyt c_6) as the e^- donor to P_{700}. Using a solution-based, self-organized platinization of the PSI nanoparticles, this study demonstrates a sodium ascorbate-cyt-PSI-Pt-H_2 electron transport and proton reduction system that yields light-dependent H_2. The system was thermostable with H_2 evolution increasing up to 55°C. In addition, stability studies have shown the H_2 evolution to be very stable, with no significant decrease over the 80 days investigated. Through simple optimization a H_2 production rate of ~5.5 μmol H_2/h/mg Chl [micro-mole H_2 per hour per milligram chlorophyll] was attained.

To further optimize the H_2 production Asc-cyt-PSI-Pt-H_2 system, response surface methodology (RSM) was employed. The process parameter studied included temperature, light intensity and platinum salt concentration. The results showed that experimental data had a good fit to the proposed model (R^2=0.99 and $p < 0.001$). Platinum salt concentration, temperature and the interaction between platinum salt concentration and temperature showed significant effects on the total H_2 yield. Light intensity had minimal effect of the total H_2 yield within the region studied. The optimum parameters for H_2 photoproduction were light intensity of 240 μE/m^2/s, [micro-eistien per square meter per second], platinum salt concentration of 636 μM [micro-mol/liter] and temperature of 31^0C.

Finally, studies that will improve the H_2 yield by increasing the kinetics of electron transfer were done. A hybrid protein was formed by engineering a gene to express a fusion of the membrane-bound [Ni-Fe] hydrogenase from *Ralstonia eutropha* H16 and the stromal-exposed subunits PsaE and PsaD of PSI from *T. elongatus*. A PsaE-free mutant of PSI was simultaneously formed by genetically disrupting the expression of the PsaE subunit of a native PSI; that will allow *in vitro* reconstitution of the desired PsaE-hydrogenase fusion protein with PsaE-free PSI.

Table of Contents

1. INTRODUCTION 1

1.1 Background 1

1.2 Scope of work 8

2. LITERATURE REVIEW 10

2.1 [Ni-Fe] hydrogenases 12

2.1.1 The active site 15

2.1.2 Activation process 17

2.1.3 Inactivation process 17

2.1.4 Thermo-tolerant and oxygen-tolerant [Ni-Fe] hydrogenases for hydrogen photo-production. 19

2.2 The hydrogenases of Ralstonia eutropha H16 21

2.3 *In vivo* strategies of hydrogen production 27

2.4 *In vitro* strategies of hydrogen production 29

2.4.1 Self assembly and platinization 29

2.4.2 Platinum Beads 32

2.4.3 Electro-separated Systems 34

2.4.4 Hydrogenase-mediated H_2 evolution 35

2.5 Photosystem I from *Thermosynechoccocus elongatus* 41

3. THERMOTOLERANT PHOTO-DEPENDENT HYDROGEN PRODUCTION BY PLATINIZED PHOTOSYSTEM I REACTION CENTERS 45

3.1 Introduction 45

3.2 Materials and methods 46

3.2.1 Growth of *Thermosynechococcus elongatus* 46

3.2.2 Isolation of trimeric PSI 46

3.2.3 Real Time H_2 Detection and Electrolysis Calibration 48

3.2.4 PSI-mediated Hydrogen Evolution 52
3.2.5 Optimized *E. coli* expression and purification of cytochrome c_6 53
3.2.6 Oxygen uptake assay to test activity of recombinant cyt c_6 53
3.3 Results and Discussion 54
3.3.1 Purification of Photosystem I from *T. elongatus* 54
3.3.2 Oxygen uptake assay to test activity of recombinant cyt c_6 57
3.3.3 Determination of rate-limiting step in PSI-mediated hydrogen evolution 58
3.3.4 Evaluation of thermostability, kinetic limitations and sustainability 62
3.3.5 Light Saturation Experiment 67
3.3.6 Peak rates of hydrogen evolution 68
3.3.7 Optimization of PSI purification for hydrogen evolution 70
3.3.8 Spectral analysis of chlorophyll in fresh and platinized PSI. 75
3.4 Conclusion 76
4. OPTIMIZATION OF THE PLATINIZATION PROCESS IN PSI MEDIATED H_2 PRODUCTION USING RESPONSE SURFACE METHODOLOGY 77
4.1 Introduction 77
4.2 Materials and methods 78
4.2.1 PSI-mediated hydrogen evolution and measurement 78
4.2.2 Screening experiments 80
4.2.3 Experimental design and data analysis 82
4.3 Results and discussion 83
4.3.1 Screening experiments 83
4.3.2 Model Fitting 85
4.3.3 Analysis of response surfaces 91
4.3.4 Optimization and validation of model 94
4.4 Summary 95

5. ENGINEERING FUSION BETWEEN HYDROGENASE AND PSAE/D PROTIENS IN *R. EUTROPHA* AND THE GENETIC DISRUPTION OF THE *psaE* AND *psaD* GENE IN *T. ELONGATUS* 96

5.1 Introduction 96

5.2 Materials and Method 101

5.2.1 Molecular biology technique 101

5.2.2 Bacterial strains and plasmids 101

5.2.3 Media and growth conditions 108

5.2.4 Isolation of genomic DNA from *T. elongatus* 108

5.2.5 Targeted mutagenesis of *psaE* and *psaD* gene 109

5.2.6 Electroporation of *T. elongatus* 114

5.2.7 Isolation of the Megaplasmid DNA 115

5.2.8 Isolation of the gene cluster coding for the *HoxKG* gene in *Ralstonia eutropha* 115

5.2.9 Genetic constructions of the hyd-PsaE and hyd-PsaD hybrid complex 115

5.2.10 Conjugative plasmid transfer and gene replacement 119

5.2.11 Purification of Hydrogenase from *Ralstonia eutropha* 119

5.2.12 SDS-Page and Western immunoblot analysis 121

5.2.13 Hydrogenase activity assay using reduced methyl viologen as electron donor 121

5.2.14 Codon optimization of *psaE* and *psaD* gene for *R. eutropha* 121

5.3 Results and discussion 123

5.3.1 Targeted Mutagenesis of *psaE* and *psaD* 123

5.3.2 Transformation of *T. elongatus* and homologous recombination 127

5.3.3 Genetic construction of hydrogenase fusion proteins 128

5.3.4 Conjugal gene replacement in *R. eutropha* 131

5.3.5 Codon optimization of *psaE* and *psaD* gene. 135

5.3.6 Construction and expression of hydrogenase fusion proteins 140

5.3.7 Purification and properties of the hydrogenase fusion proteins 143
5.3.8 H_2-evolving activity on purified hydrogenase fusion proteins 148
5.4 Summary 154
6. CONCLUSION AND FUTURE DIRECTION 156
6.1 Conclusion 156
6.2 Future directions 157
REFERENCES 160
APPENDIX 180
Appendix I – HPLC method for PSI purification 181
Appendix II – Temperature stability of cytochrome c_6 and temperature stability comparism of *Synechocystis PCC6803* and *T. Elongatus (*Circular dichroism spectroscopy) 184
Appendix III – Comparison of hydrogen evolution using no detergent and 0.03% DM in buffer. 186
Appendix IV – Raw data for hydrogen evolution used in the design of experiment (DOE). 187
VITA 191

List of Figures

Figure 1.1 Photosynthetic electron transport chain (adapted from GTL Roadmap, U.S Department of Energy Office of Science, August 2005). 3

Figure 2.1 Figure adapted from Paula *et al* [53]shows enzymes directly involved in hydrogen metabolism in cyanobacteria. 11

Figure 2.2 Figure adapted from Vignais *et al* shows a schematic representation of the phylogenetic tree of [Ni-Fe]-hydrogenases 14

Figure 2.3 Scheme of the active site of standard Ni-Fe hydrogenase (adapted from De Lacy *et al*, 2007)……. 15

Figure 2.4 Scheme of the different redox states of the active site of standard Ni-Fe hydrogenases (adapted from De Lacey et al [62]). 16

Figure 2.5 Figure adapted from Vignais *et* al,(2004) shows a schematic structures of the active site of [NiFe] -Hyrogenases 18

Figure 2.6 The three [Ni-Fe] hydrogenases of *R. eutropha* H16 (Figure adapted from Burgdorf *et a*l [59]) ……..23

Figure 2.7 Figure of the genetic and physical map of megaplasmid pHG1 from Schwartz, E., *et al* (with permission).. 26

Figure 2.8 Experiment to determine the $K_{I(app)}^{O_2}$ stepwise gas injections (Figure from Ludwig *et al*, 2009). …….. 27

Figure 2.9 Schematic of the electron flow in the photosystem I catalytic nanoparticle.. 31

Figure 2.10 Construction of the PSI/1, 6-hexanedithiol/nanoparticle bioconjugate (adapted from Grimme *et al*, 2008).. 33

Figure 2.11 Schematic view of an electro-separated system for hydrogen evolution (Figure from Krassen *et al*, 2009) [111]. 35

Figure 2.12 Figure adapted from *Ihara et al*, 2006. **A)** Assembly diagram of the hydrogenase-PSI complex from PsaE-fused hydrogenase and PsaE-free PSI [77]. 37

Figure 2.13 Schematic of the electron transfer steps process in the photo-induced hydrogen evolution system (adapted from Qian *et al*, 2009) [116]. 40

Figure 2.14 Trimeric PSI as viewed from the stromal side (PDB entry 1JB0). 43

Figure 3.1 Schematic of platinized system for hydrogen evolution. 46
Figure 3.2 Schematic representations of the experimental apparatus for hydrogen evolution measurement. ……50
Figure 3.3 Real time calibration of hydrogen sensor.. 51
Figure 3.4 PSI isolation and confirmation of trimeric arrangement of the purified protein. . 56
Figure 3.5 Oxygen uptakes by isolated PSI from *T. elongatus.* 57
Figure 3.6 Sequence of addition on fresh PSI and Energy-dispersive X-ray spectroscopy. 61
Figure 3.7 Sequence of addition on platinized PSI complex. 62
Figure 3.8 Thermal and temporal stability of H_2 evolution. 65
Figure 3.9 Comparison of yields of hydrogen evolution for *T. elongatus* (red) and *Synchocystis* (green) PSI with increasing temperature. 66
Figure 3.10 Light saturation curve for platinized PSI preparation. 68
Figure 3.11 Peak rates of hydrogen evolution.. 70
Figure 3.12 Optimization of the PSI purification steps for hydrogen evolution. 72
Figure 3.13 Hydrogen evolution activities of PSI samples using different detergents. 74
Figure 3.14 Spectral analysis of chlorophyll loss.. 75
Figure 4.1 Raw data from hydrogen evolution..... 79
Figure 4.2 Spectral irradiance of red light (red) and white light (black) showing region of PSI absorbance. 84
Figure 4.3 Prediction profiler showing effect of white and red light on H_2 yield. 85
Figure 4.4 Bivariate fit of H_2 yield by platinum salt concentration.. 87
Figure 4.5 Studentized residual plots for total H_2 yield. 90
Figure 4.6 Plot of actual yield verses predicted yield. 90
Figure 4.7 Response surface and contour plots on the combined effects of independent variables on the total H_2 yield.. 93
Figure 4.8 Prediction profiler for the different variables. 94
Figure 4.9 Hydrogen evolution at optimum condition.. 95
Figure 5.1 Structure of PsaC (pink), PsaD (blue) and PsaE (turquoise) subunits of PSI showing the putative docking site of ferredoxin/flavodoxin. 98

Figure 5.2 Overview of the formation of a hybrid H_2 evolving complex using MBH from *R. eutropha* and PSI from *T. elongatus* (adapted from Ihara et al [77]). 99
Figure 5.3 This illustrates how a psaE-Hyd fusion protein may be able to assemble with PSI either *in vitro* or *in vivo.*..... 100
Figure 5.4 Schematics of fusions between *T. elongatus* PsaE and PsaD and MBH from *R. eutropha*……101
Figure 5.5 Construction of a clone for generating a deletion mutation for the gene encoding PsaE subunit of PSI for *T. elongatus*. 110
Figure 5.6 Genetic constructions of hydrogenase and PsaE fusion protein for homologous recombination in *R. eutropha*. 118
Figure 5.7 PsaE knockout gene construct.. 124
Figure 5.8 Plasmid pCKmTe carrying a gene encoding the thermostable kanamycin nucleotidyltransferase.. 125
Figure 5.9 PsaD knockout gene construct.. 126
Figure 5.10 Transformation and homologous recombination in *T. elongatus*. 128
Figure 5.11 Isolation of the megaplasmid DNA and cloning of the *hoxK* and *hoxG* gene. . 130
Figure 5.12 Modified *hoxK* gene for homologous recombination.. 130
Figure 5.13 Conjugation in *R. eutropha*. 133
Figure 5.14 Selection of positive screens after conjugation and sequence verification. 134
Figure 5.15 Relative adaptiveness of h*oxK* sequence in *R. eutropha.*..... 136
Figure 5.16 PsaE-Linker 1 sequence; (A) before adaptation and (B) after adaptation. 138
Figure 5.17 PsaD-Linker 1 sequence; (A) before adaptation and (B) after adaptation. 139
Figure 5.18 Synthesized codon optimized *psaE* and *psaD* gene cloned into a EcorV digested pBluescript II SK derivative lacking its multiple cloning sites yielding plasmids pBSK-psaE and pBSK psaD_Linker respectively (EpcohBiolabs). 140
Figure 5.19 Models of the wild type and mutant hydrogenases (adapted from Schwarze *et al*[192]). ……..141
Figure 5.20 Subcellular localization of HoxK-PsaEL1 in *R. eutropha HFEL1* mutant strain. ……..142
Figure 5.21 SDS PAGE of partially purified MBH hydrogenase. 143

Figure 5.22 SDS- PAGE and Immunoblot analysis of purified wild type and mutant hydrogenase proteins.. 146
Figure 5.23 Relative intensities of HoxK proteins in Wild type and mutant strains from equal amounts of protein. 147
Figure 5.24 Sodium dithionite reduced methyl viologen hydrogen activity assay..... 149
Figure 5.25 H_2 evolution activities of from wild type cells and mutants cells of *R. eutropha*…… ……....150
Figure 5.26 Bar graphs of the corrected H_2 evolution activities of hydrogenase fusion proteins compared to wild type MBH purified from the soluble extract of from the membrane…….. 152

List of tables

Table 1.1 Organisms exhibiting hydrogenase activity 5

Table 2.1 Hydrogenase enzymes that may be used for *in vivo* and *in vitro* hydrogen production ……..20

Table 4.1 Level and code for the central composite design. 80

Table 4.2 Fractional factorial design with two center points for white and red light. 81

Table 4.3 Experimental design for the three variables and experimental and predicted results under different conditions. 86

Table 4.4 Parameters estimates for the full quadratic model and their relative significance in total H_2 yield. 89

Table 4.5 ANOVA for response surface reduced quadratic model. 89

Table 5.1 Bacterial strains and plasmid. 102

Table 5.2 Oligonucleotide primers used for targeted mutagenesis on *psaE* and *psaD* gene. 111

Table 5.3 Comparison of CAI score with similar *hoxk* gene from other organisms..... 137

Table 5.4 H_2 evolution activities of hydrogenase fusion proteins from the soluble extract compared to wild type MBH purified from the membrane. 151

Table 5.5 Corrected H_2 evolution activities of hydrogenase fusion proteins compared to wild type MBH purified from the soluble extract of from the membrane. 153

1. INTRODUCTION

Provision of an abundant, clean and secure sustainable energy source is one of the key future challenges facing mankind. Total annual global energy consumption is predicted to increase by 57% from 2004 to 2030 [1] and the world petroleum production rate is predicted to reach its peak before the middle of the century [2]. To date, most of this energy demand has been provided by fossil fuels. Given the dire environmental implications of pollution, the potential for anthropogenic global warming, and the growing consternation over finite oil supplies, an alternative source of energy is necessary. New approaches towards clean and sustainable energy are currently underway and sustainably produced hydrogen is considered to be a highly efficient energy carrier and fuel [3]. Hydrogen is the most abundant element in the universe and it can be used as a sustainable fuel to produce clean energy with the only byproduct being water. Unlike fossil fuel, molecular hydrogen is not present in great quantities on earth; it is a *carrier* of energy and not a source. A number of key challenges must be overcome for hydrogen to be used broadly in a sustainable future energy infrastructure such as in fuel cells to produce electricity.

1.1 Background

At present hydrogen is produced mainly from fossil fuels, biomass and water. Nearly 90% of the hydrogen produced is from the steam reforming of natural gas or light oil [4], which results in the emission of carbon dioxide. This process is also limited by the availability of natural gas reserves. Hydrogen can also be produced from the electrolysis of water, which involves the conversion of electrical energy to chemical energy in the form of hydrogen and oxygen gases. Photo-biological hydrogen production with the energy of sunlight is envisaged as a viable alternative energy. Solar energy is the most abundant and accessible sustainable energy source, although it is a diffuse one. Solar energy is by far the largest (178,000 TW/year) when compared to other sources of renewable energy; however, solar energy technologies are relatively expensive when compared to fossil fuel [3].

A broad range of organisms have developed complex molecular machinery for the efficient conversion of sunlight to chemical energy over the past 3 billion years [3]. It has been known since the turn of the century that microorganisms have the capability to produce hydrogen

[3, 5]. The metabolism of hydrogen in photosynthetic microorganisms such as algae has been studied since the 1930s and early 1940s [6, 7]. Gaffron demonstrated, using electron transport inhibitors, that algae were able to photo-produce H_2 via noncyclic electron flow through Photosystem I (PSI) to a hydrogenase [8]. Further, it was shown [9, 10] that these algae are capable of simultaneously producing oxygen and hydrogen, with the ratio of H_2 to O_2 at 1.9, approaching the theoretical ratio of 2.0 [9]. *In vitro* preparations of bacterial hydrogenases have been used to produce hydrogen since at least the 1950s [11]. Oxygenic phototrophs such as green plants, algae and cyanobacteria transfer electrons generated through water splitting through photosystem II (PSII), the b_6f complex, a redox mediator, photosystem I (PSI), and eventually to ferredoxin (Fd) where it is used by Fd-$NADP^+$ reductase (FNR) to reduce $NADP^+$ to NADPH for CO_2 fixation in the Calvin cycle (Figure 1.1) [12]. PSII catalyzes the first step of the electron transport chain and is powered by photons captured by its antenna system. Upon excitation PSII generates a chlorophyll radical cation (P_{680}^+), reduces a plastoquinone molecule (Q_A) and through a series of redox active components catalyzes the water oxidation reaction providing electron for the electron transport chain [3]. This electron is passed along to PSI via plastoquinone (PQ) and the Cyt b_6f complex. The primary electron donor in PSI is P_{700}, a chlorophyll species that in its excited state has a potential of approximately -1.2 V. P_{700} is the site of the light induced charge separation of PSI in both cyanobacteria and higher plants [13]. Electron transfer from the Cyt b_6f complex to P_{700} occurs via a soluble electron transfer protein, cytochrome c_6 (heme protein) or plastocyanin (copper protein). Higher plants use plastocyanin (PC) for this reaction, whereas some algae use either plastocyanin or cytochrome c_6 (cyt c_6) depending on the relative availability of copper and iron in the medium. Many cyanobacteria, like *Thermosynechococcus elongatus (T. elongatus)* use only cytochrome c_6 as the electron transfer protein. The electron from PSI is transferred to ferredoxin (Fd) before being used for $NADP^+$ reduction. Under anaerobic conditions, hydrogenase can provide an alternate path for the electrons resulting in the formation of hydrogen. Soluble hydrogenase enzymes are located on the stromal side of the thylakoid membrane, where the formation of molecular hydrogen takes place. H^+ released into the thylakoid lumen by PSII, generates a H^+ gradient that drives ATP production via ATP synthase [3].

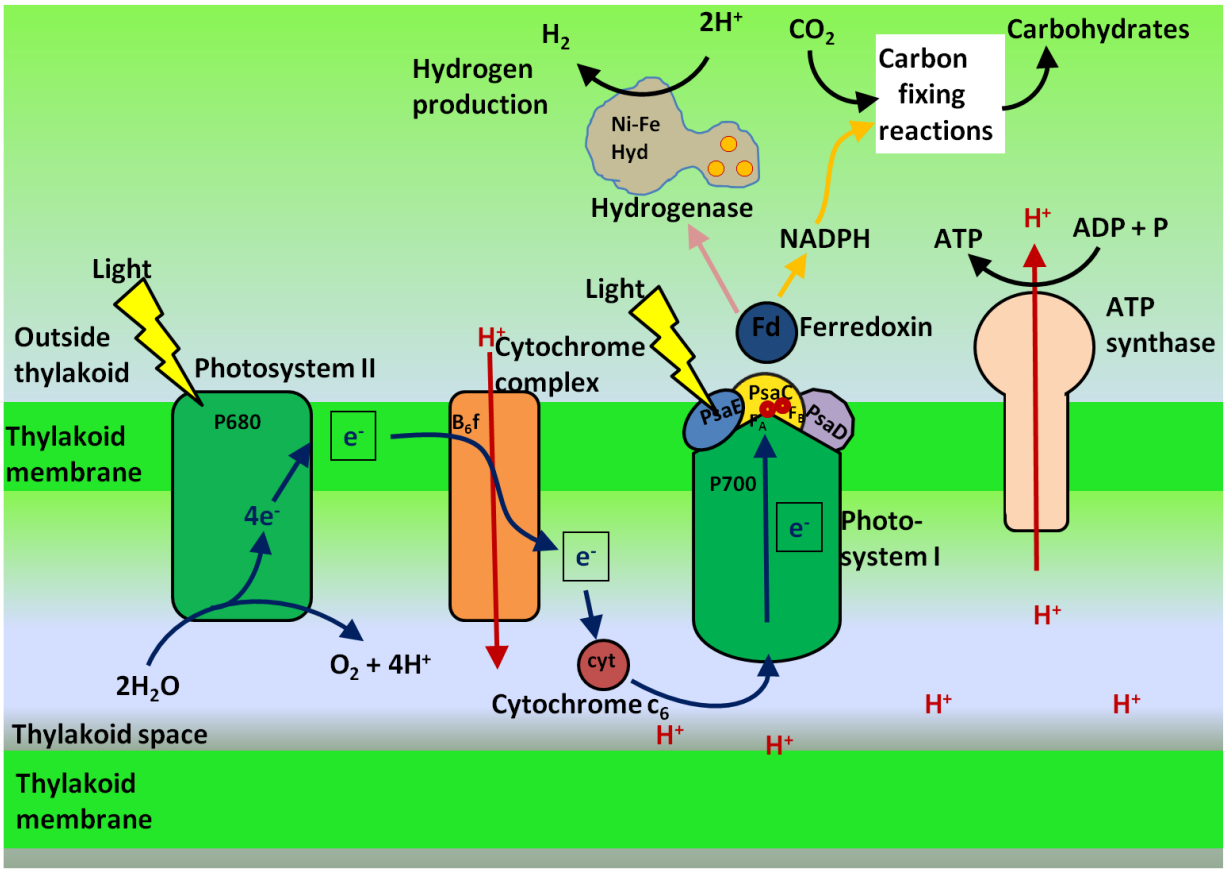


Figure 1.1 Photosynthetic electron transport chain (adapted from GTL Roadmap, U.S Department of Energy Office of Science, August 2005).

Hydrogenases are catalysts provided by nature to produce hydrogen or to utilize it as energy source. Hydrogenases catalyze the reversible oxidation of molecular hydrogen and they play a central role in microbial energy metabolism. They catalyze the reversible reaction; $H_2 \leftrightarrow 2H^+ + 2e^-$. This reaction's direction is dependent on the redox potential of the component that interacts with the enzyme. Hydrogenases are metalloproteins that are found in Archea, anaerobic bacteria and some eukaryotes, such as unicellular green algae, anaerobic ciliates, and anaerobic fungi [14]. A large number of organisms have been reported to show hydrogenase activity as given in Table 1.1.

Table 1.1 Organisms exhibiting hydrogenase activity

Organism	**Reference**
Cyanobacteria	
Synechocystis sp. PCC 6803	[15]
Synechococcus elongatus	[15]
Anabaena cylindrical	[16]
Nostoc muscorum	[17]
Microcystis aeruginosa	[18]
Spirulina platensis M-185	[19]
Anacystis nidulans	[20]
Green Algae	
Chlamydomonas reinhardtii	[21]
Scenedesmus obliquus	[21]
Ulva lactuca	[22]
Chlorella fusca	[23]
Photosynthetic Bacteria	
Thiocapsa roseopersicina	[24]
Rhodosprillum rubrum	[25]
Rhodopseudomonas capsulata	[26]
Chlorobium thiosulfatophilum	[27]
Rhodomicrobium vannielii	[28]
Rubrivivax gelatinosus	[29]
Non-photosynthetic Bacteria	
Ralstonia eutropha (formerly Alcaligines eutrophus)	[30]
Escherichia coli	[31]
	[32]

Table 1.1 Continued

Organism	Reference
Desulfovibrio vulgaris	[33]
Desulfomicrobium baculatum	[34]
Clostridium pasteurium	[35]
Azobacter vinelandii	[36]
Rhizobium leguminosarum	[37]
Methanobacterium sp.	

Hydrogenases can be largely classified into three groups based on the metals in their active sites: i) the nickel-iron, [Ni-Fe] hydrogenases, ii) the iron only, [Fe-Fe] hydrogenases, and iii) the [Fe] hydrogenases or iron-sulfur-free hydrogenase (initially called metal free hydrogenase). These three classes of hydrogenases are found to be phylogenetically distinct and utilize a completely different set of regulatory and assembly processes [38]. X-ray crystal structures of the [Ni-Fe] hydrogenase (Figure 1.2A) and the [Fe-Fe] hydrogenase (Figure 1.2B) have revealed that these two enzymes are structurally different and that they catalyze the same reaction using very different metal active site [39]. The [Ni-Fe] hydrogenases are heterodimeric periplasmic membrane enzymes containing a large and small subunit (Figure 1.2A). The large subunit contains the nickel binding site and electrons are delivered to this center via three Fe-S clusters located in the small subunit [40]. This type of hydrogenase is wide spread among all bacterial families and has been well characterized. [Fe-Fe] hydrogenases possess only [Fe-S] clusters and an iron cofactor with a unique structure of six iron atoms (Figure 1.2B). They consist of two subunits like the [Ni-Fe] hydrogenase but with iron in the active site. These enzymes are found to exist in monomeric, dimeric and multimeric forms [41]. [Fe-Fe] hydrogenases are irreversibly inactivated by the presence of oxygen while [Ni-Fe] hydrogenases are reversibly inactivated [42]. [Fe]-hydrogenases, as opposed to the [Ni-Fe] and [Fe-Fe], lack Fe–S clusters and are found only in a small group of methanogenic archea [43]. Its active site

contains a labile light sensitive cofactor [44] with a single iron, most likely Fe(II) that binds two CO ligands [45-47]. The crystal structure of the apoenzyme was reported in 2006 [48]. Oxygen sensitivity of hydrogenases is one of the main difficulties encountered for the use of these enzymes for H_2 production. A critical requirement for the photo production of H_2 is the use of a hydrogenase that is not only tolerant to O_2 but also catalytically active in O_2. Also since solar energy is required by these photosynthetic microorganisms to produce H_2 the need of hydrogenases that are thermal tolerant is important.

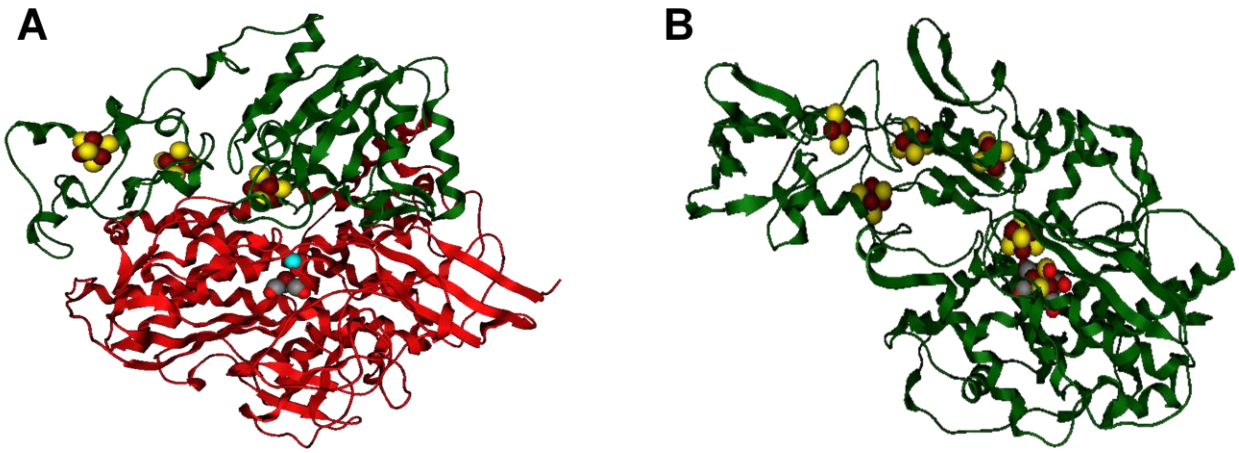


Figure 1.2 A) Crystal structure of [Ni-Fe] hydrogenase from *Desulfovibrio gigas*. Coordinates are from the Protein Databank file 1FRV. B) Crystal structure of [Fe-Fe] hydrogenase from *Clostridium pasteurianum*. Coordinates are from the Protein Databank file 1FEH.

The current interest in the use of hydrogen as an alternative to fossil fuels has led to the interest in bio-hydrogen production and research into hydrogenases will play an important role in this area. Hydrogenases that are oxygen tolerant, thermo-tolerant and highly efficient can be used *in vitro* or *in vivo* in microorganism to maximize photo-biological hydrogen production. PSI from plants, algae, and cyanobacteria has been shown to mediate hydrogen evolution both *in vivo* and *in vitro*. It has been demonstrated that chemically platinized thylakoid membrane can photosynthetically split water in molecular hydrogen and oxygen [49, 50]. In this platinized thylakoid, hydrogen is produced by proton reduction adjacent to the reducing site of the PSI complexes on the stromal side of the thylakoid membrane. This reaction is catalyzed by platinum particles.

1.2 Scope of work

In this work, hydrogen evolution capabilities of PSI from the thermophillic cyanobacteria, *Thermosynechococcus elongatus* has been characterized by a "re-wiring" of the electron transport pathway of PSI that permits a productive interface with a platinum nanoparticle catalyst, and then studying the hydrogen evolving properties of the system [51]. This cyanobacterium only encodes a c-type cytochrome (cyt c_6) that functions as the primary donor to P_{700}. Using a solution-based, self-assembled platinization of the PSI nanoparticles, the electron transport pathway NaAsc-Cyt-PSI-Pt-H_2 was established, which yields hydrogen in a light-dependent fashion. Metallic platinum was photo-precipitated at the reducing (stromal) end of PSI according to the reaction, $[PtCl_6]^{2-} + 4e^- + h\nu \rightarrow Pt\downarrow + 6Cl^-$ where it interacts with electrons (as a result of photo-induced charge separation) on the stromal side of PSI and catalyzes the evolution of molecular hydrogen. The system is thermostable with hydrogen evolution rates increasing up to 55^0C. In addition, stability studies have shown the hydrogen evolution to be stable for > 80 days [51].

This work also seek to address issues associated with the use of expensive platinum catalysts and their limited reserves limiting the implementation and long-term sustainability of this hydrogen evolving system. The use of an oxygen-tolerant hydrogenase that will work efficiently with thermophillic cyanobacterium PSI will be advantageous. The production of hydrogen *in vivo* by algae and cyanobacteria is short-lived because the hydrogenase enzyme is

inhibited by the presence of oxygen. This work focuses on *in vitro* hydrogen evolution by engineering a “hard wired” protein complex consisting of an oxygen-tolerant hydrogenase from *Ralstonia eutropha H16* and PSI from *Thermosynechococcus elongatus* as a light dependent hydrogen evolving complex.

2. LITERATURE REVIEW

Photobiological production of hydrogen could be a potential environmentally friendly alternative energy because H_2 gas is renewable using sunlight as the primary source of energy and does not liberate CO_2 during conversion to electricity or motion by combustion or use of a fuel cell. In microorganisms like cyanobacteria and green algae, two kinds of enzymes are involved in catalyzing H_2 production, hydrogenases and nitrogenases (Figure 2.1). Nitrogenases mediate the reduction of molecular nitrogen to ammonium with the consumption of reducing power (mediated by ferredoxin) and ATP [52]. However, nitrogenases can catalyze the reduction of protons to produce hydrogen in the absence of nitrogen gas. Nitrogenase enzymes are extremely oxygen-labile [52]. Hydrogenase enzymes are the central feature of hydrogen metabolism and are essential to many microorganisms because they play a vital role in anaerobic metabolism, such as methanogenic, acetogenic, nitrogen-fixing, sulfur-reducing and photosynthetic bacteria, which are of great interest for biotechnological applications. These enzymes catalyze either the consumption or the production of molecular hydrogen. H_2 production by nitrogenase is an energy consuming process due to hydrolysis of ATP molecules (4 per 1 mol of H_2) whereas hydrogenase mediated hydrogen production by cyanobacteria and green algae is better due to the zero requirement of ATP [52].

Cyanobacteria are able to perform oxygenic photosynthesis via PSI and PSII using water as an electron donor. This microorganism uses two types of [Ni-Fe] hydrogenases for hydrogen metabolism (Figure 2.1).

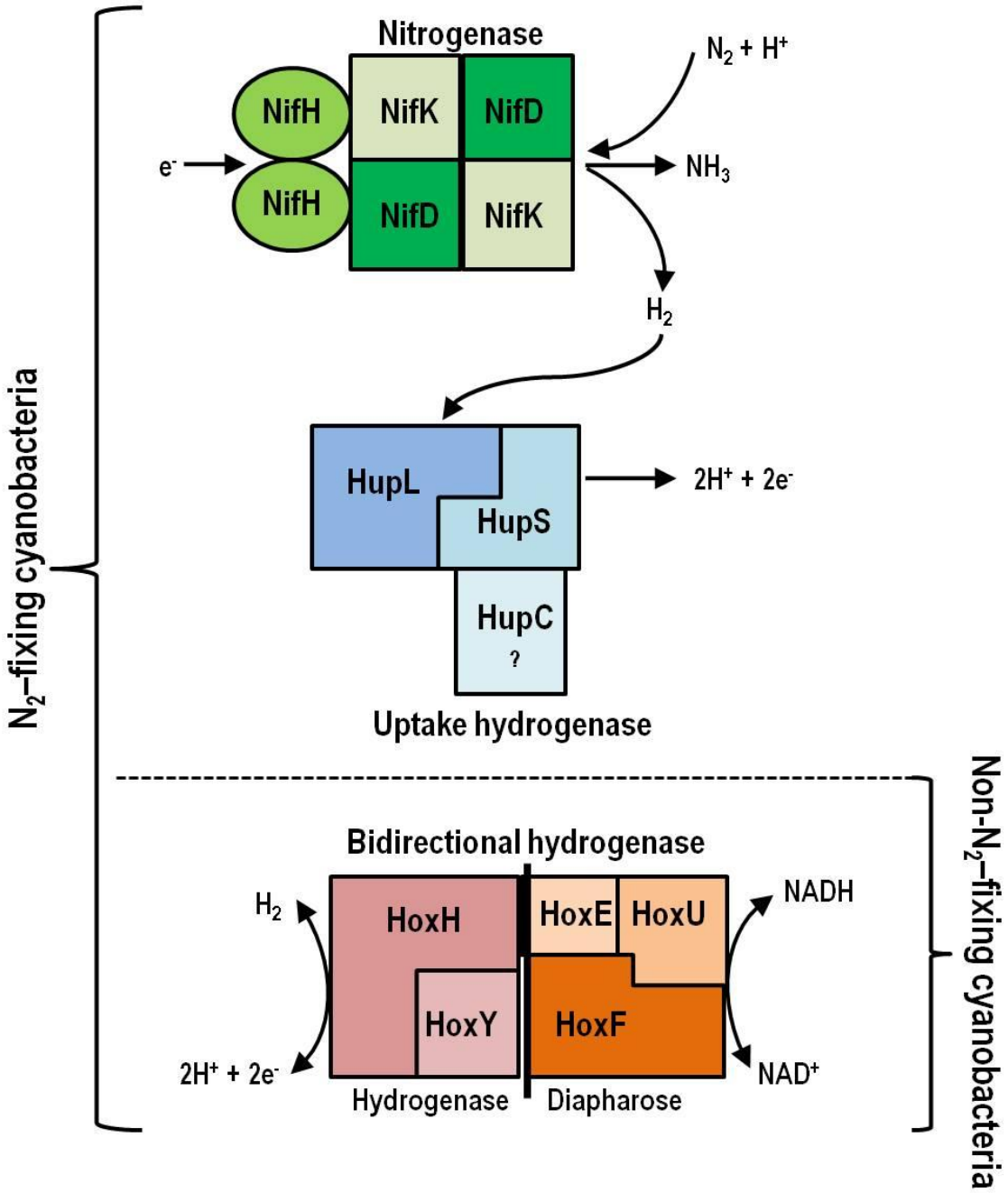


Figure 2.1 Figure adapted from Paula *et al* [53]shows enzymes directly involved in hydrogen metabolism in cyanobacteria. The uptake hydrogenase is present in most of the N_2-fixing strains tested while the bidirectional enzyme seems to be present in non-N_2-fixing and N_2-fixing strains but is not a universal enzyme [53].

2.1 [Ni-Fe] hydrogenases

[Ni-Fe] hydrogenases have been the most numerous and best studied class of hydrogenases. On the level of quaternary structure, they contain an approximately 60 kDa large subunit that houses the Ni-Fe active site and a small subunit that houses the Fe-S clusters [40]. Further studies using infrared spectroscopy revealed the presence of three non-protein ligands, 1 CO and 2 CN^- bound to the Fe atom [42]. The [Ni-Fe-Se] hydrogenases, which are widely distributed among sulfate-reducing bacteria, belong to a sub-group of the [Ni-Fe] class and contain equivalent amounts of nickel and selenium on a molar basis [54]. [Ni-Fe] hydrogenases have been classified into four groups based on the functions of the enzymes [55, 56] as shown in Figure 2.2.

The uptake [Ni-Fe] hydrogenases, or Group 1 [Ni-Fe] hydrogenases, are membrane bound hydrogen uptake enzymes (generally referred to as Hup proteins) that allow the cells to use hydrogen as an energy source. They link the oxidation of hydrogen to the reduction of anaerobic acceptors such as NO_3^-, SO_4^{2-} or CO_2 in anaerobic respiration or to O_2 in aerobic respiration, with the recovery of energy in form of proton motive force [38]. They are connected to the quinone pool of the respiratory chain in the membrane by a third subunit, a di-heme cytochrome *b*, which, together with the hydrophobic C-terminus of the small subunit, anchors the hydrogenase dimer to the membrane. Electrons from H_2 are donated to the quinone pool and the energy of H_2 oxidation is recovered by vectorial proton transfer [38]. They are characterized by the presence of a long signal peptide (containing 35 – 50 amino acid residues) at the N-terminus of their small subunits. The signal peptide contains a conserved motif recognized by a specific protein translocation pathway known as the membrane targeting and translocation (Mtt) or twin-arginine translocation (Tat) pathway, and serves as signal recognition to target the fully folded heterodimer to the membrane and the periplasm [38]. The hyperthermophilic hydrogen-oxidizing bacterium *Aquifex aeolicus* contains three hydrogenases two of which belong to this group [57]. Other members of Group 1 are the periplasmic *Desulfovibrio gigas* hydrogenase [40], *Thiocapsa roseopersicina* [58], *Ralstonia eutropha* [59], *Wolinelia succinogenes* [60] and *E. coli* hydrogenase-1 and 2.

In Group 2 are the cytoplasmic H_2 sensors and cyanobacterial uptake [Ni-Fe] hydrogenases. The small subunit of the enzymes of Group 2 does not contain a signal peptide at its N-terminus and the enzymes are therefore not exported but remain in the cytoplasm [55]. Group 2 is sub-divided into Group 2a and Group 2b. Group 2a includes the cyanobacterial uptake hydrogenases (called HupSL) like that in *Anabeana variabilis* and a third hydrogenase from *Aquifex aeolicus* [38]. Group 2b includes the regulatory hydrogenases HupUV or HoxBC; these enzymes have been identified in *Bradyrhizobium japonicum, R. eutropha, Rhodobacter capsulatus, T. roseopersicina and Rhodopseudomonas palustris* [56]. H_2 sensing hydrogenases are insensitive to oxygen, in contrast to the majority of hydrogenases. A possible reason is that the main gas channel leading to the Ni-Fe active site is too narrow for oxygen, due to the presence of amino acids bulkier than the standard [Ni-Fe] hydrogenase [61].

Bidirectional heteromultimeric cytoplasmic [Ni-Fe] hydrogenases are in Group 3. This group of hydrogenases can be subdivided into cofactor 420 (F420, 8-hydroxy-5-deazaflavin) reducing, NADP –reducing, MV-reducing and bidirectional NADP/NAD- reducing [56]. They are termed bidirectional because physiologically, they function reversibly, oxidizing or evolving hydrogen. This group of enzymes has been discovered in *Methanothermobacter marburgensis, R. eutropha, T. roseopersicina, Allichromatium vinosium, Synechocystis* PCC6803 and *Geobacter sulfurreducens* [56].

In Group 4 are the H_2-evolving, Energy –conserving membrane-associated hydrogenases. The multimeric enzymes (six subunits or more) of this group reduce protons from water to dispose of excess reducing equivalents produced by anaerobic oxidation resulting in hydrogen evolution and energy conservation. Members of this group of hydrogenases have been discovered in *E. coli* (hydrogenase 3), *Rhodospirillum rubrum, Methanothermobacter marburgensis, Carboxydothermus hydrogenoformans, Desulfurvibrio gigas*, hyperthomophillic *archeon, Pyrococcus furiosus* and the CO- linked hydrogenase in *Rubrivivax gelatinosus* [56].

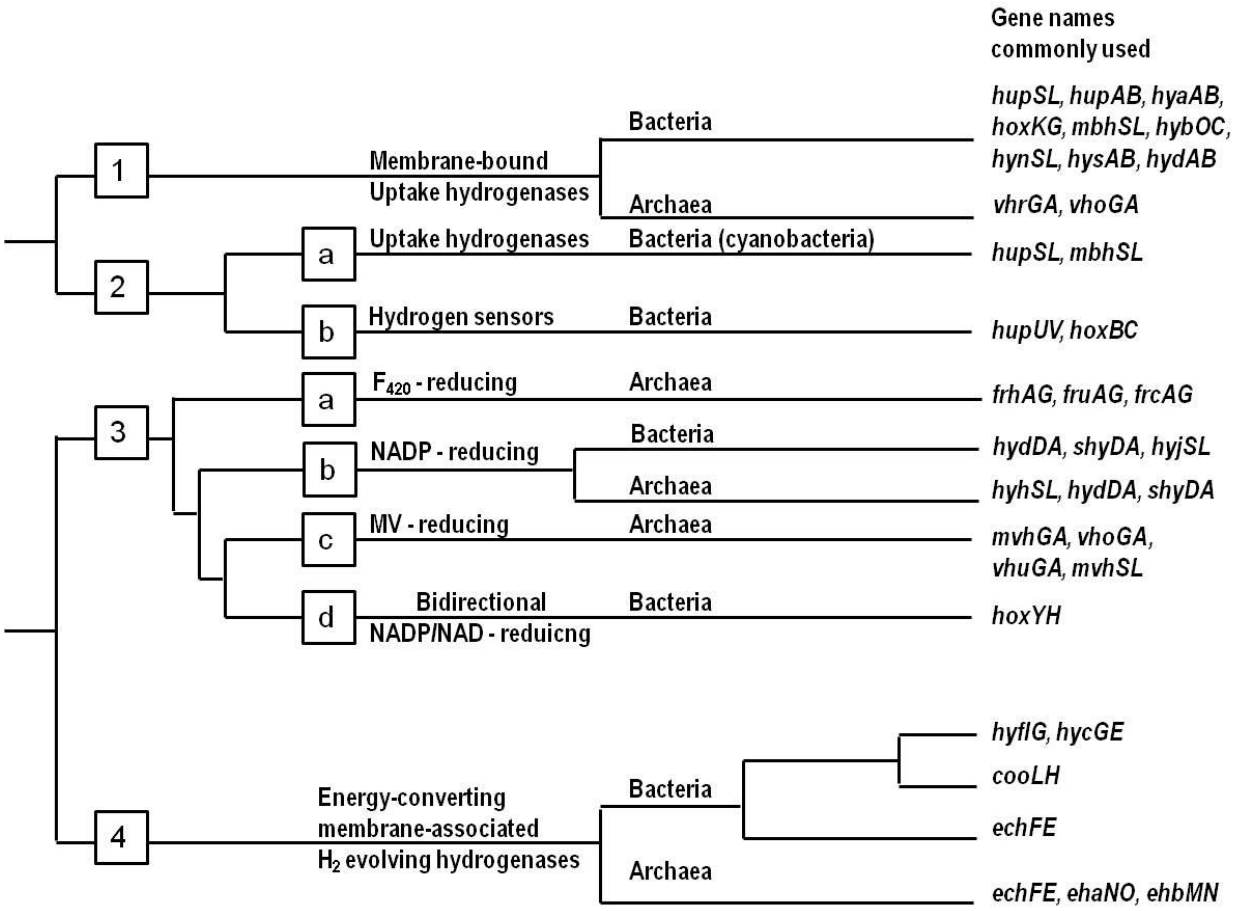


Figure 2.2 Figure adapted from Vignais *et al* shows a schematic representation of the phylogenetic tree of [Ni-Fe]-hydrogenases based on the complete sequences of the small and the large subunits (the same tree was obtained with each type of subunit), originally established by ref [38].

2.1.1 The active site

The crystallographic analysis of the [Ni-Fe] hydrogenase from *Desulfovibrio gigas* by Volbeda et al. has shown that its active site is buried in the large subunit and contains two metal ions, one of which is nickel [40]. The Ni-Fe active site is coordinated by two conserved CxxC motifs, one located in the N-terminal region and the other located at the C-terminal region of the polypeptide. The crystal structure of Ni-Fe hydrogenase from *D. gigas* is shown in Figure 1.2A. The [4Fe-4S] cluster closest to the [Ni-Fe] site is called the "proximal" cluster and the [4Fe-4S] cluster close to the protein surface is called the "distal" cluster with the "medial" [3Fe-4S] cluster in the middle. These clusters act as a "wire" to transfer electrons to and from the active site, as well as a reservoir able to store up to three electrons. The active site is stabilized in the protein by four cysteine ligands (Figure 2.3): C530 and C65, which are linked to the Ni and C533 and C68, which are bridging ligands of both Ni and Fe [62]. Some [Ni-Fe] hydrogenases have cystiene sulfur replaced by a selenium atom [54]. The enzyme isolated under aerobic conditions exhibits two Ni-related electron paramagnetic resonance (EPR) signals Ni-A ('unready' state) and Ni-B ('ready' state) [40]. A third EPR signal named Ni-C appeared gradually upon reduction with H_2 or chemical reductants which corresponds to the catalytically active state whereas the Ni-A and the Ni-B states were inactive towards hydrogen [62]. A number of additional states where observed by EPR and are shown in Figure 2.4.

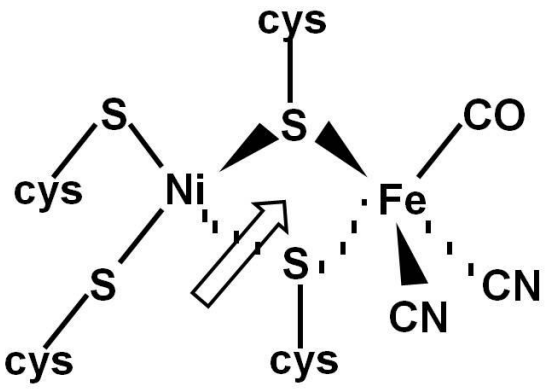


Figure 2.3 Scheme of the active site of standard Ni-Fe hydrogenase (adapted from De Lacy *et al*, 2007). The arrow indicates the vacant coordination site for binding of substrate or inhibitors [62].

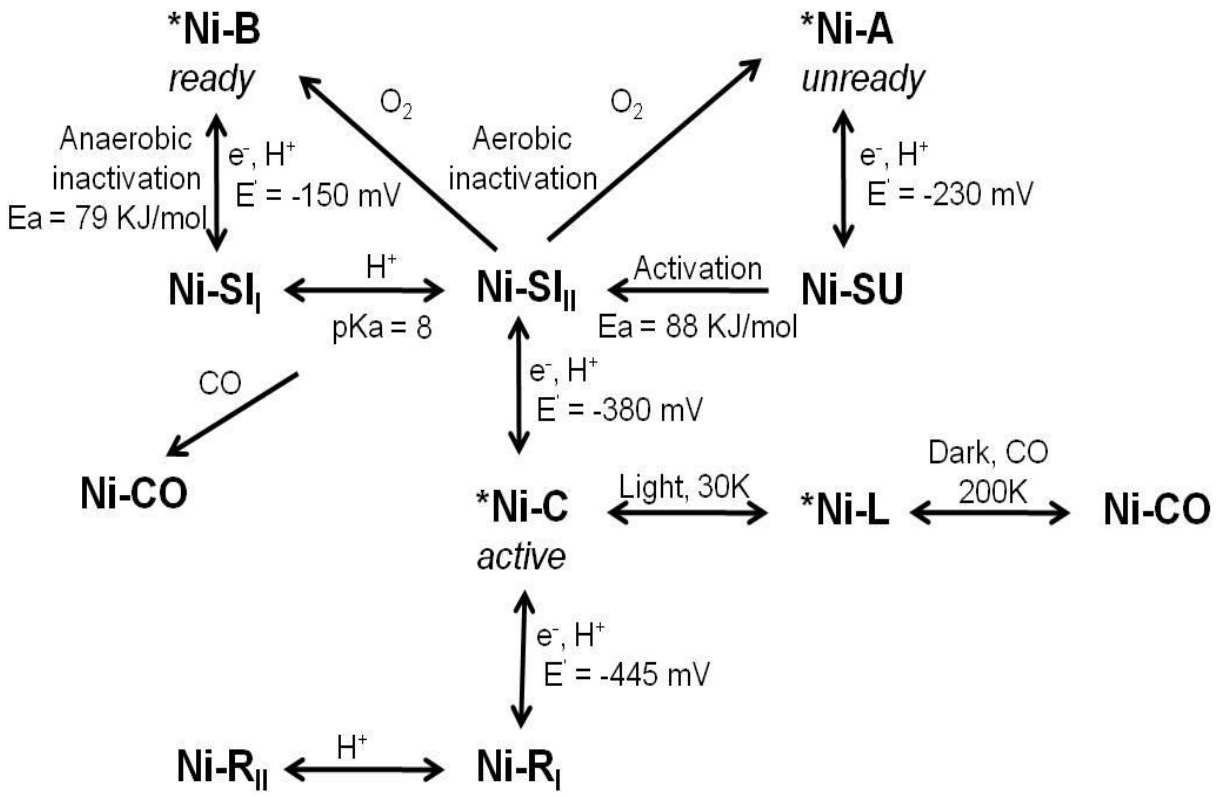


Figure 2.4 Scheme of the different redox states of the active site of standard Ni-Fe hydrogenases (adapted from De Lacey et al [62]). The paramagnetic EPR-active states are marked with an asterisk. The formal redox potentials (at pH 8.0), energy barriers, and p*K*a correspond to those measured by FTIR-spectroelectrochemistry of *D. gigas* hydrogenase by De Lacey et al [62].

2.1.2 Activation process

[Ni-Fe] hydrogenases such as that from *D. gigas* can be isolated aerobically but are then inactive in assays where H_2 is the reductant or in hydrogen-deuterium and hydrogen-tritium exchange assays. They have to be activated under reducing conditions in the absence of oxygen. It was proposed that in the oxidized enzyme the H_2-binding site (now known to be the Ni-Fe center) is inactive or blocked by oxygen, so that activation of the hydrogenase requires electron transfer into the H_2-binding site from elsewhere in the electron-transfer chain [62]. Ni-B ('ready' state) becomes active quickly upon reduction, while Ni-A ('unready' state) needs a long incubation period under reducing conditions before becoming active. Low potential electron donors or electron sources such as electrodes can be used as the reductant. In concentrated hydrogenase preparations, activation can be by intermolecular electron transfer between hydrogenase molecules or by residual traces of low-potential carriers such as cytochrome or ferredoxin from the bacterial source material [62].

2.1.3 Inactivation process

It has been known for several decades that [Ni-Fe] hydrogenases become reversibly inactivated by a trace amount of oxygen as shown in Figure 2.5. It has been reported that different ratios of the 'unready' Ni-A and 'ready' Ni-B are obtained depending on the condition of exposure to the gas, but the mechanism of the inactivation process is still not well understood. The most recent X-ray diffraction data of Ni-Fe hydrogenases in the oxidized state points to a monatomic oxygen species bridging the two metals in Ni-B, whereas, for Ni-A, a diatomic oxygen species was favored as a bridging ligand [63]. Hydrogenases from oxygen tolerant bacteria have been found to bear an additional *hypX* gene. A *hypX*- mutant of *R. eutropha* grew slowly under standard aerobic conditions, and the purified hydrogenase did not contain the extra nickel-bound CN, suggesting that, in the cell, the third cyanide is provided by the *hypX* protein [59]. [Ni-Fe] hydrogenases can undergo anaerobic inactivation by increased redox potential. Also [Ni-Fe] hydrogenases are inhibited by CO, which is a competitive inhibitor of most [Ni-Fe] hydrogenases. [Ni-Fe-Se] hydrogenases are generally more sensitive to CO inhibition than [Ni-Fe] hydrogenases and the inhibition effect is reversed by increasing the H_2 pressure [62]. CO-induced hydrogenase from *Rhodospirillum rubrum*, hyperthermophilic hydrogenase from

Pyrococcus furiosus and the O_2 – tolerant hydrogenase from *R. eutropha* are completely insensitive to CO.

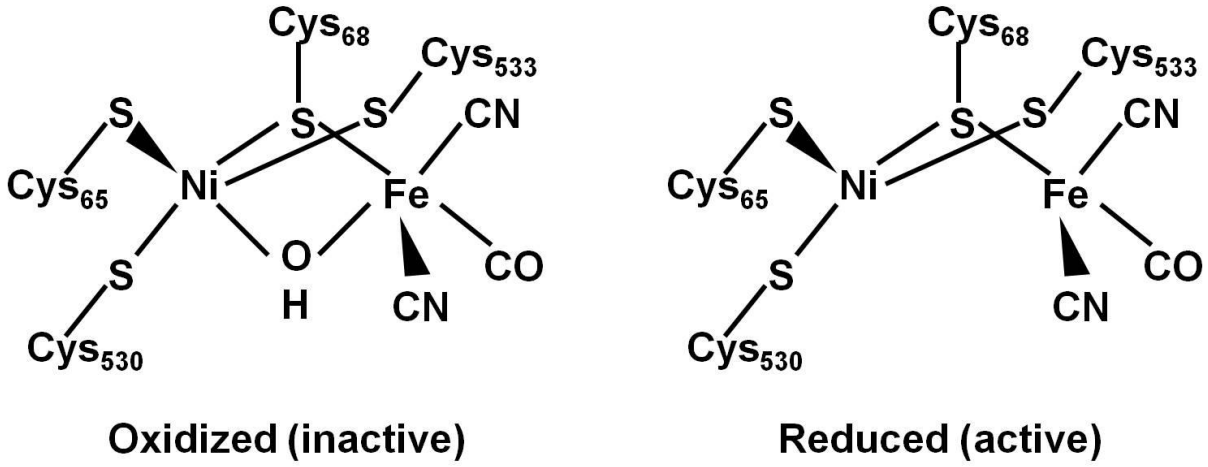


Figure 2.5 Figure adapted from Vignais *et* al,(2004) shows a schematic structures of the active site of [NiFe] -Hyrogenases: the oxidized inactive form corresponds to the Ni-A state and the reduced active form to the Ni-C state [38].

2.1.4 Thermo-tolerant and oxygen-tolerant [Ni-Fe] hydrogenases for hydrogen photo-production.

The photobiological production of H_2 gas, using water as the only electron donor, is a property of two types of photosynthetic microorganisms: green algae and cyanobacteria. In these organisms, photosynthetic water splitting is functionally linked to H_2 production by the activity of hydrogenase enzymes. Cyanobacteria possess two functionally different types of [Ni-Fe]-hydrogenases (Figure 2.1), an uptake and a bidirectional enzyme, both of which are oxygen sensitive [12]. The uptake hydrogenase (encoded by *hupSL*) catalyzes the consumption of the H_2 produced during N_2-fixation, while the bidirectional enzyme (HoxEFUYH) probably plays a role in fermentation and/or acts as an electron valve during photosynthesis [53]. Oxygen sensitivity to hydrogenases is one of the main difficulties encountered for the use of these enzymes for H_2 production. A critical requirement for the photo production of H_2 is the use of a hydrogenase that is not only tolerant to O_2 but also catalytically active in O_2. Also since solar energy is required by these photosynthetic microorganisms to produce H_2 the need of hydrogenases that are thermally tolerant is important.

Some hydrogenases are O_2-tolerant, like the soluble NAD- dependent hydrogenase of *R. eutropha*, which contains a modified metallocenter, encoded by the *hypX* gene, with an extra CN^- ligand [12, 56, 59, 62]. O_2-tolerant bacterial [Ni-Fe]-hydrogenase from *Rubrivivax gelatinosus* [29] could be used to produce H_2 but they are also CO sensitive. Hydrogenase in the purple sulfur photosynthetic bacterium *Thiocapsa roseopersicina* is also O_2-tolerant [64]. The [Ni-Fe-Se] hydrogenase from *Desulfomicrobium baculatum* has also shown high electrocatalytic stability after prolonged exposure to air [65]. Thermotolerant hydrogenases are commonly found in thermophilic and hyperthermophilic microorganism like *Thermococus kodakaraensis*, an anaerobic, sulfur-reducing hyperthermophilic archeon [66]. *T. roseopersicina* is remarkably active at high temperature [64]. The hyperthermophilic archeon *Pyrococcus furiosus* contains two cytoplasmic H_2-evolving hydrogenases (I and II) [67]. *Pyrococcus furiosus* is not only thermotolerant but oxygen tolerant. Engineering an extra CN^- ligand (like the *hypX* gene in *R. eutropha*) to occupy the uncoordinated site of the Ni-Fe metal cluster in these hydrogenases might improve O_2 tolerance, provided that the enzyme remains active. Table 2.1 gives a list of

proposed hydrogenases that may be used *in vivo* or *in vitro* with cyanobacteria to produce hydrogen.

Table 2.1 Hydrogenase enzymes that may be used for *in vivo* and *in vitro* hydrogen production

Organism	**Organism Metabolism**	**Thermo tolerant**	**Oxygen Tolerant**	**Hydrogenase Type**	**Gene Type**	**Ref**
Ralstonia eutropha	lithoautrophs	No	Yes	Cytoplasmic	*hox*	[68]
Thermococcus kodakaraensis	Sulfur-reducing hyperthermophilic archea bacteria	Yes	No	Cytoplasmic	*hyh*	[66]
Pyrococcus furiosus	hyperthermophilic archea bacteria	Yes	No	Cytoplasmic	*hyd*	[67]
Thiocapsa roseopersicina	Purple sulfur photosynthetic bacteria	Yes	Yes	Cytoplasmic	*hox*	[64]
Rubrivivax gelatinosus	Photysnthetic bacteria	Yes	No	Membrane containing CO-	-	[29]
Desulfomicrobium baculatum	lithoautophs	No	Yes	periplasmic	*hox*	[65]
Synechocystis PCC 6803	cyanobacteria	No	No	-	*hox*	[69]

The best sources of hydrogenases, both for basic research and for future biotechnological applications would be microorganisms that are inexpensive to cultivate. *T. roseopersicina* could be a good candidate for photobiological hydrogen production since the [Ni-Fe] hydrogenase from this organism is not only oxygen tolerant but thermally stable [24, 70-73]. The possibility of using this hydrogenase is limited by the fact that an active hydrogenase (*hydSL*) enzyme has not yet being produced outside of its original host due to the complicated maturation mechanism characteristic of [Ni-Fe] hydrogenases [74] and the unusual structural gene coding for the *hyd*-hydrogenase [75]. Previous attempts to express active [Ni-Fe] hydrogenase from *T. roseopersicina* in *E. coli* failed presumably because of the incompatibility of the maturation system [76]. The hydrogenase from *T. roseopersicina* is not yet accessible to genetic engineering. The hydrogenase from *Ralstonia eutropha* (formerly *Alcaligenes eutophus*) is also a good candidate for photobiological hydrogen evolution because its insensitivity to oxygen. A wealth of information is available on the biosynthesis, overproduction and biochemical properties of the membrane-bound hydrogenase from *Ralstonia eutropha* [77]. The hydrogenase from *R. eutropha* is accessible to genetic engineering and the heterodimeric membrane bound hydrogenase strongly resembles the composition of standard [Ni-Fe] hydrogenases from *Desulfovibrio vulgaris* [78]. Although hydrogenase synthesis in *R. eutropha* is temperature sensitive and ceases above 33^0C [79], Zimmer *et al*. [80] in their work have shown that a single amino acid substitution (Gly-468-Val) in the C-terminal part of HoxA is responsible for temperature tolerance. The point mutation in the *HoxA* helix-turn-helix motif was sufficient to raise the maximum lithoautotrophic growth temperature by as much as 4^0C [80]. By taking advantage of the tightly clustered genes for the membrane-bound [Ni-Fe] hydrogenase of *R. eutropha*, broad-host-range recombinant plasmids has been constructed carrying the entire membrane-bound hydrogenase (MBH) operon encompassing 21 genes [81]. This complex MBH biosynthetic apparatus was actively produced in hydrogenase-free host.

2.2 The hydrogenases of Ralstonia eutropha H16

The facultative chemilithoautotrophic β- proteobacterium *Ralstonia eutropha* harbors three distinct [Ni-Fe] hydrogenases (Figure 2.6) which are encoded on megaplasmid pHG1 [59]. It is a well studied class of the 'Knallgas' bacteria since it can thrive on a mixture of CO_2, H_2 and

O_2 [59]. The three [Ni-Fe] hydrogenases are fully functional in the presence of O_2, in contrast to standard hydrogenases, which make these hydrogenases of great interest in relation to its potential use for hydrogen photo-production.

The heterodimeric membrane-bound hydrogenase (MBH) consist of the gene product HoxG and HoxK that faces the periplasm. Its two hydrogenase subunits, HoxG (67.1 kDa), that harbours the [Ni-Fe] active site and the small subunit, HoxK (34.6 kDa), resemble those of the prototypic hydrogenase of *D. gigas* and are anchored via the C-terminal end of the small subunit to a membrane-integral *b* type cytochrome, HoxZ [82]. The cytochrome *b* serves as the primary electron acceptor and connects the MBH with the ubiquinone pool of the respiratory chain [83]. The physiological role of the MBH is in H_2 uptake. The MBH operon of *R. eutropha* contains 21 genes including the three structural genes *hoxKGZ* , the specific accessory genes *hoxMLOQRTV*, the *hyp* genes *hypABFCDEX,* responsible for Ni-Fe center assembly, and the regulatory genes *hoxABCJ* [59, 82]. By subcloning the entire MBH gene cluster of *R. eutropha* into a broad-host-range vector, the H_2 - oxidizing capability could be transferred even to hydrogenase- free recipients such as *Pseudomonas stutzeri* [81]. The temperature optimum for the MBH is 45^0C [79, 84]. The MBH can produce H_2 sustainably in the presence of oxygen and air as long as the H_2 produced is removed continuously [85], thus proving the feasibility for biological H_2 production in air.

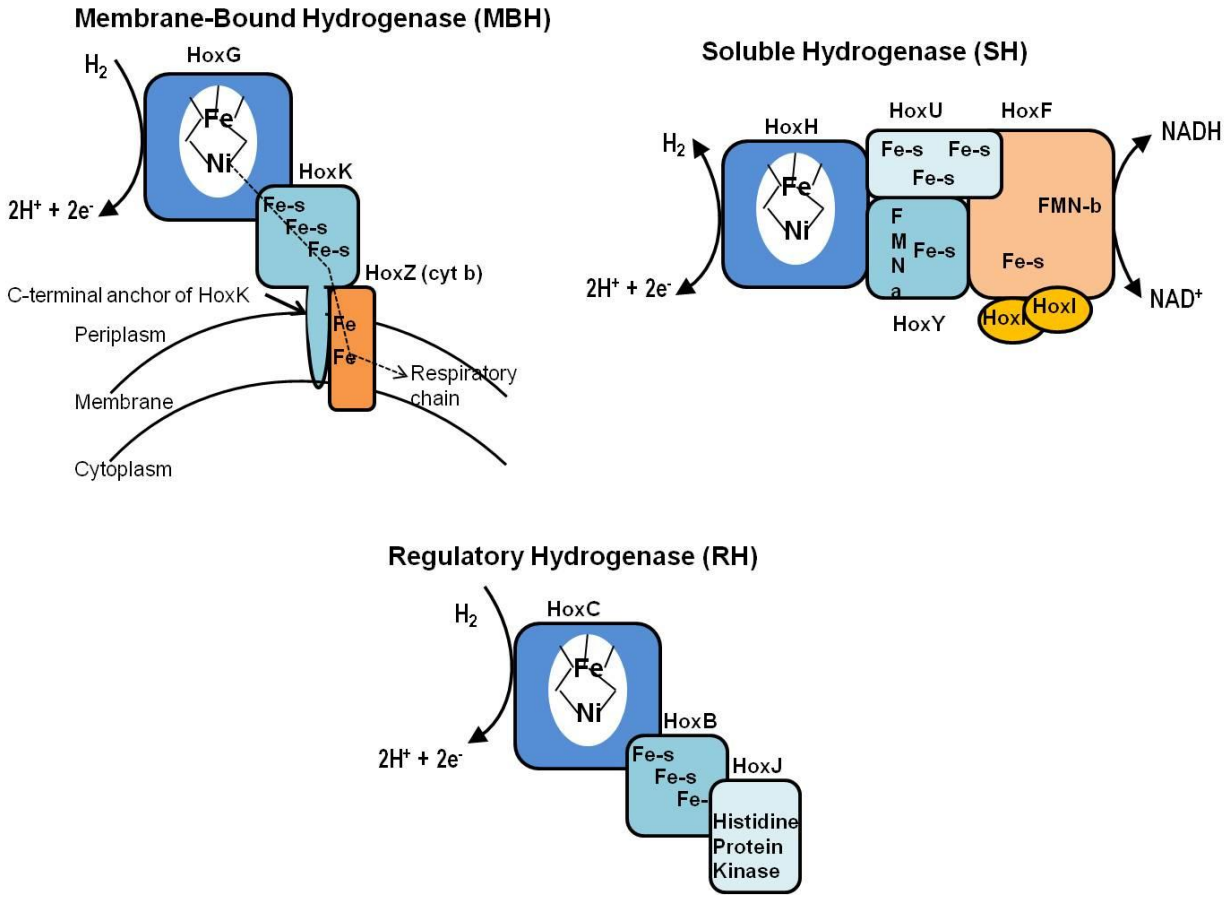


Figure 2.6 The three [Ni-Fe] hydrogenases of *R. eutropha* H16 (Figure adapted from Burgdorf *et a*l [59])

The second energy-linked [NiFe]-hydrogenase (soluble hydrogenase) in *R. eutropha* resides in the cytoplasm. It belongs to the group of multimeric, so-called bidirectional hydrogenases [59]. The soluble hydrogenae (SH) consists of two modules: the heterodimeric hydrogenase encoded by the genes *hoxH* and *hoxY* and the heterodimeric, flavin-containing NADH dehydrogenase (diaphorase) moiety encoded by *hoxF* and *hoxU* (Figure 2.6). Recently, a second flavin mononucleotide (FMN) cofactor also essential for activity, and two additional subunits each encoded by *HoxI* gene were discovered in the SH [59]. The function of the SH within the bacterial cell is to provide reducing equivalents (NADPH) for autotrophic carbon dioxide fixation and the expense of hydrogen. This hydrogenase is stable up to about 33^0C [79, 84].

The third [Ni-Fe] hydrogenase in *R. eutropha* is not involved in energy-linked processes but in transcriptional regulation [59]. The soluble, heterodimeric regulatory hydrogenase (RH) is encoded by *HoxB* and *HoxC,* and acts as a hydrogen sensor in contact with the histidine protein kinase *HoxJ*. The *HoxJ* complex detects the presence of hydrogen in the environment and transmits the signal via phosphorylation/de-phosphorylation to a response regulator which triggers expression of the MBH and SH genes [59].

The MBH from *R. eutropha* is accessible to genetic engineering, taking advantage of the fact that the genes coding for the MBH subunits are tightly linked with the clusters of hydrogenase accessory genes [81]. All structural, accessory and regulatory genes for active MBH are arranged in a large operon on the self-transmissible megaplasmid pHG1 [82]. The complete nucleotide sequence of the 452 kbp has been determined as shown in Figure 2.7 and has been deposited in the GenBank DNA sequence database under accession number AY305378 [86]. Spectroscopic analysis by FTIR and EPR has shown that almost all functional [Ni-Fe] states, which have been characterized in the standard [Ni-Fe] hydrogenases of anaerobic bacteria, were found in the MBH with one remarkable exception. There was no indication of the presence of the oxygen-inactivated Ni-A state under any conditions [87]. Ni-A represents a state in which an oxygen species, presumably a peroxo ligand [63], blocks the active site. The resulting unready, inactive enzyme requires long hours of incubation in the presence of H_2 to regain catalytic activity. The soluble, hexameric NAD^+-reducing hydrogenase and the cytoplasmic H_2 sensing

hydrogenases of *R. eutropha* also share this exceptional ability of being quickly reactivated after exposure to O_2. Direct electrochemical methods have been used to determine apparent inhibition constants for O_2 inhibition of H_2 oxidation ($K_{I(app)}^{O_2}$) for the MBH from *R. eutropha* [88]. The $K_{I(app)}^{O_2}$ values for the MBH from *R. eutropha* were at least 2 orders of magnitude higher than that those of the "standard" [Ni-Fe] hydrogenase from *D. vulgaris.* The experiment to determine the $K_{I(app)}^{O_2}$ was done by stepwise gas injection as shown in Figure 2.8. An electrode modified with MBH enzyme for *R. eutropha* was held under 100% H_2 at -8 mV versus SHE, pH 5.5, 30^0C, rotating at 4500 rpm. Aliquots of O_2 were injected into the headspace of the cell, causing the current to fall before the cell was flushed with H_2 [88].

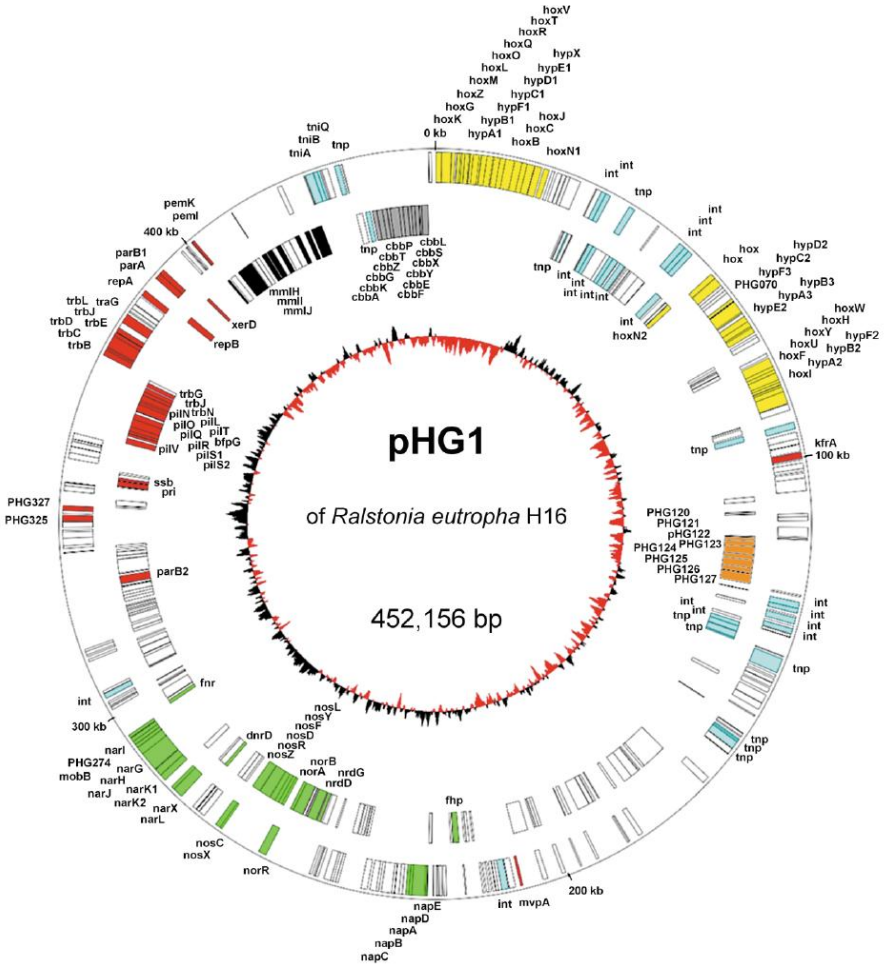


Figure 2.7 Figure of the genetic and physical map of megaplasmid pHG1 from Schwartz, E., *et al* (with permission). The outer and inner circle of boxes indicates genes transcribed in the clockwise and counterclockwise direction, respectively. ORFs are color-coded as follows: yellow, H_2 oxidation; grey, CO2 fixation; green, de-nitrification; red, plasmid maintenance and transfer; black, degradation of aromatics; orange, iron uptake; blue, recombinases. ORFs with no functional assignment are left uncolored [86].

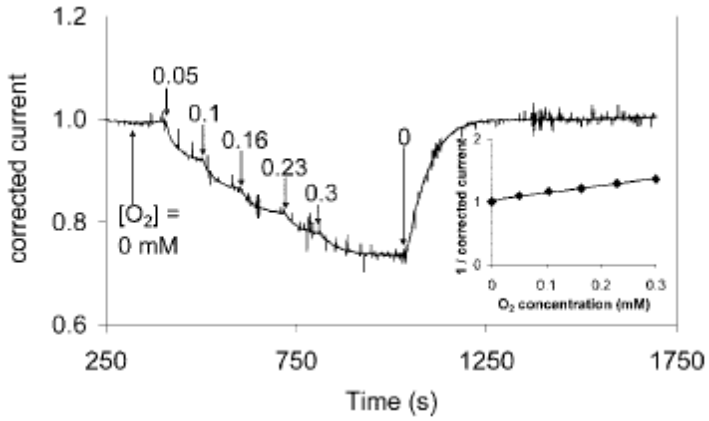


Figure 2.8 Experiment to determine the $K_{I(app)}^{O_2}$ stepwise gas injections (Figure from Ludwig *et al*, 2009). The insert shows the plot used to calculate $K_{I(app)}^{O_2}$ [88].

2.3 *In vivo* strategies of hydrogen production

Under appropriate conditions various algae and cyanobacteria can produce H_2 when illuminated with photosynthetically active light (380 – 720 nm) [89]. This implies that there is existence of a coupling mechanism linking the light-induced redox reactions with the H_2 – producing dark enzymatic reactions. There are two different modes of coupling among O_2 – evolving organisms. The first coupling involves the enzyme hydrogenase and is found in green and red algae. The second type of coupling involves the catalytic activity of the nitrogen fixing enzyme, nitrogenase and is found only in particular species of cyanobacteria [89].

Gaffron and Rubin[8] reported light-dependent evolution of H_2 in different algae via non cyclic electron flow from organic H^+ donor through PSI to hydrogenase where H_2 is released. The reported rates of hydrogen production in the range of 10 – 93 μl H_2 h^{-1} μl $cell^{-1}$ from different algae [8]. It was later shown that these algae were capable of simultaneously producing O_2 and H_2, with a ratio of H_2 to O_2 at 1.9, approaching the theoretical rate of 2.0 [9, 10]. Greenbaum and co-workers demonstrated the existence of a low-level but continuous electron transport pathway based on oxygenic photosynthesis [50, 90, 91]. This pathway is distinct from a fermentative pathway of electron transport for H_2 production reported by Gaffron, Gibbs, and co-workers [92-96]. However, it is now clear that both of these electron-transport processes have

limitations in both sustainability and yield. In vivo photosynthetic H_2 production with H_2O as the source of electrons cannot be sustained beyond a few minutes because O_2, derived from the water splitting activity of Photosystem II (PSII), functions to both inactivate the hydrogenase activity as well as to down regulate hydrogenase expression [12]. On the other hand, hydrogen evolution derived from the catabolism of endogenous substrates in green algae, does not have the reservoir capacity to sustain high rates of electron transfer to the photosynthetic apparatus.

Although the incompatibility of simultaneous photoproduction of O_2 and H_2 remained problematic for many years [97], in the late 1990's a simple and elegant solution was reported [98]. By using a nutrient-induced two-stage growth cycle the processes of oxygen evolution and hydrogen production may be separated temporally and sustained for hours. Using replete media in stage 1, normal oxygenic photosynthesis occurs; however in the second stage, the algae were deprived of sulfur-containing nutrients making them unable to repair PSII thus attenuating oxygen evolution. This altered the normal pathways of electron transport in the chloroplast and electrons were now derived from substrate donation directly into photosynthetic electron transport without PSII via one or more catabolic processes. These electrons were then provided to a hydrogenase via PSI yielding hydrogen. This system has been shown to work in *Chlamydomonas* and has been studied in some detail [99].

Hydrogen evolution activity of [Ni-Fe] hydrogenases from *T. roseopersicina, D. vulgaris* and *R. eutropha* has been achieved by coupling them with cyanobacterial photosystem I and their physiological partners. Experiments have been performed to increase *in vivo* hydrogen production by introducing the hydrogenase of *T. roseopersicina* into anaerobically adapted cells of *Synechococcus* PCC7942 by electroporation [64]. In the presence of 20 µM reduced methylviologen, saturating light (tungsten, 120µmol. $m^{-2}.s^{-1}$) and using a Clark-type electrode, hydrogen evolution was measured. The addition of *Thiocapsa* hydrogenase exhibited a threefold increase in hydrogen evolution (183nmol .mg Chl^{-1}. h^{-1}) as compared with cells subjected to electroporation without the addition of *Thiocapsa* hydrogenase (56.9nmol .mg Chl^{-1}. h^{-1}). However, within 45min of washing and re-suspending the electroporated cells, the hydrogen evolution decreased significantly [64]. This decline in activity was attributed to the lack of

accessory gene clusters that play a crucial role in the biosynthesis of the functional hydrogenase, besides the structural genes for the small and large subunits.

2.4 *In vitro* strategies of hydrogen production

Cell-free photoproduction of H_2 requires the isolation of stable, photochemically active photosynthetic complexes and coupling them with suitable hydrogen catalyst to produce H_2. In biochemically isolated PSI reaction centers, photon absorption initiates a vectorial electron transfer sequence that generates a 1 V potential over a distance of 6 nm [100], a reaction that is completed within 150 ns [101]. The quantum yield of the photochemical reaction is close to 100% [102, 103]. By coupling the low-potential electron-emergent end of PSI complexes (-0.6 V versus SHE) to either platinum nanoparticles [51, 104, 105] or covalently linked hydrogenase [77, 106], the photochemically produced electrons can catalyze the reduction of protons to hydrogen *in vitro.* One of the major advantages of *in vitro* H_2 production systems is that different components used to engineer a functional system do not all have to be derived from one organism. This allows a greater degree of flexibility for optimizing the performance of the complete system [89]. One major technical challenge with the *in vitro* H_2 production systems is the preparation of stable components that can withstand high light intensity, severe temperature fluctuations, oxygen and chemical degradation for long periods of time.

2.4.1 Self assembly and platinization

It has been demonstrated that chemically platinized thylakoid membrane can photosynthetically split water in molecular hydrogen and oxygen [49, 50]. In this platinized thylakoid, hydrogen is produced by proton reduction adjacent to the reducing site of the PSI complexes on the stromal side of the thylakoid membrane. This reaction is catalyzed by platinum particles. Subsequently, a technique to specifically platinize PSI complexes by photo-precipitation of hexachloroplatinate ($[PtCl_6]^{2-}$) on the reducing side of PSI, was developed [51, 104, 105, 107] as shown in Figure 2.9. At pH of 6.4 – 7 and at room temperature platinum clusters wereformed at the reducing side of PSI according to the reaction, $[PtCl_6]^{2-} + 4e^- + h\nu \rightarrow Pt\downarrow + Cl^-$, which then catalyzed the photoproduction of molecular hydrogen. The source of electrons for ($[PtCl_6]^{2-}$) reduction can be molecular hydrogen or reducing electrons from the light-activated PSI reaction center itself [107]. It has been further discovered that metals other

than platinum such as osmium and ruthenium can be photo-precipitated onto photosynthetic membranes and are capable of photo-catalytic hydrogen production [108].

Hydrogen evolution has been reported for PSI complexes isolated from spinach [104, 105]. Plastocyanin (PC) was required for rapid re-reduction of PSI as well as photo-induced hydrogen evolution. Sodium ascorbate (NaAsc) was used as the sacrificial electron donor with PC acting as a relay between NaAsc and the luminal side of PSI. For the solution based NaAsc-PC-PSI-Pt system, a maximum hydrogen evolution rate of ~2 µmol/h/mg Chl was reported [105]. Furthermore, the initial rates of hydrogen evolution (~0.03 µmol/h/mg Chl) was determined to increase about 3 –fold (~0.09 µmol/h/mg Chl) by cross-linking the PC to PSI [104]. *In situ* platinization and hydrogen evolution has also been demonstrated in trimeric PSI isolated from the thermophilic cyanobacterium, *Thermosynechococcus elongatus* [51]. This organism utilizes only c-type cytochrome (Cyt c_6) as the primary electron donor to P700. It has been demonstrated that a NaAsc- Cyt c_6-PSI-Pt system based on this cytochrome is capable of evolving H_2 in a Cyt c_6- and light- dependent fashion. H_2 was produced at temperatures up to 55^0C and was temporally stable for > 85 days. A maximum hydrogen evolution rate of ~5.5 µmol/h/mg Chl was reported for this system [51].

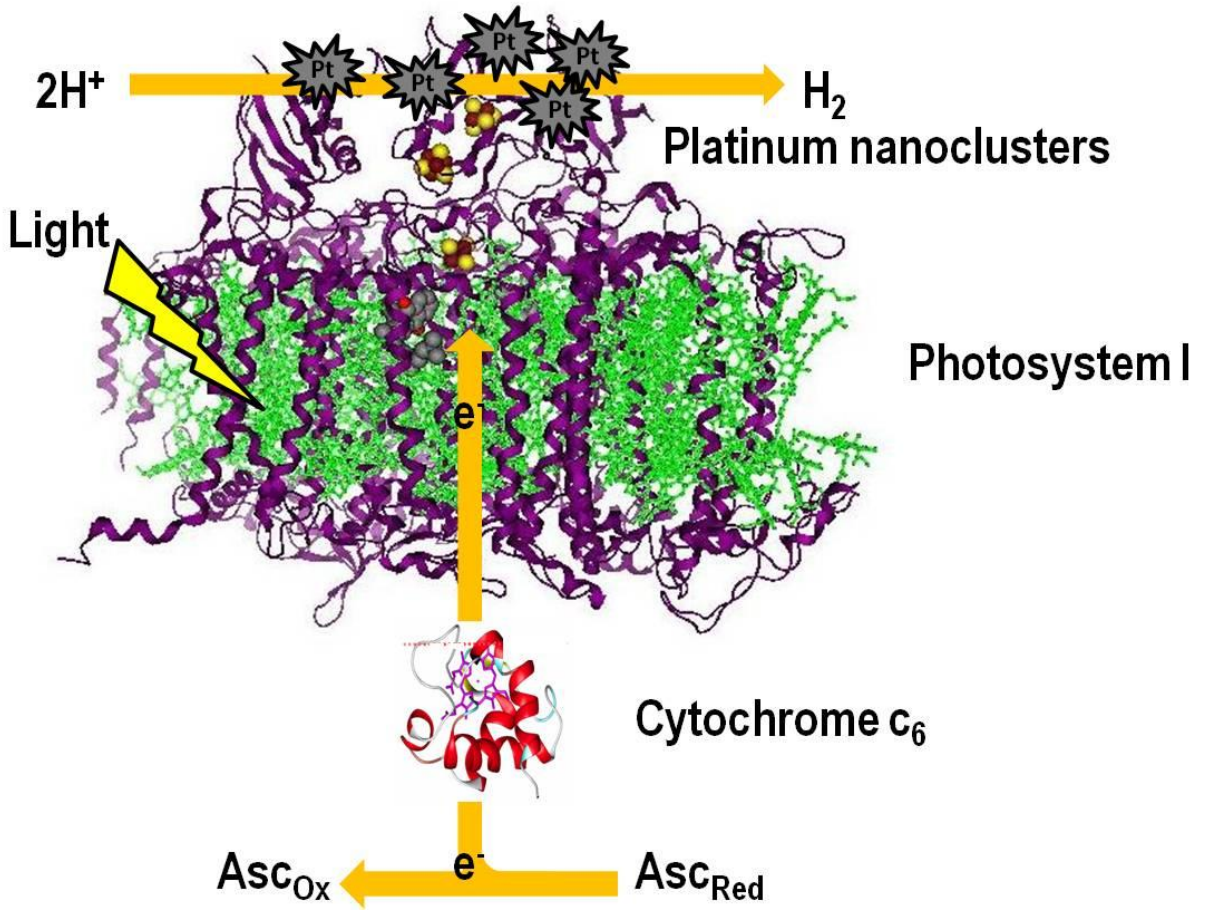


Figure 2.9 Schematic of the electron flow in the photosystem I catalytic nanoparticle. The monomeric form of the *T. elongatus* PSI is shown with chlorophyll cofactors and the protein colored by secondary structure (helical regions in purple, beta sheets in yellow and unstructured regions in brown). A partially docked form of the cyt c6 is shown, providing the rereduction of P700, deriving electrons from the oxidation of ascorbate ($Asc^{Red} \rightarrow Asc^{Ox} + e^-$). The platinum clusters on the stromal surface of PSI are shown as grey stars catalyzing the reduction of protons to hydrogen with electrons of lower potential via the energy of the absorbed photon, and PSI.

2.4.2 Platinum Beads

Photosystem I/dithiol molecular wire/ metal nanoparticle bioconjugates have been shown to catalytically generate H_2 gas when continuously illuminated [109, 110]. In the work of Grimme *et al* (2008), native PSI from the cyanobacterium *Synechocystis sp. PCC 6803*, was rebuilt to incorporate a recombinant form of PsaC subunit containing a free cysteine that allowed the covalent attachment of preformed 3 nm Pt particles or 12 nm Au particles using dithiol linkers (Figure 2.10). Using NaAsc as the sacrificial electron donor and 2, 6-dichlorophenolindophenol (DPIP) as mediator, and at saturating white light, PSI/molecular wire/ Pt bioconjugates generated 9.6 µmol/h/mg Chl [109]. Addition of 5 µM cyt c_6 increased the rate of hydrogen production by the Pt nanoparticles to 9.3 µmol h^{-1} mg Chl^{-1}. In order to maximize H_2 production of the PSI/molecular wire/Pt bioconjugates, PC isolated from spinach leaves was cross-linked to spinach PSI core complexes that had been rebuilt using the $Cys_{13}Gly$ variant of PsaC and different molecular wire lengths were used [110]. Bioconjugates constructed from the PC cross-linked spinach PSI evolved H_2 at rate of 98.6 µmol h^{-1} mg Chl^{-1}. Using 1, 8-octanedithiol, 1, 10-decanedithiol, 1, 4-benzenedithiol and 4, 4'-biphenyldithiol as molecular wires, hydrogen evolution rates of 49.0 µmol h^{-1} mg Chl^{-1}, 16.0 µmol h^{-1} mg Chl^{-1}, 150.5 µmol h^{-1} mg Chl^{-1} and 92.5 µmol h^{-1} mg $Chl^{-1}$where obtained, respectively. A onetime H_2 evolution rate of 312 µmol h^{-1} mg Chl^{-1} was obtained at optimal conditions including; solution buffered at pH 6.0, cross-linked PC, rebuilt spinach PSI, and the use of 1, 4-benzenedithiol to connect PSI to the Pt nanoparticles [110].

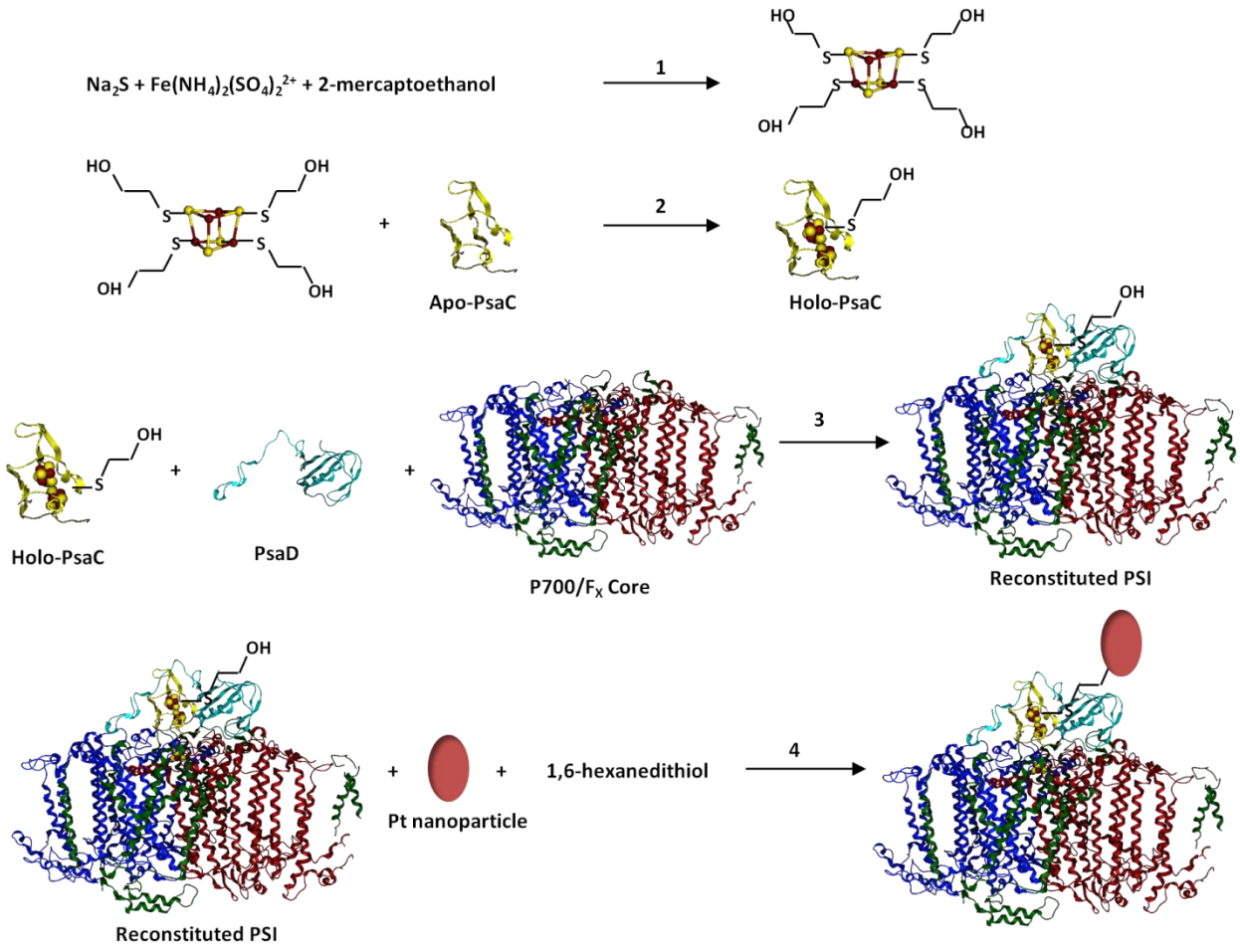


Figure 2.10 Construction of the PSI/1, 6-hexanedithiol/nanoparticle bioconjugate (adapted from Grimme *et al,* 2008). PS I was rebuilt by combining reconstituted PsaC and P700/F_X cores in the presence of PsaD. The 2-mercaptoethanol ligand to the F_B cluster was displaced, and PS I was covalently linked to a Pt or Au nanoparticle by 1, 6-hexanedithiol [109].

2.4.3 Electro-separated Systems

A viable hydrogen-evolving surface has been developed that employed the combination of immobilized PSI from *Synechocystis sp. PCC 6803* and the membrane-bound hydrogenase (MBH) form *Rasltonia eutropha H16* to provide a platform for H_2 production [111]. In this study PSI-hydrogenase hybrid complex was attached on a gold electrode by genetic engineering a decahistindine tag on the periplasmic side of the membrane integral PsaF subunit of PSI (Figure 2.11). This allowed for site-oriented attachment of PSI-hydrogenase fusion protein to the gold electrode surface *via* histidine/Ni-NTA interaction. Electrons provided by the gold electrode were transferred to PSI via a soluble electron carrier, N-methylphenazonium methyl sulfate (PMS) and then channeled to the hydrogenase upon light excitation of P700. This PSI-MBH hybrid complex produced H_2 at the rate of 4500 ± 1125 mol H_2/min/mol hybrid complex [111].

The [Fe-Fe] hydrogenase CrHydA1 from photosynthetic green algae *Chlamydomonas reinhardtii* has been mobilized onto a gold surface which has been modified by different carboxy-terminated self-assembled monolayers [112]. In the presence of the electron mediator, methyl viologen, hydrogen was produced at a rate of 85 mol H_2/min/mol protein.

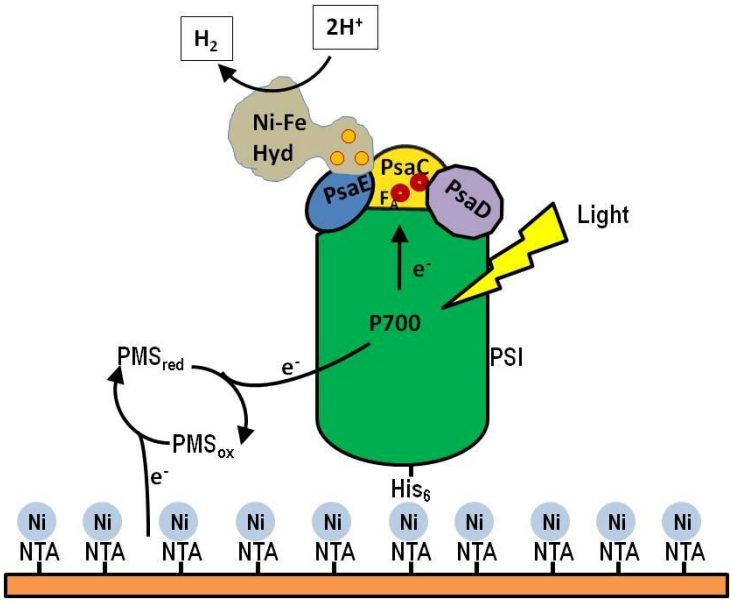


Figure 2.11 Schematic view of an electro-separated system for hydrogen evolution (Figure from Krassen *et al*, 2009) [111].

2.4.4 Hydrogenase-mediated H_2 evolution

Ihara and coworkers demonstrated light-driven hydrogen production by a hybrid complex of a [Ni-Fe] hydrogenase and the cyanobacterial photosystem I [77, 106]. While it is possible to use aqueous *in vitro* mixtures of PSI and hydrogenase, the formation of direct fusion proteins of hydrogenase and PSI have demonstrated five times the hydrogen evolution rate of mixtures of the native complexes. This was determined in the recent experiments of Ihara *et al* in which PSI was directly coupled with a hydrogenase enzyme for the first time. They first reported an artificial fusion of the membrane bound [Ni-Fe] hydrogenase from *R. eutropha* H16 and the peripheral PSI subunit PsaE of the cyanobacterium *Thermosynechococcus elongatus* [77]. The resulting hydrogenase-PsaE fusion protein associated with the PsaE-free PSI spontaneously and photo-produced hydrogen at a rate of 0.58 µmol/h/mg Chl (Figure 2.12A). Although the hydrogenase/PSI complex served as a direct light-to-H_2 conversion system *in vitro*, hydrogen evolution activity was totally suppressed by adding ferrodoxin (Fd) and ferrodoxin-$NADP^+$-reductase (FNR). In order to establish a H_2 photoproduction system in which the activity was not interrupted by Fd and FNR, PsaE from *Synechocystis* PCC6803, corresponding to the Fd-binding site was cross-linked with cytochrome c_3 from *D. vulgaris* [106]. This complex was then

stoichiometrically assembled with PsaE-free PSI from *Synechococcus elongatus* to form the cyt c_3/PSI complex (Figure 2.12B). Consequently, in the simultaneous presence of hydrogenase, Fd, and FNR, the light-driven H_2 production by the hydrogenase/*cyt* c_3/PSI complex was observed (0.30 μmol H_2/h/mg Chl). These results suggest that the *cyt* c_3/PSI complex may produce H_2 *in vivo* [106].

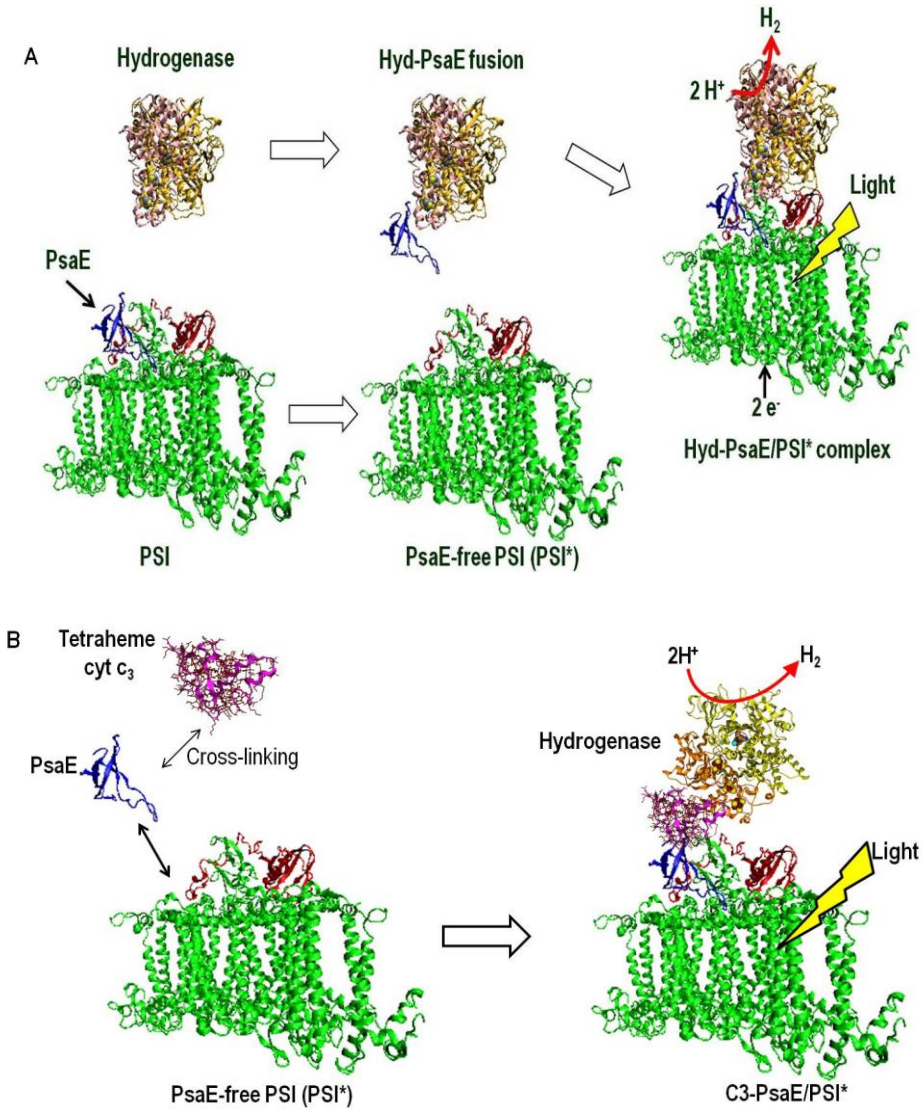


Figure 2.12 Figure adapted from *Ihara et al*, 2006. **A)** Assembly diagram of the hydrogenase-PSI complex from PsaE-fused hydrogenase and PsaE-free PSI [77]. B) Putative structure of the hydrogenase/cyt c_3-PsaE/PsaE-free PSI complex [106]. The cofactors are shown in red and PsaE is shown in blue.

A Photosystem I/molecular wire/hydrogenase system for hydrogen production in a manner similar to that for the Pt nanoparticles has been reported [113]. The HydA protein of [Fe-Fe] hydrogenase from *C. acetobutylium* was linked to PSI from *Synechocystis* PCC6803. The F_B cluster of the Cys_{13}Gly variant of PsaC on PSI was covalently linked to the distal [4Fe-4S] of the Cys_{97}Gly variant the HydA (hydrogenase) enzyme using 1, 6-hexanedithiol as the molecular wire [113]. The variant HydA enzyme had a hydrogenase activity (hydrogen evolution) of 11.5 mol H_2/s/mol H_2ase which was significantly lower than the wild type enzyme activity of 80.6 mol H_2/s/mol H_2ase. Cyt c_6, NaAsc and DPIP were added in the dark as soluble electron donor and photo-induced hydrogen evolution occurred at the rate of 3.9 µmol/h/mg Chl. The drawback for the Fe-Fe] hydrogenase from *C. acetobutylium* is that, like almost all hydrogenases, they are inhibited by oxygen.

H_2 evolution by direct electron transfer from a dithionite- reduced spinach PSI to both hydrogenase I and hydrogenase II from *Clostridium pasteurianum* was observed in the dark [114]. hydrogen evolution rate of 0.01 µmol/h/mg H_2ase (610 nmol/min/mg H_2ase) was observed with purified *C. pasteurianum* hydrogenase mixed with 5 mM dithionite and PSI core complex at 0.96 mg chl/ml. Light dependent H_2 evolution was also observed, using high potential electron donors to PSI, hydrogenase I and purified PSI or thylakoids [114]. In that system, NaAsc and dithiothreitol served as electron donors to PSI. The rate of hydrogen evolution with the purified PSI was 0.00003 µmol/h/mg H_2ase (2.1 nmol/min/mg H_2ase) at 2.4 µM PSI and 0.0003 µmol/h/mg H_2ase (12.1 nmol/min/mg H_2ase) with thylakoids. *C. pasteurianum* hydrogenases are inhibited in the presence of oxygen. A lower level of photo-induced hydrogen evolution was observed with thylakoids and the purified hydrogenase from *Rhodococcus* MR11, an enzyme that is not affected by oxygen [114]. Hydrogen evolution by spinach chloroplast mixed with *Clostridium kluyveri* hydrogenase and ferredoxin has also be reported [97]. The coupling of spinach chloroplast PSI to a *clostridial* hydrogenase and ferredoxin was first noted by Arnon *et al* [115]. An H_2 evolution rate of 4.0 µmol/h/mg Chl was observed with the basic system of chloroplast-ferrodoxin-hydrogenase [97]. Addition of a PSI electron donor, NaAsc and DPIP (with 3-(3, 4-dichlorophenyl)-1, 1-dimethyl-urea, DCMU added to block PSII) resulted in a 6-fold stimulation of the rate of H_2 evolution (26.7 µmol/h/mg Chl). Benemann *et al* in 1973

reported that the oxygen produced during the reaction of the basic system accounted for the relatively low rates of hydrogen evolved compared to those observed with PSI electron donors [97].

The capability of *Thiocapsa* hydrogenase to utilize the electron transfer mediators, ferredoxin and cytochrome c_6, of cyanobacterial origin has been determined [64]. Hydrogen evolution was measured amperemetrically using a Clark-type electrode at 30^0C under strict aneorobic conditions. Electron transfer mediators were added at different concentrations and the reaction was started by the addition of 50µL of the hydrogenase solution. A K_m value of 0.88mM was determined using ferredoxin as the electron transfer mediator [64]. In comparison, the K_m value of 0.55mM for methylviologen as the electron transfer mediator demonstrates a higher affinity of hydrogenase for methylviologen than for ferrodoxin. EPR spectroscopy and inhibitor studies on the hydrogenase from *T. roseopersicina* revealed that methylviologen interacts directly with the Ni-containing H cluster of the active center [64, 78] whereas recent X-ray structure determination of the hydrogenase from *Desulfovibrio gigas* [40] indicates that the interaction of natural electron mediators with the Fe-S centers of the small subunit is very likely.

An artificial system containing photosystem I from *Synechocystis* PCC6803, *Thiocapsa* hydrogenase, methylviologen (MV^{2+}) and mercaptoacetic acid (electron donor) had been shown to evolve hydrogen in the presence of light [116]. A 600W tungsten lamp was used to irradiate the sample solution and a 0.05mM phosphate was used to buffer the solution. A schematic of the electron transfer step used is shown in Figure 2.13.

The cytoplasmic hydrogenase from *Thiocapsa roseopersicina* NCIB 8347, has been purified, characterized and investigated for *in vitro* hydrogen production [73]. The cell concentration and the specific hydrogenase activity were increased when *T. roseopersicina* NCIB 8347 was photo-autotrophically cultivated with the addition of nutrients every 24 hours. The optimum pH and temperature for the H_2 evolution of the purified enzyme was 7.0 and 70^0C, respectively, and those for optimum cell growth were 7.0 and 25^0C, respectively. The purified hydrogenase, at 50^0C and pH 7.0, evolved H_2 gas for approximately 10 days under *in vitro*

conditions, using sodium dithionite and methyl viologen as the electron donor and carrier, respectively.

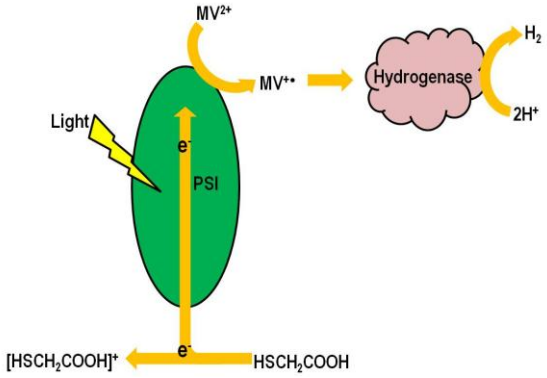


Figure 2.13 Schematic of the electron transfer steps process in the photo-induced hydrogen evolution system (adapted from Qian *et al*, 2009) [116].

2.5 Photosystem I from *Thermosynechoccocus elongatus*

The light-to-hydrogen conversion by the hydrogenase-PSI complex is a new concept that may be used to improve the hydrogen evolution ability of phototropic organisms like cyanobacteria [77]. A significant prior research that has bearing on the hydrogen evolution by a hydrogenase-PSI complex has been done. PSI isolated from a thermophillic cyanobacterium, *Thermosynechococcus elongatus* has been used for this study. This cyanobacteria PSI is a highly uniform, symmetric, disk-shaped nanoparticle with dimensions of ~12 X 40nm [117]. In addition, this complex forms a very stable trimer *in vivo*. A further advantage is the availability of a high-resolution X-ray diffraction crystal structure [118] and the ability to genetically transform *T. elongatus* [119, 120], which will enable the engineering for more rapid re-reduction via cyt c_6 and the ability to employ novel immobilization coupling chemistry and/or formation of directed fusion with specific subunits. Finally, this protein is stable at ambient as well as increased temperatures [121, 122].

T. elongatus is a thermophillic cyanobacterium that has been isolated from the Beppu hot springs in Japan. Photosystem I isolated from *T. elongatus* is a large subunit protein complex embedded into the photosynthetic thylakoid membrane [117]. It catalyses the light induced electron transfer from cyt c_6 on the luminal side of the membrane to ferredoxin or flavodoxin on the stromal side of the membrane. In cyanobacteria, PSI exists as a trimer with a molecular weight of more than 1 million Da [123]. The structure at 2.5 Å resolution showed that each monomer contains 12 proteins, 96 chlorophylls (Chl), 22 carotenoids, 3 [4Fe-4S] and 127 cofactors [118]. The center of one monomeric unit is built by the large subunits PsaA (silver) and PsaB (brown) as shown in Figure 2.14. The small membrane intrinsic subunits are: PsaF (ice blue), PsaI (purple), PsaJ (blue). The membrane extrinsic stromal proteins are depicted in yellow (PsaC), cyan (PsaD) and lime (PsaE). The electron transfer chain is functionally the most important part of PSI. It is located at the center of the monomeric PSI complex [124]. It consist of the P700 special pair, which is the primary electron donor and three 4Fe-4S clusters (F_x, F_A and F_B) as shown in Figure 2.14C. The two terminal Fe-S clusters, F_A and F_B, are bound to the extrinsic subunit, PsaC (8.9 kDa). The structure of Photosystem I in combination with mutagenesis studies that identified the ligands for F_A and F_B showed that the proximal cluster with a center-to-center distance of 12 A^o to F_x is F_A and the terminal Fe-S cluster with a distance

of 22 A^o to F_x is F_B [124]. *T. elongatus* utilizes only a c-type cyt (cyt c_6) as the primary electron donor to P_{700}.

The PSI reaction center is robust and has a number of favorable properties for application as a photochemical module. The antenna chlorophylls in PSI provide a large optical cross section. Since there are nearly 100 chlorophyll molecules per P_{700} in each PSI reaction center, up to 1000 photons can be absorbed per second [113]. Regardless of its wavelength, every absorbed photon generates a charge-separated $P_{700}^+ F_B^-$ state, thus the quantum yield of PSI approaches 1.0 [113]. The 1.01V of Gibbs free energy stored in the charge-separated $P_{700}^+ F_B^-$ state represents a remarkable 59% conversion efficiency for a red photon and 38% conversion efficiency for a blue photon [125, 126]. This results in a high thermodynamic efficiency of charge separation. PSI delivers electrons at a redox potential sufficiently low to drive H_2 production. The F_B cluster has a pH-independent redox potential of -580 mV [125, 126], which is 166 mV more reducing that the half-cell potential for H^+/H_2 couple at pH 7.0 ($2H^+ + 2e^- \leftrightarrow H_2$) [113]. This makes the reduction of protons to H_2 thermodynamically favorable with sufficient electromotive force to drive the reaction forward. Also, various methods have been pioneered for the biochemical removal[127-129] and reconstitution [128, 130, 131] of PSI with recombinant PsaC, PsaD (15.3 kDa) and PsaE (8 kDa) proteins [132, 133]. Finally, the chemical removal and reinsertion of F_x, F_A, and F_B clusters and site-directed mutagenesis of the proteins that constitute PSI has been reported [134-138].

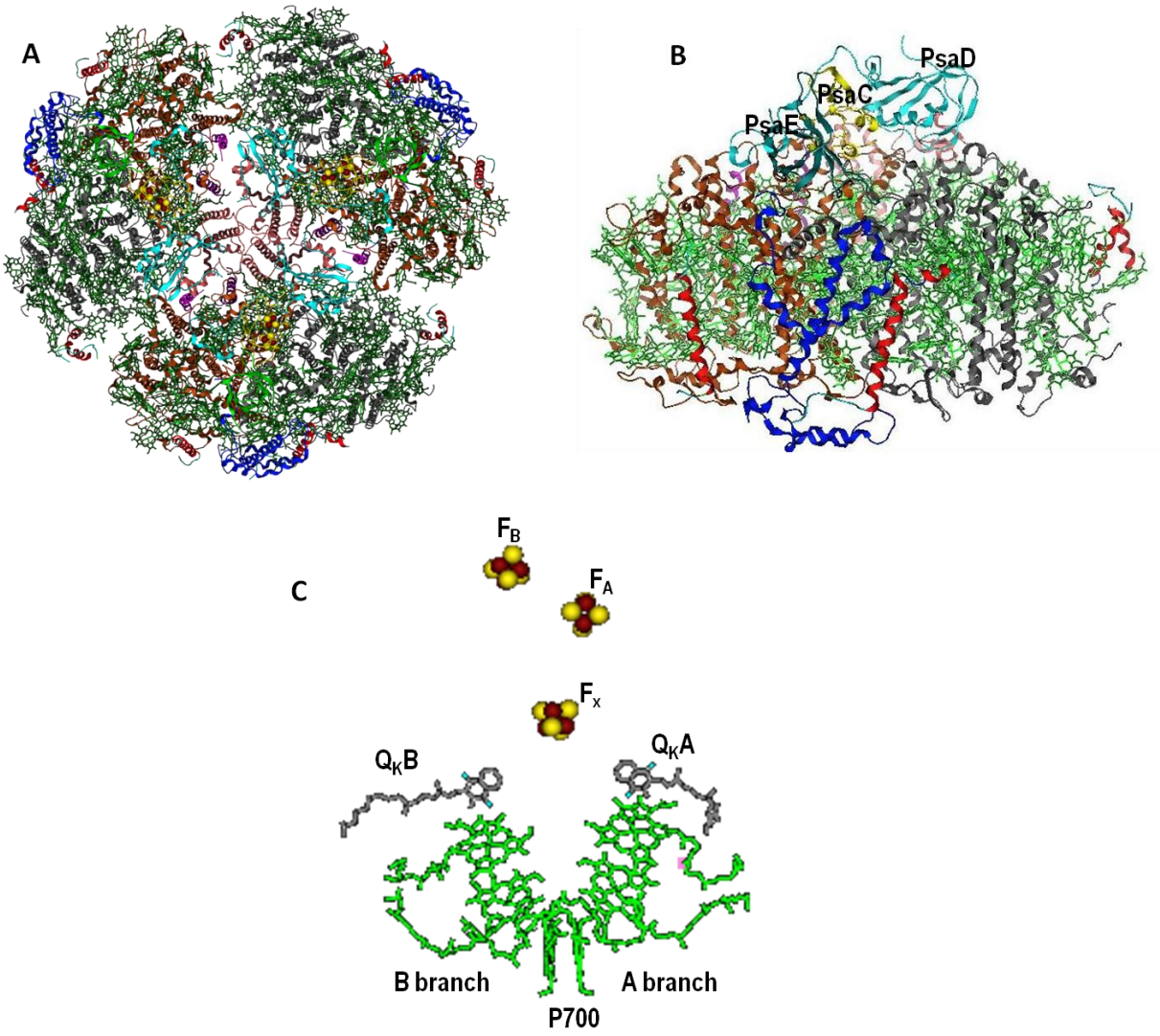


Figure 2.14 Trimeric PSI as viewed from the stromal side (PDB entry 1JB0). **B)** Side view of the whole PSI monomer along the membrane plane. **C)** The electron transport chain showing the arrangement of the electron transfer cofactors [124].

In summary, there has been active research in the area of biological hydrogen production. Oxygen sensitivity of the hydrogenases, temporal and thermal stability of the proteins and low rates of hydrogen evolution have continued to prevent the implementation of this technology. Significant recent research advances have been shown to pave the way for success in improving stability and rates of photosynthetic hydrogen evolution. In this work, we characterize the *in vitro* hydrogen evolution capabilities of PSI from *T. elongatus* using the platinum based system and also the naturally oxygen tolerant [Ni-Fe] hydrogenase from *R. eutropha*.

3. THERMOTOLERANT PHOTO-DEPENDENT HYDROGEN PRODUCTION BY PLATINIZED PHOTOSYSTEM I REACTION CENTERS

3.1 Introduction

There has been considerable interest in using green algae to produce hydrogen as a fuel since, in principle; they can employ the highly efficient process of photosynthesis to produce H_2 from two simple yet renewable resources, sunlight and water. Previous work has identified two independent pathways of *in-vivo* H_2 production; oxygenic photosynthesis reported by Greenbaum and co-workers [50, 90, 91] and the fermentative pathway of electron transport for H_2 production reported by Gaffron, Gibbs, and co-workers [92, 93, 95, 96]. However, it is now clear that both of these electron-transport processes have limitations in both how long H_2 production was sustained and the yield.

An alternative approach to *in vivo* photosynthetic hydrogen production has been proposed that employs biochemically-isolated PSI reaction centers that have kinetic and structural properties that are unsurpassed by synthetic systems. By coupling the low-potential electron-emergent end of PSI complexes to platinum nanoparticles [104, 105], the photochemically produced electrons can catalyze the reduction of protons to hydrogen *in vitro.* The fact that PSI has been shown to be active in both the solid-state [139] and in solution (this work) for many months suggests that this system will be able to produce a highly stable, cell-free hydrogen-evolving system that may prove to be a feasible, solar-driven energy solution [140]. Furthermore, future improvements may allow direct electron extraction from water using a coupled PSII to PSI system capable of recapitulating the photosynthetic electron transport chain in a new hybrid nanoparticle similar to what has been done in solution (22).

This work is directed toward demonstrating that a cell-free system derived from the thermophilic cyanobacterium, *Thermosynechococcus elongatus*, can provide a stable, thermotolerant, hydrogen-evolving nanoparticle. Using two biological components, PSI isolated from cultivated *T. elongatus* cells and a recombinant form of *T. elongatus* cyt c_6 expressed in *E. coli* and platinum metal, hydrogen evolution in an entirely resolved system is reported (Fig 3.1).

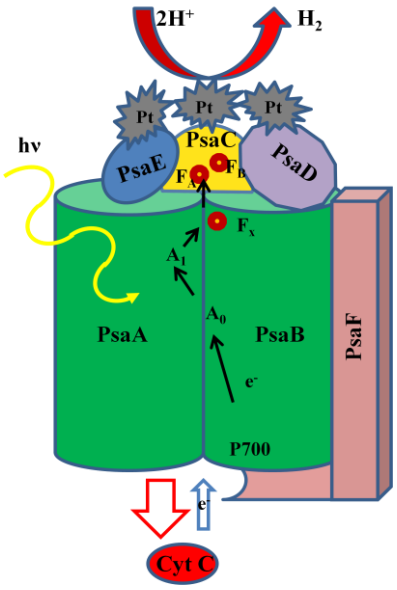


Figure 3.1 Schematic of platinized system for hydrogen evolution.

3.2 Materials and methods

3.2.1 Growth of *Thermosynechococcus elongatus*

The thermophilic cyanobacterium *T. elongatus BP-1* wild type was grown in 2L airlift fermenters (Bethesda Research Labs, Bethesda MD) and in some cases a 5L- BIOFLO 3000 batch/continuous bioreactor (New Brunswick Scientific) in NTA media. The temperature was held at 56°C with continuous illumination by fluorescent lights. The light level was increased as the cultures approached higher densities to a maximum of 50 µE/m^2/s. Cells were collected during late log phase by centrifugation for 10 minutes at 7,000 *g*, and washed once in wash buffer, 20 mM 2-(*N*-morpholino)ethanesulphonic (MES) pH 6.4, 5 mM $MgCl_2$, and 5 mM $CaCl_2$ before storage at -80°C until use for PSI preparation.

3.2.2 Isolation of trimeric PSI

Purification of trimeric PSI was carried following protocol established by Fromme *et al* [141] with modifications. Frozen cells were thawed and resuspended in lysozyme buffer (10 mM $CaCl_2$, 10 mM $MgCl_2$, 50 mM HEPES at pH 8.0 and 500 mM sorbitol). The resuspended cells were adjusted to chlorophyll-a content of 1 mg ml^{-1} and homogenized using a Dounce homogenizer. The chlorophyll a was measured using a spectrophotometer. After chlorophyll

extraction in 90% methanol, the chlorophyll-a was estimated from the extinction coefficient at 665 nm by the equation; (µg Chl a)/ml = Abs_{665} x 13.9 (1 cm path length). Lysozyme was then added to 0.2% (w/v) and the mixture was incubated in the dark for 45 min at 37 ^{0}C with gentle shaking. The resulting mixture was centrifuged for 10 min at 7,000g and the light blue supernatant was discarded. The pellet was resuspended in lysis buffer (10 mM $CaCl_2$, 10 mM $MgCl_2$, 20 mM MES at pH 6.4 and 500 mM Sorbitol). The volume was adjusted again so that the chlorophyll a concentration was 1 mg ml^{-1}; the mixture was then passed twice through a chilled French Press (SLC Aminco) at a cell pressure of 20,000 psi. The highly fluorescent lysate was centrifuged at ~50,000g for 20 min, and the supernatant was discarded. The crude membrane fragments collected in the pellet were washed in wash buffer (10 mM $CaCl_2$, 10 mM $MgCl_2$, 20 mM MES at pH 6.4) once, washed the second time with wash buffer supplemented with 3 M NaBr and then finally in the initial wash buffer. The final washed membrane fragments were adjusted to a chlorophyll a concentration of 1 mg ml^{-1} and dodecyl–maltoside (DM) was added to a final concentration of 0.6% w/v and the mixture incubated for 20 min at 20 ^{0}C in darkness with gentle stirring. The insoluble material was removed from the solubilized membrane mixture by centrifugation at 50,000g for 30 min. The supernatant was separated immediately from the pellet and then loaded onto 10 - 30% sucrose gradients with 60% cushion; all solutions in the gradient also contained wash buffer and 0.03% DM. Density gradient centrifugation was performed at ~80,000g at 10 ^{0}C for 16 h. The lowest green band contained (Fig. 3.4A) the trimeric PSI complex; these bands were pooled using a large syringe. Pooled PSI samples were dialyzed against 20 mM MES pH 6.4, 10 mM $CaCl_2$, 10 mM $MgCl_2$ and 0.03% DM. to remove sucrose, and then loaded onto a POROS 20HQ (Applied Biosystems) anion exchange column (BioCAD 202 Chromatography workstation) and eluted with a non-linear 0 to 400 mM MgSO4 gradient. The method used for the HPLC is shown in Appendix I. The MgSO4 was removed by dialyzing against 20 mM MES pH 6.4, 10 mM $CaCl_2$, 10 mM $MgCl_2$ and 0.03% DM. The chlorophyll a concentration was measured and aliquots were stored at -80 ^{0}C for future use.

3.2.3 Real Time H_2 Detection and Electrolysis Calibration

An in-house developed continuous flow system was used for hydrogen detection as shown in Figure 3.2 [105]. A humidified N_2 stream flowing at 50mL/min carried the H_2 produced in the reaction chamber to an in-line Figaro tin oxide hydrogen sensor (model TGS821, Figaro Engineering Inc., Osaka, Japan). The signal from the hydrogen sensor was transmitted to a NI-Data acquisition box (National Instrument) via a bridge amplifier. The data acquisition box was interfaced to a personal computer. The hydrogen sensor was calibrated using an in-line electrolysis cell connected to a Keithley 6220 constant current source. A steady-state calibration step of electrolysis current was discharged through the cell containing 1mM potassium hydroxide (Fig. 3.3A). Faraday's first law of electrolysis was then used to convert the applied current into absolute rates of hydrogen production (Fig. 3.3B). Faraday's law can be summarized by

$$m = \left(\frac{Q}{F}\right)\left(\frac{M}{z}\right) \tag{3.1}$$

Where

m is the mass of the substance liberated at an electrode,

Q is the total electric charge passed through the substance,

F = 96,485 C mol^{-1} is the Faraday constant,

M is the molar mass of the substance,

Z is the valency number of ions of the substance.

In a simple case of constant-current electrolysis, $Q = It$ leading to

$$m = \left(\frac{It}{F}\right)\left(\frac{M}{z}\right) \tag{3.2}$$

and then to

$$n = \left(\frac{It}{F}\right)\left(\frac{1}{z}\right) \tag{3.3}$$

where *n* is the amount of substance (number of moles) liberated: ($n=m/M$) and *t* is the total time the constant current was applied.

Moisture traps were kept on ice to minimize the H_2O vapor reaching the tin oxide hydrogen sensor. The sample was illuminated by means of a dual Fiber-Lite A3200 fiber-optic

illuminator with an OSRAM 150 W quartz halogen lamp (Dolan-Jenner Industries). A Schott red glass filter that blocked light of wavelengths shorter than 600 nm was used for red light illumination, so the visible light transmitted to the reaction was limited to 600-900 nm. The light intensity was measured with a Licor quantum flux meter (Model Li-189). For the light saturation and temperature dependence experiments, a Fisher Scientific fiber-optic illuminator (Model 12-562-36) fitted with dual fiber-optic cables was used, and an USHIO 150 W halogen projector lamp (USHIO INC) calibrated using the LI-1800 portable spectroradiometer (LI-COR). At each power setting on the fiber-optic illuminator, the micro-processor-controlled LI-1800 spectroradiometer was used for rapid acquisition of spectroradiometric and photometric data.

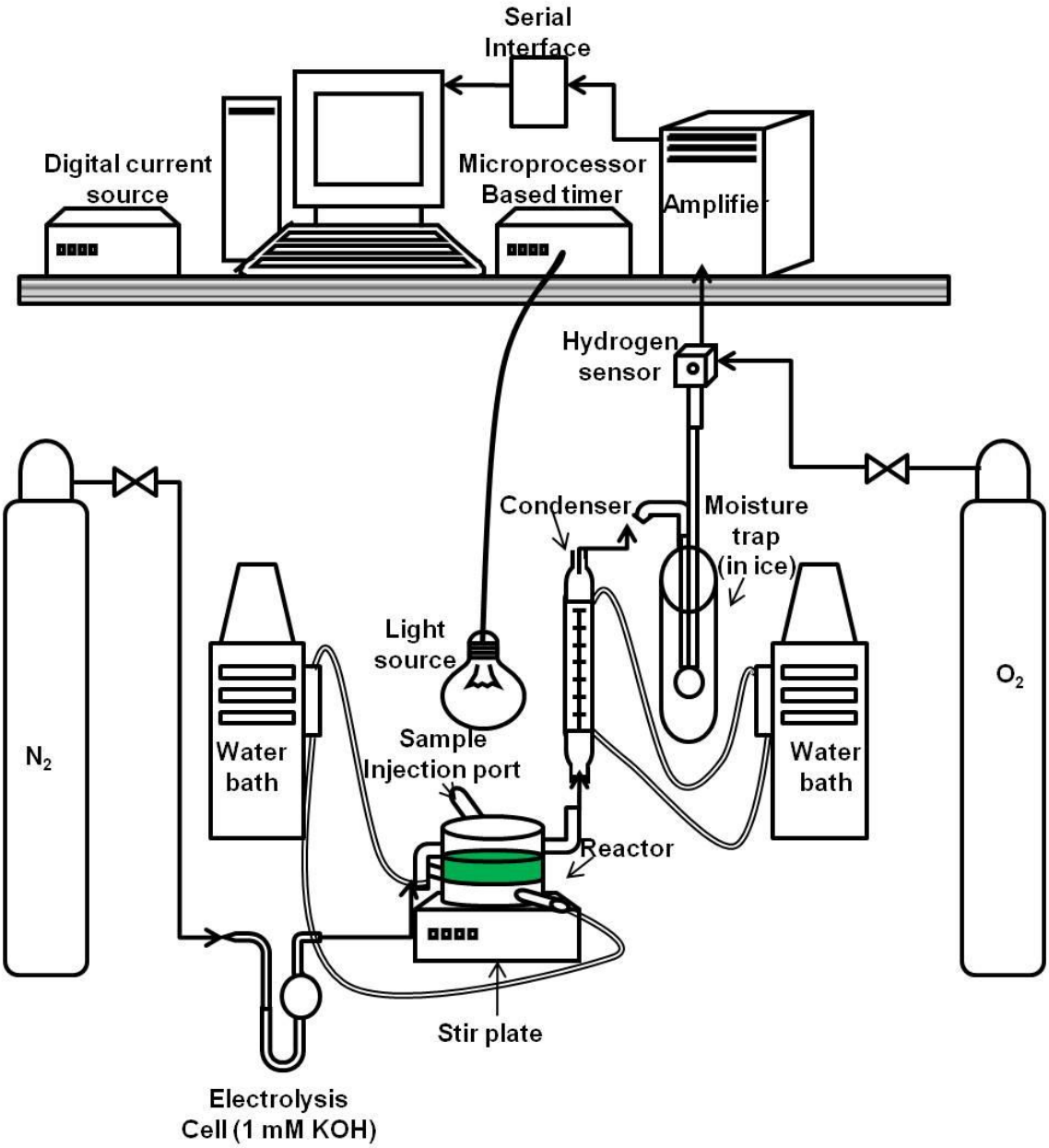


Figure 3.2 Schematic representations of the experimental apparatus for hydrogen evolution measurement.

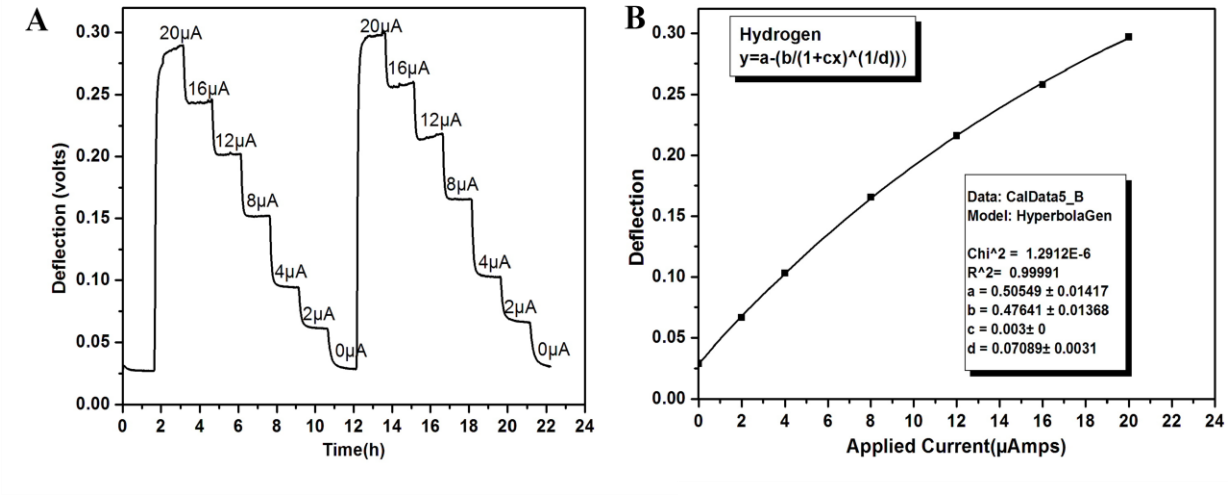


Figure 3.3 Real time calibration of hydrogen sensor. **A)** Raw data from the electrolysis step showing the deflection as the applied current is changed. **B)** Plot of the deflection versus the applied current is fit into a hyperbolic equation yielding parameters for the conversion of the sensor deflection to hydrogen produced (using Faraday's law of electrolysis).

3.2.4 PSI-mediated Hydrogen Evolution

Platinization reactions were carried out by incubation of cyt c_6, PSI (*T. elongatus* or *Synechocystis*) and 0.5 mM $Na_2[PtCl_6]$ in a thermostatically controlled photo-bioreactor as described previously [105], except that 20 mM MES at pH 6.4 was used to buffer the reaction. The molar ratio of cyt c_6 to *T. elongatus* PSI was maintained at 10:1, unless otherwise stated. Typical reactions contained PSI (80 µg chlorophyll ml^{-1}), 282 µmol cyt c_6, 0.5 mM $Na_2[PtCl_6]$, 20 mM MES buffer pH 6.4 and 20 mM (1 mM in some cases) NaAsc, at 25 ^{0}C. All reaction components, except NaAsc, were combined and injected into the photo-bioreactor. After anaerobosis was achieved (~1 h) the NaAsc was added to the reaction. Samples were illuminated as described above. A Chrontrol Model XT microprocessor-based timer was used to cycle the light on and off at intervals of 2 h. The photo-bioreactor was shielded from external light. After 24 h of the light catalyzed platinization and hydrogen evolution, the reaction mixture was dialyzed in 20 mM MES buffer pH 6.4, to remove excess hexachloroplatinate. In some cases, sucrose density gradient centrifugation was used to remove small analytes but had the additional effect of separation of the PSI complexes and cyt c_6.

Temperature–activity measurements were carried out as described above using the dialyzed platinized PSI preparation. The reactions were carried out in 20 mM MES pH 6.4 with 20 mM NaAsc as the sacrificial electron donor. No additional cyt c_6 or $Na_2[PtCl_6]$ were added to these reactions. An external water bath was used to incrementally increase the temperature during successive 2 h light on/off cycles, allowing the reaction to equilibrate during the dark cycles. A thermocouple was inserted into the reaction mixture to directly measure the temperature of the reaction. For long-term stability, hydrogen evolution was measured as above, and the data were integrated as a function of time with a smoothing window of 13 data points (Fig. 3.8b), demonstrating the compatible yield upon long-term storage. For the peak yield experiment in Fig. 3.10, the PSI complexes were platinized as described above, except that the chlorophyll and hexachloroplatinate concentrations were reduced to 5 µg ml^{-1} and 70 µM, respectively. After ten light cycles, the PSI complexes were recovered and purified by density gradient centrifugation. The purified PSI complexes were resuspended in reaction media at a cyt c_6 to P_{700} molar ratio of 75, with an illumination level of ~1,200 µE m^{-2} s^{-1}, NaAsc concentration of 100 mM and a temperature of 25 ^{0}C.

3.2.5 Optimized *E. coli* expression and purification of cytochrome c_6

The gene (petJ) for cyt c_6, has been cloned using gene-specific primers (manuscript in review). Applying an optimized expression system, large amounts (>10 mg/l) of the mature length holoenzyme was purified via immobilized metal affinity chromatography (IMAC) followed by anion exchange chromatography. This cyt c_6 was obtained from an MS student, Natalie Meyers in the laboratory of Dr Barry Bruce at the University of Tennessee, Knoxville.

3.2.6 Oxygen uptake assay to test activity of recombinant cyt c_6

Oxygen uptake experiments where performed in two biological oxygen monitors (YSI Incorporated, Model 5300). This two-channeled instrument utilizes a Clark type polarographic oxygen probes. A thin gas permeable membrane stretched over the end of the probe isolates the electrodes from the environment. These probes were immersed in magnetically stirred air-tight sample chambers. The temperature in the sample chamber was controlled by an external water bath. The four sample chambers were held in place with locking nylon hold down rings and sealed in the bath with two rubber o-rings [142]. All the assays were carried out in 5 ml glass cuvettes at 30° C. The electrodes were calibrated under aerobic conditions with constant stirring in the dark and the reading on the amplifier was set to 100.0% saturation by oxygen in air at these conditions. For the light saturation experiments, a Fisher Scientific fiber-optic illuminator (Model 12-562-36) fitted with dual fiber-optic cables was used. Typical reaction mixtures contained PSI (0.03mg chl a/ml), 20 mM NaAsc, 0.1 mM MV and 20 mM MES pH 6.4 containing 0.02% detergent n-dodecyl-β-D-maltopyranoside (DM) (Sigma-Aldrich). The presence of MV inhibits the recombination reaction between the electron acceptor side of the reaction center and $P700^{ox}$, as can be expected if MV is reduced by PSI [143-145]. NaAsc was used as the electron donor and cyt c_6 used as the electron carrier. Data from the oxygen uptake monitor was interfaced to a personal computer via National Instruments, model USB-6211 data acquisition box. To obtain the rate of oxygen uptake in μmol O_2 / (mg chlorophyll $\times$hr) the following equation was used:

$$\frac{\mu \text{l } O_2}{\text{hr} \times \text{ml}} \times 1.2875 \frac{\text{g } O_2}{\text{l } O_2} \times \frac{\text{mol } O_2}{32 \text{ g } O_2} \times \frac{1}{\text{M PSI}} \times \frac{\mu \text{M PSI}}{96 \mu \text{M chl}} \times \tag{3.1}$$

$$\frac{\mu\text{mol chl}}{893\mu\text{g chl}} \times \frac{10^3\,\mu\text{g chl}}{\text{mg chl}} = \frac{\mu\text{mol O}_2}{\text{mg chl} \times \text{hr}},$$

1.2874 g/l is the density of oxygen at 30°C, calculated using the ideal gas law and "M" is the mass of PSI added to the reaction medium.

3.3 Results and Discussion

3.3.1 Purification of Photosystem I from *T. elongatus*

Photosystem I (PSI) was isolated from the thermophilic cyanobacteria *Thermosynechococcus elongatus.* In the PSI preparation, the lowest chlorophyll- containing band of the sucrose gradient typically contained nearly pure trimeric PSI (Fig. 3.4A). Since Tris-Tricine SDS-PAGE (Fig 3.4B) revealed the presence of a small amount of phycobiliproteins, anion exchange chromatography was later used to ensure consistent purity and to concentrate the final PSI trimers (Fig 3.4D). Transmission electron microscopy (TEM) on the purified complexes provided supporting evidence for the uniformity and purity of the trimeric PSI nanoparticles (Fig 3.4C). A scaled outline of the PSI trimer structure as determined by Jordan *et al* [118] has been included for reference. The solvent- accessible surfaces of each of the monomers as shown in red, blue and purple and their three respective stromal exposed surfaces shown in green. Outlines of these were drawn in red and placed over several of the nanoparticles observed in the TEM, further confirming the uniformity of the PSI preparation.

Unlike plants, this cyanobacterium only encodes a c-type cytochrome (cyt c_6) that functions as the primary donor to P_{700} *in vivo*. The complete *T elongatus* genome [146] revealed only one cyt c_6 gene that contains a signal peptide. Thus to maximize the rate of hydrogen evolution in this system, it was necessary to have this cytochrome available in large quantities. Applying an optimized expression system, large amounts (>10 mg/l) of the mature length holoenzyme were purified via immobilized metal affinity chromatography (IMAC) followed by anion exchange chromatography. Circular dichroism spectroscopy was used to observe the thermostability of both PSI and cyt c_6 by monitoring the non-covalent pigment organization of PSI and the protein primary structure of cyt c_6. These experiments indicated that T_m for the

coordination of the bulk chlorophyll is ~55°C for PCC 6803 and >67°C for *T. elongatus* (Appendix II).

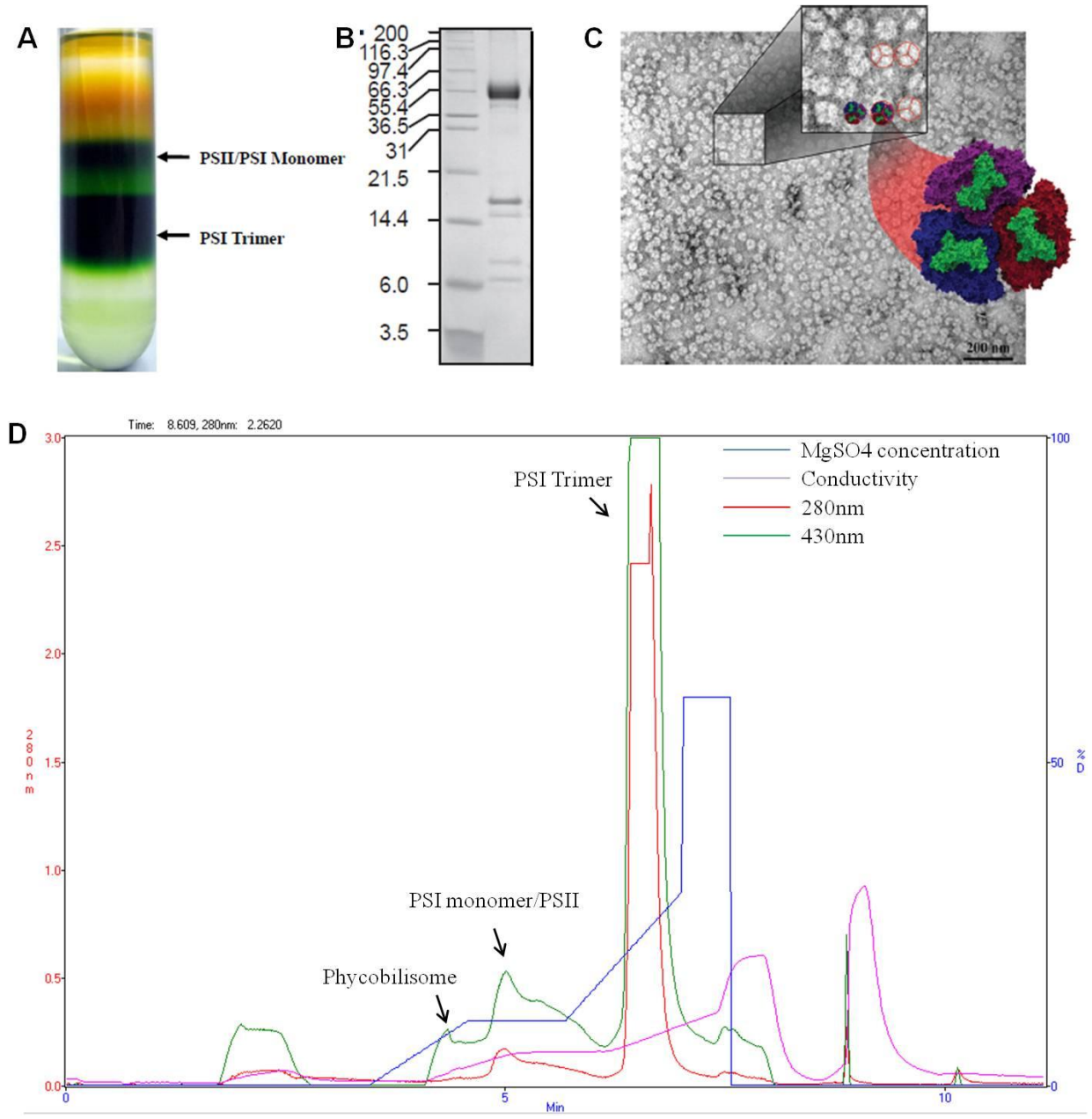


Figure 3.4 PSI isolation and confirmation of trimeric arrangement of the purified protein. **A)** Typical 10-30% sucrose density gradient displaying complete resolution of trimeric PSI from monomer and PSII. **B)** Tris-Tricine SDS-PAGE of PSI preparations from *Thermosynechococcus elongatus*. **C)** TEM of purified trimeric PSI. The inset is further magnified 2.5x and directly compared with an appropriately scaled spacefilling model of PSI (transmembrane elements are of each monomer are red, blue or purple, and stromal external subunits are green). **D)** High

pressure liquid chromatography (HPLC) elution profile of Trimeric PSI form sucrose gradient. Trimeric PSI was eluted by applying a step gradient of 0 – 400 mM $MgSO_4$.

3.3.2 Oxygen uptake assay to test activity of recombinant cyt c_6

In order to determine if the recombinant cyt c_6 was capable of P_{700} re-reduction, the methyl viologen mediated uptake of oxygen, using the purified trimeric PSI was done. This assay is light driven yet requires rapid re-reduction of P_{700}^+ to sustain the O_2 uptake. The concentration dependence of cyt c_6's ability to re-reduce P_{700}^+ was also explored. This is shown in Figure 3.5, where the molar excess of cyt c_6 was increased from 1 to 50 molar excess of the PSI concentration. As the amount of cyt c_6 is increased in the reaction, the rate of O_2 consumption increases. This results shows that cyt c_6 re-reduces PSI in a light dependent fashion since oxygen uptake occurred only in the presence of light. This result also suggests that there is a weak interaction between cytochrome c_6 and PSI from *T. elongatus* which is in agreement with literature [147].

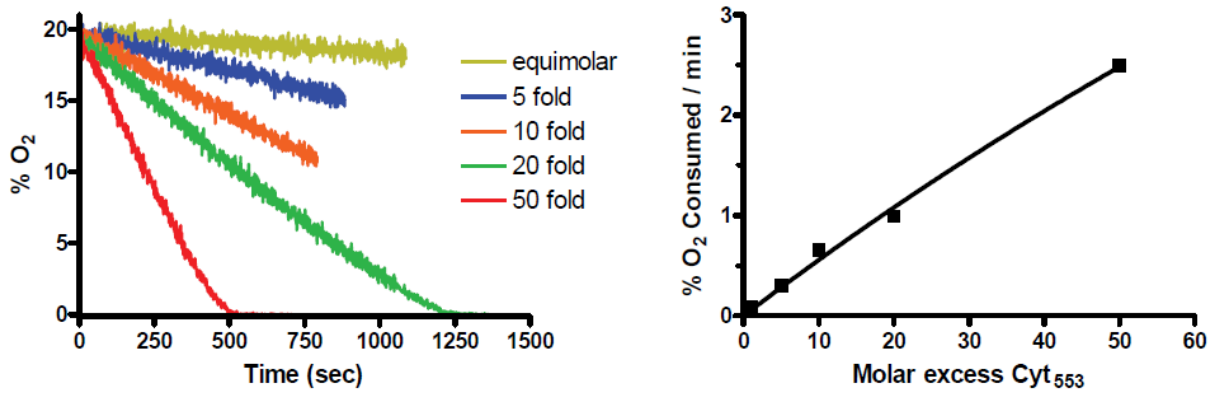


Figure 3.5 Oxygen uptakes by isolated PSI from *T. elongatus*. This assay monitors methyl violgen mediated oxygen uptake. The change in oxygen content is totally dependent on the presence of light, cyt c_6, MV and ascorbate. The data on the left is plotted as the rate of oxygen uptake as a function of the molar excess of cyt c_6.

3.3.3 Determination of rate-limiting step in PSI-mediated hydrogen evolution

Although PSI-mediated photo-production of hydrogen has been demonstrated with PSI isolated from spinach leaves [104, 105] and cyanobacteria [77, 106], this is the first report of a similar reaction being carried out by a thermophillic cyanobacterial system. Initial experiments were carried out to investigate the parameters under which T. elongatus PSI can support photo-dependent hydrogen evolution and also to study the stability of the system. A sequence-of-addition-reaction was carried out to demonstrate how the additions of each reagent affect the rate of photo-dependent hydrogen production. The first experiment was performed with unplatinized PSI complexes. The initial reaction containing PSI and $[PtCl_6]^{2-}$ was allowed to proceed for 2 light/dark (L/D) cycles. After the second light cycle, NaAsc was added in the dark and the rate of hydrogen evolution was continuously monitored at 25°C (Fig. 3.6A). Cytochrome c_6 was then added after 6 L/D cycles. Very low hydrogen evolution (0.0605 nmol per light cycle) was observed that was still light-dependent prior to the addition of ascorbate or cytochrome c_6. This low level remained unchanged even after the addition of 1 mM ascorbate indicating that ascorbate has a very poor ability to reduce P_{700}. However, the addition of cyt c_6 supported a rapid burst of hydrogen evolution that was short lived, decreasing sharply to about 25% of this level by the start of the next light cycle. One possible reason for this rapid hydrogen evolution may have been supported by a large pool fully reduced cyt c_6, following illumination this pool becomes depleted by the next light cycle. With time the system comes to equilibrium, with the rate of cyt c_6 reduction by Asc matching the level of P_{700} photo-oxidation. Another reason may be that the system experiences an initial burst of hydrogen under platinization conditions with high light intensity, high platinum concentration to PSI ratio. This may have caused the system to turnover very fast reaching its threshold precipitation in the first light cycle. It has been reported that upon reaching threshold precipitation and beyond, the peak rate of hydrogen production is observed atthe beginning of the cycle and decreases as that cycle continues [105].

To demonstrate that the platinum catalyst is truly integrated into the PSI nanoparticle we removed the PSI sample after the 13 L/D cycles shown in Fig. 3.6A and re-isolated PSI via sucrose density gradient centrifugation. This separateed the trimeric PSI from the platinum salts, cyt c_6, and any free metallic Pt nanoclusters formed during the first 13 L/D cycles. The PSI complexes were recovered and dialyzed overnight as described in Materials and Methods. These

particles were then evaluated for their platinum content by energy-dispersive X-ray spectroscopy shown in Fig. 3.6B. It is clear that this sample contains platinum as indicated by the energy levels of the emitted X-rays at 2.05, 11.07/11.25, and 9.36/9.44 KeV. Also the presence of carbon (0.28 KeV), nitrogen (0.39 KeV), oxygen (0.52 KeV), magnesium (1.25/1.30 KeV), sulphur (2.31 KeV), chlorine (2.62 KeV) and iron (6.4 KeV) were indicated by the energy levels of the emitted X-rays. Finally, the catalytic activity of this platinized PSI was verified by its hydrogen evolving ability with no additional Pt required as shown in the second sequence-of-addition reaction (Fig. 3.7). As before, only low level light-induced hydrogen evolution was observed without either ascorbate or cyt c_6. The fact that no increase in hydrogen evolution was detected upon ascorbate addition indicated that the re-isolated PSI did not still contain any cyt c_6. However, when cyt c_6 was added in the reaction vessel there was a burst of hydrogen production in the next light cycle. The rate of hydrogen evolution increased approximately 80-fold following the addition of cyt c_6. This experiment indicates that the initial treatment shown in Fig. 3.6A results in the integration of platinum into PSI. The hydrogen evolving ability of these platinized PSI nanoparticles still requires cyt c_6 as an electron donor, presumably to facilitate rapid re-reduction of P_{700} following photo-oxidation. Although the molecular nature of this platinization is not known, electron microscopy analysis indicates that the platinum probably forms electron dense complexes associated with PSI (Fig. 3.6C). Similar experiments using single-turnover saturating flashes of light and thylakoid membranes suggested that the minimum number of platinum atoms needed to observe the onset of hydrogen evolution was not more than 50, whereas a stable platinum metal catalyst developed at about 500 atoms [107]. Following this burst in hydrogen evolution, an initial decay in hydrogen evolution with each additional light cycle was observed. This decay can be fit to a single exponential decrease with time as is shown in Figure 3.7 with a half-life of 3.8 h. However, this decay does eventually decreases and the hydrogen evolution rate approaches a steady state rate. This decay suggests that for short times, some component involved in hydrogen evolution is either being degraded or is possibly damaged during the illumination. There are two potential explanations for this behavior; the first is that the platinum catalyst could be experiencing poisoning. Platinum and other platinum group metal catalysts are sensitive to fouling or poisoning by a wide range of compounds including sulfur containing compounds[148], heterocyclic nitrogen-containing compounds[149], and other

surface adsorbing molecules. Chlorophyll, a 5-membered heterocycle, is a known poison for some metal-based catalysts[150]. It is possible that either free chlorophyll or some other degradation product is responsible for this decrease in activity. The second potential is that free chlorophyll could be lost from PSI over time, leading to a direct decrease in the antenna size and rate of photon capture. A measurable loss of Chl from the PSI complex was observed during extended periods (> 24 h). This Chl release could account for the initial change in hydrogen evolution rate over time, either by poisoning of the platinum catalyst or by simply reducing the amount of chlorophyll available for photon capture in PSI or some combination of these processes.

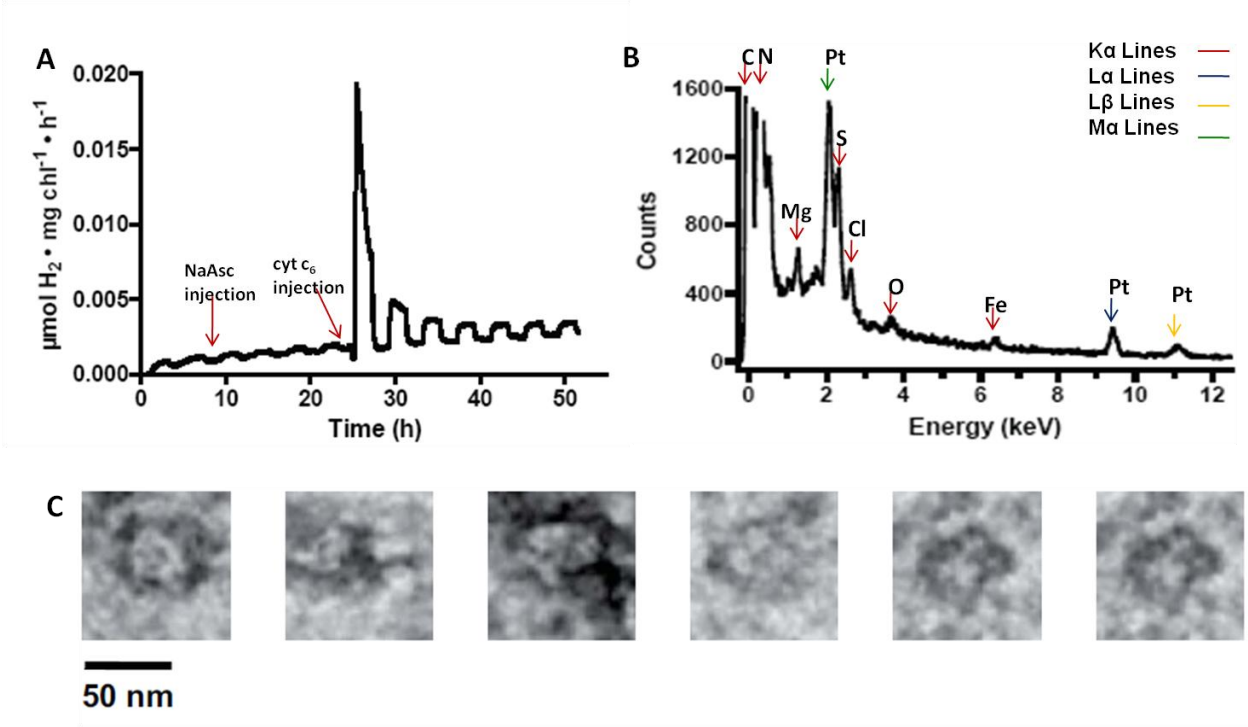


Figure 3.6 Sequence of addition on fresh PSI and Energy-dispersive X-ray spectroscopy. **A)** Sequence of addition on fresh PSI preparation. PSI at a Chl concentration of 80 µg/ml and 0.5 mM $[PtCl_6]^{2-}$ were added at time t = 0 at a temperature of 25°C. 1 mM NaAsc was injected through a side port into the photo-reactor at t = 7.18 h in the dark as indicated with an arrow. 9.4 µM cyt c_6 was then added into the system at time t = 24.58 h in the dark as indicated with an arrow. **B)** Energy-dispersive X-ray spectroscopy to confirm the presence of Pt nanoclusters. **C)** TEM of individual PSI particles showing electron dense particles following platinization and staining with 0.5% potassium phosphotungstic acid. Images were collected on a Hitachi H800 TEM at 50,000x magnification. Six individual particles are shown to reveal the somewhat irregular electron dense labeling that may represent the bound metallic platinum.

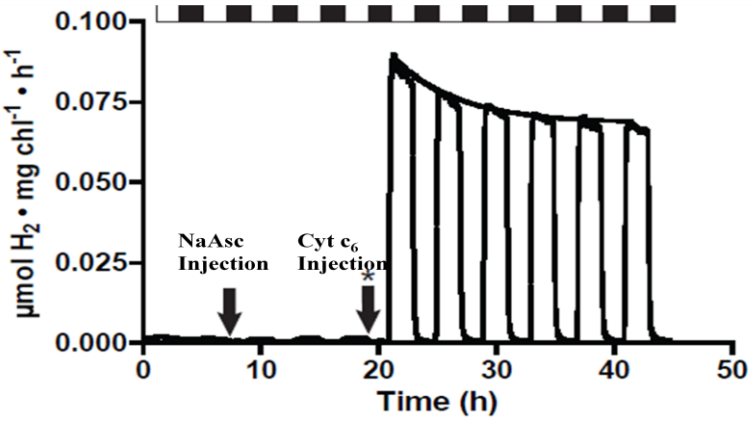


Figure 3.7 Sequence of addition on platinized PSI complex. Cyt c_6-free platinized PSI was initially added at time t = 0.1 mM NaAsc was added at time t = 7.5 h and 9.4 µM cyt c_6 was then added at time t = 20.09 h. The activity of hydrogen evolution was continuously monitored at 25^0C.

3.3.4 Evaluation of thermostability, kinetic limitations and sustainability

To evaluate this cell-free hydrogen evolution system for sustained H_2 evolution, an extended experiment that tested one lot of platinized PSI repeatedly over a 3 month period was done. The initial platinization of PSI was conducted using a 10:1 ratio of cyt c_6 to PSI in the presence of NaAsc and hexachloroplatinate for 60 h at 25°C; three representative L/D cycles are shown on the left of Fig. 3.8A. Upon termination of the reaction, the PSI preparation was dialyzed overnight (indicated as S1) to remove small reactant molecules and by-products (Fig. 3.8A). There was no visible precipitation of platinum in the reaction. The dialyzed PSI preparation was re-introduced to the reaction vessel, fresh NaAsc was added; H_2 production was observed without the addition of hexachlororplatinate further demonstrating that the Pt catalyst was stably associated with PSI. After 170 h of hydrogen evolution at 25°C, shown schematically as S2, the temperature was increased to 60°C for 20 h to determine if the system was thermally stable, as expected for thermophilic cyanobacterial proteins. The H_2 evolution rate at 60°C was not only stable but actually increased by 80%. Following this temperature increase the platinized Pt-PSI biomimetic catalyst was stored at 4°C for an extended period of 64 days (S3) and the rate

of hydrogen evolution was re-measured at 25°C for 29 L/D cycles and observed to be comparable to the rates observed earlier at 25°C, however. Finally, the sample was stored another 5 days (S4) and then retested, showing only a slight decrease from the initial values. These data show that our PSI preparations maintain operational stability for extended time periods. By comparing the initial activity to that remaining after ~2064 h there was no evidence of significant decrease as is shown in Fig. 3.8B.

Study of temperature dependence on the rate of hydrogen photo-evolution was performed in order to optimize this for the cyanobacterial PSI and cyt c_6 system. Recall that in the previous experiment, the rate increased 80% when the temperature was raised to 60^{o}C, even though the reaction has been running for 170 h at that point. Temperature-activity measurements were carried out using a dialyzed platinized PSI preparation in the presence of MES and NaAsc. Fig. 3.8C shows the temperature dependence of the hydrogen evolution rate. The yield of hydrogen evolution integrated over the initial 2 h light cycle at 25°C was about 0.97 nmol H_2 mg Chl^{-1}. When the temperature was increased to 45°C, the integrated yield hydrogen evolution increased to about 9.29 nmol H_2 mg Chl^{-1}. The highest rate of hydrogen evolution was observed at 55^{o}C with a yield of 14.8 nmol H_2 mg Chl^{-1}. This indicates ~15-fold increase in the sustained rate of hydrogen evolution as the temperature is increased from 25-55°C, which is the physiological growth temperature for *T. elongatus*. Further increase in the temperature of the reaction resulted in a slow decrease in the rate of hydrogen evolution. This observed thermostability was not surprising since the thermal stability of the two biological components (Appendix II) had already been confirmed, cyt c_6 and PSI, which have a T_m of 81°C and ~90^{o}C, respectively. A slight decrease in the hydrogen evolution rate as a function of temperature was observed (Fig. 3.8C). Interestingly however, a similar decrease in the rate of hydrogen evolution with subsequent L/D cycles where the temperature was fixed at 25°C was observed (Fig. 3.7). Fitting both of these observed decreases in hydrogen evolution (Fig. 3.7 and Fig. 3.8C) to a single exponential decay indicates a similar decay constant. The similarity in this decay suggested that there is some systemic component that was losing its activity during multiple L/D cycles. The only consumable component in our system is the NaAsc that is added in excess to facilitate the re-reduction of cyt c_6. It is possible that during the extended length of these experiments that the

NaAsc is either literally used up or possibly degrades to some inactive product. To test the potential role of NaAsc consumption during the course of this experiment we ran an extended experiment until the rate of hydrogen evolution reached a plateau, at which point a new aliquot of fresh NaAsc was injected. In Figure 3.8D, an immediate increase of ~80% that is very stable and free from decay was observed.

To compare the temperature dependence of hydrogen production for PSI from *T. elongatus* and *Synechocystis PCC 6803*, the integrated yield of hydrogen for a 2-h light cycle was measured and plotted against temperature (Fig 3.9A and 3.9B). The experiments were carried out two different reactor set up and carried out under different light intensity as a result; the yields in Figure 3.9A were normalized to the yield at 25^0C for easy visualization of the effect of temperature on hydrogen yield. It is clear that for *T. elongatus* the hydrogen yield increased up to 55 ^{0}C before it began to decrease (Fig. 3.9B); however, the hydrogen yield for *Synechocystis PCC* 6803 decreased steadily and was barely detectable at 60 ^{0}C. The experiments above illustrate the thermal (>55 ^{0}C) and temporal and storage (>2,000 h) stability achievable with these hydrogen-evolving nanoparticles. The hydrogen evolution rates shown in Fig. 3.7 (~80 nmol H_2 h^{-1} (mg chlorophyll)$^{-1}$) equal or exceed those previously reported using platinized PSI from plants [104, 105].

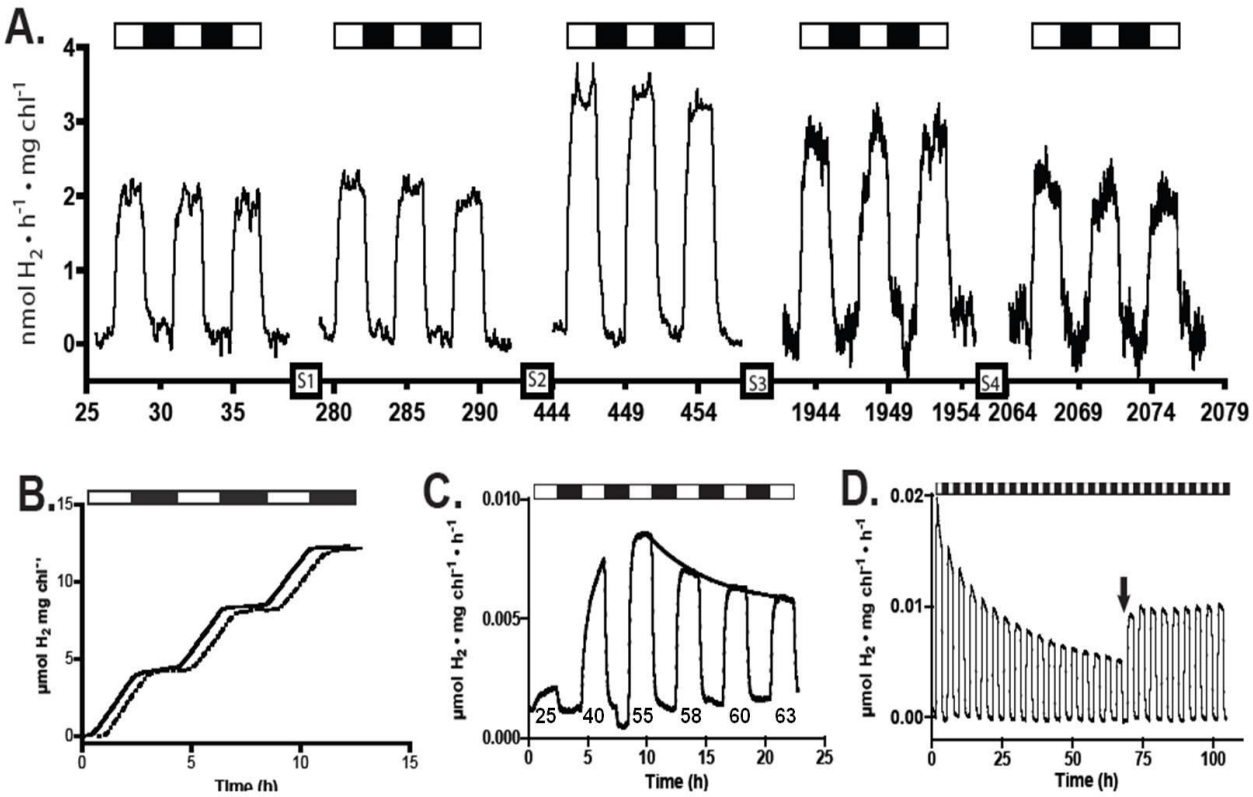


Figure 3.8 Thermal and temporal stability of H_2 evolution. **A)** Temporal stability. The platinization was stopped after 60 h and dialyzed to remove excess platinate (S1). After 170 h of L/D cycles with comcominant hydrogen evolution at 25°C, the temperature was increased to 60°C for 20 h. The reaction mixture was stored for 64 days at 4°C (S2), later warmed to 25°C, and re-exposed to 2 h light/dark cycles as before. **B)** Integrated H_2 yield of three light/dark cycles. Integrated H_2 yield before initial storage (solid line) and after final storage (dashed line) were plotted. **C)** Temperature-activity measurements. Temperature was changed during the 2h light off cycle to equilibrate before actinic light exposure. **D)** Temporal stability and role of donor consumption. 2 mM NaAsc was initially present, and 1 mM NaAsc was added at t = 68 h as indicated by the arrow. Decreased activity is fit by a single exponential in panels **(C)** and **(D)**.

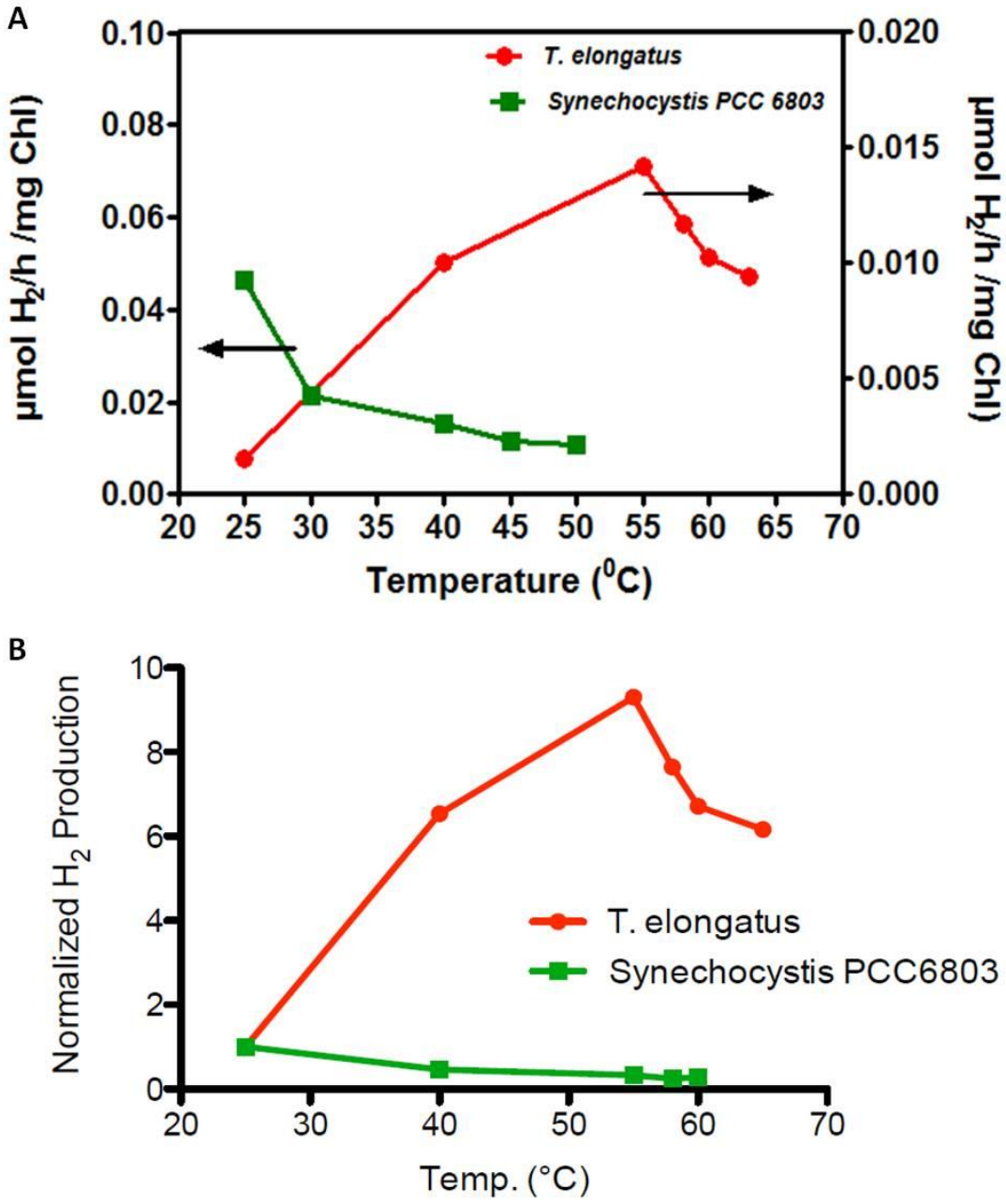


Figure 3.9 Comparison of yields of hydrogen evolution for *T. elongatus* (red) and *Synchocystis* (green) PSI with increasing temperature. Integrated hydrogen yield over 2h light cycles are normalized by their respective 25°C yields. **A)** Raw hydrogen yield **B)** Normalized yields of hydrogen evolution.

3.3.5 Light Saturation Experiment

The light saturation experiment was performed with platinized *T. elongatus* PSI nanoparticles similar to those described above. The hydrogen production rate increased with increasing light intensity (Fig. 3.10) and began to plateau as the light intensity approached 800 μE m^{-2} s^{-1}, however, this curve is sigmoidal with a distinct lag phase. Considering the photons as substrate for PSI, regular kinetic analysis may be applied since H_2 production is proportional to PSI activity. Although these data do not result in a good fit to a simple single-substrate kinetic model (blue line), it can be fit to a cooperative model (red line) with a Hill coefficient of ~2.5. The Hill coefficient is a measure of cooperativity in a binding process. A Hill coefficient of 1 indicates independent binding, a value greater than 1 shows that an enzyme has more than one substrate binding site and that the binding of one substrate to the enzyme facilitates binding of other substrate molecules. The shape of this curve is different from the light saturation response for monomeric PSI isolated from spinach [105], which was linear in the low light region. Because the *T. elongatus* PSI (Fig. 3.4C) is trimeric, the platinum catalyst can potentially accept electrons from more than one of the PSI P_{700} in the trimeric complex. Such cooperativity between adjacent PSI monomers explains how a single electron from a single P_{700} could facilitate molecular hydrogen production, which requires two electrons to reduce two protons. This sigmoidal response indicates that at higher light levels the probability of simultaneously photo-exciting two PSI reaction centers increases within a trimer, thus yielding a higher and 'cooperative' mechanism of hydrogen production. Another difference between the spinach and *T. elongatus* light responses was the light level at which the hydrogen yield was observed to plateau. In spinach, the plateau was at ~200 μE m^{-2} s^{-1}, whereas in *T. elongatus* the plateau was at ~800 μE m^{-2} s^{-1}. This may be the result of the considerable difference in the chlorophyll antennae-to-P700 ratio in the organisms. The plant PSI has much larger antennae, approaching ~300 chlorophyll/P_{700} whereas the *T. elongatus* PSI is ~95 chlorophyll/P_{700}. This approximately threefold difference in antenna size would account for the difference in light dependence.

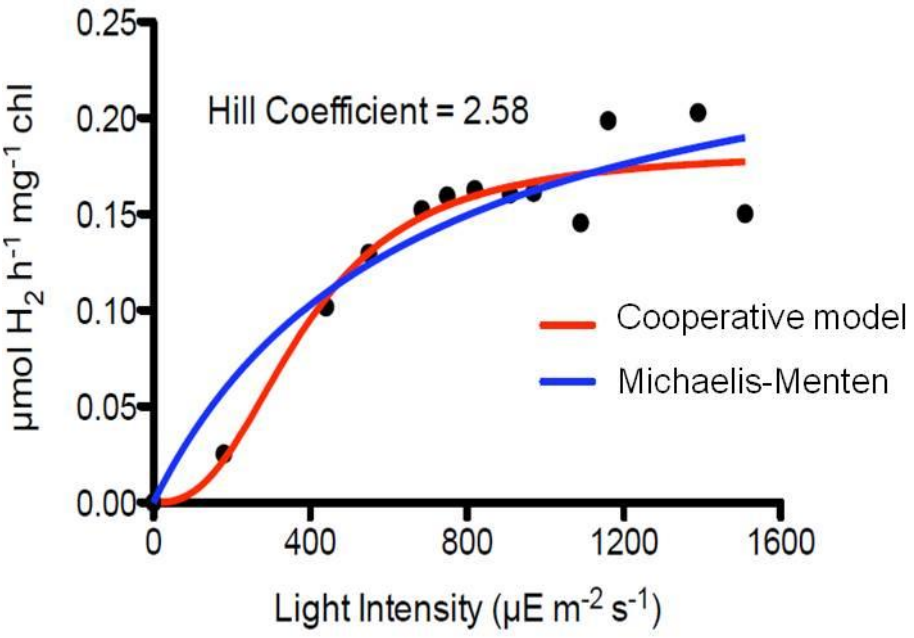


Figure 3.10 Light saturation curve for platinized PSI preparation. Previously platinized PSI (20 µg chlorophyll ml^{-1}) was used to determine hydrogen production as a function of light intensity. The data were fit to a single site kinetic model, that is, with no cooperativity (blue line), and a cooperative model (red line).

3.3.6 Peak rates of hydrogen evolution

The hydrogen evolution rates shown in Figs. 3.6 & 3.7 (>80 nmol H_2h^{-1}mg Chl^{-1}) are equal or higher than what have been previously reported using platinized PSI from plants. Hydrogen evolution rates of approximately 12 nmol H_2 h^{-1} mg Chl^{-1} have been reported for spinach PSI and plastocyanin, PC [151]. In Evans *et al.*, rates of 30 nmol H_2 h^{-1} mg Chl^{-1} and 90 nmol H_2 h^{-1} mg Chl^{-1} were reported for free and cross-linked spinach PC to PSI systems respectively[104]. This hydrogen evolving system is remarkable due to its thermostability (>55°C), its extended temporal and storage stability (>2000 h), and its simple mode of self-assembly. The system has also been shown to evolve hydrogen under continous operation for > 500 h (data not shown). A novel bioengineered system has been reported[152] that utilized preformed platinum/gold nanoparticles coupled directly to a cyanobacterial PSI to evolve hydrogen. This elegant study reported much higher rates than was attained in this study, >45 µmol H_2 h^{-1} mg Chl^{-1}. Unlike our self-assembled *in situ* platinization procedure, this group

"rebuilt" the native PSI to incorporate a recombinant form of the PsaC subunit containing a free cysteine thiol that allowed the covalent attachment of preformed Pt/Au nanoparticles. An experiment was performed to determine if this *in situ* platinized PSI complex can produce similar rates of hydrogen production as reported by Grimme *et al* [109]. The PSI complexes were platinized as described above, except that the chlorophyll and hexachloroplatinate concentrations were reduced to 5 μg ml^{-1} and 70 μM, respectively. After 10 light cycles, the PSI complexes were recovered and purified by density gradient centrifugation. To determine the peak hydrogen evolving capacity of our self-assembled platinized PSI, we ran this final experiment under as similar as possible to those conditions used in Grimme *et al.* Specifically, illumination levels of ~1200 μE $m^{-2}s^{-1}$, cyt c_6 to P_{700} molar ratio of 75, NaAsc concentration of 100 mM, and at 25°C was used for the experiment. Under these conditions, a much improved maximum rate of >5.5 μmol H_2 h^{-1} mg Chl^{-1} was obtained (Fig 3.11). The rate observed in this study is of the same magnitude as reported for the tethered, PSI nanoparticle complex. This indicates that *in situ* platinization of PSI complexes can yield high rates of H_2 production without the restrictions associated with re-engineering the PSI complex and synthesis of tethered metal nano-catalysts. Interestingly, there is also the possibility that the tethered system is using an alternative path of electron transport since hydrogen yield is stimulated < 5-fold upon the addition of cyt c_6, possibly functioning as simply a chlorophyll dye-sensitized solar driven catalyst[153]. This system using similar ratios reveals a stimulation of ~60-fold increase upon cyt c_6 addition as is shown in Fig. 3.6 and 3.7. A final advantage of the *in situ* approach is that it requires at least a 50-fold lower level of platinum salts (70 μM vs. 3.4 mM Na_2PtCl_6) than the tethered system. Our peak rates described above are also higher than the hydrogen evolution rates of ~580 nmol H_2 h^{-1} mg Chl^{-1} have been reported using a [NiFe]-hydrogenase from *Ralstonia eutropha* fused directly to PsaE of PSI from *Synechocystis* PCC 6803[154].

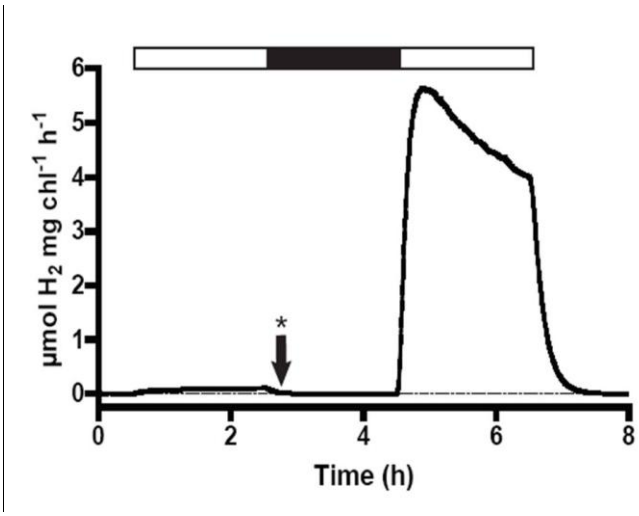


Figure 3.11 Peak rates of hydrogen evolution. Platinized PSI complex (5 µg chl ml^{-1}), 100mM NaAsc, and 4.4 µM cyt c_6 in 20mM MES buffer pH 6.4. White light from a halogen bulb light source was used at an intensity of about 1200 µE m^{-2} s^{-1}. Cyt c_6 was added into the system at time t = 2.8 h in the dark as indicated with an arrow.

3.3.7 Optimization of PSI purification for hydrogen evolution

The final purification step in PSI isolation was varied to determine its effect on hydrogen evolution activity and thermal stability of the complex. The PSI complex was purified as described in the materials and method up to the isolation of the PSI trimer from sucrose gradient density centrifugation. Three different samples were prepared in order to test hydrogen evolution activity. The first PSI sample was directly from the sucrose gradient. The second sample was harvested from the sucrose gradient and directly loaded onto a POROS 20HQ (Applied Biosystems) anion exchange column (BioCAD 202 Chromatography workstation) and eluted with a non-linear 0 to 400 mM MgSO4 gradient and buffer containing 0.02% Triton. For the third PSI sample, pooled PSI samples were dialyzed against 20 mM MES pH 6.4, 10 mM $CaCl_2$, 10 mM $MgCl_2$ and 0.03% DM for about 6 h to remove sucrose slowly, and then loaded onto a POROS 20HQ (Applied Biosystems) anion exchange column (BioCAD 202 Chromatography workstation) and eluted with a non-linear 0 to 400 mM MgSO4 gradient and buffer containing 0.03% DM. Each sample was platinized for 6 L/D cycles and subsequently re-isolated by sucrose gradient density centrifugation (Fig. 3.12 A). In the first panel in Figure 3.12A there is presence of an orange band (Na_2PtCl_6) suggesting that platinization process was much slower when

compared to the other two samples. This may have been a result of high detergent concentration during solubilization of the thylakoid membrane. Also the second sample (from sucrose gradient to HPLC) formed larger particle size after platinization and aggregates were present in the sample as shown in the third panel in Figure 3.12A. DM was determined to be a better detergent than Triton. Detergents have found widespread use in solubilization, reconstitution and crystallization of membrane proteins [155-157]. However, not all types of detergents are suitable for each membrane protein as they can inactivate the proteins [157]. This can be caused by either the nature of the detergent (ionic/bile salts/nonionic/zwitterionic) or the sensitivity of the protein to removal of specific lipids. Little is known about the specific interactions of detergents with membrane proteins and often it is not clear why one type is more suitable than another. TEM images of all three platinized samples are shown in Figure 3.12C. The TEM images for the three different samples are similar except that the sample in Triton (2^{nd} panel) seemed to form more aggregates as also observed in the sucrose gradient density centrifugation. Hydrogen evolution activity on the three PSI samples (Fig. 3.12B) at varying temperatures reveal that the PSI sample that was dialyzed before HPLC and eluted in DM show the highest activity of 0.42 µmol H_2 h^{-1} mg Chl^{-1} at 55^0C. This rate was higher than the rate from the PSI sample from sucrose gradient (0.1 µmol H_2 h^{-1} mg Chl^{-1}) and the rate from the PSI preparation from sucrose gradient directly to HPLC (0.32 µmol H_2 h^{-1} mg Chl^{-1}) but which displayed an optimum temperature of 45^0C.

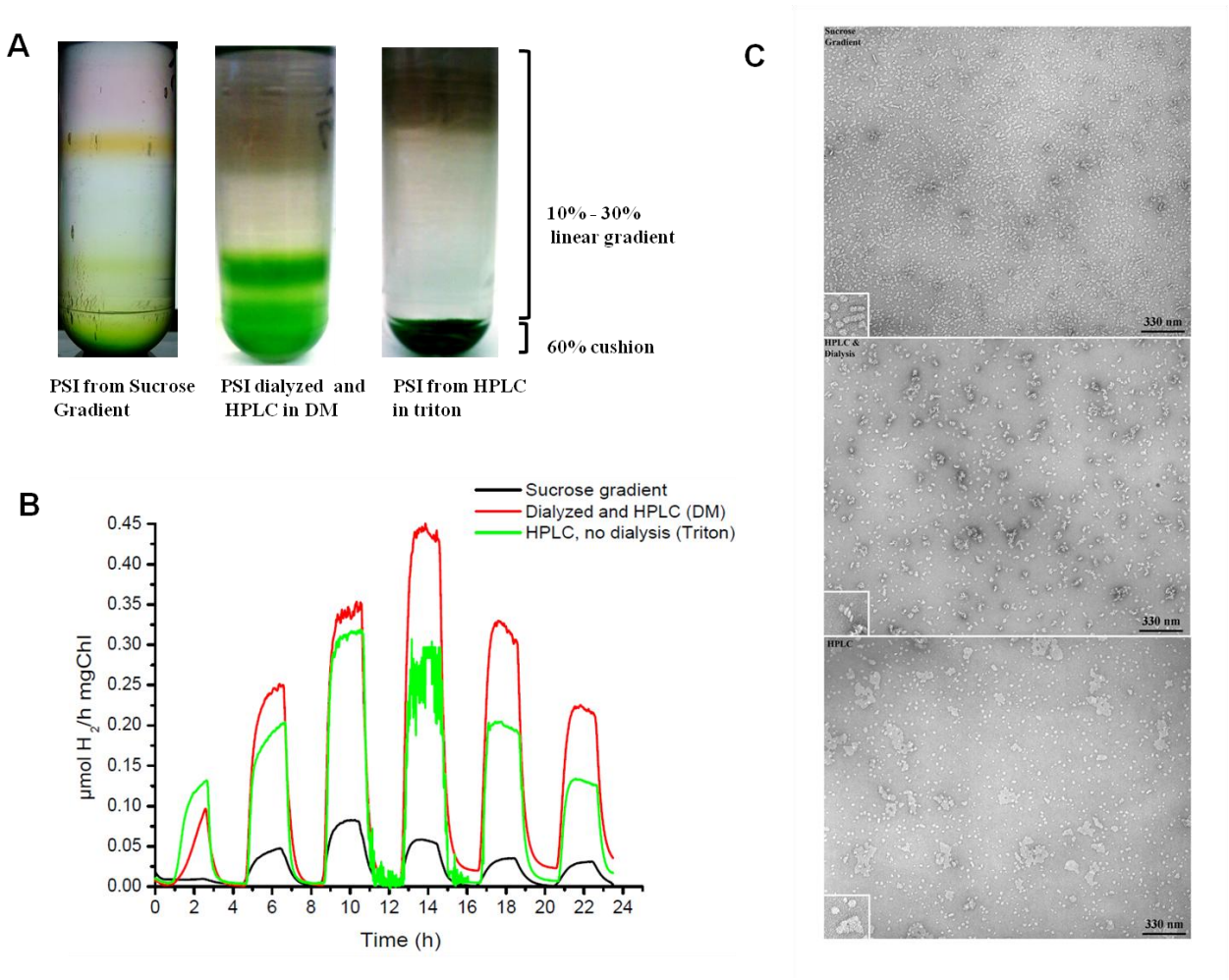


Figure 3.12 Optimization of the PSI purification steps for hydrogen evolution. **A)** Sucrose gradient of the various PSI samples. **B)** Hydrogen evolution activity of the various PSI samples. Platinized PSI complex (40 µg chl ml^{-1}), 10mM NaAsc, and 10 molar excess cyt c_6 in 20mM MES buffer pH 6.4. Red light was used at an intensity of about 400µE m^{-2} s^{-1}. **C)** TEM images of the platinized PSI samples.

To determine the effect of the detergent used in the buffer for hydrogen activity assay, the same lot of purified PSI was tested for hydrogen evolution using Triton, DM and no detergent. In Figure 3.13, addition of no detergent to the buffer resulted in the highest initial activity of 0.065 µmol H_2 h^{-1} mg Chl^{-1}. This initial rate was more than 2 times higher than rates of hydrogen produced by the sample containing 0.03 % triton (0.028 µmol H_2 h^{-1} mg Chl^{-1}) and more than 4 times higher than rates of hydrogen produced by the sample containing 0.02 % DM (0.015 µmol H_2 h^{-1} mg Chl^{-1}), although the samples formed aggregates. These experiments were carried out at 25^0C. A lower rate was also observed in Figure 3.12 for the sample containing DM at 25^0C but seems to more stable at higher temperature. The rates of all three samples decayed with time and reached the same rate after about 40 h (Appendix III).

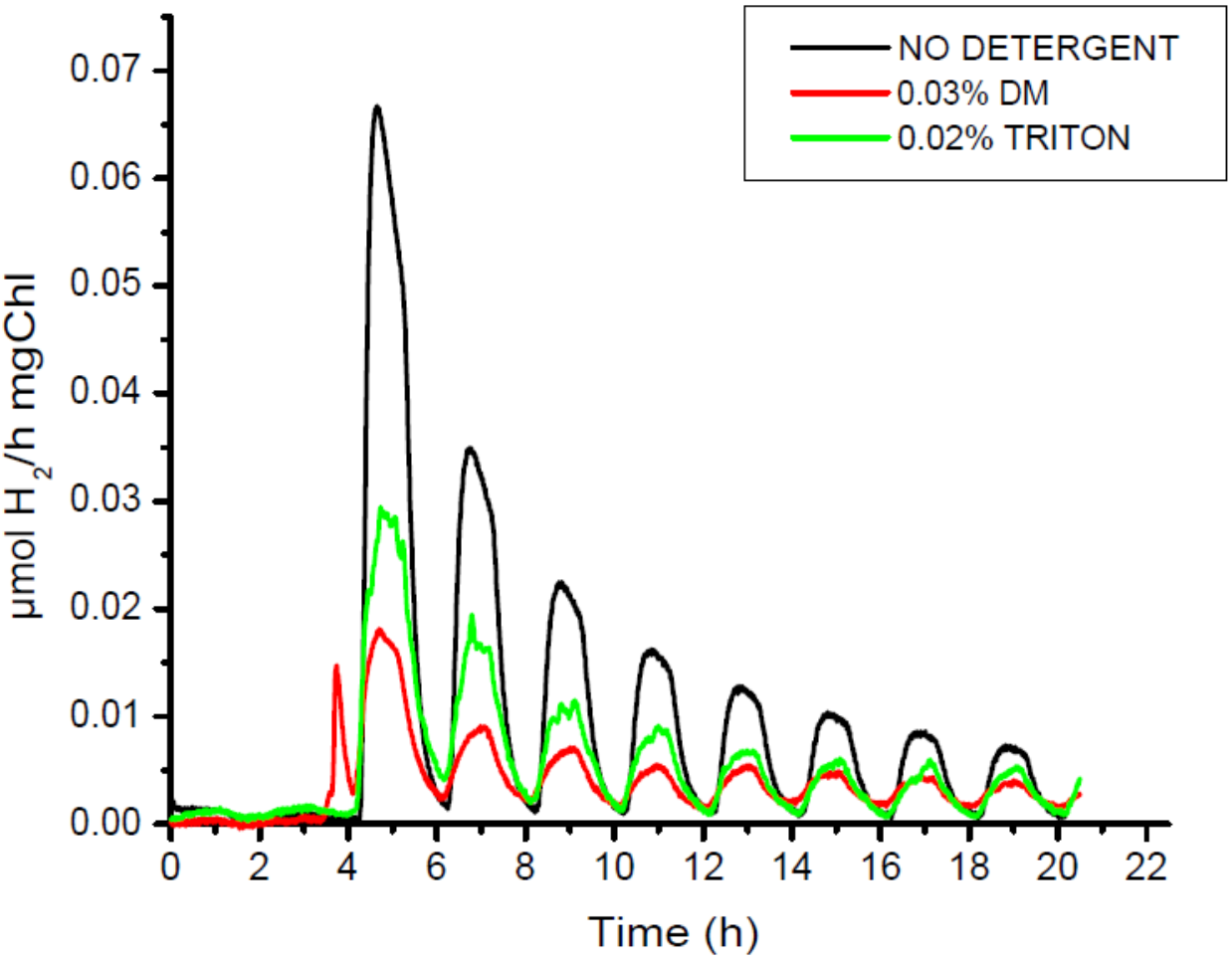


Figure 3.13 Hydrogen evolution activities of PSI samples using different detergents. Platinized PSI complex (20 µg chl ml^{-1}), 10 mM NaAsc, and 10 molar excess cyt c_6 in 20 mM MES buffer pH 6.4. DM, triton and no detergent were used in the buffer during platinization and also during hydrogen evolution activity. White light was used at an intensity of about 400 µE m^{-2} s^{-1}.

3.3.8 Spectral analysis of chlorophyll in fresh and platinized PSI.

Hydrogen evolution was carried out for 14 L/D cycles w/ platinized PSI complexes (90 µg Chl/ml, 10 mM NaAsc, 10 molar excess cyt c6 to PSI ratio, 20 mM MES, pH 6.4) at 30°C and illumination w/ 300 µE m^{-2} s^{-1}. Mock samples were treated similarly yet they were placed in a second reactor that was kept in the dark. After 56 h (equivalent to 14 L/D cycles) 1.5 ml samples were removed from both the mock treatment and the hydrogen evolving sample and centrifuged at 50,000 g. The supernatant was collected and the remaining green pellet was resuspended in 1 ml of 90% methanol, shaken using a MP Biomedical FastPrep-24 and spun at 21,000 g for 5 min. This methanol extraction was further diluted 10 fold and the spectra was collected on a Cary 50 Bio UV/Visible spectrometer using a 1 mm path length quartz cuvette. The 50,000 g supernatant was also measured yet this sample was not extracted in 90% methanol nor was it diluted as shown in Figure 3.14. This study demonstrates that some chlorophyll was lost from the hydrogen evolving PSI particles that have been platinized.

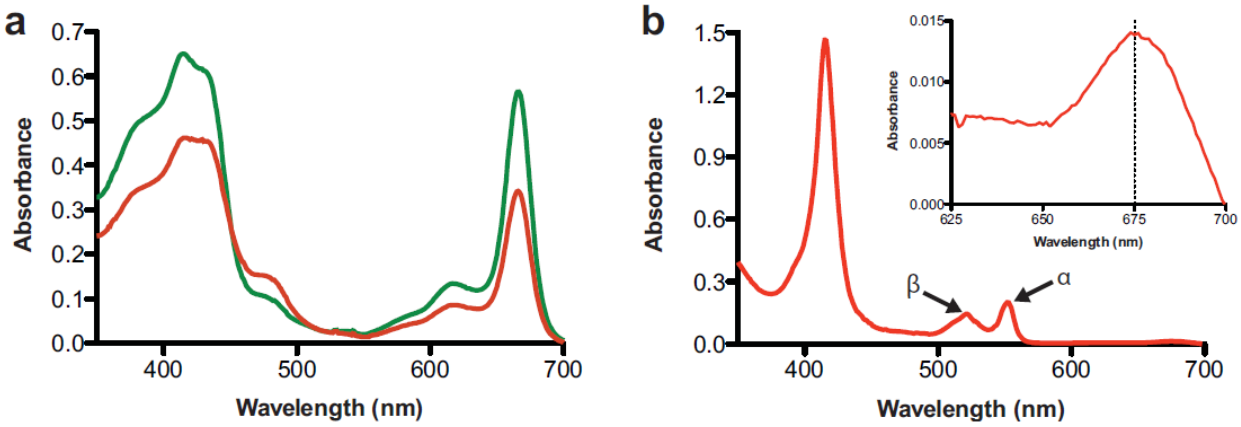


Figure 3.14 Spectral analysis of chlorophyll loss. **A)** Spectra of the mock PSI treatment (green lines) and the hydrogen evolving sample (red lines) after 56 h (14 L/D) after extraction with 90% methanol. **b)** Spectrum of the 50,000 g supernatant following 14 L/D cycles of hydrogen evolution. The inset represents an enlargement of the chlorophyll absorbance at 675 nm. The arrows indicate α- and β- peaks of the cyt c_6 that also remains in the supernatant.

3.4 Conclusion

In these experiments, the potential of a cell-free hydrogen-evolving system using only two biological components, PSI isolated from cultivated *T. elongatus* cells and a recombinant form of *T. elongatus* cyt c_6 expressed in *E. coli* and platinum metal has been demonstrated. This light driven catalytic production is both temporally and thermally stable. Simple optimization of this self-organized system leads to rates close to those recently reported by researchers working with synthetically attached catalysts. In chapter 4 the optimization of the platinization process for improved H_2 production is discussed.

Replacing the very expensive platinum with a hydrogenase enzyme will result in a more sustainable hydrogen evolution system. Platinum and other platinum group metal catalysts are sensitive to poisoning by a wide range of compounds including sulfur containing compounds [158], heterocyclic nitrogen-containing compounds [159], and other surface adsorbing molecules, this may pose a problem on the pt-PSI system. While it is possible to use aqueous *in vitro* mixtures of PSI and hydrogenase, the formation of direct fusion complexes of hydrogenase and PSI have demonstrated five times the hydrogen evolution rate of mixtures of the native proteins. Therefore, we need to replace the platinum catalyst in our current construct with an oxygen tolerant Ni-Fe hydrogenase and to form a hybrid protein by engineering a gene to express a fusion of a hydrogenase from *Ralstonia eutropha* H16 and the stromal-exposed subunit PsaE of PSI from *T. elongatus*. A PsaE/D-free mutant of PSI has to be created in parallel by genetically disrupting the expression of the PsaE/D subunit of a native PSI that will allow *in vitro* reconstitution of the desired PsaE-hydrogenase fusion protein with PsaE-free PSI. The genetic disruption of the *psaE* and *psaD* gene in *T. elongatus* and the formation of the PsaE/D – hydrogenase fusion are discussed in chapter 5.

4. OPTIMIZATION OF THE PLATINIZATION PROCESS IN PSI MEDIATED H_2 PRODUCTION USING RESPONSE SURFACE METHODOLOGY

4.1 Introduction

In situ platinization and hydrogen evolution has also been demonstrated in trimeric PSI isolated from the thermophillic cyanobacterium, *T. elongatus* [51]. As discussed earlier, this organism utilizes only c-type cytochrome (cyt c_6) as the primary electron donor to PSI. It has been demonstrated that a NaAsc- cyt c_6-PSI-Pt system based on this cytochrome is capable of evolving H_2 in a cyt c_6- and light- dependent fashion. H_2 was produced at temperatures up to 55^0C and showed both storage and temporally stable for > 85 days. A maximum hydrogen evolution rate of ~5.5 µmol/h/mg Chl was reported for this system [51] by increasing the light intensity and the PSI to cyt c_6 ratio. However, the effect of the various process variables on the rate of H_2 production has not been explored. Process variable optimization by the classical method of changing one variable while fixing the others constant is very laborious, time consuming and requires a lot of materials. Single-variable optimization methods are monotonous and can also lead to misinterpretation of results that are used to select factors that will have a significant effect in a process. A more elegant approach is the use of response surface methodology (RSM); a commonly used method to efficiently optimize a multi-variable process with minimum number of experiments. This method has been widely used to optimize phototrophic hydrogen production processes [160-163].

In this chapter, H_2 evolution using platinized PSI isolated from the thermophillic cyanobacterium, *T. elongatus* was investigated. Response surface methodology (RSM) using a central composite design was employed to determine the individual and interactive effects of the concentration of platinum salt, light intensity and temperature on the platinization process and H_2 evolution of this system.

4.2 Materials and methods

4.2.1 PSI-mediated hydrogen evolution and measurement

T. elongatus was grown and PSI isolated as described above (Section 3.2.1 and 3.2.2). Platinization reactions were carried out by incubation of cyt c_6, PSI (*T. elongatus*) and different concentration of $Na_2[PtCl_6]$ in a thermostatically controlled photo-bioreactor as described previously [51], and buffered with 20 mM MES at pH 6.4. The molar ratio of cyt c_6 to *T. elongatus* PSI was maintained at 10:1. Typical reactions contained PSI (50 µg chl ml^{-1}), 282 µmol cyt c_6, $Na_2[PtCl_6]$ (50 µM, 275 µM, and 500 µM), 20 mM MES buffer pH 6.4 and 10 mM sodium ascorbate (NaAsc), at varying temperatures (25^0C, 35^0C and 45^0C) . An external water bath was used to control the reactor temperature. The light intensity was also varied during the platinization experiment (120 µE/m^2/s^{-1}, 210 µE/m^2/s^{-1}, and 300 µE/m^2/s^{-1}). All reaction components were combined and injected into the photo-bioreactor. N_2 gas was allowed to flow through the mixture for ~ 1 h to purge air off the system. After anaerobosis was achieved, samples were illuminated as described above. The photo-bioreactor was shielded from external light and a Chrontrol Model XT microprocessor-based timer was used to cycle the USHIO 150 W halogen projector lamp (USHIO INC, Tokyo, Japan) on and off at intervals of 2 h. After 24 h of the light catalyzed platinization and hydrogen evolution (Fig. 4.1A), the platinized PSI containing was re-isolated from the reaction mixture by sucrose density gradient centrifugation and dialyzed in 20 mM MES buffer pH 6.4, to remove excess hexachloroplatinate, small analytes and cyt c_6. The re-isolated platinized PSI was put back into the reactor for the hydrogen evolution experiment without additional $Na_2[PtCl_6]$ (Fig. 4.1B). For the hydrogen evolution phase of the experiment the reaction medium composition, the light intensity, and temperature were kept constant (10 mM NaAsc, light intensity of 280 µE/m^2/s^{-1} at 35^0C). The rate of hydrogen production was measured in micromoles of hydrogen produced per hour per mg chlorophyll a (µmol H_2/h/mg chl). The total (integrated) hydrogen yield for the first 3 cycles (Fig. 4.1B) was measured for each experiment and used for statistical analysis. Raw data for all experiments are shown in Appendix IV.

For the screening experiments to determine the effect of light wavelength on the rate of H_2 production, full spectrum white light and filtered red light were used. For a light source, a

Fisher Scientific fiber-optic illuminator (Model 12-562-36) fitted with dual fiber-optic cables was fitted with an USHIO 150 W halogen projector lamp (USHIO INC, Tokyo, Japan) calibrated using the LI-1800 portable spectroradiometer (LI-COR Biosciences, Lincoln, Nebraska, USA). At each power setting on the fiber-optic illuminator, the micro-processor-controlled LI-1800 spectroradiometer was used for rapid acquisition of photometric data. Quantum integration for the calculation of light intensity was done between wavelengths of 650 and 750 nm. A high pass red filter with a 590 nm cut-off was placed at the end of the light source, in the case of the red light experiments.

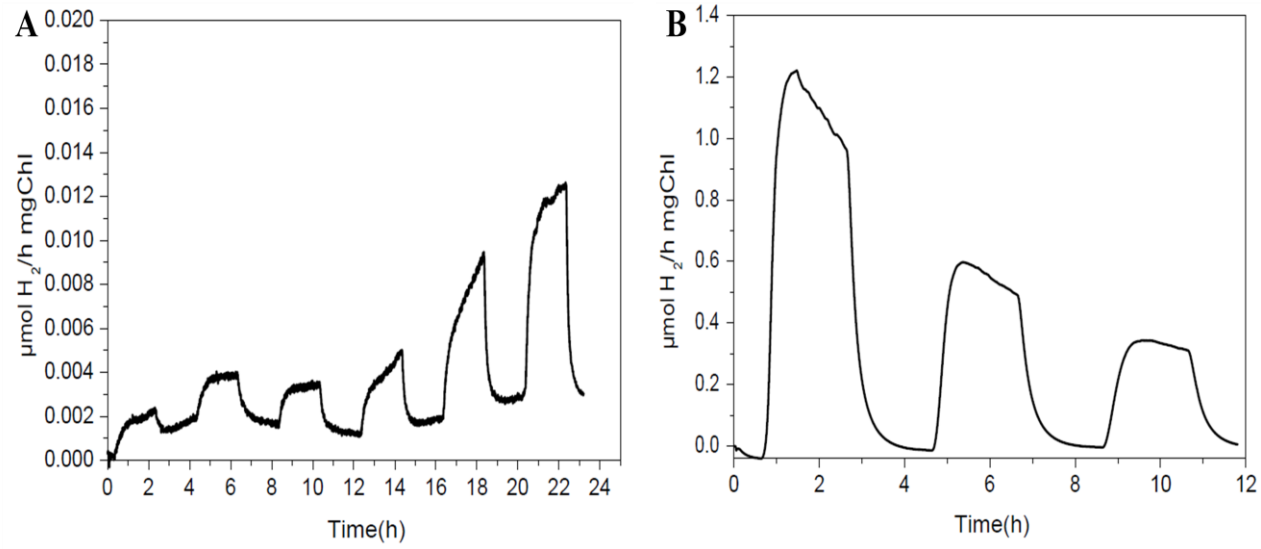


Figure 4.1 Raw data from hydrogen evolution. **A)** *In situ* platinization and hydrogen evolution. **B)** Hydrogen evolution from re-isolated Pt-PSI complexes.

4.2.2 Screening experiments

Preliminary experiments were carried out to screen the appropriate parameters affecting H_2 yield. Light intensity, platinum salt ($Na_2[PtCl_6]$) concentration and temperature were determined as important factors affecting the rate of H_2 production. A screening experiment was done to determine the effect of light color (red or white, as described above) on the H_2 yield. Previous experiments (Appendix IV) indicated that the use of white light during platinization led to a different H_2 yield when compared to red light at the same intensity. The experimental design was based on a 2^{k-1} fractional factorial design (where *k* as the number of factors) with 4 center points blocked by light color as shown in Table 4.2. The level and the code of variables considered in this study are shown in Table 4.1.

Table 4.1 Level and code for the central composite design.

Variables	Symbols	Coded Levels		
		-1	0	+1
Light Intensity ($\mu E/m^2/s^{-1}$)	X_1	120	210	300
Platinum Concentration (μM)	X_2	50	275	500
Temperature (^0C)	X_3	25	35	45

Table 4.2 Fractional factorial design with two center points for white and red light.

Run	Light color	Light Intensity (µE /m/s)	Platinum conc.(µM)	Temp. (^oC)	Total yield (µmol H_2/h/mg chl)	ln(Total yield) (µmol H_2/h/mg chl)
1	White	120	50	45	0.0565	-2.8728
2	White	120	500	25	2.7849	1.0242
3	White	300	500	45	0.0979	-2.3236
4	White	300	50	25	0.0886	-2.4237
5	White	210	275	35	2.5578	0.9391
6	White	210	275	35	2.1938	0.7856
7	Red	120	50	45	0.0776	-2.5562
8	Red	120	500	25	3.3550	1.2104
9	Red	300	500	45	2.0106	0.6984
10	Red	300	50	25	4.0594	-5.4397
11	Red	210	275	35	1.5552	0.4416
12	Red	210	275	35	1.0053	0.0053

4.2.3 Experimental design and data analysis

Based on the screening experiments, the mean total yield of white light was less than the red light so red light was used for the subsequent experiments. Platinum salt ($Na_2[PtCl_6]$) concentration and temperature were selected as independent variables for evaluation in this study. RSM was applied to evaluate the effects of these variables on the rate of H_2 production. The experimental design was based on a three-factor face-centered central composite design (CCD). Face centered central composite design, a cubic design, contains axial points that are situated at a distance α from the center of the design. α takes a value of ±1 in the design [164]. The total number of experimental points (N) in a central composite design [165] can be calculated by the equation

$$N = 2^k \text{ (factorial points)} + 2k \text{ (axial points)} + n_0 \text{ (center points)} \quad (4.1)$$

In equation 4.1, N is the number of experimental points, k is the number of independent factors, and n_0 is the number of center points. Thus for this design the total number of experimental points was 16 (k = 3, n_0 =2). The original experimental design had 16 experimental points; however, 1 additional point was replicated to argument error estimates (Table 4.3). Experiments at the center point were conducted for evaluation of experimental error. The level and the code of variables considered in this study are shown in Table 4.1.

Cumulative H_2 yield was predicted from RSM. JMP 8 software was used in the experimental design, data analysis, model buildings, and three-dimensional response surface plot. The model was built based on the variables with confidence levels of 95%. Analysis of variance (ANOVA) was performed to evaluate the adequacy of the generated mathematical model.

4.3 Results and discussion

4.3.1 Screening experiments

A screening experiment was done to determine the effect of light color (red or white) on the rate of photo-dependent H_2 production. Spectral irradiance of red light (red) and white light (black) used for the experiment, overlaid with the absorbance PSI in this region are shown in Figure 4.2. The light intensities used were calculated from the integration of the region between 650 and 750 nm for both white and red light. The absorption of PSI in this region as shown in the PSI spectrum is as a result of the chlorophyll. As can be seen in the figure 4.2 this region contains the photosynthetically active wavelengths for PSI excitation. The spectral irradiance for the red light was in the range of 600 – 850 nm and the spectral irradiance for the white light was in the range of 400 – 800 nm. The experimental design was based on a fractional factorial design with 4 center points blocked by light color as shown in Table 4.2. Light intensity, platinum salt concentration and temperature were variables used in this experiment. The highest yield for both the red and white light were at 25^0C temperature, light intensity at 120 µE /m^2/s and platinum salt concentration at 500 µM. The blocking effect of light color was not significant however, the mean total yield for white light (1.2965 µmol H_2/mg chl) was less than red light (2.0105 µmol H_2/mg chl) as shown in the figure 4.3, and therefore red light was preferred. The prediction profiler was used as a "manual optimizer" to locate a good starting point for a more formal optimization algorithm. Subsequent experiments were done using red light.

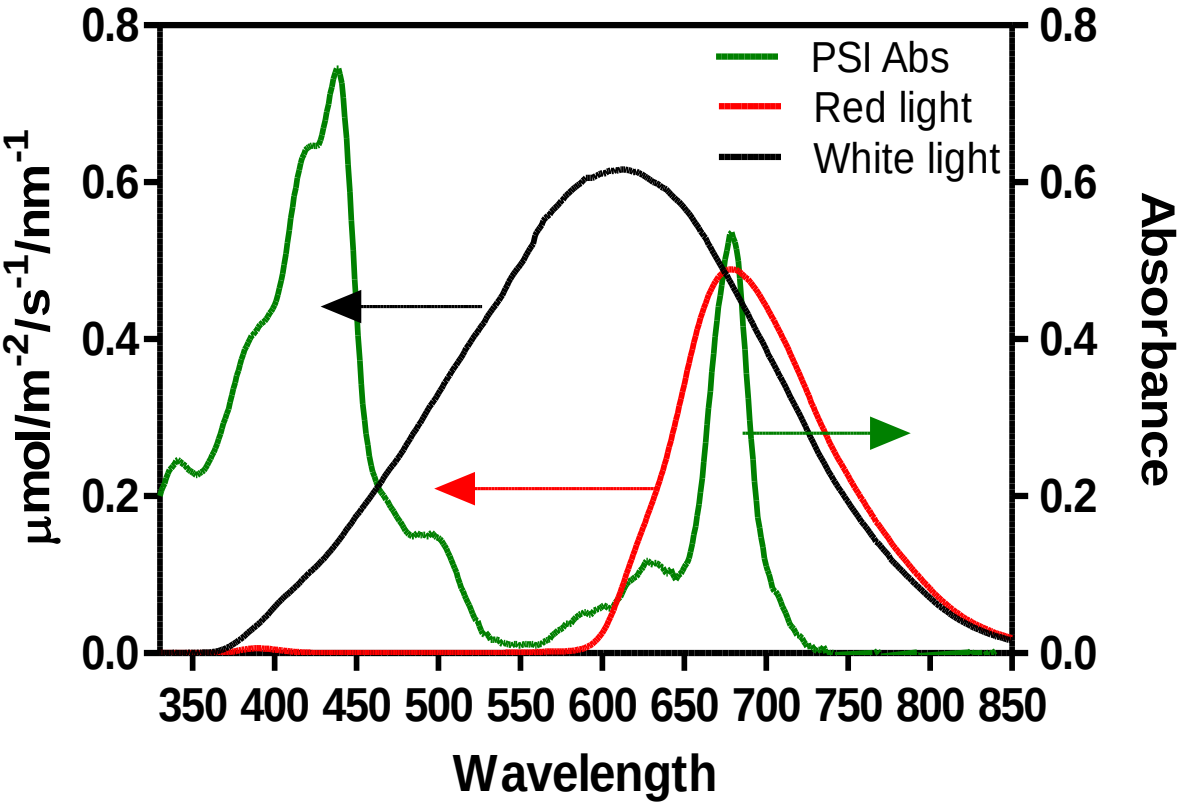


Figure 4.2 Spectral irradiance of red light (red) and white light (black) showing region of PSI absorbance. The light intensities used were calculated from the integration of the region between 650 and 750 nm.

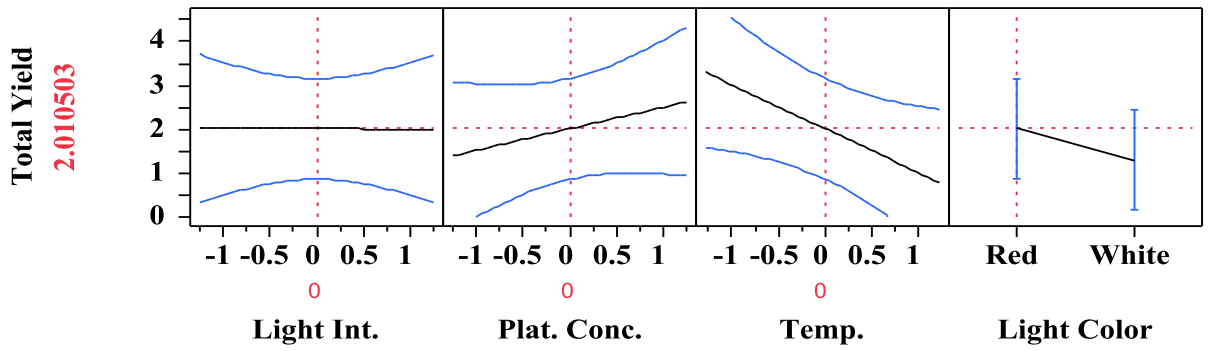


Figure 4.3 Prediction profiler showing effect of white and red light on H_2 yield.

4.3.2 Model Fitting

To minimize the experimental runs and time for optimizing variables involved in the photo-production of H_2, an experimental design was adopted on the basis of response surface methodology. This was necessary because preparation of the materials and hydrogen evolution experiments were very laborious and time consuming. The levels of the independent variables were not changed after the screening experiments. The actual and predicted yields from all seventeen experimental runs are listed in Table 4.3. Data transformations were needed for the response of H_2 yield to meet the assumption of normality of the residuals that made the ANOVA valid because raw H_2 yield data could not be fitted very well [164, 166, 167]. Preliminary analysis of the data was carried out by checking for outliers and plotting H_2 yield against each independent variable (data not shown). There was no presence of outliers in the data but the plot for H_2 yield against platinum salt concentration (Fig. 4.4A) indicates that platinum concentration was the most active variable and the yield varied unequally as the platinum salt concentration increased. Therefore, natural logarithm of yield transformation (Fig. 4.4B) was necessary to address skewness and increasing unequal variability of the yield [168].

Table 4.3 Experimental design for the three variables and experimental and predicted results under different conditions.

Light Intensity (X1)	Platinum Conc. (X2)	Temp. (X3)	Total Yield	ln(Total Yield)	Predicted ln(Total Yield)	Predicted Total Yield
-1	-1	-1	0.0100	-4.6022	-4.8004	0.0082
-1	-1	1	0.0776	-2.5562	-2.5854	0.0754
-1	0	0	0.6687	-0.4024	0.1108	1.1171
-1	1	-1	3.3550	1.2104	1.1149	3.0492
-1	1	1	1.9924	0.6894	0.4991	1.6473
0	-1	0	0.0517	-2.9627	-3.0405	0.0478
0	0	-1	0.3698	-0.9948	-0.9389	0.3907
0	0	0	1.5552	0.4416	0.2622	1.2998
0	0	0	1.0053	0.0053	0.2622	1.2998
0	0	1	1.2021	0.1841	0.0904	1.0946
0	1	0	6.0040	1.7924	1.8315	6.2430
1	-1	-1	0.0043	-5.4397	-5.5987	0.0037
1	-1	-1	0.0026	-5.9576	-5.5986	0.0037
1	-1	1	0.0484	-3.0276	-2.9224	0.0538
1	0	0	1.5955	0.4672	-0.0848	0.9187
1	1	-1	2.7784	1.0219	1.0608	2.8886
1	1	1	2.0106	0.6984	0.9063	2.4752

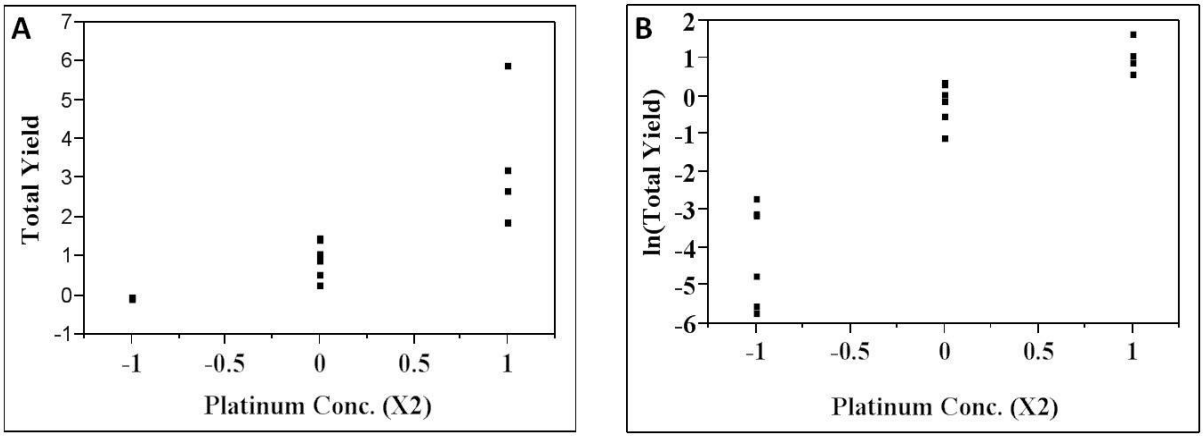


Figure 4.4 Bivariate fit of H_2 yield by platinum salt concentration. **A)** Raw data **B)** Transformed data.

The experiments were run in a random order to minimize the effect of uncontrolled variables. In Figure 4.5, the plot of the residuals versus observation order of experiments indicated that the order in which the experiments were run had no influence on the data obtained which also implied that the model was adequate. The mathematical model representing the transformed total H_2 yield as a function of the independent variables; light intensity (X_1), platinum salt concentration (X_2) and temperature (X_3) within the region under investigation was expressed by the following equation:

$$\text{Ln (Total } H_2 \text{ Yield)} = 0.2689 - 0.1173X_1 + 2.4555X_2 + 0.5346X_3 - 0.2593X_1^2 - 0.8768X_2^2 - 0.6971X_3^2 - 0.7321X_2X_3 \quad (4.2)$$

In general, exploration and optimization of a fitted response surface may produce poor or misleading results unless the model exhibits a good fit, so it was essential to check the model adequacy. The ANOVA data was used to evaluate the significance of the constructed quadratic models and model terms after eliminating the insignificant ones without damaging model hierarchy. The significance of each coefficient was determined by the t – values and p – values which are listed in Table 4.5. The larger the magnitude of t-test value and the smaller the p- values the more significant the corresponding parameter [160]. It can be seen that the linear effect, quadratic effect and interaction effect of light intensity had p- values that were more than

0.05 as shown in the parameter estimates table 4.4, indicating that light intensity had no significant effect on the model. Therefore, all two-factor light intensity interaction terms were dropped from the model (light intensity-platinum conc. and light intensity-temperature) as shown in equation 4.2. The analysis also revealed that the platinum salt concentration and temperature had a strong linear effect on the response. The interaction between platinum salt concentration and temperature also had a significant effect on the response. The ANOVA (analysis of variance) in Table 4.6 showed the adequacy of the fitted quadratic model with p-value of < 0.0001 which was much less than 0.05. The p-value for lack of fit was 0.4861 (> 0.05) further indicating that there was no significant lack of fit in the fitted model. The model coefficient of multiple determination, R^2 was found to be 0.99, this indicates that 99% of variation observed in the natural logarithm of the H_2 yield could be attributed to terms (light intensity, platinum salt concentration, temperature, and platinum-temperature interaction) in the model while 1% is due to random error. The adjusted -R^2 in the model was 0.97. In this study, R^2 and adjusted -R^2 were close to each other, which indicated that all used terms in the model were necessary for constructing the correct model. A simple graphical method was also used to assist in analyzing the data from the experiment. In Figure 4.6, the actual-by-predicted plot shows that the underlying error distribution is normal as the data plots resemble a straight line within a confidence interval of 95%.

Table 4.4 Parameters estimates for the full quadratic model and their relative significance in total H_2 yield.

Term	Estimate	Std Error	t Ratio	Prob>|t|
Intercept	0.2622174	0.176969	1.48	0.1820
X_1 (120,300)	-0.097778	0.115038	-0.85	0.4235
X_2 (50,500)	2.4359819	0.115038	21.18	<.0001*
X_3 (25,45)	0.5151298	0.115038	4.48	0.0029*
X_1* X_2	0.1860438	0.127664	1.46	0.1884
X_1* X_3	0.1153239	0.127664	0.90	0.3964
X_2* X_3	-0.707683	0.127664	-5.54	0.0009*
X_1* X_1	-0.249225	0.230104	-1.08	0.3147
X_2* X_2	-0.866736	0.230104	-3.77	0.0070*
X_3* X_3	-0.68697	0.230104	-2.99	0.0204*

Table 4.5 ANOVA for response surface reduced quadratic model.

Source	DF	Sum of Squares	Mean Square	F Ratio	Prob > F
Model	9	95.8309	10.6479	75.9799	<.0001*
Residual Error	7	0.98098	0.1401		
Lack of Fit	5	0.7517	0.1503	1.3112	0.4861
Pure Error	2	0.2293	0.1147		
Total	16	98.8119			

R-Square = 0.9899, R-Square Adj. 0.9768

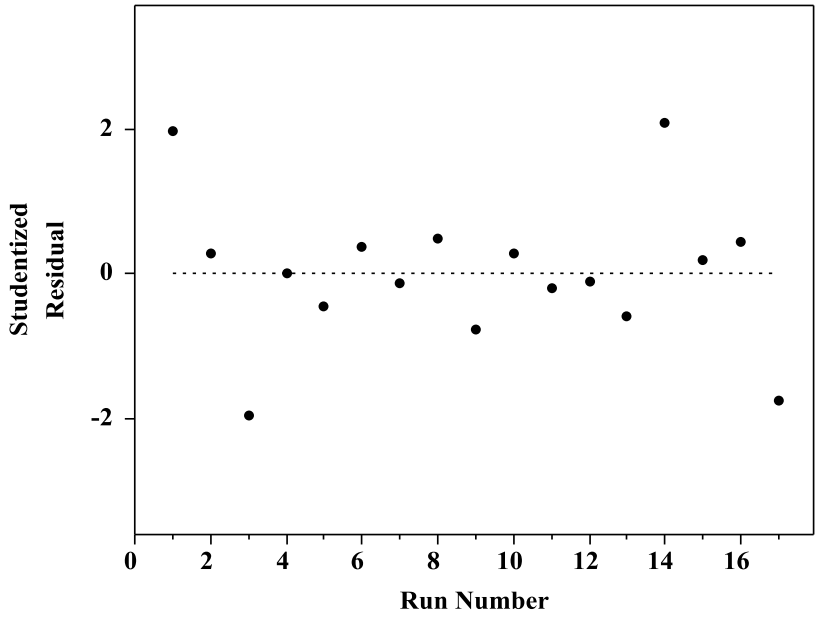


Figure 4.5 Studentized residual plots for total H_2 yield.

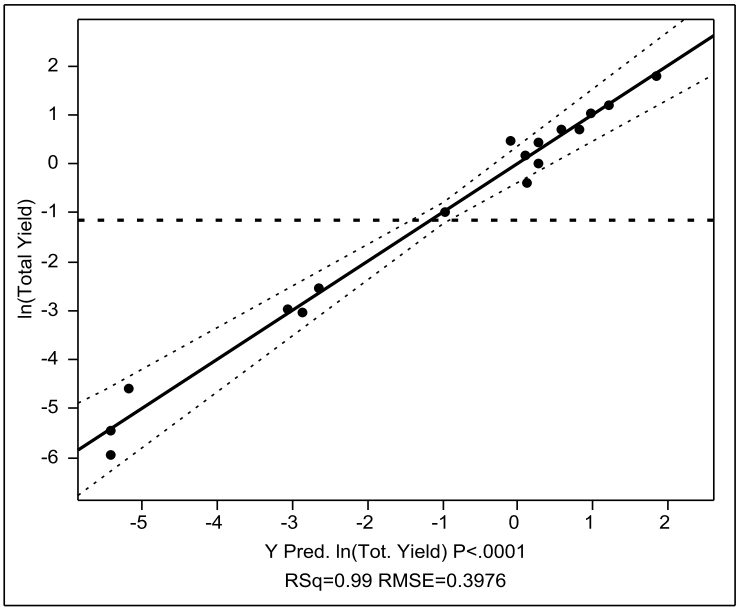


Figure 4.6 Plot of actual yield verses predicted yield.

4.3.3 Analysis of response surfaces

In order to illustrate the effect of the independent variables on the total H_2 yield, surface responses of the model were constructed by varying two variables within the experimental range and holding the third value at the central point. Figure 4.7A shows the effect of light intensity and platinum salt concentration on the total H_2 yield at a fixed temperature. At low light intensity, increasing platinum salt concentration increased the total H_2 yield. Similarly, at high light intensity, increasing platinum salt concentration increased the total H_2 yield. Platinum salt concentration had a significant effect on the model as shown in Table 4.5. At low platinum salt concentration, increasing the light intensity had minimal effect on the total H_2 yield; this was likely because platinum salt was the limiting reagent in the formation of the Pt nanoparticles that drives the photoproduction of H_2 and increasing the light intensity did not have a significant effect. A slight increase in total H_2 yield up to light intensity of about 230 $\mu E /m^2 /s$ was observed at high platinum concentration. In general the independent variable, light intensity, did not have a significant effect on the model as indicated by the p-value shown in Table 4.5.

Figure 4.7B depicts the effect of light intensity and temperature on the total H_2 yield. At both low and high temperatures, increasing the light intensity had minimal effect on the total H_2 yield. Similarly, at high and low light intensities, changing the temperature did no significantly affect the total H_2 yield. This result suggests that the interactive effect of light intensity and temperature on the total H_2 yield was not significant.

As shown in Figure 4.7C, at low platinum salt concentration, the total H_2 yield increased with increasing temperature. At high platinum salt concentration, increasing the temperature had a negative effect on the total H_2 yield. PSI was isolated from a thermophillic organism and increasing the temperature increases the rate of electron transfer [51] and hence the formation of the Pt nanoparticle but at high platinum concentration, increasing temperature probably results in the formation of large platinum clusters that tend to become very unstable for H_2 production thus reducing the H_2 yield. At both low and high temperatures increasing the platinum salt concentration increases the H_2 yield. Figure 4.7C shows that the two variables were interdependent. In other words, there was significant interactive effect between temperature and platinum salt concentration on the H_2 yield.

Considering all effects of different variables, the platinum salt concentration and temperature had significant effect on the total H_2 yield. Light intensity did not have significant effect on the total H_2 yield. Other factors such as PSI concentration, PSI/cyt c_6 ratio, time and pH can affect the total H_2 yield, but these factors were not considered in the present study. Therefore, further investigation is still necessary to evaluate the effect of these variables on the total H_2 yield.

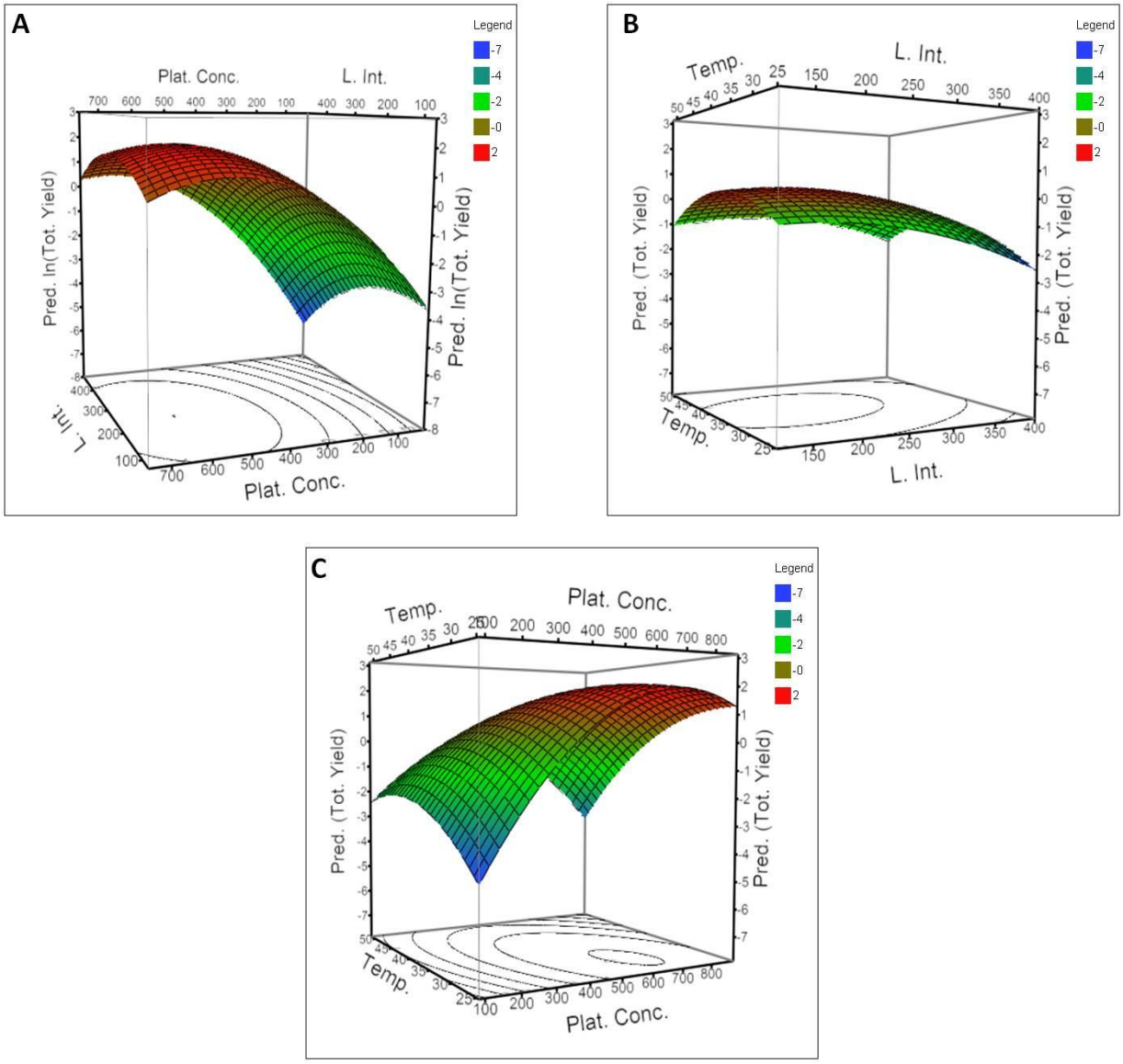


Figure 4.7 Response surface and contour plots on the combined effects of independent variables on the total H_2 yield. **A)** Light intensity and platinum salt concentration; **B)** light intensity and temperature **C)** platinum salt concentration and temperature. The scales on the y-axes are the natural log of the predicted yield.

4.3.4 Optimization and validation of model

Using the fitted model to optimize factor setting shows that the optimum setting is outside the range of the data, but visual observation of the surface and contour plots in Figure 4.7 show that yield should be maximized at about light intensity of 240 μE/m^2/s, platinum salt concentration of 636 μM and temperature of 31^{0}C. The predicted optimum was ~ 8.17μmol H_2/mg chl. The canonical form of the fitted model indicates that the surface is steepest along the platinum axis as also shown in the prediction profiler (Fig. 4.8). H_2 evolution experiment was carried out at light intensity of 240 μE/m^2/s, platinum salt concentration of 636 μM and temperature of 31^{0}C to validate the model (Figure 4.9). The H_2 yield for the validation experiment was 8.02 μmol H_2/mg chl.

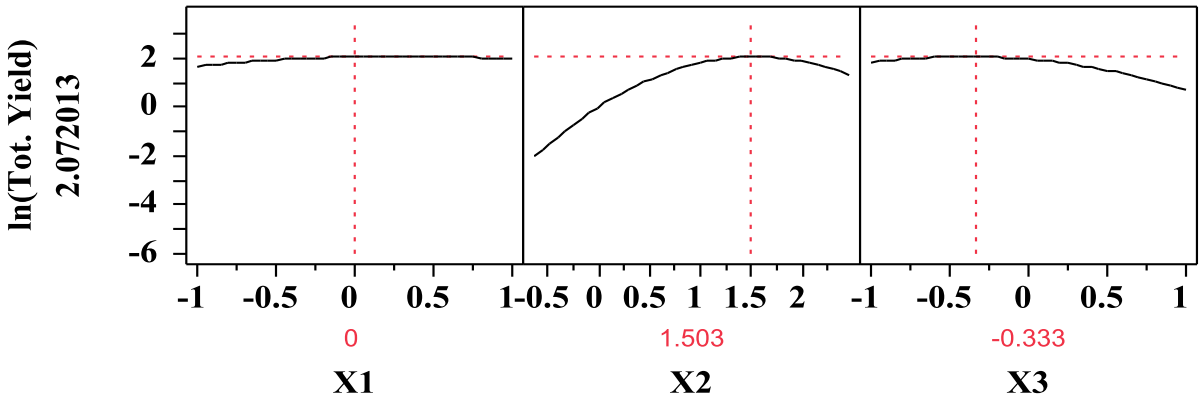


Figure 4.8 Prediction profiler for the different variables. Light intensity (X_1), platinum salt concentration (X_2) and temperature (X_3).

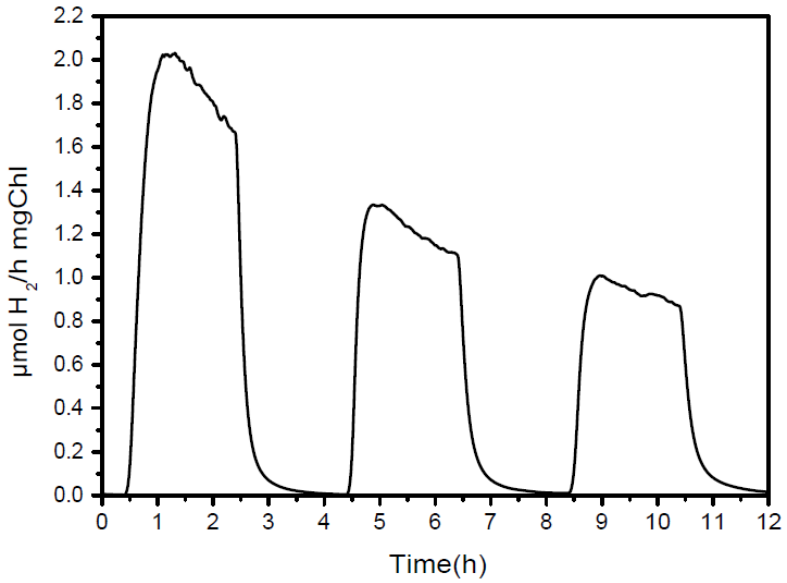


Figure 4.9 Hydrogen evolution at optimum condition. (Light intensity of 240 µE/m^2/s, platinum salt concentration of 636 µM and temperature of 31^0C).

4.4 Summary

This is the first study investigating the possible effects of light intensity, platinum salt concentrations and temperature on the platinization process for photo-dependent H_2 production. Screening experiments using fractional factorial design were used to determine the effect of light spectrum (white vs. red) on the rate of H_2 production. The mean total yield of red light was relatively larger than the mean total yield for white light. The result shows that the second-order polynomial model could be used to optimize H_2 yield in Pt-PSI hydrogen evolving system. Platinum salt concentration, temperature and the interaction between platinum salt concentration and temperature showed significant effects on the total H_2 yield. Light intensity had minimal effect of the total H_2 yield within the region studied. The optimum parameters for H_2 photoproduction were at light intensity of 240 µE/m^2/s, platinum salt concentration of 636µM and temperature of 31^0C. Response surface methodology (RSM) is an effective technique for analyzing and optimizing the pt-PSI photo-dependent H_2 production. This method of optimization was efficient with respect to both time and material resources.

5. ENGINEERING FUSION BETWEEN HYDROGENASE AND PSAE/D PROTIENS IN *R. EUTROPHA* AND THE GENETIC DISRUPTION OF THE *psaE* AND *psaD* GENE IN *T. ELONGATUS*

5.1 Introduction

The rate of photobiological H_2 production in algae is limited by two factors;(1) the [Fe-Fe] hydrogenases are highly sensitive to O_2 and thus does not tolerate the exposure to O_2 released during photolysis of water [169] and (2) the photon efficiency is relatively low because of the Ferrodoxin-mediated electron transfer from PSI to hydrogenase has to compete with the electron transfer channel to the Calvin-Benson- Bassham (CBB) cycle [169]. An ideal approach has been reported by Ihara and co-workers [77] to circumvent these problems by coupling an O_2-tolerant [Ni-Fe] hydrogenase with PSI in phototrophic organisms. Direct coupling of hydrogenase to PSI is an attractive new option to enhance light-driven H_2 production. The availability of molecular genetics, genomic information and synthetic biology offers new possibilities to creating microorganism possessing enhanced synthetic functions.

PSI is one of the two photochemically active complexes that take part in the photosynthetic electron transfer across the thylakoid membranes of cyanobacteria. The three stromal subunits of the PSI complex, PsaC, PsaD and PsaE, participate in the docking of ferredoxin/flavodoxin on the stromal side of the membrane [118, 123] as shown in Figure 5.1. A basic patch formed by PsaD, PsaE and PsaA may be involved in the docking of the negatively charged ferredoxin via electrostatic interactions. This docking site was first suggested based on the low resolution 6Å structure of PSI [170]. PsaC contains the two final electron carriers of PSI (the Fe-S clusters, F_A and F_B) from where the electrons are transferred to ferredoxin/flavodoxin and is shielded by PsaE and PsaD [118, 171]. The large number of interactions between PsaD and the adjacent subunits of PSI suggests a stabilizing role of PsaD on the stromal ridge and explains why it is needed for correct orientation of PsaC subunit [117]. Interactions between PsaE and the C-terminal region of PsaF has been shown with mutagenesis and cross-linking studies [172]. The interactions of PsaE with PsaC and PsaD are relatively weak and the geometry of the stromal structure formed by PsaC and PsaD does not dramatically change in the absence of PsaE [117]. PsaD and PsaE subunits have been shown to assemble into isolated

thylakoid, specifically into the PSI complex without the need for any cytosolic factors or the presence of nucleoside triphosphates (NTPs) [173, 174]. The mechanism of the assembly of PsaE and PsaD into the thylakoids and/or isolated PSI complexes have been reported [175, 176]. These studies show that electrostatic interactions facilitate the stable assembly of PsaE and PsaD within PSI and that a newly introduced PsaE or PsaD assembles into the PSI complex via an exchange mechanism [175, 176]. The fusion of a hydrogenase protein and PsaE has also been shown to associate with PsaE-free PSI spontaneously and to accept electron from PsaE-free PSI [77]. The terminal-bound Fe-S clusters F_A and F_B of PSI have redox potentials between -440 and -480 mV [177], which is in the range of the H^+/H_2 couple (-420 mV). Thus, although hydrogenase and PSI are not physiological redox partners, an electron transfer between both components is thermodynamically feasible. Electron transfer between PSI and free hydrogenase *in vitro* has been reported [114]. A stable deletion mutation for the *psaE* gene from the cyanobacterium *Synechocystis sp. PCC 6083* has been generated by transforming the organism with cloned DNA in which the *psaE* gene for 8-kDa subunit was replaced by a gene conferring resistance to kanamycin [178]. This transformation method has also been used to generate a PsaD- free mutant of *Synechocystis sp. PCC 6083* [179]. In this chapter, I describe the genetic engineering of an oxygen tolerant membrane-bound Ni-Fe hydrogenase from *R. eutropha* to express a fusion of a hydrogenase from *R. eutropha* and the stromal-exposed subunit PsaE/D of PSI from *T. elongatus*. A PsaD- and PsaE-free mutant of PSI was simultaneously generated by genetically disrupting the expression of the PsaE and PsaD subunit of a native PSI; this will allow *in vitro* reconstitution of the desired PsaD and PsaE-hydrogenase fusion protein with PsaE/D-free PSI (Figure 5.2).

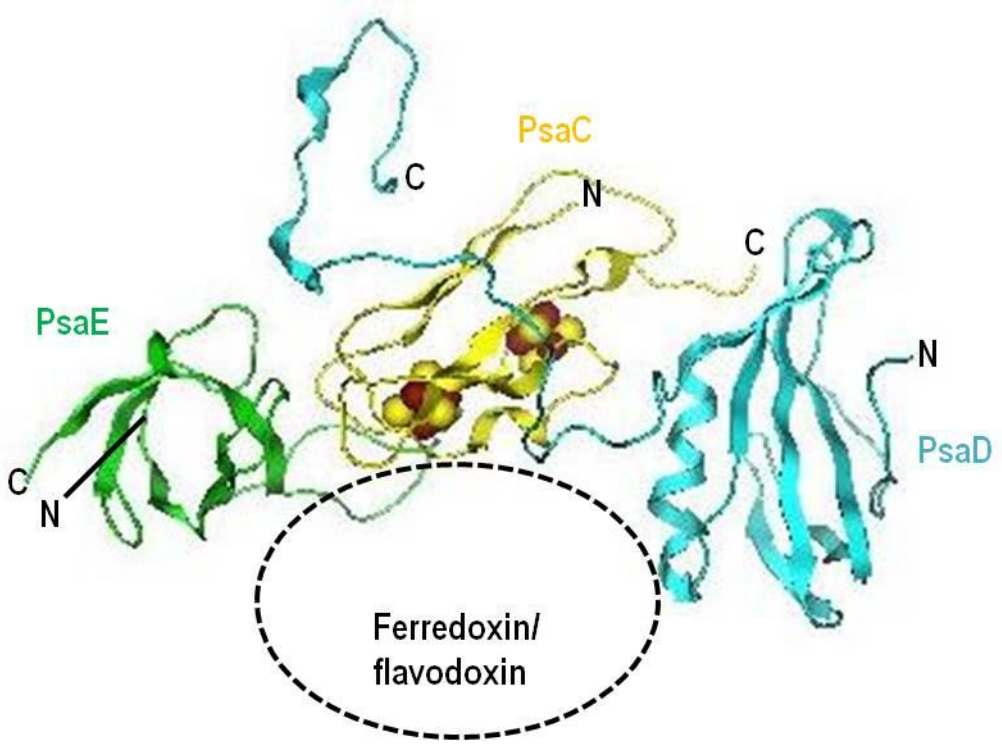


Figure 5.1 Structure of PsaC (pink), PsaD (blue) and PsaE (turquoise) subunits of PSI showing the putative docking site of ferredoxin/flavodoxin. Structural model of PSI trimer at 2.5 Å with view along the membrane normal from the stromal side (adapted from Jordan *et al*, 2001 [118]).

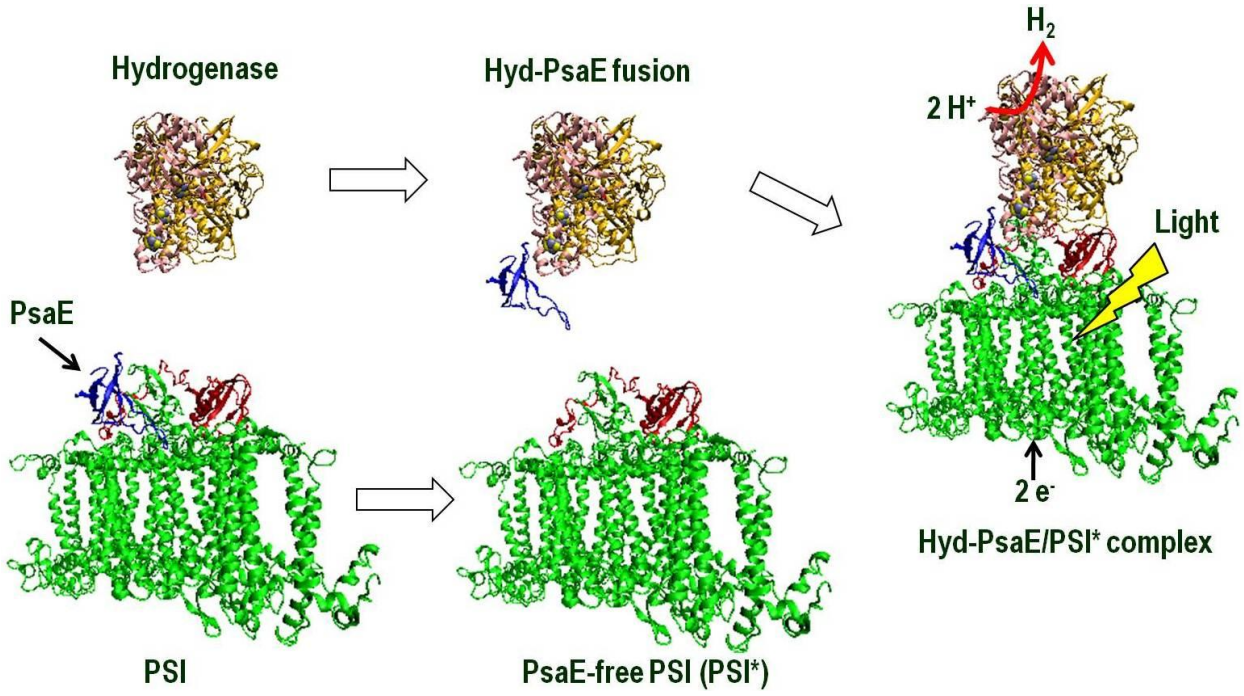


Figure 5.2 Overview of the formation of a hybrid H_2 evolving complex using MBH from *R. eutropha* and PSI from *T. elongatus* (adapted from Ihara et al [77]).

A structural model of how a hydrogenase may be engineered to interact with *T.elongatus* PSI is shown in Figure 5.3. In this hypothetical structure, PsaD and PsaE are used to form fusion complexes with the hydrogenase. Crosslinking experiments have shown that the PsaD and PsaE polypeptides are the docking polypeptides for ferredoxin and PsaE polypeptide is in close proximity to the PsaD polypeptide in the stromal side of the thylakoid membrane [180]. They are also involved in strengthening the binding of PsaC to PSI [175].



Figure 5.3 This illustrates how a psaE-Hyd fusion protein may be able to assemble with PSI either *in vitro* or *in vivo.* Cyt c_6 (bottom, pink) docking to PSI (green) and PsaE (top, blue) crosslinked with [Ni-Fe] hydrogenase (purple). All of the cofactors are shown in space filling mode, and in each case the edge-to-edge distances are < 20 Ang. suggesting rapid electron transport (created by Micheal Vaughn, Bruce Laboratory UTK).

Engineered crosslinking of PSI and the MBH of *R. eutropha* was performed *in vitro* using the original protocol of Ihara *et al* [77]. In this study the fusion of the MBH (*hoxKGZ)* to PSI from *T. elongatus* was done in two different ways (Figure 5.4) using three different linker lengths which are to determine the complex that results in the production of the highest hydrogen.

I. Fusion of the MBH from *R. eutropha* and PsaE subunit of PSI from *T.elongatus.*
II. Fusion of the MBH from *R. eutropha* and PsaD subunit of PSI from *T.elongatus.*

Six histidine were also introduced on the C- terminal end of the fusion protein for protein purification and for western blot analysis with antibodies against histidine.

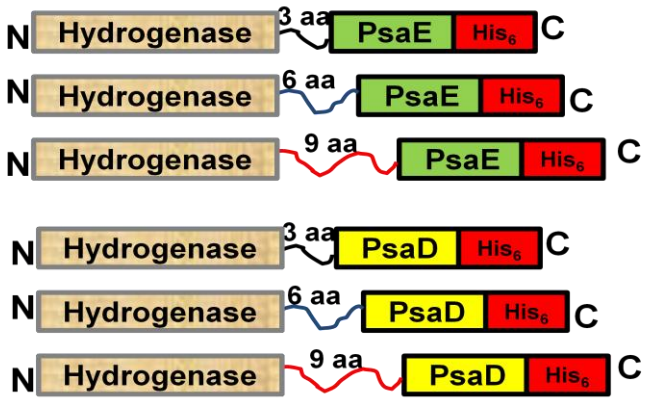


Figure 5.4 Schematics of fusions between *T. elongatus* PsaE and PsaD and MBH from *R. eutropha.*

5.2 Materials and Method

5.2.1 Molecular biology technique

DNA manipulation, cloning and PCR was performed using the general procedures described previously [181] or the manufacturers' instructions. The nucleotide sequences of all plasmid constructs and PCR product subclones were confirmed by sequencing.

5.2.2 Bacterial strains and plasmids

Bacterial strains and plasmids are listed in Table 5.1. *Ralstonia eutropha H16* (ATCC 17699, DSM 428) is the wild-type strain harboring the endogenous megaplasmid pHG1. *Ralstonia eutropha HF387* is a derivative of *Ralstonia eutropha H16* that lacks the bidirectional soluble hydrogenase because of an in-frame deletion in the structural gene, HoxH [182]. *Ralstonia eutropha HF387* is a kind gift from Oliver Lenz (Institut fur Biologie, Humboldt-Universitat zu Berlin, Berlin, Germany). *T. elongatus* BP-1 was also used for this study.

E. coli GC5 (Sigma-Aldrich) and NovaBlue (Novagen) were used as host in standard cloning procedures and for the production of double stranded plasmids for sequencing. *E coli S17-1*, the mobilizing strain, is a special *E. coli* donor strain that carries the transfer genes of the broad host range IncP-type plasmid RP4 integrated in its chromosome [183]. *E. coli S17-1* served as a donor in conjugative gene transfer.

Table 5.1 Bacterial strains and plasmid.

Strains and Plasmids	**Relevant characteristic(s)**	**Source or reference**
T. elongatus		
BP-1	Wild type	[184]
ΔPsaE	*psaE* deletion in *T. elongatus*	This work
ΔPsaD	*psaD* deletion in *T. elogatus*	This work
R. eutropha		
H16	Wild type	ATCC 17699
HF387	Inframe deletion of the structural gene *hoxH* resulting in the deletion of the soluble hydrogenase.	[185]
HF387H	Derivative of HF 387, MBH - His_6	This work
HFEL1	Derivative of HF 387, HoxK - PsaEL1- His_6	This work
HFEL2	Derivative of HF 387, HoxK – PsaEL2- His_6	This work
HFEL3	Derivative of HF 387, HoxK – PsaEL3- His_6	This work
HFDL1	Derivative of HF 387, HoxK - PsaDL1- His_6	This work
HFCON	Derivative of HF 387, HoxK – His_6 with deletion of *hoxZ* anchor region	This work
E. coli		
GC5	*F^- F80lacZDM15 D(lacZYA-argF)U169 endA1relA1 gyrA96 hsdR17 (rk^-, mk^+) phoA supE44 thi-1 λ^- T1R*	Sigma-Aldrich
S17-1	*Tra^+ recA pro thi hsdR, chr.:RP4-2*	[183]
Novablue	*Amp^R recA- , endA- , lacI*	Novagen

Table 5.1 continued

Strains and Plasmids	Relevant characteristic(s)	Source or reference
Plasmids		
pLO3	Tet^R sacB RP4 OriT colE1 ori	[186]
pGEM-T Easy	Amp^R, lacZ, f1 ori, T7 gene promoter, Sp6 gene promoter	Promega
pPsaE	4074 bp fragment containing psaE gene in pGEM-T easy vector.	This work
pPsaD	4244 bp fragment containing psaD gene in pGEM-T easy vector.	This work
pCKmTe	Km^R	[119]
pPsaEHIII	Derivative of pPsaE containing one HindIII site.	This work
pPsaEHIII2x	Derivative of pPsaE containing two HindIII sites.	This work
pPsaDHIII	Derivative of pPsaD containing one HindIII site.	This work
pPsaDHIII2x	Derivative of pPsaD containing two HindIII sites.	This work
pPsaEKmTe	Derivative of pPsaE containing HindIII ligated Km^R.	This work
pPsaDKmTe	Derivative of pPsaD containing HindIII ligated Km^R.	This work
pHoxKGRe	2666 bp fragment containing hoxK and hoxG gene in pGEM-T easy vector.	This work
pHoxKGRemod	1698 bp fragment containing hoxK and hoxG gene in pGEM-T easy vector.	This work

Table 5.1 continued

Strains and Plasmids	Relevant characteristic(s)	Source or reference
Plasmids		
pGEM-HoxKG	Derivative of pHoxKGRemod containing xbaI site at the 5' end of the anchor region of hoxK and BamHI site at 3' end of hoxK.	This work
pGEM-HoxKGC	Derivative of pHoxKGRemod containing BamHI site at the 5' end of the anchor region of hoxK and BamHI site at 3' end of hoxK.	This work
pGEM-PE1	Derivative of pPsaE containing ser-gly-gly linker sequence and six C-terminal histidine codons.	This work
pGEM-PE2	Derivative of pPsaE containing ser-gly-gly-ser-gly-gly linker sequence and six C-terminal histidine codons.	This work
pGEM-PE3	Derivative of pPsaE containing ser-gly-gly-ser-gly-gly -ser-gly-gly linker sequence and six C-terminal histidine codons.	This work
pGEM-PD1	Derivative of pPsaD containing ser-gly-gly linker sequence and six C-terminal histidine codons.	This work
pGEM-PD2	Derivative of pPsaD containing ser-gly-gly-ser-gly-gly linker sequence and six C-terminal histidine codons.	This work
pGEM-PD3	Derivative of pPsaD containing ser-gly-gly-ser-gly-gly -ser-gly-gly linker sequence and six C-terminal histidine codons.	This work
	Derivative of pGEM-HoxKG containing psaE gene equipped with a ser-gly-gly linker sequence and six C-terminal histidine codons.	This work

Table 5.1 continued

Strains and Plasmids	Relevant characteristic(s)	Source or reference
Plasmids		
pGEM-PE1-HoxKG	Derivative of pGEM-HoxKG containing psaE gene equipped with a ser-gly-gly linker sequence and six C-terminal histidine codons.	This work
pGEM-PE2-HoxKG	Derivative of pGEM-HoxKG containing psaE gene equipped with a ser-gly-gly-ser-gly-gly linker sequence and six C-terminal histidine codons.	This work
pGEM-PE3-HoxKG	Derivative of pGEM-HoxKG containing psaE gene equipped with a ser-gly-gly-ser-gly-gly -ser-gly-gly linker sequence and six C-terminal histidine codons.	This work
pGEM-PD1-HoxKG	Derivative of pGEM-HoxKG containing psaD gene equipped with a ser-gly-gly linker sequence and six C-terminal histidine codons.	This work
pGEM-PD2-HoxKG	Derivative of pGEM-HoxKG containing psaD gene equipped with a ser-gly-gly-ser-gly-gly linker sequence and six C-terminal histidine codons.	This work
pGEM-PD3-HoxKG	Derivative of pGEM-HoxKG containing psaD gene equipped with a ser-gly-gly-ser-gly-gly -ser-gly-gly linker sequence and six C-terminal histidine codons.	This work
pLO3-PE1-HoxKG	Derivative of pGEM-PE1-HoxKG in pLO3.	This work

Table 5.1 continued

Strains and Plasmids	Relevant characteristic(s)	Source or reference
Plasmids		
pLO3-PE2-HoxKG	Derivative of pGEM-PE2-HoxKG in pLO3.	This work
pLO3-PE3-HoxKG	Derivative of pGEM-PE-3HoxKG in pLO3.	This work
pLO3-PD1-HoxKG	Derivative of pGEM-PD1-HoxKG in pLO3.	This work
pLO3-PD2-HoxKG	Derivative of pGEM-PD2-HoxKG in pLO3.	This work
pLO3-PD3-HoxKG	Derivative of pGEM-PD3-HoxKG in pLO3.	This work
pGEM-HoxKGcon	Derivative of pGEM-HoxKGC lacking 50 bp encoding the anchor region of HoxK.	This work
pLO3-HoxKGcon	Derivative of pGEM-HoxKGcon in pLO3.	This work
pGEM-HoxKGBglII	Derivative of pGEM-HoxKGRemod containing a BglII site	This work
pGEM-HoxKGHis	Derivative of pGEM-HoxKGRemod containing six histidine codon and the 3' end of hoxK.	This work
pLO3-HoxKGHis	Derivative of pGEM-HoxKGHis in pLO3.	This work

Table 5.1 continued

Strains and Plasmids	Relevant characteristic(s)	Source or reference
Plasmids		
pBSK-psaE	pBluescript II SK derivative lacking its multiple cloning sites containing psaElinker1 sequence.	EpochBiolabs
pBSK psaD_Linker	pBluescript II SK derivative lacking its multiple cloning sites containing psaDlinker1 sequence.	EpochBiolabs
pBSK-psaEL2	pBSK-psaE derivative in pGEM containing linker 2 sequence.	This work
pBSK-psaEL3	pBSK-psaE derivative in pGEM containing linker 3 sequence.	This work
pBSK-psaDL2	pBSK psaD_Linker derivative in pGEM containing linker 2 sequence.	This work
pBSK-psaDL3	pBSK psaD_Linker derivative in pGEM containing linker 3 sequence.	This work

5.2.3 Media and growth conditions

Ralstonia eutropha strains were grown in a modified Luria broth containing 0.25% sodium chloride and buffered with 50mM MOPS (morpholinepropanesulfonic acid, pH 7.0), LSLB-MOPS as described previously [187]. *Ralstonia eutropha* strains were grown heterotrophically in synthetic medium containing 0.2% fructose and 0.2% glycerol as carbon and energy sources [188]. Sucrose-resistant transconjugants of *sacB*-haboring strains were selected on LSLB plates containing 15% sucrose [189]. *E. coli* strains were grown in LB medium or on solid LB containing 1.5% agar. Antibiotics were added when appropriate. 15µg/ml of tetracycline was used for *Ralstonia eutropha* strains and for *E.coli*, 100µg/ml of ampicillin and 15µg/ml of tetracycline were used [187]. *T. elongatus* was grown as descirbed in section 3.2.1.

5.2.4 Isolation of genomic DNA from *T. elongatus*

Cells were harvested during late log phase by centrifugation for 10 minutes at 7,000 *g*. Cell lysis and DNA isolation were performed as previously described [190]. The cell pellet was resuspended in TE buffer (100 mM Tris and 10 mM EDTA, pH 8) and the incubated with 25 mg/ml lysozyme at 37°C for 80 minutes. 10% SDS was added to the sample and vortexed mildly, after which it was incubated at 25°C for 10 minutes. 20 mg/ml proteinase-K was added and incubated at 65°C for 60 minutes. Neutralization solution 3M potassium acetate, pH 5.5) was then added and mixed gently (to avoid DNA shearing) by inverting 4 – 6 times prior to incubating on ice for 4 minutes. The lysate was centrifuged for 10 minutes at 10,000 g to remove cell debris. The clear supernatant containing genomic DNA was transferred to a new microcentrifuge tube and saturated buffered phenol: chloroform: iso-amyl alcohol (24:24:1) was added and centrifuged at 14,000 *g* for 4 minutes. The clear aqueous solution and white middle layer was pooled to a new microcentrifuge tube, leaving the bottom organic layer containing dissolved cellular component. This phenol-chloroform extraction was repeated once. Chloroform: iso-amyl alcohol (24:1) was added to the clear aqueous solution and centrifuged as above. The DNA contained in the aqueous portion was pooled carefully and transferred to another microcentrifuge tube. DNA was precipitated upon addition of chilled 100% EtOH, after gentle mixing and incubation at -20°C for 60 minutes. Precipitated DNA was pelleted by

centrifugation at 14,000 *g* for 15 minutes, after which EtOH was aspirated from the pellet. Pellets were left exposed to air for drying and then resuspended in TE buffer.

5.2.5 Targeted mutagenesis of *psaE* and *psaD* gene

The *psaE* gene from *T. elongatus* was amplified using primers 1 and 2 (Table 5.2) and cloned as a 4074bp fragment from the genomic DNA into the pGEM-T Easy (Promega) cloning vector by TA cloning to form plasmid pPsaE. The actual size of the *psaE* subunit is 231bp. The lengths of the remaining flanking sequence were 1878 and 1973 bp, enough for homologous recombination after transformation. Primers 5 and 6 were used to introduce the first HindIII restriction site by site-directed mutagenesis 78 bp downstream of the N-terminus of the *psaE* gene in plasmid pPsaE giving plasmid pPsaEHIII. Primers 7 and 8 were used to introduce a second HindIII site 231 bp downstream of the *psaE* start codon on plasmid pPsaEHIII yielding plasmid pPsaEHIII2x. 153 bp of the *psaE* gene was digested from pPsaEHIII2x using the HindIII restriction enzyme and re-ligated with a HindIII-digested kanamycin resistant gene (pCkmTe) that has been codon optimized for expression in *T. elongatus* yielding plasmid pPsaEKmTe (Figure 5.5). A similar approach was taken to clone the gene coding for the PsaD subunit of PSI. PCR amplification using primers 3 and 4 was used to amplify 4224 bp of genomic DNA carrying *psaD* gene (420 bp). This fragment was cloned into the pGEM-T Easy Vector by TA cloning. Primers 9 and 10 were used to introduce the first HindIII restriction site by site-directed mutagenesis 113 bp downstream of the N-terminus of the *psaD* gene in plasmid pPsaD to form plasmid pPsaDHIII. Primers 11 and 12 were used to introduce a second HindIII site 293 bp downstream of the *psaD* start codon on plasmid pPsaDHIII yielding plasmid pPsaDHIII2x. 179 bp of the *psaD* gene was digested from pPsaDHIII2x using HindIII restriction enzyme and re-ligated with HindIII-digested kanamycin resistant gene (pCkmTe) that has been codon optimized for expression in *T. elongatus* yielding plasmid pPsaDKmTe. The plasmids were verified by agarose gel electrophoresis and DNA sequencing.

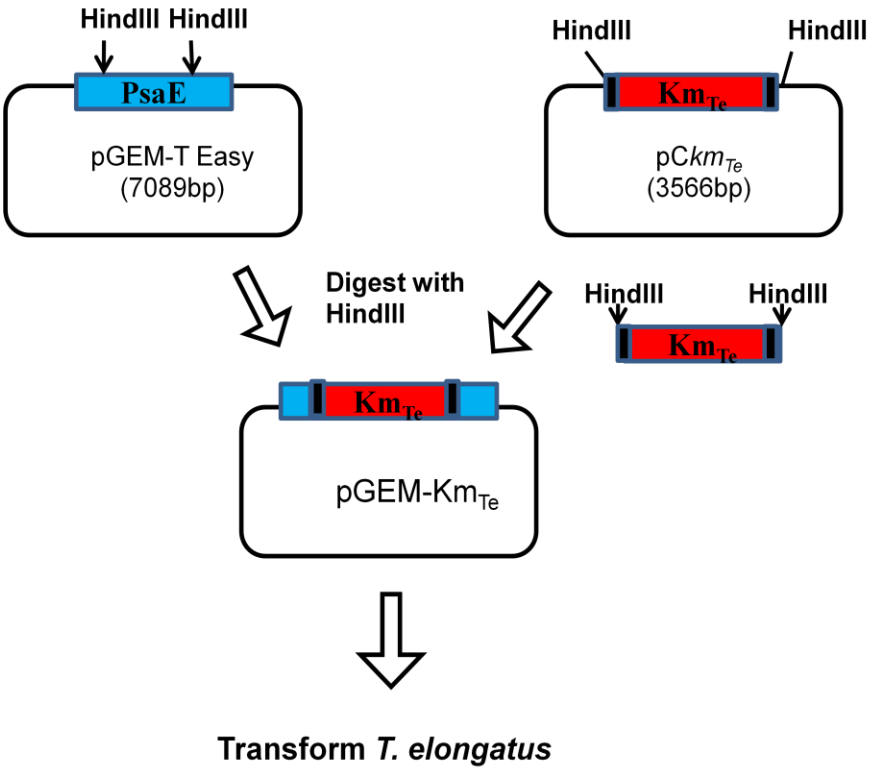


Figure 5.5 Construction of a clone for generating a deletion mutation for the gene encoding PsaE subunit of PSI for *T. elongatus*.

Table 5.2 Oligonucleotide primers used for targeted mutagenesis on *psaE* and *psaD* gene.

Designation	**(#)**	**DNA Sequence 5' – 3'**
psaE_upper	1	CCCGATCGAGAGCCAGAATTGGTGCGTGC
psaE_lower	2	GCGATCGCTTCCCTACTTGCCACCGTCAG
psaD_upper	3	CTGGTTATCACTGTTGTTGCGTTAGTCCTGCTGGGC
psaD_lower	4	CCAGTTGGCCACTGCGGTTCAGTTCGGG
PsaE_HindIII_mutant_upper	5	GGATTCAGGGCGGAGAAGCTTGACTTTAGAACCACG
PsaE_HindIII_mutant_lower	6	CGTGGTTCTAAAGTCAAGCTTCTCCGCCCTGAATCC
PsaEHindIIIx2mutant_upper	7	GCACTTCGTGAAGCGCAAGCTTATTTGTGTTC
PsaEHindIIIx2mutant_lower	8	GAACACAAATAAGCTTGCGCTTCACGAAGTGC
PsaD_HindIII1x_upper	9	GCCCCAAAGAGCAAGCTTTTGAGATG
PsaD_HindIII1x_lower	10	CATCTCAAAAGCTTGCTCTTTGGGGC
PsaDHindIII2x_upper	11	CCATCCCAAGCTTGGCGTTTTCCCTG
PsaDHindIII2x_lower	12	CAGGGAAAACGCCAAGCTTGGGATGG
HoxK_upper_primer	13	GATTCGGCAAGTCGGGGATCCTGGTAG
HoxK_lower_primer	14	GGCCTGTTTATACAGTGTGCCGATGG
HoxKGmodified_upper	15	GGAGACAGGTTATGGTCGAAACATTTTATGAAGTC
HoxKGmodified_lower	16	ATG AAAGGGCCCAAGCTGACCACTCTCG
HoxK_xbaIupper	17	GATGGCTTTTGGGACAATCTAGAATTCTACGATCGTC TGACCG
HoxK_xbaIlower	18	CGGTCAGACGATCGTAGAATTCTAGATTGTCCCAAAA GCCATC
HoxK_BamHILower2	19	GTCAGACGATCGTAGAAGGATCCTTTGTCCCAAAAGC CATCCTCG

Table 5.2 continued

Designation	**(#)**	**DNA Sequence 5' – 3'**
HoxK_BamHIUpper2	20	CGAGGATGGCTTTTGGGACAAAGGATCCTTCTACGATCGTCTGAC
HoxKlower_BamHIfurther	21	CGTTTCCCCGGCGGCTTAGGATCCACTGCCGCTGGTTTCGTTC
HoxKupper_BamHIfurther	22	GAACGAAACCAGCGGCAGTGGATCCTAAGCCGCCGGGGAAACG
PsaELinker1_upper	23	GGTACAATCCGGATCCCTAGTGGTGGTGGTGGTGGTGTTTACCTTTTTTGG
PsaELinker1_lower	24	ATAATTTAAATTCTAGAATTCTACGATTCCGGAGGACAACGTGGTTCTAAAGTCAAG
PsaELinker2V2_upper	25	CACGTTGTCCTCCGCTTCCTCCGGAATCG
PsaELinker2V2_lower	26	CGATTCCGGAGGAAGCGGAGGACAACGTG
PsaELinker3V2_upper	27	CACGTTGTCCTCCGCTTCCTCCGCTTCCTCGCCAATCG
PsaELinker3V2_lower	28	CGATTCCGGAGGAAGCGGAGGAAGCGGAGGACAACGTG
PsaD_Linker1_upper	29	ATTTAAATTCTAGAATTCTACGATTCCGGAGGAACAACACTCACTGGGCAACC
PsaD_Linker2_upper	30	ATTTAAATTCTAGAATTCTACGATTCCGGAGGAAGCGGAGGAACAACACTCACTGGGCAA
PsaD_Linker3_upper	31	ATTCTAGAATTCTACGATTCCGGAGGAAGCGGAGGAAGCGGAGGAACAACACTCACTGGG
PsaD_Linker_lower	32	GGTACAATCCGGATCCCTAGTGGTGGTGGTGGTGGTGTGGATCGTAGGGCTTTTT
Hox_T_Mutant_upper	33	CGATTATCAAGGTCCCGGGGTGGTGCCCTCC
Hox_T_Mutant_lower	34	GGAGGGCACCCCGGGACCTTGATAATCG
HoxKgenome_upper	35	GCCAATACCAATACAGAAATTAGGAGCTCGGTTATGGTCG

Table 5.2 continued

Designation	**(#)**	**DNA Sequence 5' – 3'**
HoxKgenomexbaI_lower	36	CGATCGTAGAATTCTAGATTGTCCCAAAAGCCATCCTC
HoxKgenomeBamHI_lower	37	CGATCGTAGAAGGATCCTTTGTCCCAAAAGCCATC
HoxkForward_primer	38	GTCGCCAAGCCAGCATTCGTG
HoxKcon_His Upper	39	GATGGCTTTTGGGACAAACACCATCACCATCACCATTAGGGATCCTAAGCCGCCGGG
HoxKcon_His Lower	40	CCCGGCTTAGGATCCCTAATGGTGATGGTGATGGTGTTTGTCCCAAAAGCCATC
Mbh fwd bglII	41	CAGTGAACACAGATCTGCCGGGGAAACGACT
Mbh rev bglII	42	AGTCGTTTCCCCGGCAGATCTGTGTTCACTG
Mbh 6his fwd_BglII	43	CACAGATCTGCTCACCATCACCATCACCATTAAGCCGCCGGGGAAACGACTGAATCA
M13 reverse	44	pGEM T-easy sequencing primer (Promega)
PsaELinker2opt_upper	45	GACAATCTAGAATTCTACGACTCGGGCGGCTCGGGCGGCCAGCGCGGCTCGAA
PsaELinker3opt_upper	46	GACAATCTAGAATTCTACGACTCGGGCGGCTCGGGCGGCTCGGGCGGCCAGCGCGGCTC
PsaDLinker2opt_upper	47	GACAATCTAGAATTCTACGACTCGGGCGGCTCGGGCGGCACCACC
PsaDLinker3opt_upper	48	GGACCATCTAGAATTCTACGACTCGGGCGGCTCGGGCGGCTCGGGCGGCACCACCCTGA
PsaDLinkeropt_lower	49	GGCGGCTTAGGATCCTTAATGGTGATGGTGATGGTG
xbaImutatuion_lower	50	GGGACAATCTGGAATTCTACGACTC
xbaImutatuion_lower	51	GAGTCGTAGAATTCCAGATTGTCCC
PsaE_UpperMet	52	GACAGTGTTGGCCATAACCGGATGACAGAAAGGAG

Table 5.2 continued

Designation	**(#)**	**DNA Sequence 5' – 3'**
PsaE_lowerTerm	53	CTCGATGAAGGCTTGCGGCTCTTTGGGAG
psaD_upper_MetStart	54	GCTACGATGCCGTTGAATCTGGTTAGAGCCCTTTTC
psaD_lower_term	55	CAAGAGGGGTTGCCAGCTTTGCATCACCAAGGTATAG

5.2.6 Electroporation of *T. elongatus*

The plasmid DNA was introduced into *T. elongatus* following protocols established by Iwai *et al* [120]. *T elongatus* wild type strain was grown as discussed in section 3.2.1 but in a 2 L bottle. 1 L of cells were harvested at mid log phase (OD_{730} = 0.804, 3.39 x 10^7 cells/ml) by centrifugation at 2000 g for 10 minutes. A hemocytometer was used to get an approximate cell count. The cells where washed once in 10 ml of 2mM TES-KOH pH 7.3 and centrifuged at 2000 g for 10 minutes. The cells were then resuspended in 10 ml of sterile deionized water and centrifuged at 2000 g for 10 minutes after which they were resuspended in about 1.6 ml deionized water to a final concentration of 2.5 x 10^{10} cells/ml. 40 µl of the cell suspension was mixed with 4 – 8 µg of DNA solution and electroporated at a field strength of 8 kV cm^{-1}. Pulsed cells were mixed with 1 ml of BG11 medium followed by shaking for 24 h at 45^0C under low light conditions (10 – 20 µE m^{-2} s^{-1}. The incubated cells were spread on a BG11 (0.8% agar) plate containing 30 µg/ml kanamycin. Antibiotics resistant transformants appeared after incubation under continuous illumination (~50 µE m^{-2} s^{-1}) for about 7 days at 45^0C. Single colonies were picked and re-streaked on BG11/kanamycin plates. Surviving transformants for PsaE deletion were named ΔPsaE and were screened by colony PCR using appropriate primers 52 and 53. PsaD deletion transformants were named ΔPsaD and was also screened by colony PCR using appropriate primers 54 and 55.

5.2.7 Isolation of the Megaplasmid DNA

Megaplasmid DNA was isolated as described previously with the following modification [191]. 1.5 ml culture of *Ralstonia eutropha H16* was grown in minimal salts media with fructose and glycerol as carbon sources for ~30 h. The cells were harvested by centrifugation at 8000 g for 1 min. The cell pellet was gently resuspended in 500 µl of lysis buffer (0.3 M sucrose, 25 mM Tris-HCl pH 8.0 and 25 mM EDTA, pH 8.0). 5 mg of lysozyme was added followed by the addition of 25 µg of RNase A. The mixture was incubated at 37^0C for 20 min without shaking. 250 µl of 2% SDS was added, mixed by inverting 5 times and then incubated for 5 min at room temperature. 250 µl of Phenol/Chloroform/Isoamyl (25:24:1) was added and the mixture was emulsified by inverting the tube 10 to 20 times. The aqueous phase was separated from the phenol phase by centrifugation at 12000g for 5 min. The aqueous phase (~700 µl) was transferred to a clean DNAse free tube. 0.1 vol. of 3M potassium (or sodium) acetate, pH 4.8 was added followed by the addition of 1 vol. of isopropanol. The mixture was incubated at room temperature for 5 min. The precipitated DNA was recovered by centrifugation at 12000 g for 10 min (may not see pellet). The supernatant was removed leaving about ~ 50 µl in the tube. 500 µl of cold (-20^0C) 70% ethanol was added, and the tube was kept at -20^0C for 30 min (or overnight). The precipitated DNA was recovered by centrifugation at -2^0C for 30 min at 12000 g. The supernatant was discarded and residual ethanol was evaporated by speed vacuum. The pellet was dissolved in 50 – 80 µl of nuclease free distilled water.

5.2.8 Isolation of the gene cluster coding for the *HoxKG* gene in *Ralstonia eutropha*

The *hoxKG* gene from *R. eutropha* [42] was amplified from the megaplasmid pGH1 by PCR using primers 13 and 15 (Table 5.2) and subsequently subcloned as a 2666-bp fragment into the cloning vector, pGEM-T easy by TA cloning resulting in plasmid pHoxKGRe.

5.2.9 Genetic constructions of the hyd-PsaE and hyd-PsaD hybrid complex

The genetic construction of the hybrid complex was done following the procedure reported by Ihara *et al.* [42] as shown in Figure 5.6. The 3' end of *hoxK* was amplified from plasmid pHoxKGRe using primers 15 and 16 (Table 5.2) to form plasmid pHoxKGRemod. Primers 17 and 18 were used to introduce an XbaI site at the 5' end of the region encoding the HoxK anchor (corresponding to Lys303 – Ser305). Similarly, primers 19 and 20 were used to

introduce a BamHI site at the 5' end of the region encoding the HoxK anchor for one of the constructs. A further BamHI site was introduced at the 3' end of *hoxK* (corresponding to Glu357 – His360) using primers 21 and 22 yielding plasmid pGEM-HoxKG for the plasmid carrying the xbaI site and pGEM-HoxKGC for the plasmid carrying the BamHI site. Digestion of pGEM-HoxKGC with BamHI restriction enzyme and self-ligation of the plasmid deleting 50 bp at the 3' end of *hoxk* resulted in plasmid pGEM-HoxKGcon. Primers 39 and 40 were used to introduce six C-terminal histidine codons on pGEM-HoxKGcon. Plasmids pGEM-PE1-HoxKG, pGEM-PE2-HoxKG and pGEM-PE1-HoxKG were generated as follows; the *T. elongatus psaE* gene from plasmid pPsaE was amplified as an XbaI/BamHI fragment with a 5' linker sequence (ser-gly-gly) and six C-terminal histidine codons using primers 23 and 24 and introduced into pGEM T-easy vector by TA cloning to yield plasmid pGEM-PE1. Plasmid pGEM-PE1 was amplified as an XbaI/BamHI fragment with a 5' linker sequence (ser-gly-gly-ser-gly-gly) and six C-terminal histidine codons using primers 25 and 26 into pGEM vector yielding plasmid pGEM-PE2. Similarly, pGEM-PE1 was amplified as an XbaI/BamHI fragment with a 5' linker sequence (ser-gly-gly-ser-gly-gly-ser-gly-gly) and six C-terminal histidine codons using primers 27 and 28 into pGEM vector to give plasmid pGEM-PE3. Plasmids pGEM-PE1-HoxKG, pGEM-PE2-HoxKG and pGEM-PE1-HoxKG were generated by ligating XbaI/BamHI digested fragments from plasmids pGEM-PE1, pGEM-PE2 and pGEM-PE3 to an equally digested plasmid pGEM-HoxKG respectively. For the generation of the pGEM-PD1-HoxKG, pGEM-PD2-HoxKG, pGEM-PD3-HoxKG plasmids, the *T. elongatus psaD* gene from plasmid pPsaD was amplified as XbaI/BamHI fragments with three different 5' linker sequence (ser-gly-gly, ser-gly-gly-ser-gly-gly, ser-gly-gly-ser-gly-gly-ser-gly-gly) and six C-terminal histidine codons using three different primer pairs (primers 29 and 32, primers 30 and 32, and primers 31 and 32 respectively) and cloned into pGEM vector to form plasmids pGEM-PD1, pGEM-PD2 and pGEM-PD3. Plasmids pGEM-PD1, pGEM-PD2 and pGEM-PD3 were then digested with XbaI and BamHI restriction enzymes and ligated to an XbaI/BamHi digested plasmid pGEM-HoxKG to yield plasmids pGEM-PD1-HoxKG, pGEM-PD2-HoxKG, pGEM-PD3-HoxKG respectively.

A mutation from C → A was found 567 bp downstream of the start codon of *hoxK* resulting in amino acid change from proline to threonine. Site directed mutagenesis using

primers 33 and 34 was used to change the A → C. A PstI restriction site was introduced into vectors pGEM-PE1/2/3-HoxKG and pGEM-PD1/2/3-HoxKG using primers 35 and 36. PstI was also introduced into vector pGEM-HoxKGcon using primers 36 and 37. For homologous recombination, SacI/PstI fragments from pGEM-PE1/2/3-HoxKG, pGEM-PD1/2/3-HoxKG and pGEM-HoxKGcon were cloned into pLO3. These products resulted to plasmids pLO3-PE1/2/3-HoxKG, pLO3-PD1/2/3-HoxKG and pLO3-HoxKGcon and were used to introduce the modified *hoxk* gene into *R. eutropha* by homologous recombination. Primer 38 was used for sequence verification. The resulting transconjugants were named HFEL1, HFEL2, HFEL3, HFDL1 and HFCON (Table 5.1).

A His_6-tag fusion to the C-terminus of the MBH small subunit HoxK was constructed as follows: primers 41 and 42 were used to introduce a BglII site at the 3' end of *hoxK* gene on plasmid pGEM-HoxKGRemod yielding plasmid pGEM-HoxKGBglII. Primers 43 (carrying a BglII site and six histidine codon) and 44 were used to amplify a region of pGEM-HoxKGBglII. A BglII-SacI fragment of the PCR product was inserted to an equally cut plasmid pGEM-HoxkGBglII resulting in plasmid pGEM-HoxKGHis. Finally, a PstI-SacI fragment from pGEM-HoxKGHis was ligated to the PstI-SacI site of the suicide vector pLO3 to give pLO3-HoxkGHis for homologous recombination in *R. eutropha*. The resulting transconjugant was named HF387H.

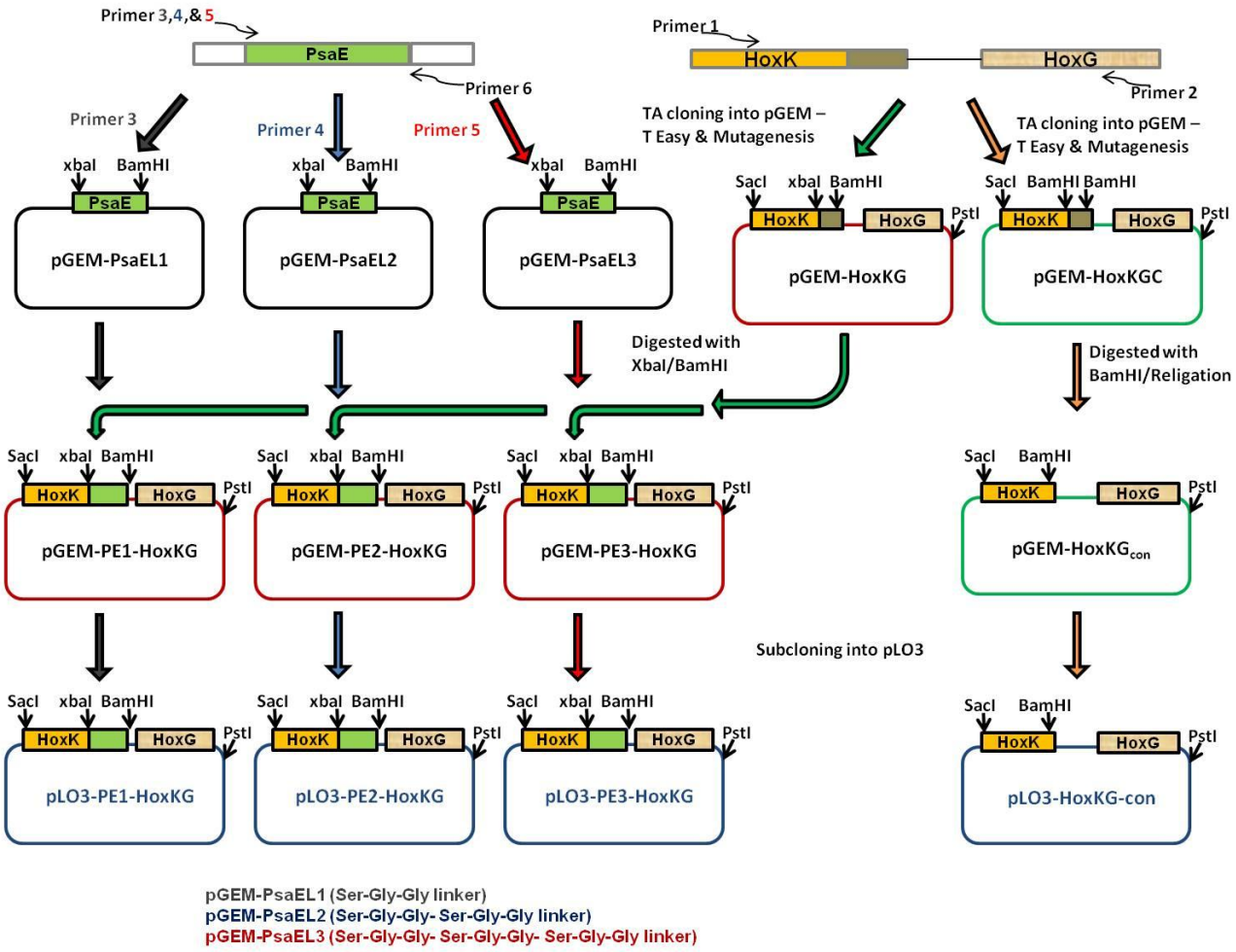


Figure 5.6 Genetic constructions of hydrogenase and PsaE fusion protein for homologous recombination in *R. eutropha*.

5.2.10 Conjugative plasmid transfer and gene replacement

Donor (*E. coli S17-1*) and recipient (*R. eutropha HF387*) strains were grown to late exponential growth phase. 1 ml of the donor strain and 3 ml of the recipient strains were concentrated by centrifugation (3500 x g for 5 min) and washed three times with LSLB-MOPS media and then resuspended in 100 µl of LSLB-MOPS media. Mobilizable plasmids were transferred from *E. coli S17-1* to *R. eutropha HF387* by a spot mating technique [183]. Spot mating was performed on D-medium agar by plating 200 µl of the mixture of donor and recipient at a cell ratio of 1:3. After 16 h of incubation at 30^0C in the dark, the cells were washed of the agar with 700 µl of FGN media and washed once with FGN media by centrifugation at 3500 g. Various dilutions of the cell suspension was plated onto FGN plates with 15µg/ml of tetracycline. Transconjugants appeared after 3 to 5 days of incubation at 30^0C. Tetracycline resistant transconjugants were picked, purified by streaking in FGN/Tet plates twice and then inoculated in LSLB-MOPS without antibiotics. The cells were grown in 2 ml culture overnight at 30^0C and 100 µl of cells were then spread on LB plates containing 15% sucrose. Sucrose resistant survivors were picked and screened by colony PCR. Each PCR was performed with a specific primer set binding the flanking regions of the homologous section because the sizes of the amplified fragment of the wild type and mutant are clearly distinguished by PCR. Megaplasmid DNA was isolated from positive screens, the modified region amplified by PCR, gel purified and then verified by DNA sequencing.

5.2.11 Purification of Hydrogenase from *Ralstonia eutropha*

Purification of the MBH_{wt}-His_6: Cells of HF387H were grown aerobically at 30^0C in 5 baffled flasks each containing 1 liter of FGN medium. The purification of the recombinant hydrogenase was done following the protocol reported by Schwarze *et al* [192] with some modifications. After 50 h the cells reached an OD_{436} of ~11 and were harvested by centrifugation (5,000 g at 4^0C for 15 min) and washed once with phosphate buffer ($Na_2HPO_4.12H_2O$ (90 g $liter^{-1}$) and KH_2PO_4 (15 g $liter^{-1}$)), and re-centrifuged. The resulting cell pellet was frozen in liquid N_2 and stored at -80 °C. The cell pellet (~20 g) was resuspended in 40 ml of Buffer A (50 mM Tris pH 8.0, 300 mM NaCl, 0.2 mM $MnC1_2$, 1 µM lupetin, 1 µM pepstatin, and 100 µM PMSF). The resuspended cells were disrupted by two passages through a chilled French press (SLC Aminco)

at a cell pressure of 20,000 psi. Cell debris and membranes were separated from the soluble protein fraction by ultracentrifugation (100,000 x g, 4^0C for 60 min). The brownish membranes were removed by scrapping with a spatula and homogenized using a Dounce homogenizer in an appropriate volume of buffer A. The membrane proteins were solubilized by adding Triton X-114 at a final concentration of 2% (w/v) and subsequently stirring on ice for 2 h. The solubilized protein was then separated by ultracentrifugation (100,000 x g, 4^0C for 20 min). The supernatant containing the solubilized membrane proteins were loaded on a HisPur cobalt column (2 ml bed volume (BV), Thermo Scientific) equilibrated with 15 BV of washing buffer (Buffer A + 10 mM imidazole). The columns were washed with 15 BV of washing buffer and bound proteins were eluted 6 x 0.5 ml of elution buffer (Buffer A + 150 mM imidazole (without Triton X-114)). The MBH-containing fractions were combined and concentrated using a centrifugal filter device (Amicon Ultra-15 (PL-30), Millipore). The buffer was changed twice by adding 10 ml of storage buffer (50 mM Tris pH 8.0, 50 mM NaCl, and 20% glycerol).

Purification of the MBH_{PsaEL1}/ MBH_{PsaEL2}/ MBH_{PsaEL3}/ MBH_{PsaDL1}/ MBH_{con}: Cells of HFEL1, HFEL2, HFEL3, HFDL1 and HFCON were grown aerobically at 30^0C in 5 baffled flasks each filled with 1 liter of FGN medium. After 50 h the cells reached an OD_{436} of ~11 and were harvested by centrifugation (5,000 x g at 4^0C for 15 min) and washed once with washed with phosphate buffer ($Na_2HPO_4.12H_2O$ (90 g $liter^{-1}$) and KH_2PO_4 (15 g $liter^{-1}$)), and re-centrifuged. The resulting cell pellet was frozen in liquid N_2 and stored at -80 °C. The cell pellet (~10 g) was resuspended in 10 ml of Buffer A. The resuspended cells were disrupted by two passages through a chilled French press (SLC Aminco) at a cell pressure of 20,000 psi. Cell debris and membranes were separated from the soluble protein fraction by ultracentrifugation (88,000 x g, 4^0C for 45 min). The resulting soluble fractions were loaded Cobalt His-pur column (2 ml bed volume (BV), Thermo Scientific) equilibrated with 15 BV of washing buffer (Buffer A + 10 mM imidazole). The columns were washed with 15 BV of washing buffer and bound proteins were eluted 6 x 0.5 ml of elution buffer (Buffer A + 150 mM imidazole (without Triton X-114)). The MBH-containing fractions were combined and concentrated using a centrifugal filter device (Amicon Ultra-15 (PL-30), Millipore). The buffer was changed twice by adding 10 ml of storage buffer (50 mM Tris pH 8.0, 50 mM NaCl, and 20% glycerol) and stored at -20^0C. All the purification steps were performed at 4^0C.

5.2.12 SDS-Page and Western immunoblot analysis

The BCA method (Pierce, USA) was applied for protein quantification using bovine serum albumin as standard. The purity of the samples was estimated by visual inspection of the SDS- polyacrylamide gel stained with Coomassie Brilliant blue G-250. For the detection of protein complexes containing hyd-PsaE/D, the respective proteins were resolved in 15% polyacrylamide-SDS gels and subsequently transferred to PVDF (Immobilon-PSQ Millipore) membranes. The *His*-tagged fusion proteins were identified by a chemiluminescent detection system an anti *His*-tag (C-term) AP-conjugated antibody (invitrogen). For immunological detection of MBH- related proteins, antisera were applied in the following dilutions: anti-HoxK serum (1:20,000) and anti-HoxG serum (1:20,000). HoxK and HoxG antisera were kind gifts from Oliver Lenz (Institut fur Biologie, Humboldt-Universitat zu Berlin, Berlin, Germany).

5.2.13 Hydrogenase activity assay using reduced methyl viologen as electron donor

The hydrogenase activity assay carried out in a 2 ml GC vial containing 1.5 ml of 50mM Tris pH 7.0, 3 mM methyl viologen and the hydrogenase sample [77]. The gas phase was flushed with N_2 for 10 min and the reaction was catalyzed by the anaerobic addition of 20 mM sodium dithionite solution. The hydrogen evolution for ~ 3 h was measured every 50 - 60 min by withdrawing 100 µl from the gas phase and analyzing it with a gas-chromatography calibrated with hydrogen. 5890 Series III (HP) GC equipped with a thermal conductivity detector and Supelco Carboxen 1000 column, was used for this assay. The evolution rate was calculated from the slope of the time dependent reaction. One unit of activity is defined as the amount of hydrogenase evolving 1µmol H_2/min/ mg protein.

5.2.14 Codon optimization of *psaE* and *psaD* gene for *R. eutropha*

Gene Designer, a synthetic biology tool for constructing artificial DNA segment, was used to codon optimize *psaE* and *psaD* gene (shown below) with their linker sequence for expression in *R. eutropha* [193]. Synthetic gene were designed based on the codon-optimized gene and used for the genetic engineering of the fusion between membrane-bound small subunit, *hoxK* and the *psaE* and *psaD* gene. Java Codon Adaptation Tool (Jcat), a free online software was also used to determine the codon adaptation of the *psaE* and *psaD* genes in *R. eutropha*.

PsaE_Linker1 Sequence

tgggacaatctagaATTCTACGACtcgggcggcCAGCGCGGCTCGAAGGTGAAGATCCTGCGCCC
GGAATCGTACTGGTACAACGAAGTGGGCACCGTGGCCTCGGTGGACCAGACCCCGG
GCGTGAAGTACCCGGTGATCGTGCGCTTCGACAAGGTGAACTACACCGGCTACTCG
GGCTCGGCCTCGGGCGTGAACACCAACAACTTCGCCCTGCACGAAGTGCAGGAAGT
GGCCCCGCCGAAGAAGGGCAAGCACCATCACCATCACCATTAGggatcctaagccgccgg

PsaD_Linker1 Sequence

tgggacaatctagaATTCTACGACtcgggcggcACCACCCTGACCGGCCAGCCGCCGCTGTACGG
CGGCTCGACCGGCGGCCTGCTGTCGGCCGCCGACACCGAAGAAAAGTACGCCATCA
CCTGGACCTCGCCGAAGGAACAGGTGTTCGAAATGCCGACCGCCGGCGCCGCCGTG
ATGCGCGAAGGCGAAAACCTGGTGTACTTCGCCCGCAAGGAACAGTGCCTGGCCCT
GGCCGCCCAGCAGCTGCGCCCGCGCAAGATCAACGACTACAAGATCTACCGCATCT
TCCCGGACGGCGAAACCGTGCTGATCCACCCGAAGGACGGCGTGTTCCCGGAAAAG
GTGAACAAGGGCCGCGAAGCCGTGAACTCGGTGCCGCGCTCGATCGGCCAGAACCC
GAACCCGTCGCAGCTGAAGTTCACCGGCAAGAAGCCGTACGACCCGCACCATCACC
ATCACCATTAAggatcctaagccgccgg

Codon optimized *psaE* and *psaD* gene were synthesized by EpochBiolabs and cloned into a EcorV digested pBluescript II SK derivative lacking its multiple cloning sites yielding plasmids pBSK-psaE and pBSK psaD_Linker. Primers 45 – 49 was used to amplify the codon optimized genes from plasmids pBSK-psaE and pBSK psaD_Linker and cloned into pGEM vector to give pBSK-psaEL2, pBSK-psaEL3, pBSK-psaDL2 and pBSK-psaDL3. XbaI-BamHI fragments of these plasmids were digested and ligated into equally cut plasmids pGEM-PE1/2/3-HoxKG and pGEM-PD1/2/3-HoxKG to form codon optimized plasmids pGEM-PE1/2/3-HoxKG and pGEM-PD1/2/3-HoxKG. XbaI site in plasmids pGEM-PE1/2/3-HoxKG and pGEM-PD1/2/3-HoxKG were removed by site directed mutagenesis using primers 50 and 51.

5.3 Results and discussion

5.3.1 Targeted Mutagenesis of *psaE* and *psaD*

A PsaE-free mutant of PSI was formed by genetically disrupting the expression of the PsaE subunit of a native PSI. A deletion derivative plasmid (pPsaEKmTe) was constructed by cloning flanking regions of *psaE* gene into pGEM-T Easy. 153 bp of the *psaE* gene was digested using HindIII restriction enzyme and then replaced with a gene that confers kanamycin resistance (Figure 5.7A) which has been codon optimized for expression in *T. elongatus* and it thermostable. This kanamycin resistant gene was obtained from plasmid pCkmTe (Figure 5.8) a kind from Dr. Kiyoshi Onai, Center for Gene Research, Nagoya University, Japan. Synthesis of the codon-optimized gene encoding the thermostable kanamycin nucleotidyltransferase and the construction of the expression cassette has been reported by Onai *et al* [119]. *T. elongatus cpcC* gene was used as the promoter in plasmid pCkmTe. The insertion of the kanamycin resistant gene into plasmid pPsaE was confirmed by digestion of the ligation product as shown in Figure 5.7B. This construct was further verified by DNA sequencing.

Similarly a *psaD* gene was constructed by cloning the *psaD* flanking gene into pGEM-T Easy vector and then digesting 179 bp of the *psaD* gene and replacing it with a kanamycin resistant gene to yield plasmid pPsaDKmTe (Figure 5.9A). The insertion of the kanamycin resistant gene into plasmid pPsaD was confirmed by digestion of the ligation product as shown in Figure 5.9B.

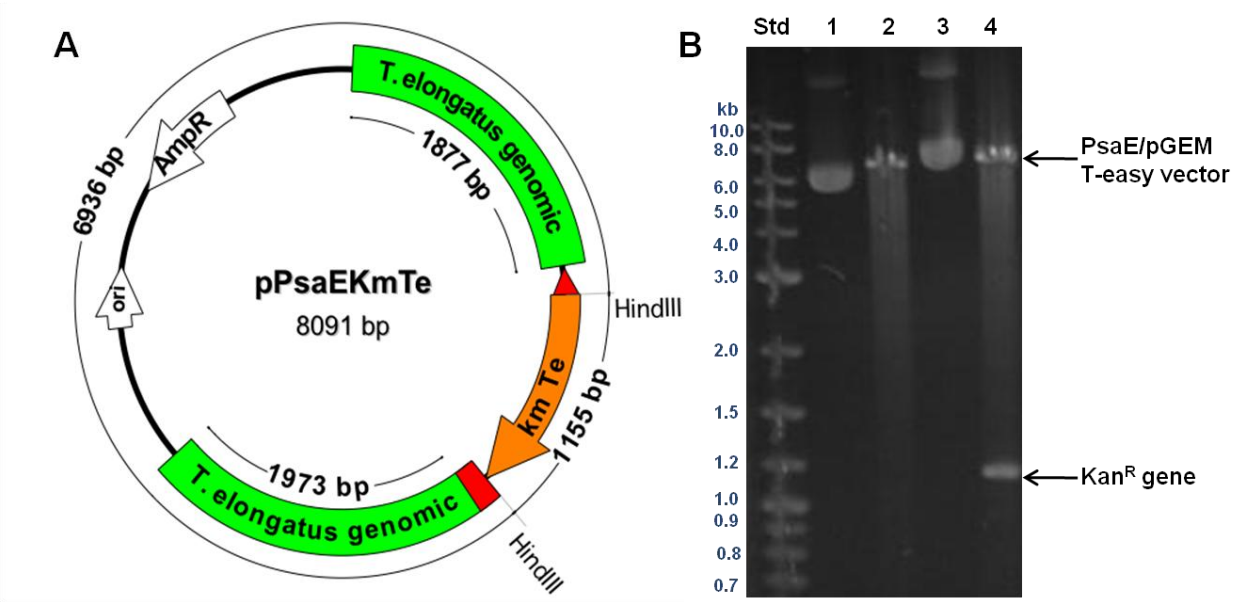


Figure 5.7 PsaE knockout gene construct. **A)** Plasmid pPsaEKmTe carrying flanking regions of PsaE and a kanamycin resistant gene. **B)** Agarose gel electrophoresis of plasmid pPsaE, digested and undigested with hindIII restriction enzyme (Lane 1 and 2 respectively) and pPsaKmTe digested and undigested with hindIII restriction enzyme (Lane 3 and 4).

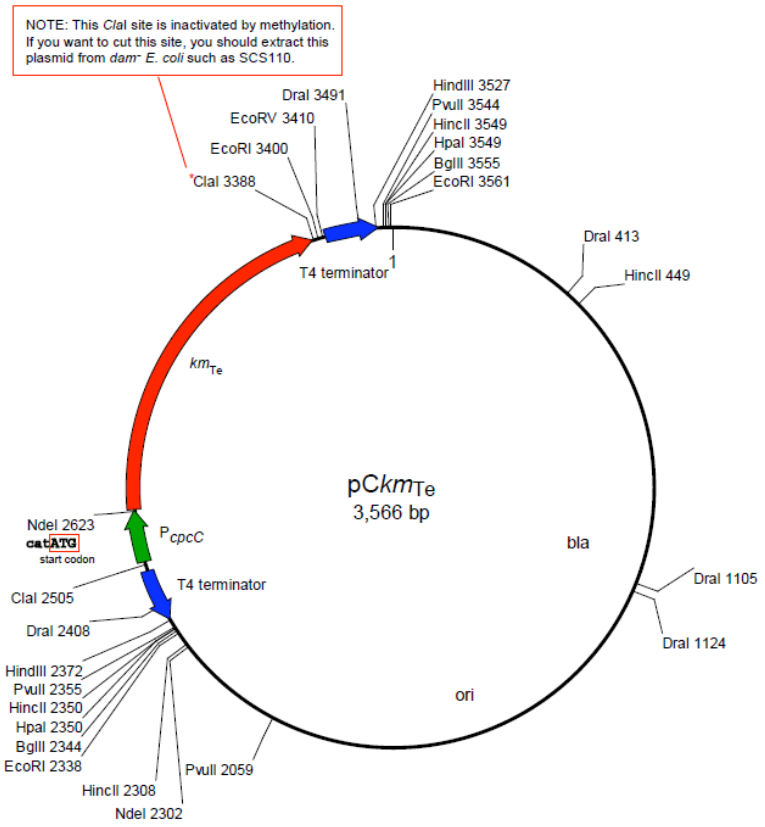


Figure 5.8 Plasmid pCKmTe carrying a gene encoding the thermostable kanamycin nucleotidyltransferase. This vector also carries *T.elongatus cpcC* promoter and to T4 terminator sequences oriented in opposite direction at both ends of the plasmid [119].

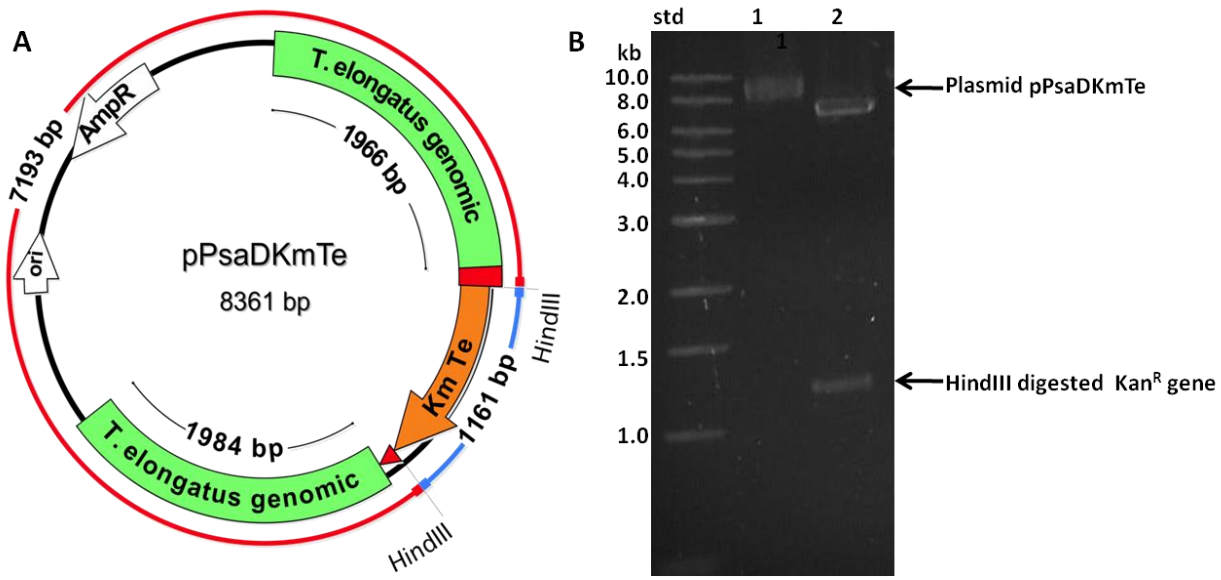


Figure 5.9 PsaD knockout gene construct. **A)** Plasmid pPsaDKmTe carrying flanking regions of PsaE and a kanamycin resistant gene. **B)** Agarose gel electrophoresis of plasmid pPsaD, digested and undigested with hindIII restriction enzyme (Lane 1 and 2 respectively) and pPsaKmTe digested and undigested with hindIII restriction enzyme (Lane 3 and 4).

5.3.2 Transformation of *T. elongatus* and homologous recombination

Transformation of *T. elongatus* was done following an improved genetic transformation protocol reported by Iwai and co-workers [120]. A targeting vector used in electroporation contained thermostable Kan^R gene (~1200 bp) with a strong cyanobacterial promoter and codon optimized for *T. elongatus.* Gel of digested vector shows size of inserted Kan^R gene (Fig 5.7B and Fig 5.9B). The flanking sequence in each targeting vector was > 1800 bp (Fig 5.7A and Fig 5.9A) to improve the efficiency of transformation. In *Synechococcus sp*. strain PCC 7942, it has been reported that the ratio of the length of the homologous sequences to that of a foreign segment interrupting it affects transformation efficiency markedly, with the efficiency increasing as the ratio increases [119]. After electroporation the plates were incubated at 45^0C with illumination at 50 μE $m^{-2}s^{-1}$ and Kan^R colonies were observed after 10-14 days (Fig 5.10A). The Kan^R colonies were re-streaked on Kan/BG-11 plates (Fig 5.10B).

The efficiency of transformation for the electroporation was low. This may have been as a result of the presence of a putative type I restriction endonuclease, *tll2230*. It has been reported that the disruption of the gene that codes for this endonulcease in *T. elongatus* increased the electroporation efficiency by about 5 times [120]. Natural transformation efficiency in the *tll2230*-disruptant strain was also significantly higher than in the wild type. Type I restriction endonuclease, *tll2230*, has been reported to be the only candidate for restriction endonuclease in *T. elongatus* genome based on sequence analysis [146]. A type II restriction endonuclease activity (SelI) from *T. elongtus* has also be reported by Miyake *et al* [194] to degrade DNA at CGCG. Colony PCR on ΔPsaD transformants showed no positive screen. Colony PCR on ΔPsaE transformants showed the presence of two species, the wild type (4086 bp) and the disrupted PsaE (5241 bp) with Kan^R gene insertion (Fig. 5.10C and Fig. 5.10D). The presence of these multiple species was not expected but may have been as a result of the presence of multiple copies of the genome [195]. It has been reported that one of the difficulty in manipulating cyanobacterial genes arises from their polyploidy i.e. the multiple copies of genomic DNA in some strains [195-197].

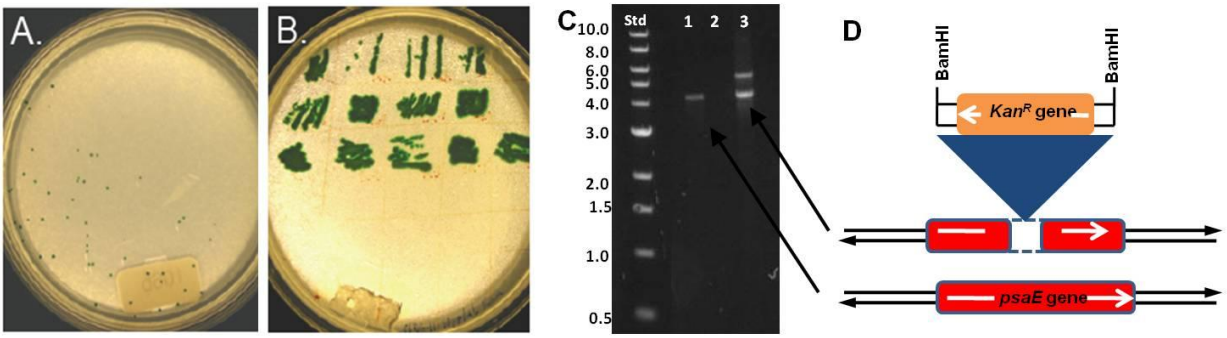


Figure 5.10 Transformation and homologous recombination in *T. elongatus*. **A)** After electroporation, *T. elongatus* cells were plated on BG-11 media containing 50 ug/ml of kanamycin; colonies were visible after 10-14 days. **B)** Individual colonies were re-streaked on fresh selective plates and cultured for 2-3 weeks. **C)** Agarose gel of colony PCR product of Kan^R transformants showing size shift of 1155 bp of inserted Kan^R gene, Lane 1 (Wild type), Lane 2 (No DNA control), Lane 3 (ΔPsaE with insertion of Kan^R gene. **D)** Genomic organization of the Kan^R gene placement upon homologous recombination in *T. elongatus.*

5.3.3 Genetic construction of hydrogenase fusion proteins

The membrane-bound hydrogenase was selected for the construction of the hybrid fusion proteins because of the oxygen tolerance of the hydrogenase. The membrane-bound hydrogenase strongly resembles the composition of a standard [Ni-Fe] hydrogenase (from *D. vulgaris*) whose crystal structure is known. Also the enzyme is accessible to genetic engineering and its biosynthesis and biochemical properties have been greatly studies.

The megaplasmid DNA for *R. eutropha* was isolated and the gene coding for small subunit, HoxK and part of the large subunit HoxG were amplified and cloned into a cloning vector for modification on the *hoxk* gene (Figure 5.11). The hyd-PsaE/D fusion proteins were constructed by substituting three different linker peptide (Ser-Gly-Gly, Ser-Gly-Gly-Ser-Gly-Gly, Ser-Gly-Gly-Ser-Gly-Gly-Ser-Gly-Gly), for the membrane anchor domain of the membrane-bound hydrogenase small subunit, HoxK. Subsequently, this was linked to the PsaE and PsaD moity from *T. elongatus* equipped with a C-terminal hexahistidine tag. A truncated

hoxK in which the terminal anchor peptide had been removed by insertion of a translational stop codon into the the corresponding gene was also formed. This protein served as a control. The gene coding for this fusion proteins were cloned into a mobilizable suicide vector (plO3) and verified agarose gel electrophoresis (Fig. 5.12 A) and sequencing. Six C-terminal histidine codons were also introduced to intact *hoxK* for introduction of hexahisitidine tag to the wild-type. The conditionally lethal suicide vector, pLO3 [186] was used for the generation of the isogenic mutants of *R. eutropha* HF387 (Fig. 5.12B).

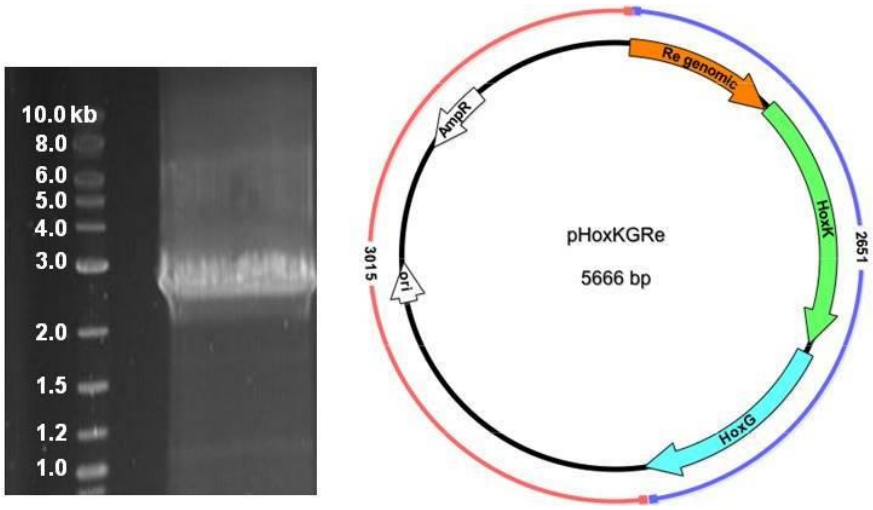


Figure 5.11 Isolation of the megaplasmid DNA and cloning of the *hoxK* and *hoxG* gene. Left panel shows agarose gel electrophoresis of PCR amplification of the *hoxK* and *hoxG* gene (2666 bp) from the megaplasmid. Right panel shows the gene construct for *hoxK* modification.

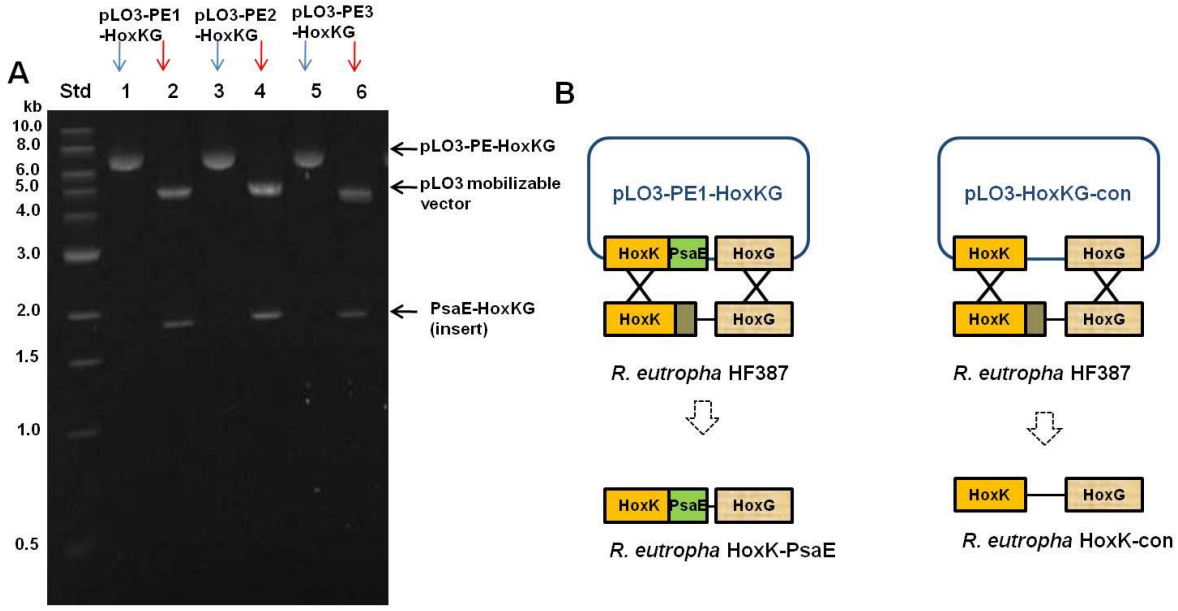


Figure 5.12 Modified *hoxK* gene for homologous recombination. **A)** Gel electrophoresis of modified *hoxK* gene linked with PsaE gene via three different linkers. pLO3-HoxKG-PsaELinker1 (lane 1) digested with PstI/SacI (lane 2). pLO3-HoxKG-PsaELinker2 (lane 3) digested with PstI/SacI (lane 4). pLO3-HoxKG-PsaELinker3 (lane 5) digested with PstI/SacI (lane 6). **B)** Homologous recombination of the modified *hoxk* with the wild type strain.

5.3.4 Conjugal gene replacement in *R. eutropha*

Bacterial conjugation is the transfer of genetic material between bacteria by cell-to-cell contact or by a bridge-like connection between to cells. It is a mechanism of horizontal gene transfer as with transformation and transduction. During conjugation the donor cell provides a conjugative or mobilizable genetic element that is most often a plasmid or transposon. To facilitate the gene exchange procedure, a mobilizable (suicide) plasmid, pLO3 [186] was used. plO3 is a ColE1 replicon outfitted with the RP4 transfer origin (*oriT*) and a conditionally lethal *B. subtilis sacB* gene [189] in addition to a tetracycline resistant gene. This vector is competent for mobilization in *R. eutrophus* but incapable of autonomous replication in this bacterium[187]. Suicide vectors are used for allelic exchange of non-selectable marker. The Tet^R phenotype of the plasmid provides a direct selection for the integration of the plasmid into the chromosome. Once the plasmid is integrated, segregants are screened by testing for the loss of the plasmid Tet^R marker using a counter-selectable marker on the plasmid. *SacB* gene on the plasmid was used as the counter-selectable marker. Expression of the *sac-B* gene is toxic for gram-negative bacteria when grown in the presence of 5% sucrose, providing a direct selection for loss of the plasmid. *sacB*-based systems for positive selection have been successfully used in gram negative bacteria. *E. coli S17-1* was used as the mobilizing (donor) strain. The donor strain carry the transfer genes of the broad host range IncP-type plasmid with chromosomally integrate RP4 derivative to promote mobilization [183]. They can utilize any gram negative bacterium as a recipient for conjugative DNA transfer.

Modified *hoxk* sequences sub-cloned in pLO3 were introduced into *R. eutropha* for allelic exchange. Conjugation was initiated by spot mating of donor and recipient strains (Fig. 5.13). Heterogenote (single crossover) recombinants were selected by screening for tetracycline resistance. Tet^R segregants were picked and purified by streaking. In a subsequent step, homogenates (double crossover) recombinants which have lost the vector sequences including the *sacB* gene were selected as sucrose-resistant survivors. During this second selection, the megaplasmid duplication is segregated by homologous recombination between the flanking direct repeats, leaving one copy of the gene on the megaplasmid. This recombination results to either the wild-type copy or the mutant copy as shown in Figure 5.14A. Megaplasmid DNA was

prepared for each of the isolates and screened for the desired modification by colony PCR. In figure 5.14A positive screen for the hyd-PsaE fusion resulted in a size shift of ~200 bp. The PCR product was further screened by restriction digest with BamHI restriction enzyme which confirmed the presence of the BamHI site found only in the mutant strain (data not shown). This same screening procedure was carried out for all the constructs (data not shown). All isolates were verified by DNA sequencing (Figure 5.14B). The sequence verified mutants were grown in FGN media as described above for the isolation of the hydrogenase fusion proteins. No expression of the protein was observed. The lack of expression of the hybrid proteins may have been as a result of rare codons in the newly introduced *psaE* and *psaD* gene from *T.elongatus.*

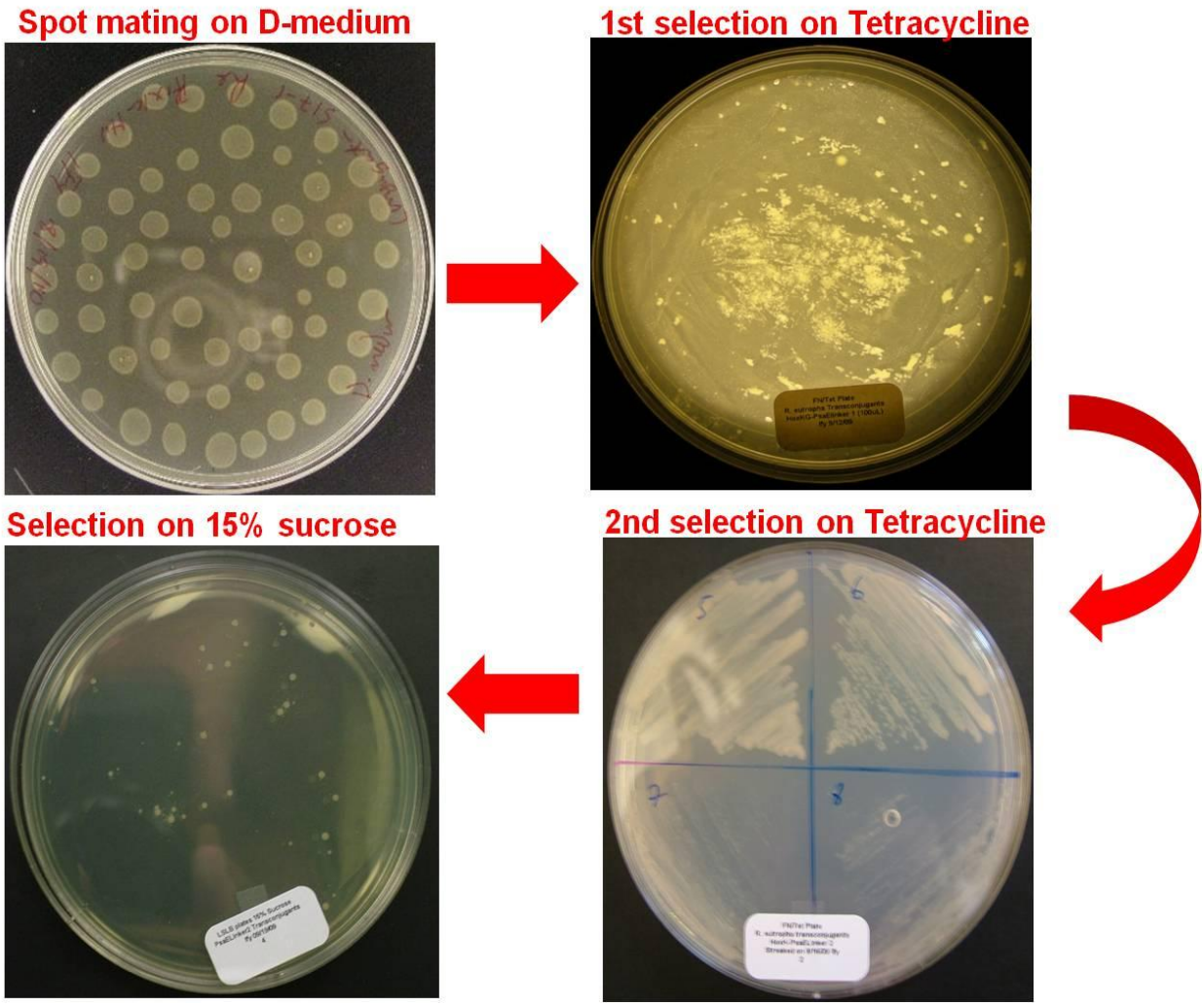


Figure 5.13 Conjugation in *R. eutropha*. Conjugation was initiated by spot mating of *R. eutropha* HF387 and *E coli S17-1*. Spots were washed off the D-medium plate and spread on FGN/Tet plate. Tet^R colonies were picked and re-streaked on FGN/Tet plate. Tet^R colonies from the second collection where then grown on LB medium overnight and spread on modified LB plates containing 15% sucrose.

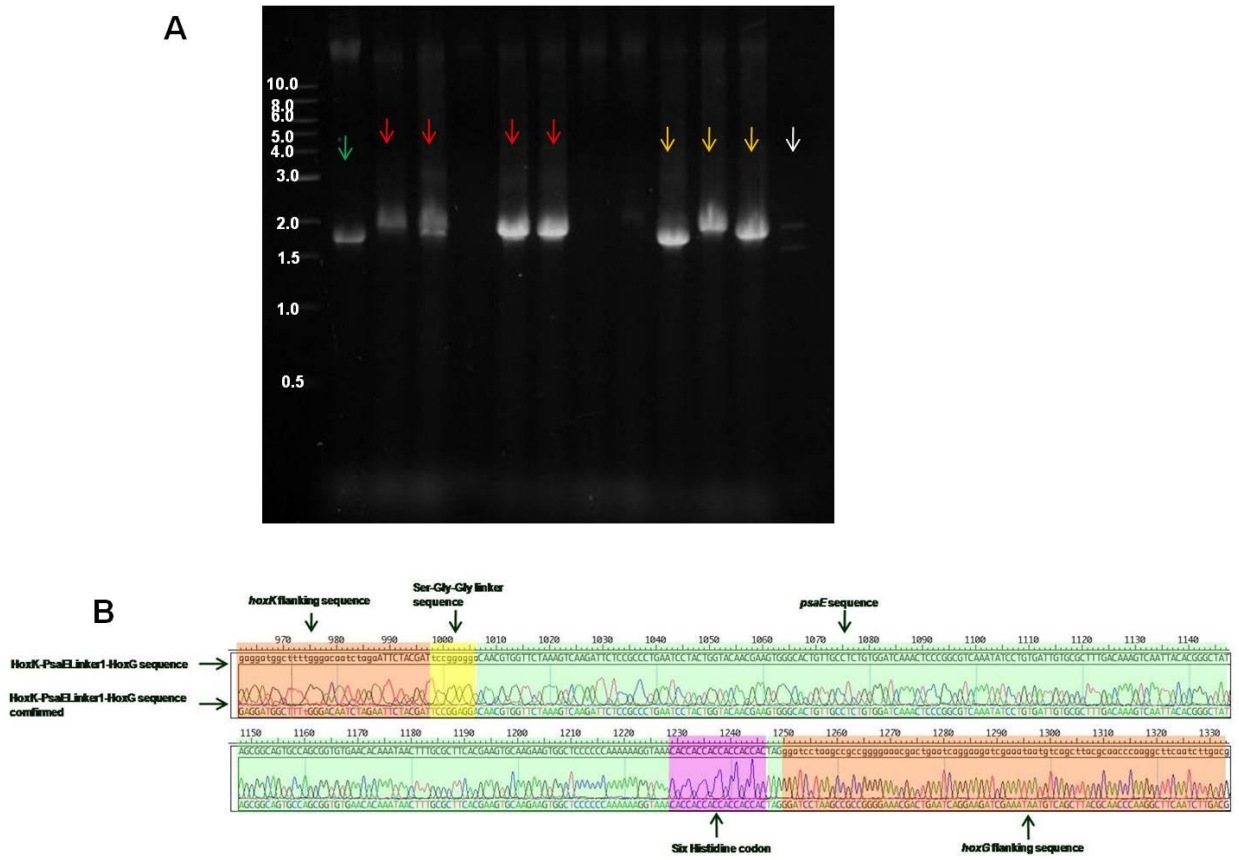


Figure 5.14 Selection of positive screens after conjugation and sequence verification. **A)** Agarose gel electropherisis of colony PCR product. Green arrow (wild type control), red arrow (Hoxk-PsaE-Linker1 mutant), yellow arrow (Hoxk-PsaE-Linker2 mutant) and white arrow (no DNA control). **B)** Electropherogram showing sequence verification of the modified *hoxk-psaE* gene *R. eutropha* transconjugants.

5.3.5 Codon optimization of *psaE* and *psaD* gene.

A codon is a series of 3 nucleotides (triplets) that encodes a specific amino acid residue in the polypeptide chain or for the termination of translation (stop codons). There are 64 different codons but only 20 different translated amino acids. The degeneracy of the genetic code enables many alternative nucleotide sequences to encode the same protein. The frequencies with which different codons are used by different organisms and different types of genes vary significantly[198] and are correlated to the population of tRNA in the cells [199]. Rare codons are not only associated with low level of protein expression due to ribosome stalling and abortive translation [200], but also been implicated in frame shift and amino acid misincorporation [201, 202]. Codon usage has also been identified as the single most important factor in prokaryotic gene expression [203]. Codon usage preference in a gene is often measured by Codon Adaptation Index (CAI score). A CAI score of 1 means that in each case only the most abundant codon is used [193]. A CAI score of 1 is not ideal because a strongly transcribed mRNA from such a gene will generate high codon concentrations for a subset of the tRNA populations, resulting in imbalanced tRNA pool, skewed codon usage pattern and increased translational error [204].

Java Codon Adaptation Tool (Jcat), free online software, was also used to determine the codon adaptation of the *hoxk, psaE* and *psaD* genes in *R. eutropha* (Fig. 5.15, 5.16 and 5.17). In figure 5.15, the h*oxK* sequence before adaptation has a CAI score of 0.331 and a GC content of 57.525. The CAI score of *hoxK* gene in it native host is low. This value was compared to CAI score in other organism with similar *hoxK* gene as shown in Table 5.3 most of which had low CAI score. The reason for this low CAI score is not very clear. The PsaE-Linker 1 sequence before adaptation had a CAI score of 0.057 (Fig. 5.16A) and a CAI score of 0.802 (Fig. 5.16B) after adaptation. Also, PsaD-Linker 1 had a CAI score of 0.096 (Fig. 5.17A) and a CAI score of 0.802 (Fig. 5.17B) after codon optimization. This low CAI score was as a result of frequently used rare codons for the *psaE* and the *psaD* genes that may have affected the expression of the hybrid protien. Codon optimized *psaE* and *psaD* gene were synthesized by EpochBiolabs and cloned into a EcorV digested pBluescript II SK derivative lacking its multiple cloning sites

yielding plasmids pBSK-psaE (Fig 5.18A) and pBSK psaD_Linker (Fig 5.18B). These codon optimized genes were then used to engineer the fusion between HoxK and PsaE/D.

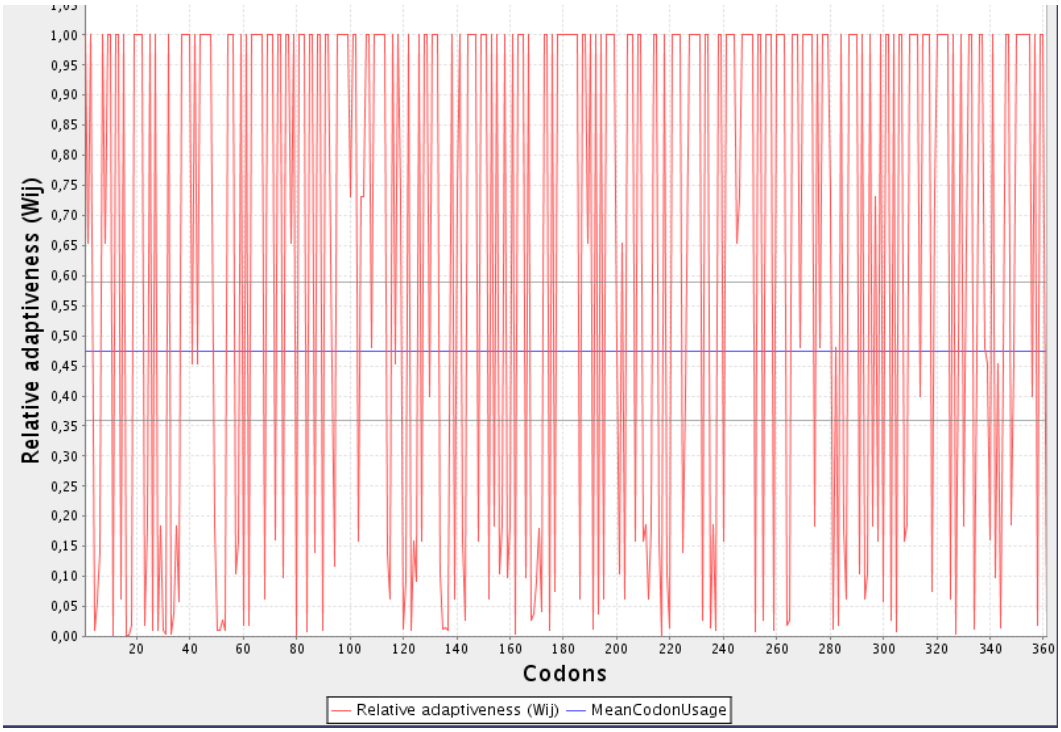


Figure 5.15 Relative adaptiveness of h*oxK* sequence in *R. eutropha*. The h*oxK* sequence before adaptation has a CAI score of 0.331 and a GC content of 57.525.

Table 5.3 Comparison of CAI score with similar *hoxk* gene from other organisms

Organism	CAI score
Ralstonia eutropha H16	0.331
Ralstonia metallidurans CH34	0.348
Methylococcus capsulatus	0.164
Polatomonas sp.	0.235
Salmonella typhimurium	0.278
Salmonella paratyphi-a	0.355
Rhidobacter sphaeroides	0.619
Azoarcus sp.	0.749

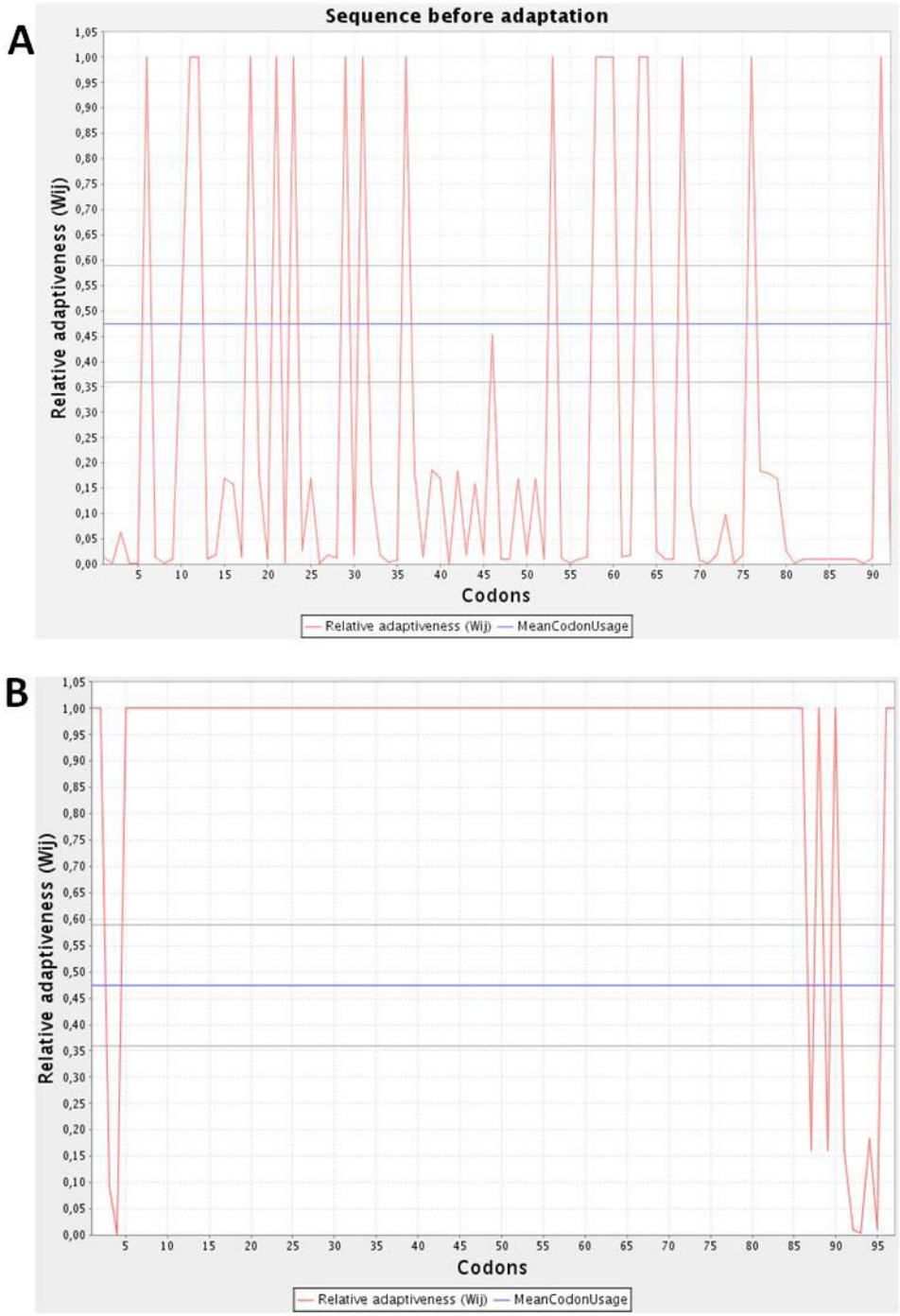


Figure 5.16 PsaE-Linker 1 sequence; (A) before adaptation and (B) after adaptation. The PsaE-Linker 1 sequence before adaptation has a CAI score of 0.057 and a GC content of 49.64 and a score of 0.802 and a GC content of 62.9 after adaptation.

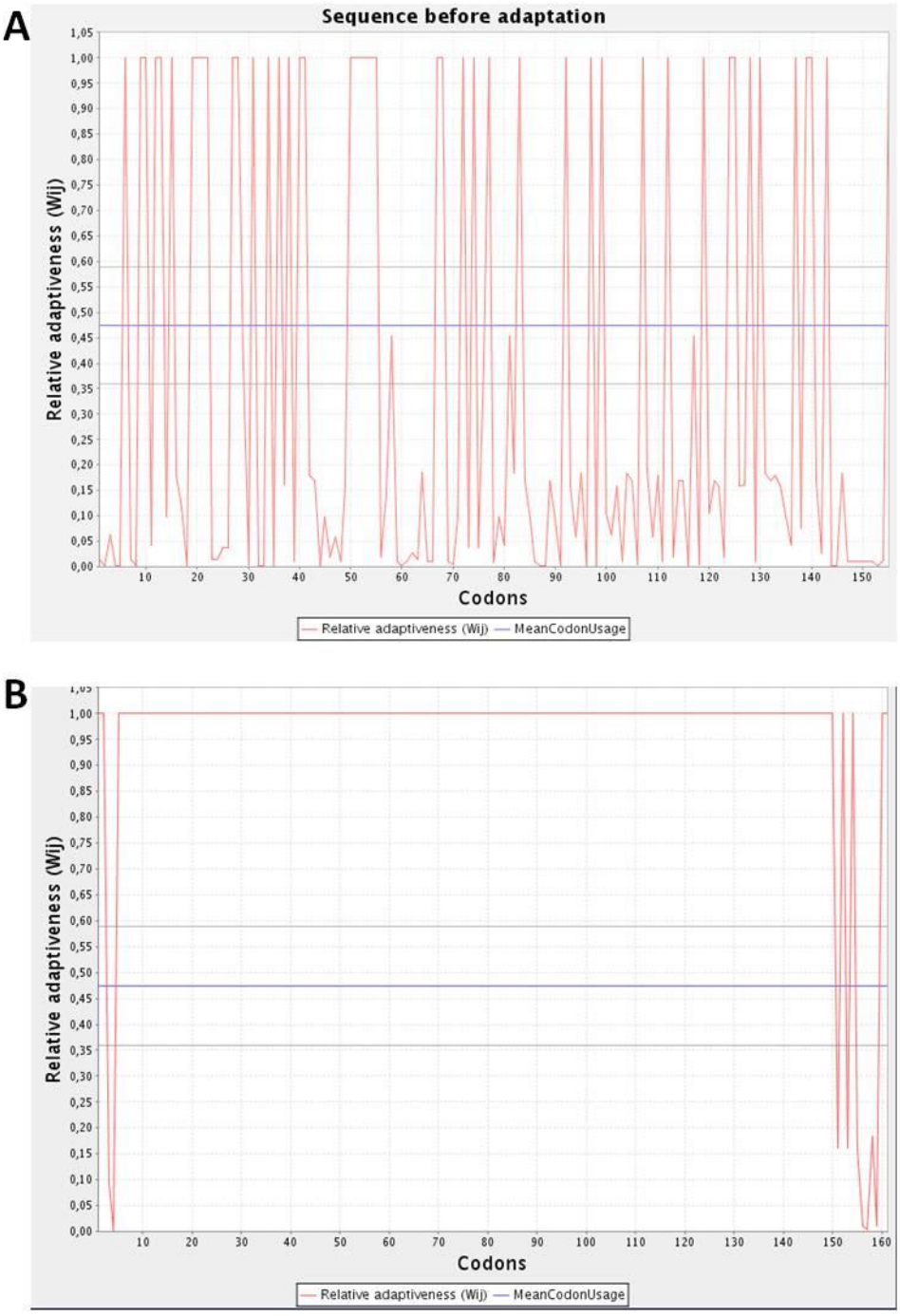


Figure 5.17 PsaD-Linker 1 sequence; (A) before adaptation and (B) after adaptation. The PsaE-Linker 1 sequence before adaptation has a CAI score of 0.096 and a GC content of 54.077 and a score of 0.876 and a GC content of 64.32 after adaptation.

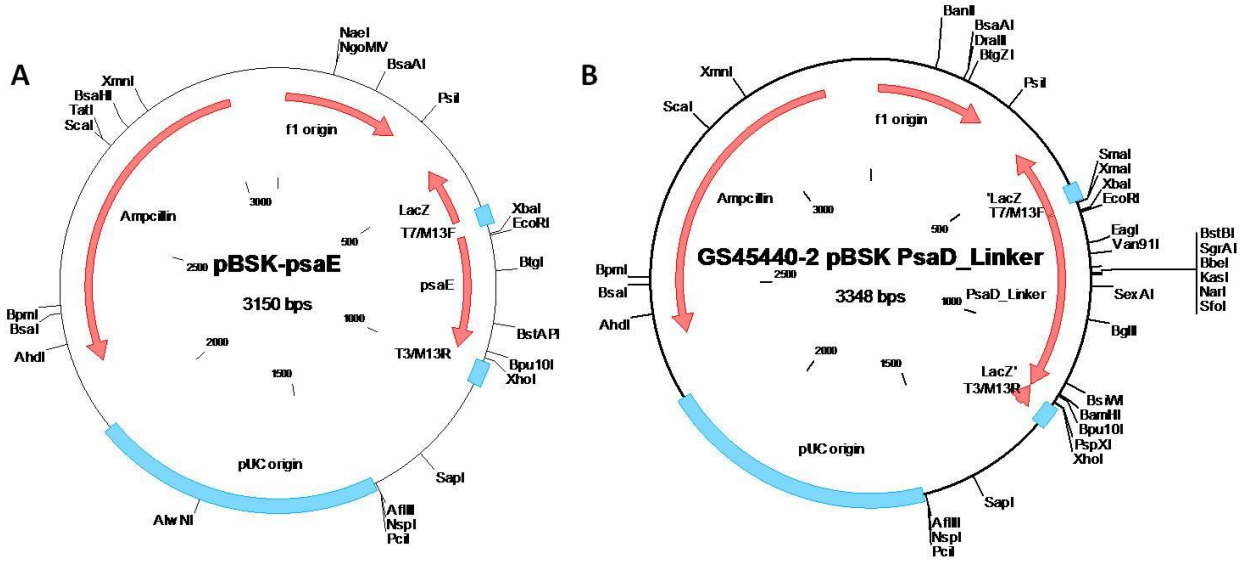


Figure 5.18 Synthesized codon optimized *psaE* and *psaD* gene cloned into a EcorV digested pBluescript II SK derivative lacking its multiple cloning sites yielding plasmids pBSK-psaE and pBSK psaD_Linker respectively (EpcohBiolabs).

5.3.6 Construction and expression of hydrogenase fusion proteins

The MBH of *R. eutropha* consists of a large subunit, HoxG, that houses the Ni-Fe active site and a small subunit, HoxK, which contains several Fe-S clusters. The MBH is connected via a C-terminal "anchor" region of HoxK to a membrane integral *b*-type cytochrome, thereby facing the membrane [82, 83, 205]. Catalytically active membrane fusion protein have been reported for light driven hydrogen production [77, 192, 206]. For construction of the hyd-PsaE and hyd PsaD fusion proteins, the C-terminal "anchor" sequence encoded at the 3' end of *hoxK* (Fig. 5.19A) was replaced by a Ser-Gly-Gly (1x, 2x and 3x) linkers followed by a sequence coding for the *T. elongatus* PSI subunit *psaE* and *psaD* equipped with a C-terminal His- tag sequence (Fig. 5.19C). The C-terminal "anchor" sequence encoded at the 3' end of *hoxK* was replaced by a His-tag sequence for the construction of the hyd-stop that served as a control (Fig 5.19B). Recombinant strains lacking the anchor region has been reported to not sustain H_2- dependent autotrophic growth due to the fact that the hydrogenase fusion proteins were incapable of establishing a proper connection to the *b*-type cytochrome, HoxZ [192].

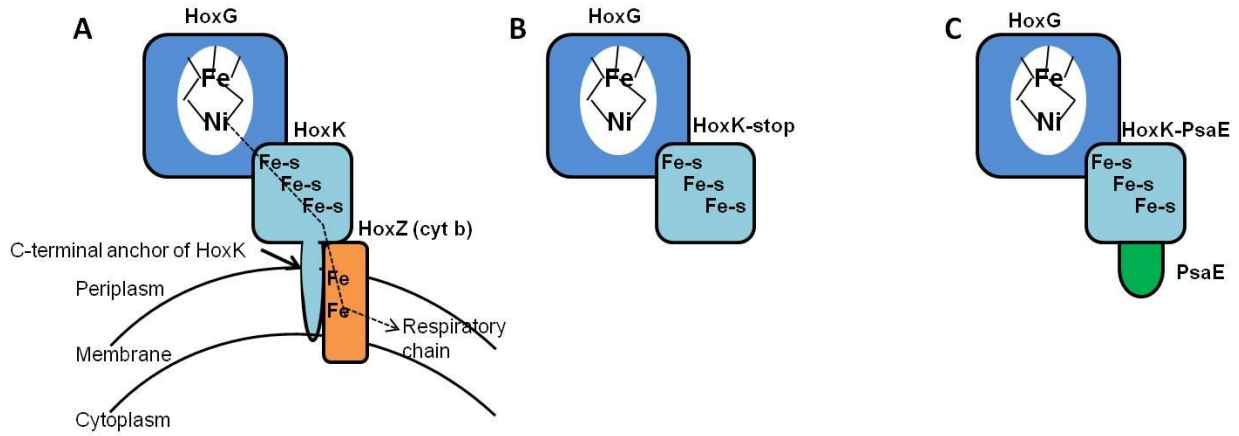


Figure 5.19 Models of the wild type and mutant hydrogenases (adapted from Schwarze *et al*[192]). **A)** Wild type MBH of *R.eutropha* H16. **B)** MBH-stop protein lacking the C-terminal anchor domain of HoxK. **C)** MBH-PsaE fusion protein lacking the C-terminal anchor domain of HoxK.

The hyd-PsaE, hyd-PsaD and hyd-stop proteins all lack the HoxK anchor peptide responsible for membrane attachment and thus these proteins were expected to be purified from the soluble protein fractions (Fig 5.20A). Immunological analysis was conducted using purified solubilized membrane and soluble fractions from the *R. eutropha* HFEL1 strain (Fig. 5.20B). Using antibodies against C-terminal His, *His*-tagged hyd-PsaE fusion protein was detected in the soluble fraction as expected. The fact that the hyd-PsaE fusion protein was found in the cytoplasm led to the conclusion that the modification of the C-terminus strongly affects the twin-arginine-dependent membrane translocation (Tat)-dependent transport competence of the fusion protein [192]. This phenomenon have also been observed in mutants of *R. eutropha* that lacked the large MBH subunit, HoxG [192]. This effect may have been as a result of the HoxK precursors been retained in the cytoplasm or stalled in the membrane within the Tat translocon.

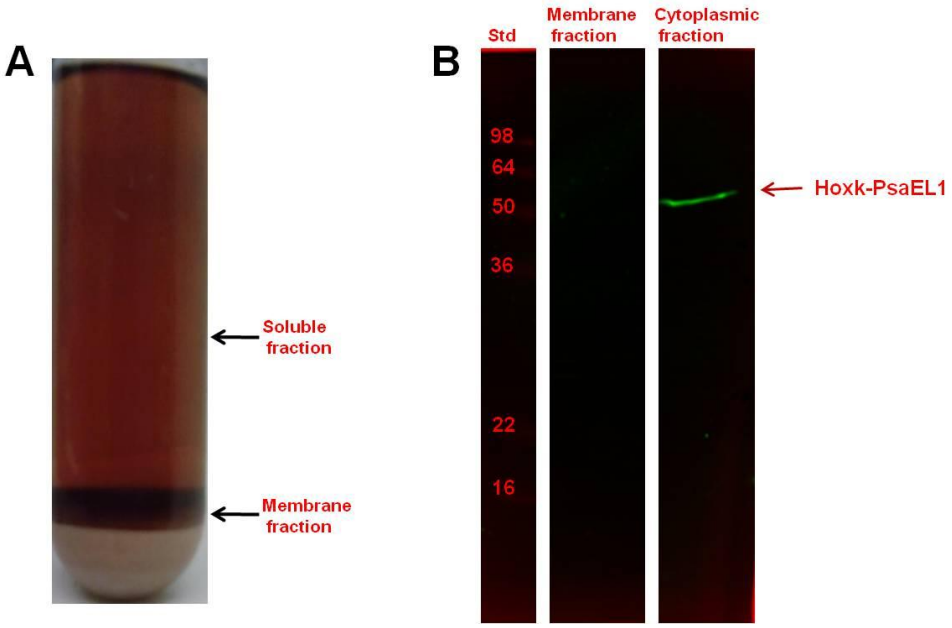


Figure 5.20 Subcellular localization of HoxK-PsaEL1 in *R. eutropha HFEL1* mutant strain. **A)** Soluble and membrane fraction after ultracentrifugation (100,000 x g at 4^0C for 60 min) of lysed cells. **B)** Purified solubilized membrane and soluble fraction were run on SDS-PAGE. Western blot analysis was done using antibodies against His.

5.3.7 Purification and properties of the hydrogenase fusion proteins

The wild type MBH from *R. eutropha H16* was partially purified as previously reported [84]. In Figure 5.21, SDS PAGE of partially purified MBH hydrogenase and Immunoblot analysis using antibodies against HoxG (Lane 3) and HoxK (Lane 4) reveals the presence of the large subunit (67 kDa) and the small subunit (35 kDa).

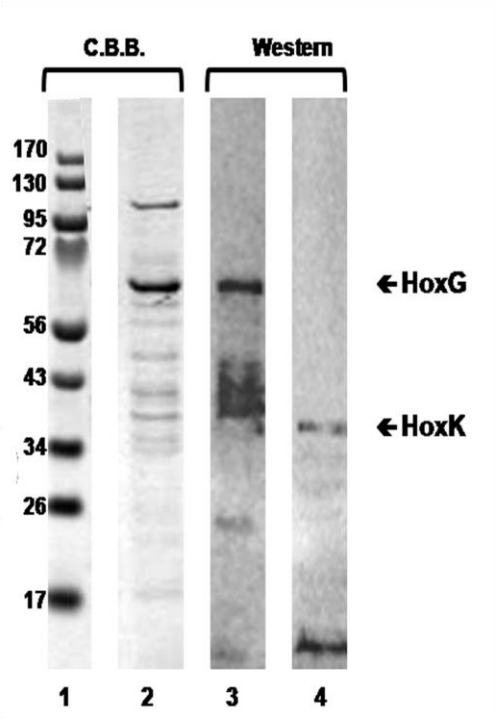


Figure 5.21 SDS PAGE of partially purified MBH hydrogenase. Protein standard (Lane 1), partially purified MBH from *R. eutropha H16* (Lane 2), Immunoblot analysis using antibodies against HoxG (Lane 3) and HoxK (Lane 4).

It has been previously demonstrated that the cytoplasmic, premature HoxK protein, designated preHoxK, co-purifies with the accessory HoxO and HoxQ proteins [192]. The preHoxK protein carries an N-terminal signal peptide of 43 amino acids that is cleaved off during translocation of the MBH through the Tat apparatus [82]. Thus C-terminally *His*-tagged hyd-PsaE was expected to occur in two protein complexes upon affinity chromatography, the mature HoxG-HoxK-PsaE and the premature preHoxK-PsaE-HoxO/Q. Soluble extracts was purified from mutant cells grown under hydrogen-derepressing conditions and applied to one-step immobilized metal affinity chromatography (IMAC) using HisPur cobalt resin. After a washing step, matrix-bound protein was eluted using 150 mM Imidizole. The eluate, designated to as HoxK-stop, HoxK-PsaEL1, HoxK-PsaEL2, HoxK-PsaEL3 and HoxK-PsaDL1 were concentrated and subjected to SDS-PAGE (Fig. 5.22). A *His*-tagged version of the wild type MBH was also isolated from the membrane fraction as described in materials and methods. Immunological analysis identified the wild type HoxK (36 kDa), premature, non translocated preHoxk-PsaELinker1 (~ 44kDa), preHoxK-PsaELinker2 (~ 44kDa), preHoxK-PsaELinker3 (~ 44kDa), and preHoxK-PsaDLinker1 (~ 51kDa). Due to the lack of the anchor peptide in the HoxK-stop protein, the corresponding HoxK derivative was found at positions corresponding to 34 kDa (preHoxK-stop). Also a 29 kDa (Hoxk-stop) band was found in a previous purification of the HoxK-stop protein (data not shown) which is in agreement with published data [192]. This was not feasible in Figure 5.22 as a result of very low concentration of the protein. Commassie blue staining revealed mainly five distinct protein band. Four of this bands were the MBH large subunit HoxG (67 kDa), HoxK or the preHoxK-PsaE and preHoxK-psaD, the chaperones HoxQ (31 kDa) and HoxO (18 kDa). The identity of the bands corresponding to position (~ 39 – 40 kDa) is unclear but seems to be highly expressed in the mutant hydrogenase lacking the membrane anchor. 5 µg of all different proteins were loaded on the gel but the wild type hydrogenase revealed a higher expression of the MBH as since in the thicker band for HoxG and HoxK (Fig. 5.22). The higher expression of the chaperones and unidentified proteins in the mutant proteins is possibly due to the lack of the anchor peptide and/or proteolysis during the purification process.

Using Biorad gel documentation system the amount of Hoxk protein in the mutant strains were quantified relative to the amount of HoxK protein in the wild type since total amount of protein for all the samples were the same (Fig. 5.23). This analysis was done based on the intensities of the bands on the Western immunoblot in Figure 5.22. It is clear for Figure 5.23 that the amount of HoxK was greater in the wild type when compared o the mutant strains as a result of much higher expression of identified proteins in the mutants. Also HoxQ and HoxO formed stable complexes with the mutant strain as seen in Figure 5.22.

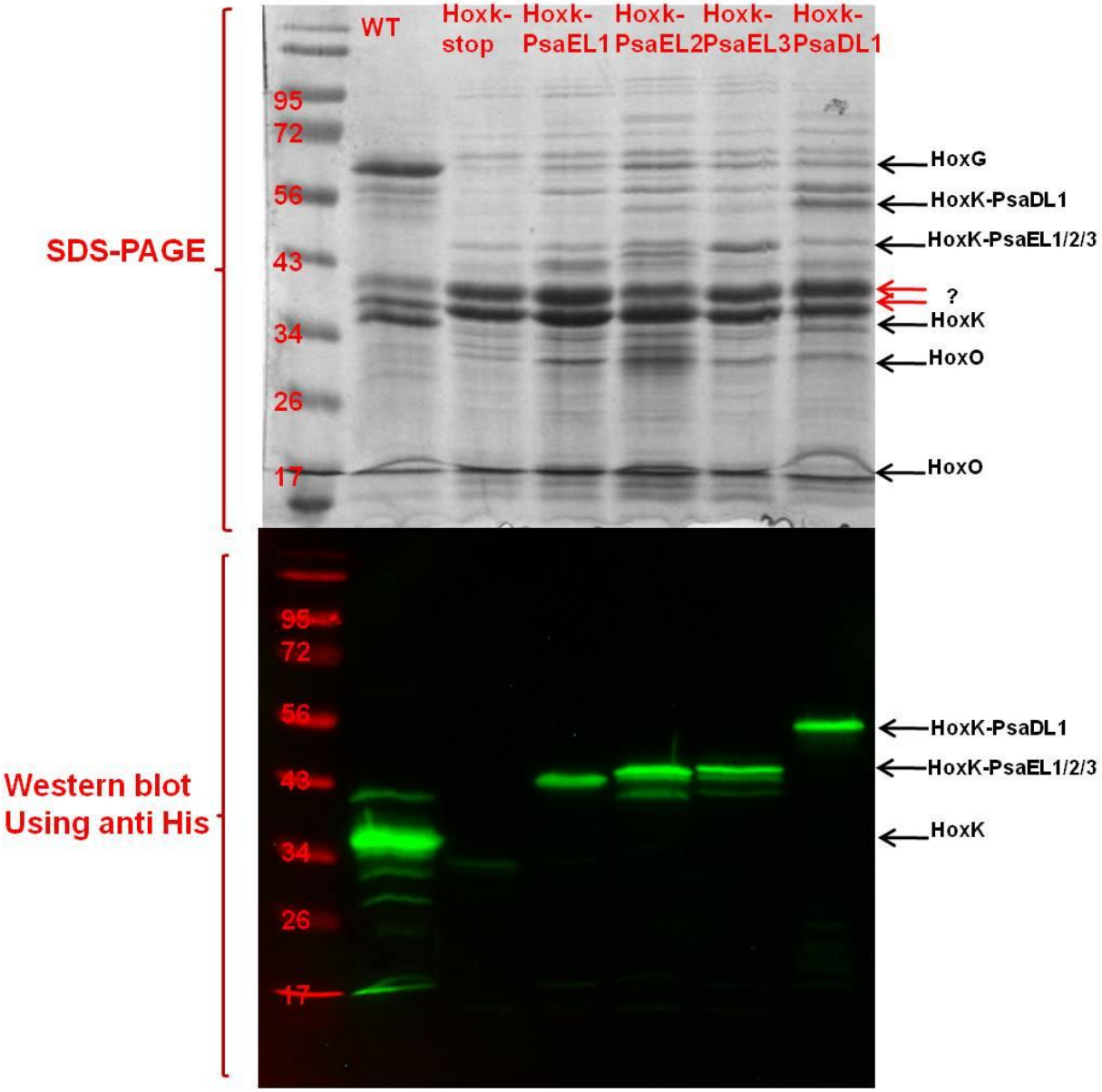


Figure 5.22 SDS- PAGE and Immunoblot analysis of purified wild type and mutant hydrogenase proteins. WT HoxK – 36 kDa, preHoxk-stop ~ 33kDa, preHoxk-PsaELinker1 ~ 44kDa, preHoxK-PsaELinker2 ~ 44kDa, preHoxK-PsaELinker3 ~ 44kDa, and preHoxK-PsaDLinker3 ~ 51kDa.

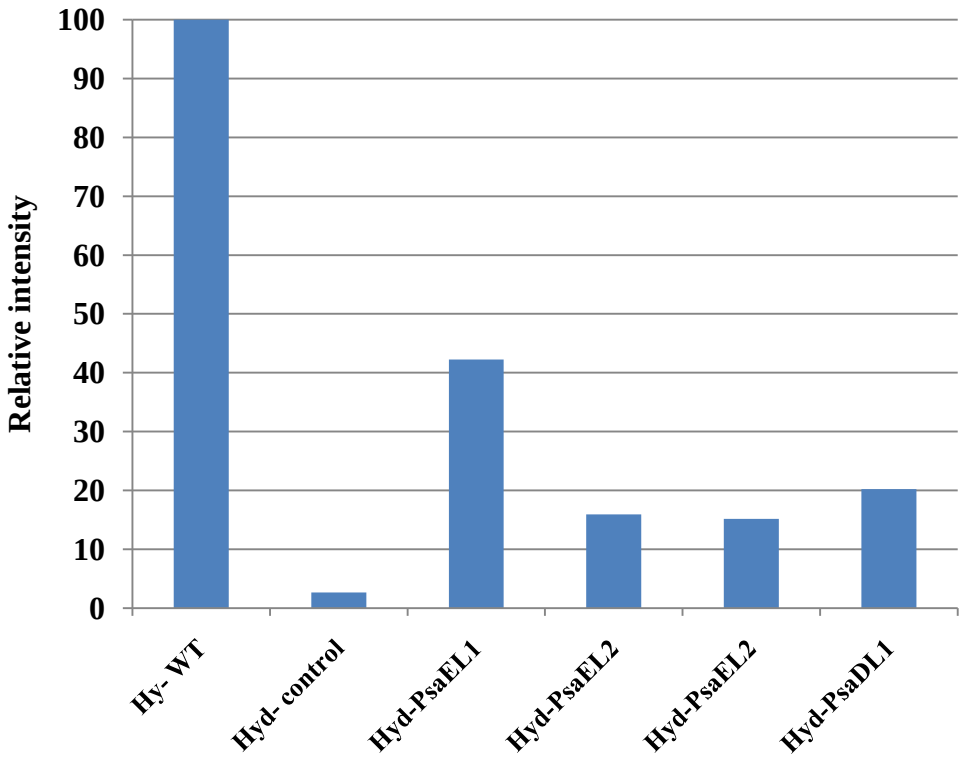


Figure 5.23 Relative intensities of HoxK proteins in Wild type and mutant strains from equal amounts of protein.

5.3.8 H_2-evolving activity on purified hydrogenase fusion proteins

The H_2 evolution activities of the MBH variants were determined using dithionite-reduced methyl viologen as the electron donor. H_2 was measured by withdrawing 100 µl aliquots from the gas phase and subsequently analyzing it with a 5890 Series III (HP) GC gas chromatograph as shown in Figure 5.24. The rate of H_2 production was calculated from the slop of the plot. In Figure 5.25, hydrogenase activity was measured for equal amounts of whole cells for the wild type and mutant strains. The mutant strains showed low hydrogenase activity which was two orders of magnitude lower than the wild type hydrogenase. Also the control strain carrying wild type hydrogenase but lacking the HoxK anchor also showed lower hydrogenase activity when compared to the wild type. Similar trend was observed in the hydrogenase activity from purified wild type and mutants proteins (Table 5.4 and Figure 5.26). The wild type hydrogenase had two orders of magnitude more H_2 evolving activity than all the hydrogenase fusion proteins and even the control protein (hyd-stop) all lacking the HoxK C-terminal anchor. The more heterogeneous protein content from mutant hydrogenase must have contributed to this observation. As seen in Figure 5.22, the wild type hydrogenase expressed more HoxK and HoxG protein per mg of protein when compared to the mutant hydrogenases. Since similar trend was observed in H_2 evolving activity from whole cells, the removal of the C-terminal anchor peptide may have affected the expression of the hydrogenase protein and probably the activity. It has been reported that maturation was severely delayed in mutants with modified C-terminus of the small subunit leading to ineffective removal of the chaperones HoxO and HoxQ from the premature hybrid protein, which in turn prevents membrane translocation [192]. The rates presented here is 30 times lower in the wild type hydrogenase and almost three orders of magnitude in mutant hydrogenase when compared to literature [192]. Although H_2-evolving activity was measured using an inversely polarized Clark-type electrode, the fact that an over-expression strain (*R. eutropha* HF632) was used for the expression of the hyd-PsaE fusion protein played a role in the higher activity reported. Membrane fractions from the over-expression strain have been shown to have about four fold higher levels of MBH activity than from extracts of the megaplasmid harboring strain (*R. eutropha* HF387) lacking the soluble hydrogenase [81]. In this work, *R. eutropha* HF387 was used as a host for conjugal gene transfer. Corrected activity based on the relative amounts of HoxK protein in the wild type and mutants is

shown in Figure 5.26 and Table 5.5. The activities showed similar trends with hyd-PsaEL1 showing the lowest activity.

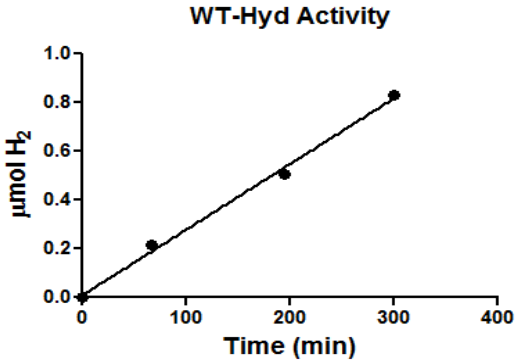


Figure 5.24 Sodium dithionite reduced methyl viologen hydrogen activity assay. H_2 was measured by withdrawing 100 µl aliquots from the gas phase and subsequently analyzing it with a Shimadzu GC gas chromatograph. The rate of H_2 production was calculated from the slop of the plot.

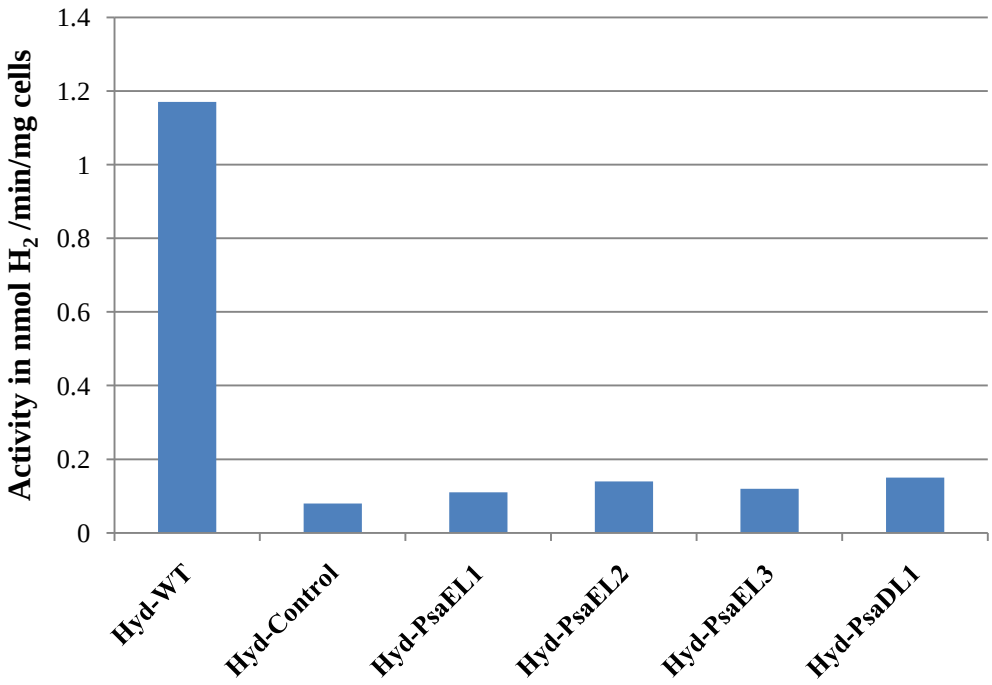


Figure 5.25 H_2 evolution activities of from wild type cells and mutants cells of *R. eutropha*.

Table 5.4 H_2 evolution activities of hydrogenase fusion proteins from the soluble extract compared to wild type MBH purified from the membrane.

Protein	**Activity nmol H_2 /min/mg protein**	**Normalized by Hyd-WT**	**Normalized by Hyd-control**	**Schwarze *et al* nmol H_2 /min/mg protein**
Hyd-WT	16.19	1.000	44.972	500
Hyd-Control	0.36	0.022	1.000	300
Hyd-PsaEL1	0.26	0.016	0.722	210
Hyd-PsaEL2	0.68	0.042	1.889	-
Hyd-PsaEL3	0.52	0.032	1.444	-
Hyd-PsaDL1	0.4	0.025	1.111	-

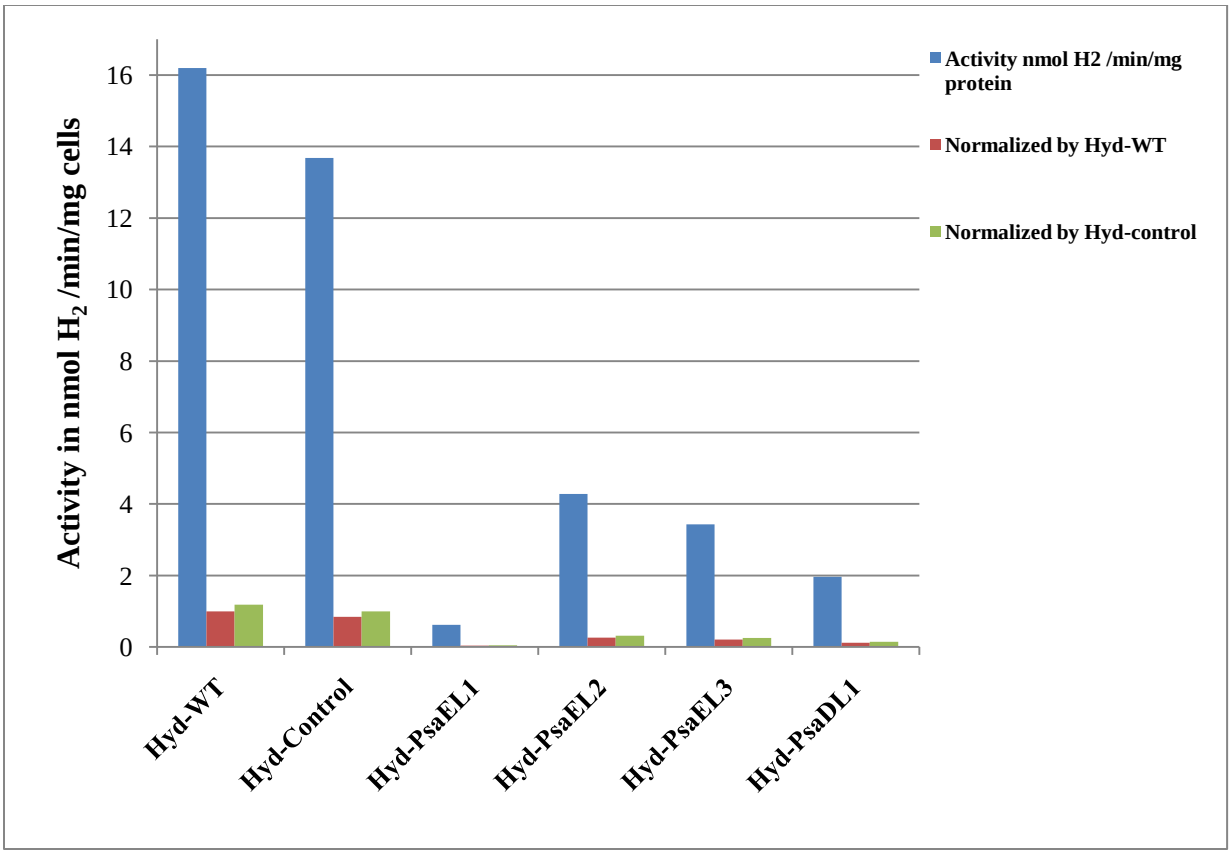


Figure 5.26 Bar graphs of the corrected H_2 evolution activities of hydrogenase fusion proteins compared to wild type MBH purified from the soluble extract of from the membrane.

Table 5.5 Corrected H_2 evolution activities of hydrogenase fusion proteins compared to wild type MBH purified from the soluble extract of from the membrane.

Protein	**Activity nmol H_2 /min/mg protein**	**Normalized by Hyd-WT**	**Normalized by Hyd-control**
Hyd-WT	16.19	1.000	1.183
Hyd-Control	13.68	0.845	1
Hyd-PsaEL1	0.624	0.039	0.046
Hyd-PsaEL2	4.284	0.265	0.313
Hyd-PsaEL3	3.432	0.212	0.251
Hyd-PsaDL1	1.96	0.121	0.143

5.4 Summary

The formation of a fusion between the MBH of *R.eutropha* and PsaE and PsaD subunits of *T. elongatus* PSI (hyd-PsaElinker1, hyd-PsaElinker2, hyd-PsaElinker3 and hyd-PsaDlinker1 has been formed). These proteins have been purified via a one step immobilized metal affinity chromatography of the soluble extracts. The hybrid proteins were catalytically active but displayed low H_2 evolution rate when compared to the wild type MBH. The hydrogenase activity of the hyd-PsaE fusion protein strain has been reported in the literature to be only 16% of that from the wild type hydrogenase protein [77]. The deletion of the small subunit membrane anchor was previously examined by Gross and co-workers [207], they reported a significant reduction in the hydrogenase activity to approximately 10%. The C-terminus small subunit structure lies adjacent to the distal Fe-S clusters and is thought to play an important role to regulate their redox potential[208]. The mutation at the C-terminus in hyd-PsaE, hyd-PsaD and hyd-stop might induce structural changes leading to significant change in the redox potential of the Fe-S clusters. Also mutant analysis showed that HoxO and HoxQ interacted with a HoxK version that lacks the C-terminal anchor peptide supporting the notion that these chaperones were associated with the signal peptide and that modifications in the C-terminal anchor peptide strongly affected the Tat- translocation efficiency of the MBH heterodimer [192]. This contaminating premature MBH forms yielded heterogeneous preHoxG-HoxK-PsaE fusion protein resulting in lower hydrogenase specific activity. A purification strategy that will allow efficient removal of the contaminating premature MBH forms has been reported [192]. HoxQ was equipped with a *His*-tag and the HoxK-PsaE protein had an additional *Strep*-tag. In a first step, soluble fractions were subjected to immobilized metal affinity chromatography allowing HoxQ complex to bind to the column. In a second step, flow through from the IMAC was loaded onto a *Strep*-Tactin Superflow column resulting in homogeneous HoxK-PsaE protein.

PsaE and PsaD subunit knockout gene has also been formed to generate PsaE-free and PsaD-free PSI T elongatus mutants. This will be used for *in vitro* reconstitution of the hydrogenase-PsaE and hydrogenase-PsaD with the PsaE-free and PsaD-free PSI to form a H_2-evolving complex. A Kan^R gene that has been codon optimized for expression in *T. elonaguts* was inserted in between the *psaE* and *psaD* gene to disrupt the expression of the protein.

Electroporation was used to introduce the modified genes into wild type *T. elongatus.* The efficiency of transformation for the electroporation was low. This may have been as a result of the presence of a putative type I restriction endonuclease, *tll2230* which when disrupted has been shown to increase the electroporation efficiency by about 5 times [120]. Colony PCR on ΔPsaD transformants showed no positive screen. Colony PCR on ΔPsaE transformants showed the presence of two species, the wild type (4086 bp) and the disrupted PsaE (5241 bp) with Kan^R gene insertion. A possible reason for this may be the presence of multiple copies of the genome which has been reported in other cyanobacterial species.

6. CONCLUSION AND FUTURE DIRECTION

6.1 Conclusion

This study have demonstrated a simple 'rewiring' of the electron transport pathway of PSI that permits a productive interface with a platinum nanoparticle catalyst. The individual components have been shown to be thermostable as well as shown enhanced hydrogen evolution rate for temperatures up to 60°C. The temporal stability of this system by its ability to evolve hydrogen for > 80 days has also been demonstrated. These properties, as well as the renewable nature of most of the key components, suggest that this mode of photosynthetic hydrogen evolution may be a sustainable source of hydrogen. Simple optimizations of this H_2 producing system have lead to rates close to those recently reported by researchers working with synthetically attached catalysts. For example, increasing the temperature to 55°C increases our rates by ~15 times which would exceed the rates of other available methods while retaining the benefit of a self-assembled system. If scaled linearly, a solar collector 1 acre in size with a solution depth of 10 cm operating at 55°C would be capable of producing a hydrogen yield with an energy equivalent to that of 300 liters of gasoline/day/hectare. This potential yield is more than an order of magnitude higher than the gasoline equivalent agricultural biomass systems such as corn based ethanol (5.43 l/day/hectare), soy based biodiesel (1.42 l/day/hectare), or projected yields of switchgrass-produced ethanol (12.1 l/day/hectare). This system is a more direct route to fuel production with no need for converting, fermenting and subsequently distilling the products of the starches and cellulose in the biomass. Moreover, other processing and transportation costs would be much lower since the bio-Pt hybrid catalyst is reused through many cycles, compared to a once-through method such as biomass accumulation and harvest.

Response surface methodology was employed to optimize the independent variables. Temperature, light intensity and platinum salt concentration on the rate of H_2 photo-production since conventional process of optimization were usually time consuming and expensive. Platinum salt concentration, temperature and the interaction between platinum salt concentration and temperature were critical factors on the total H_2 yield. Light intensity had minimal effect of the total H_2 yield within the region studied. The optimum parameters for H_2 photoproduction were at light intensity of 240 $\mu E/m^2/s$, platinum salt concentration of 600 - 650 μM and

temperature of 31^0C. Screening experiments using fractional factorial design was successfully used to determine the effect of light color (white vs. red) on the rate of H_2 production. The screening and optimization methodology used in this study represents valuable tools for the development of an optimized process for PSI dependent H_2 production.

The formation of a fusion between the MBH of *R.eutropha* and PsaE and PsaD subunits of *T. elongatus* PSI has been genetically engineered. The *psaE* and *psaD* genes from *T.* elongatus were optimized for improved expression in *R. eutropha.* These proteins have been purified via a one step immobilized metal affinity chromatography of the soluble extracts. The hybrid proteins were catalytically active but displayed low H_2 evolution rate when compared to the wild type MBH. PsaE-free and PsaD-free mutants of PSI were simultaneously formed by genetically disrupting the expression of the PsaE and PsaD subunit of a native PSI; this will allow *in vitro* reconstitution of the desired PsaE-hydrogenase and PsaD-hydrogenase fusion protein with PsaE-free and PsaD-free PSI respectively. These modified *psaE* and *psaD* gene were introduced into *T. elongatus* by electroporation. The efficiency of transformation was low and positive screen were identified only in the ΔPsaE mutants.

6.2 Future directions

Further research needs to be done to understand the formation of pt particles on PSI for H_2 evolution. High resolution TEM may provide information on the deposition of pt particles on the stromal side of PSI. Optimum conditions for the *in situ* platinization of PSI complexes need to be explored. Response surface methodology (RSM) has been shown to be an effective technique for analyzing and optimizing the pt-PSI photo-dependent H_2 production. The effect of process variables such at buffer pH, PSI concentration, PSI to cyt c_6 ratio, length of time for platinization, NaAsc concentration on the overall rate of H_2 production and the stability of the pr-PSI complexes should be researched.

Hydrogenases are a structurally and functionally diverse group of enzymes that catalyze the reversible oxidation of molecular hydrogen. [Ni-Fe] hydrogenases are the most widespread and the mechanism of their biosynthesis is currently the best understood. The metallo-clusters in

[Ni-Fe] hydrogenases are reversibly deactivated by oxygen and carbon-monoxide, although some [Ni-Fe] hydrogenases are oxygen tolerant. Inactivation by oxygen poses a great problem in the use of these enzymes in H_2 production. Structural studies of these hydrogenases will be important in directing protein engineering in rendering these enzymes oxygen tolerant. Another desirable property of [Ni-Fe] hydrogenases to be used in photo-biotechnological applications is thermal stability. Thermotolerant hydrogenases are found in thermophilic and hyperthermophilic microorganism. Studies of H_2 metabolism and regulation will also be important in engineering microorganisms at the cellular level to maximize H_2 production. It will not be surprising to find that many uncultivated species of microorganism will contain novel type of hydrogenases that has not yet been discovered, given the importance of H_2 metabolism to microorganism. Optimization of the purification of the fusion proteins and the linker lengths in this study will be important in generating homogenous hybrid proteins with ideal linker length for electron transport. A purification strategy that will allow efficient removal of the contaminating premature MBH forms needs to be employed. One strategy being to equip HoxQ with a *His*-tag and the HoxK-PsaE protein had an additional *Strep*-tag. Another strategy will be to engineer fusions between PsaE and PsaD and MBH with intact anchor region since the complex formation of HoxQ/O is as result of disrupting the membrane anchor. This strategy may also improve the hydrogenase activity since it has been well established that the disruption of the anchor region affects the transport competence of the MBH and may also result in structural changes in the protein conformation, and hence leading to reduced activity. Formation of direct fusion between the hydrogenase-PsaE and hydrogenase-PsaD with the PsaE-free and PsaD-free mutants of PSI will efficiently determine the fusion protein that will result in the optimum H_2 photo-production. Exploring not only the C-terminal fusion complexes but also N-terminal fusion complexes may lead to some interesting findings. Both wild type and mutant MBH proteins display very low expression protein levels making it difficult to characterize the protein due to limited materials. Design of an Overexpression vector for the over expression of the MBH protein in its native host or possibly in *E. coli* will be of great importance. EPR and FTIR studies on wild type and mutant MBH proteins will provide useful information on the redox states, redox transitions and the intermolecular interactions within the catalytic center [87].

Improved method for efficient electroporation of *T. elongatus* needs to be developed. It has been reported that the disruption of the gene that codes for this endonulcease in *T. elongatus* increased the electroporation efficiency by about 5 times [120]. Type I restriction endonuclease, *tll2230*, has been reported to be the only candidate for restriction endonuclease in *T. elongatus* genome based on sequence analysis [146]. Improved selection method for *T. elongatus* transconjugants need to be developed. Conjugation can also be explored for the transfer of genetic material in *T. elongatus.* Congjugal gene transfer has been successful in other cyanobacterial species.

REFERENCES

1. *International Energy Outlook 2007* Energy information administration, May 2007. **Report #:DOE/EIA-0484(2007)**.
2. Tsoskounogiou, M., G. Ayerides, and E. Tritopoulou, *The end of cheap oil: Current status and prospects.* Energy Policy, 2008. **36**(10): p. 3797-3806.
3. Kruse, O., et al., *Photosynthesis: a blueprint for solar energy capture and biohydrogen production technologies.* Photochemical & Photobiological Sciences, 2005. **4**(12): p. 957-970.
4. Das, D. and T.N. Veziroglu, *Hydrogen production by biological processes: a survey of literature.* International Journal of Hydrogen Energy, 2001. **26**(1): p. 13-28.
5. Pakes, W.C.C. and W.H. Jollyman, *The bacterial decompostion of formic acid into carbon dioxide and hydrogen.* J. Chem. Soc., 1901. **79**: p. 386-391.
6. Gaffron, H., *Reduction of carbon monoxide with molecular hydrogen in green algae.* Nature, 1939. **143**: p. 204-205.
7. Gaffron, H., *Carbon dioxide reduction with molecular hydrogen in green algae.* American Journal of Botany, 1940. **27**: p. 273-283.
8. Stuart, T.S. and H. Gaffron, *Mechanism of Hydrogen Photoproduction by Several Algae .2. Contribution of Photosystem-Ii.* Planta, 1972. **106**(2): p. 101-&.
9. Greenbaum, E., *Photosynthetic Unit of Hydrogen Evolution.* Science, 1977. **196**(4292): p. 879-880.
10. Greenbaum, E., *Simultaneous Photoproduction of Hydrogen and Oxygen by Photosynthesis.* Biotechnology and Bioengineering, 1980. **22**: p. 1-13.
11. Gest, H., *Properties of cell-free hydrogenases of Escherichia coli and Rhodospirillum rubrum.* Journal of Bacteriology, 1952. **63**(1): p. 111-121.
12. Ghirardi, M.L., et al., *Hydrogenases and hydrogen photoproduction in oxygenic photosynthetic organisms.* Annual Review of Plant Biology, 2007. **58**: p. 71-91.
13. Fay P., V.B.C., ed. *The Cyanobacteria*. 1987, Elsevier Sci. Publ.: Amsterdam. 1 - 27.
14. Maeda, T., V. Sanchez-Torres, and T.K. Wood, *Escherichia coli hydrogenase 3 is a reversible enzyme possessing hydrogen uptake and synthesis activities.* Applied Microbiology and Biotechnology, 2007. **76**(5): p. 1035-1042.

15. Frenkel, A., H. Gaffron, and E.H. Battley, *Photosynthesis and Photoreduction by the Blue Green Alga, Synechococcus Elongatus, NÃ¤g.* Biological Bulletin, 1950. **99**(2): p. 157-162.
16. Fujita, Y., H. Ohama, and A. Hattori, *HYDROGENASE ACTIVITY OF CELL-FREE PREPARATION OBTAINED FROM THE BLUE-GREEN ALGA, ANABAENA CYLINDRICA*. 1964. p. 305-314.
17. Ward, M.A., *Whole cell and cell-free hydrogenases of algae.* Phytochemistry, 1970. **9**(2): p. 259-266.
18. Asada, Y. and S. Kawamura, *Hydrogen Evolution by Microcystis-Aeruginosa in Darkness.* Agricultural and Biological Chemistry, 1984. **48**(10): p. 2595-2596.
19. Asada, Y. and S. Kawamura, *Screening for cyanobacteria that evolve molecular hydrogen under dark and anaerobic conditions.* Journal of Fermentation Technology, 1986. **64**(6): p. 553-556.
20. Peschek, G.A., *Anaerobic hydrogenase activity in Anacystis nidulans H2-dependent photoreduction and related reactions.* Biochimica et Biophysica Acta (BBA) - Bioenergetics, 1979. **548**(2): p. 187-202.
21. Hartman, H. and A.I. Krasna, *Studies on Adaptation of Hydrogenase in Scenedesmus.* Journal of Biological Chemistry, 1963. **238**(2): p. 749-&.
22. Frenkel, A.W. and C. Rieger, *Photoreduction in Algae.* Nature, 1951. **167**(4260): p. 1030-1030.
23. Kessler, E., ed. *Algal Physiology and Biochemistry*. 1974, Blackwell, Oxford: Berkeley and Los Angeles, Carlifornia. 454 - 473.
24. Gogotov, I.N., N.A. Zorin, and E.N. Kondrateva, *Purification and Properties of Hydrogenase from Phototropic Bacterium Thiocapsa-Roseopersicina.* Biochemistry-Moscow, 1976. **41**(5): p. 685-690.
25. Ormerod, J.G. and H. Gest, *Symposium on Metabolism of Inorganic Compounds .4. Hydrogen Photosynthesis and Alternative Metabolic Pathways in Photosynthetic Bacteria.* Bacteriological Reviews, 1962. **26**(1): p. 51-&.

26. Klemme, J.H., *Studies on Photoautotrophic Growth of New Isolated Nonsulfur Purple Bacteria at Expense of Molecular Hydrogen.* Archiv Fur Mikrobiologie, 1968. **64**(1): p. 29-&.
27. N. Pfenning, N.G.T., *The Phototrophic Bacteria*, in *Bergeys Manual of Determinative bacteriology*. 1974, William and Wilkins: Baltimore. p. 24 - 64.
28. Hoare, D.S. and S.L. Hoare, *Hydrogen Metabolism by Rhodomicrobium Vannielii.* Journal of Bacteriology, 1969. **100**(2): p. 1124-&.
29. Maness, P.-C., et al., *Characterization of the Oxygen Tolerance of a Hydrogenase Linked to a Carbon Monoxide Oxidation Pathway in Rubrivivax gelatinosus*. 2002. p. 2633-2636.
30. Repaske, R., *Electron Transport System of Hydrogenomonas Eutropha .1. Diphosphopyridine Nucleotide Reduction by Hydrogen.* Journal of Biological Chemistry, 1962. **237**(4): p. 1351-&.
31. Stephenson, M. and L.H. Stickland, *Hydrogenase: A bacterial enzyme activating molecular hydrogen. I. The properties of the enzyme.* Biochemical Journal, 1931. **25**(1): p. 205-214.
32. Yagi, T., M. Honya, and N. Tamiya, *Purification and Properties of Hydrogenases of Different Origins.* Biochimica Et Biophysica Acta, 1968. **153**(3): p. 699-&.
33. Parkin, A., et al., *The Difference a Se Makes? Oxygen-Tolerant Hydrogen Production by the [NiFeSe]-Hydrogenase from Desulfomicrobium baculatum.* Journal of the American Chemical Society, 2008. **130**(40): p. 13410-13416.
34. Korkes, S., *Enzymatic Reduction of Pyridine Nucleotides by Molecular Hydrogen.* Journal of Biological Chemistry, 1955. **216**(2): p. 737-748.
35. Hyndman, L.A., R.H. Burris, and P.W. Wilson, *Properties of Hydrogenase from Azotobacter-Vinelandii.* Journal of Bacteriology, 1953. **65**(5): p. 522-531.
36. Dixon, R.O.D., *Hydrogen Uptake and Exchange by Pea Root Nodules.* Annals of Botany, 1967. **31**(121): p. 179-&.
37. Bryant, M.P., B.C. McBride, and R.S. Wolfe, *Hydrogen-Oxidizing Methane Bacteria .I. Cultivation and Methanogenesis.* Journal of Bacteriology, 1968. **95**(3): p. 1118-&.

38. Vignais, P.M. and A. Colbeau, *Molecular biology of microbial hydrogenases.* Current Issues in Molecular Biology, 2004. **6**: p. 159-188.
39. Fontecilla-Camps, J.C., et al., *Structure/Function Relationships of [NiFe]- and [FeFe]-Hydrogenases.* Chemical Reviews, 2007. **107**(10): p. 4273-4303.
40. Volbeda, A., et al., *Crystal-Structure of the Nickel-Iron Hydrogenase from Desulfovibrio-Gigas.* Nature, 1995. **373**(6515): p. 580-587.
41. Florin, L., A. Tsokoglou, and T. Happe, *A novel type of iron hydrogenase in the green alga Scenedesmus obliquus is linked to the photosynthetic electron transport chain.* Journal of Biological Chemistry, 2001. **276**(9): p. 6125-6132.
42. Adams, M.W.W., *The structure and mechanism of iron-hydrogenases.* Biochimica et Biophysica Acta (BBA) - Bioenergetics, 1990. **1020**(2): p. 115-145.
43. Carmen, Z., et al., *H₂-forming methylenetetrahydromethanopterin dehydrogenase, a novel type of hydrogenase without iron-sulfur clusters in methanogenic archaea*. 1992. p. 511-520.
44. Seigo, S., et al., *The Cofactor of the Iron-Sulfur Cluster Free Hydrogenase Hmd: Structure of the Light-Inactivation Product13*. 2004. p. 2547-2551.
45. Shima, S., et al., *Mossbauer Studies of the Iron-Sulfur Cluster-Free Hydrogenase: The Electronic State of the Mononuclear Fe Active Site.* Journal of the American Chemical Society, 2005. **127**(29): p. 10430-10435.
46. Lyon, E.J., et al., *Carbon Monoxide as an Intrinsic Ligand to Iron in the Active Site of the Iron-Sulfur-Cluster-Free Hydrogenase H2-Forming Methylenetetrahydromethanopterin Dehydrogenase As Revealed by Infrared Spectroscopy.* Journal of the American Chemical Society, 2004. **126**(43): p. 14239-14248.
47. Korbas, M., et al., *The Iron-Sulfur Cluster-free Hydrogenase (Hmd) Is a Metalloenzyme with a Novel Iron Binding Motif*. 2006. p. 30804-30813.
48. Pilak, O., et al., *The Crystal Structure of the Apoenzyme of the Iron-Sulphur Cluster-free Hydrogenase.* Journal of Molecular Biology, 2006. **358**(3): p. 798-809.
49. Greenbaum, E., *Platinized Chloroplasts - a Novel Photocatalytic Material.* Science, 1985. **230**(4732): p. 1373-1375.

50. Greenbaum, E., *Energetic efficiency of hydrogen photoevolution by algal water splitting.* Biophysical Journal, 1988. **54**(2): p. 365-368.
51. Iwuchukwu, I.J., et al., *Self-organized photosynthetic nanoparticle for cell-free hydrogen production.* Nat Nano. **5**(1): p. 73-79.
52. Asada, Y. and J. Miyake, *Photobiological hydrogen production.* Journal of Bioscience and Bioengineering, 1999. **88**(1): p. 1-6.
53. Paula, T., et al., *Cyanobacterial hydrogenases: diversity, regulation and applications*. 2007. p. 692-720.
54. Garcin, E., et al., *The crystal structure of a reduced [NiFeSe] hydrogenase provides an image of the activated catalytic center.* Structure, 1999. **7**(5): p. 557-566.
55. Vignais, P.M., B. Billoud, and J. Meyer, *Classification and phylogeny of hydrogenases.* Fems Microbiology Reviews, 2001. **25**(4): p. 455-501.
56. Vignais, P.M. and B. Billoud, *Occurrence, classification, and biological function of hydrogenases: An overview.* Chemical Reviews, 2007. **107**(10): p. 4206-4272.
57. Brugna-Guiral, M., et al., *[NiFe] hydrogenases from the hyperthermophilic bacterium Aquifex aeolicus: properties, function, and phylogenetics.* Extremophiles, 2003. **7**(2): p. 145-157.
58. Rakhely, G., et al., *Cyanobacterial-type, heteropentameric, NAD(+)-reducing NiFe hydrogenase in the purple sulfur photosynthetic bacterium Thiocapsa roseopersicina.* Applied and Environmental Microbiology, 2004. **70**(2): p. 722-728.
59. Burgdorf, T., et al., *[NiFe]-hydrogenases of Ralstonia eutropha H16: Modular enzymes for oxygen-tolerant biological hydrogen oxidation.* Journal of Molecular Microbiology and Biotechnology, 2005. **10**(2-4): p. 181-196.
60. Gross, R., J. Simon, and A. Kroger, *The role of the twin-arginine motif in the signal peptide encoded by the hydA gene of the hydrogenase from Wolinella succinogenes.* Archives of Microbiology, 1999. **172**(4): p. 227-232.
61. Buhrke, T., et al., *Oxygen tolerance of the H-2-sensing [NiFe] hydrogenase from Ralstonia eutropha H16 is based on limited access of oxygen to the active site.* Journal of Biological Chemistry, 2005. **280**(25): p. 23791-23796.

62. De Lacey, A.L., et al., *Activation and inactivation of hydrogenase function and the catalytic cycle: Spectroelectrochemical studies.* Chemical Reviews, 2007. **107**(10): p. 4304-4330.
63. Volbeda, A., et al., *Structural differences between the ready and unready oxidized states of [NiFe] hydrogenases (vol 10, pg 239, 2005).* Journal of Biological Inorganic Chemistry, 2005. **10**(5): p. 591-591.
64. Schnackenberg, J., et al., *In vitro and in vivo coupling of Thiocapsa hydrogenase with cyanobacterial and algal electron mediators.* Journal of Bioscience and Bioengineering, 1999. **88**(1): p. 30-34.
65. Reisner, E., et al., *Visible Light-Driven H2 Production by Hydrogenases Attached to Dye-Sensitized TiO2 Nanoparticles.* Journal of the American Chemical Society, 2009. **131**(51): p. 18457-18466.
66. Kanai, T., S. Ito, and T. Imanaka, *Characterization of a cytosolic NiFe-hydrogenase from the hyperthermophilic archaeon Thermococcus kodakaraensis KOD1*. Journal of Bacteriology, 2003. **185**(5): p. 1705-1711.
67. Ma, K., R. Weiss, and M.W.W. Adams, *Characterization of Hydrogenase II from the Hyperthermophilic Archaeon Pyrococcus furiosus and Assessment of Its Role in Sulfur Reduction*. 2000. p. 1864-1871.
68. Burgdorf, T., A.L. De Lacey, and B. Friedrich, *Functional analysis by site-directed mutagenesis of the NAD(+)-reducing hydrogenase from Ralstonia eutropha.* Journal of Bacteriology, 2002. **184**(22): p. 6280-6288.
69. Cournac, L., et al., *Sustained photoevolution of molecular hydrogen in a mutant of Synechocystis sp strain PCC 6803 deficient in the type I NADPH-dehydrogenase complex.* Journal of Bacteriology, 2004. **186**(6): p. 1737-1746.
70. Serebryakova, L.T., N.A. Zorin, and I.N. Gogotov, *Purification and Properties of Hydrogenase Bound to Chromatophores from Phototropic Bacterium Thiocapsa-Roseopersicina.* Biochemistry-Moscow, 1977. **42**(4): p. 571-575.
71. Sasikala, K., Ramana, ChV., Rao, P. R., and Kovacs, K. L., *Anoxygenic photosynthesis bacteria: physiology and advances in hydrogen production technology*. Advances in Applied Microbiology. Vol. 38. 1993: Academic Press Inc. 211 - 215.

72. Kovacs, K.L., et al., *The hydrogenases of Thiocapsa roseopersicina.* Biochemical Society Transactions, 2005. **33**: p. 61-63.
73. Kim, M.S., E.H. Choi, and Y.K. Oh, *Characterization of hydrogenase from purple sulfur bacterium Thiocapsa roseopeysicina and its prolonged in vitro hydrogen evolution.* International Journal of Hydrogen Energy, 2008. **33**(5): p. 1496-1502.
74. Kovacs, K.L., et al., *Hydrogenases, accessory genes and the regulation of [NiFe] hydrogenase biosynthesis in Thiocapsa roseopersicina.* International Journal of Hydrogen Energy, 2002. **27**(11-12): p. 1463-1469.
75. Rakhely, G., et al., *Unusual organization of the genes coding for HydSL, the stable [NiFe]hydrogenase in the photosynthetic bacterium Thiocapsa roseopersicina BBS.* Journal of Bacteriology, 1998. **180**(6): p. 1460-1465.
76. Mura, G.M., et al., *The [Ni-Fe] hydrogenase from the thermophilic bacterium Acetomicrobium flavidum*. 1996. p. 829-836.
77. Ihara, M., et al., *Light-driven hydrogen production by a hybrid complex of a [NiFe]-hydrogenase and the cyanobacterial photosystem I.* Photochemistry and Photobiology, 2006. **82**(3): p. 676-682.
78. Adams, M.W.W., L.E. Mortenson, and J.S. Chen, *Hydrogenase.* Biochimica Et Biophysica Acta, 1980. **594**(2-3): p. 105-176.
79. Friedrich, C.G. and B. Friedrich, *Regulation of Hydrogenase Formation Is Temperature Sensitive and Plasmid Coded in Alcaligenes-Eutrophus.* Journal of Bacteriology, 1983. **153**(1): p. 176-181.
80. Zimmer, D., et al., *Temperature Tolerance of Hydrogenase Expression in Alcaligenes-Eutrophus Is Conferred by a Single Amino-Acid Exchange in the Transcriptional Activator Hoxa.* Journal of Bacteriology, 1995. **177**(9): p. 2373-2380.
81. Lenz, O., et al., *Requirements for heterologous production of a complex metalloenzyme: the membrane-bound [NiFe] hydrogenase.* Journal of Bacteriology, 2005. **187**(18): p. 6590-6595.
82. Schubert, T., et al., *Chaperones specific for the membrane-bound [NiFe]-hydrogenase interact with the Tat signal peptide of the small subunit precursor in Ralstonia eutropha H16.* Molecular Microbiology, 2007. **66**(2): p. 453-467.

83. Bernhard, M., et al., *Functional and structural role of the cytochrome b subunit of the membrane-bound hydrogenase complex of Alcaligenes eutrophus H16.* European Journal of Biochemistry, 1997. **248**(1): p. 179-186.
84. Schink, B. and H.G. Schlegel, *Membrane-Bound Hydrogenase of Alcaligenes-Eutrophus .1. Solubilization, Purification, and Biochemical-Properties.* Biochimica Et Biophysica Acta, 1979. **567**(2): p. 315-324.
85. Goldet, G., et al., *Hydrogen production under aerobic conditions by membrane-bound hydrogenases from Ralstonia species.* Journal of the American Chemical Society, 2008. **130**(33): p. 11106-11113.
86. Schwartz, E., et al., *Complete nucleotide sequence of pHG1: A Ralstonia eutropha H16 megaplasmid encoding key enzymes of H-2-based lithoautotrophy and anaerobiosis.* Journal of Molecular Biology, 2003. **332**(2): p. 369-383.
87. Saggu, M., et al., *Spectroscopic Insights into the Oxygen-tolerant Membrane-associated [NiFe] Hydrogenase of Ralstonia eutropha H16.* Journal of Biological Chemistry, 2009. **284**(24): p. 16264-16276.
88. Ludwig, M., et al., *Oxygen-tolerant H-2 Oxidation by Membrane-bound [NiFe] Hydrogenases of Ralstonia Species COPING WITH LOW LEVEL H-2 IN AIR.* Journal of Biological Chemistry, 2009. **284**(1): p. 465-477.
89. Weaver, P.F., S. Lien, and M. Seibert, *Photobiological Production of Hydrogen.* Solar Energy, 1980. **24**(1): p. 3-45.
90. Greenbaum, E., *Photosynthetic hydrogen and oxygen production- Kinetic studies.* Science, 1982. **215**(4530): p. 291-293.
91. Greenbaum, E., R.R.L. Guillard, and W.G. Sunda, *Hydrogen and oxygen photoproduction by marine algae.* Photochemistry and Photobiology, 1983. **37**(6): p. 649-655.
92. Maione, T.E. and M. Gibbs, *Hydrogenase-mediated activities in isolated chloroplasts of Chlamydomonas reinhardii.* Plant Physiology, 1986. **80**(2): p. 360-363.
93. Stuart, T.S. and H. Gaffron, *Kinetics of hydrogen photoproduction by adapted Scenedesmus.* Planta, 1971. **100**(3): p. 228-&.

94. Stuart, T.S. and H. Gaffron, *Kinetics of H2 photoproduction by Scenedesmus.* Plant Physiology, 1971. **47**: p. 32-&.

95. Stuart, T.S. and H. Gaffron, *Mechanism of hydrogen photoproduction by several algae 2. Contribution of photosystem II.* Planta, 1972. **106**(2): p. 101-&.

96. Stuart, T.S. and H. Gaffron, *Mechanism of hydrogen photoproduction by several algae 1. Effect of inhibitors of photophosphorylation.* Planta, 1972. **106**(2): p. 91-&.

97. Benemann, J.R., et al., *Hydrogen Evolution by a Chloroplast-Ferredoxin-Hydrogenase System.* Proc Natl Acad Sci U S A, 1973. **70**(8): p. 2317-2320.

98. Melis, A., et al., *Sustained photobiological hydrogen gas production upon reversible inactivation of oxygen evolution in the green alga Chlamydomonas reinhardtii.* Plant Physiology, 2000. **122**(1): p. 127-135.

99. Melis, A., *Photosynthetic H2 metabolism in Chlamydomonas reinhardtii (unicellular green algae).* Planta, 2007. **226**(5): p. 1075-86.

100. Lee, I., et al., *Measurement of electrostatic potentials above oriented single photosynthetic reaction centers.* Journal of Physical Chemistry B, 2000. **104**(11): p. 2439-2443.

101. Brettel, K., *Electron transfer and arrangement of the redox cofactors in photosystem I.* Biochimica Et Biophysica Acta-Bioenergetics, 1997. **1318**(3): p. 322-373.

102. Zankel, K.L., D.W. Reed, and R.K. Clayton, *Fluorescence and Photochemical Quenching in Photosynthetic Reaction Centers.* Proceedings of the National Academy of Sciences of the United States of America, 1968. **61**(4): p. 1243-&.

103. Hiyama, T., *Quantum Yield and Requirement for the Photooxidation of P-700.* Physiologie Vegetale, 1985. **23**(5): p. 605-610.

104. Evans, B.R., et al., *Enhanced photocatalytic hydrogen evolution by covalent attachment of plastocyanin to photosystem I.* Nano Letters, 2004. **4**(10): p. 1815-1819.

105. Millsaps, J.F., et al., *Nanoscale photosynthesis: Photocatalytic production of hydrogen by platinized photosystem I reaction centers.* Photochemistry and Photobiology, 2001. **73**(6): p. 630-635.

106. Ihara, M., et al., *Photoinduced hydrogen production by direct electron transfer from photosystem I cross-linked with cytochrome c(3) to [NiFe]-hydrogenase.* Photochemistry and Photobiology, 2006. **82**(6): p. 1677-1685.
107. Greenbaum, E., *Interfacial photoreactions at the photosynthetic membrane interface: an upper limit for the number of platinum atoms required to form a hydrogen-evolving platinum metal catalyst.* The Journal of Physical Chemistry, 1988. **92**(16): p. 4571-4574.
108. Lee, J.W., R.T. Collins, and E. Greenbaum, *Molecular Ionic Probes: A New Class of Hill Reagents and Their Potential for Nanofabrication and Biometallocatalysis.* The Journal of Physical Chemistry B, 1998. **102**(11): p. 2095-2100.
109. Grimme, R.A., et al., *Photosystem I/molecular wire/metal nanoparticle bioconjugates for the photocatalytic production of H-2.* Journal of the American Chemical Society, 2008. **130**(20): p. 6308 - 6308.
110. Grimme, R.A., C.E. Lubner, and J.H. Golbeck, *Maximizing H-2 production in Photosystem I/dithiol molecular wire/platinum nanoparticle bioconjugates.* Dalton Transactions, 2009(45): p. 10106-10113.
111. Krassen, H., et al., *Photosynthetic Hydrogen Production by a Hybrid Complex of Photosystem I and [NiFe]-Hydrogenase.* ACS Nano, 2009. **3**(12): p. 4055-4061.
112. Krassen, H., et al., *Immobilization of the [FeFe]-hydrogenase CrHydA1 on a gold electrode: Design of a catalytic surface for the production of molecular hydrogen.* Journal of Biotechnology, 2009. **142**(1): p. 3-9.
113. Lubner, C.E., et al., *Wiring Photosystem I for Direct Solar Hydrogen Production.* Biochemistry. **49**(3): p. 404-414.
114. McTavish, H., *Hydrogen Evolution by Direct Electron Transfer from Photosystem I to Hydrogenases*. 1998. p. 644-649.
115. Arnon, D.I., A. Paneque, and A. Mitsui, *Photoproduction of Hydrogen Gas Coupled with Potosynthetic Phosphorylation.* Science, 1961. **134**(348): p. 1425-&.
116. Qian, D.J., et al., *Photoinduced hydrogen evolution in an artificial system containing photosystem I, hydrogenase, methyl viologen and mercaptoacetic acid.* Chinese Chemical Letters, 2008. **19**(5): p. 607-610.

117. Fromme, P., P. Jordan, and N. Krauss, *Structure of photosystem I.* Biochim Biophys Acta, 2001. **1507**(1-3): p. 5-31.

118. Jordan, P., et al., *Three-dimensional structure of cyanobacterial photosystem I at 2.5 A resolution.* Nature, 2001. **411**(6840): p. 909-17.

119. Onai, K., et al., *Natural transformation of the thermophilic cyanobacterium Thermosynechococcus elongatus BP-1: a simple and efficient method for gene transfer.* Molecular Genetics and Genomics, 2004. **271**(1): p. 50-59.

120. Iwai, M., et al., *Improved genetic transformation of the thermophilic cyanobacterium, Thermosynechococcus elongatus BP-1.* Plant and Cell Physiology, 2004. **45**(2): p. 171-175.

121. Sambongi, Y., et al., *Cytochrome c from a thermophilic bacterium has provided insights into the mechanisms of protein maturation, folding, and stability.* European Journal of Biochemistry, 2002. **269**(14): p. 3355-3361.

122. Fontana, A., *Analysis and modulation of protein stability.* Curr Opin Biotechnol, 1991. **2**(4): p. 551-60.

123. Fromme, P., et al., *Structure and function of photosystem I: interaction with its soluble electron carriers and external antenna systems.* FEBS Letters, 2003. **555**(1): p. 40-44.

124. Grotjohann, I. and P. Fromme, *Structure of cyanobacterial Photosystem I.* Photosynthesis Research, 2005. **85**(1): p. 51-72.

125. Ke, B., R.E. Hansen, and H. Beinert, *Oxidation-Reduction Potentials of Bound Iron-Sulfur Proteins of Photosystem I.* Proceedings of the National Academy of Sciences of the United States of America, 1973. **70**(10): p. 2941-2945.

126. Heathcote, P., et al., *Role of Membrane-Bound Iron-Sulfur Centers-a and Centers-B in Photosystem-I Reaction Center of Spinach-Chloroplasts.* Biochimica Et Biophysica Acta, 1978. **503**(2): p. 333-342.

127. Parrett, K.G., et al., *Purification and Properties of the Intact P-700 and Fx-Containing Photosystem-I Core Protein.* Biochimica Et Biophysica Acta, 1989. **973**(2): p. 324-332.

128. Li, N., et al., *Polypeptide Composition of the Photosystem-I Complex and the Photosystem-I Core Protein from Synechococcus Sp Pcc-6301.* Biochimica Et Biophysica Acta, 1991. **1059**(2): p. 215-225.

129. Golbeck, J.H., et al., *Isolation of the Intact Photosystem-I Reaction Center Core Containing P700 and Iron-Sulfur Center Fx.* Febs Letters, 1988. **228**(2): p. 268-272.

130. Parrett, K.G., T. Mehari, and J.H. Golbeck, *Resolution and Reconstitution of the Cyanobacterial Photosystem-I Complex.* Biochimica Et Biophysica Acta, 1990. **1015**(2): p. 341-352.

131. Golbeck, J.H., et al., *Reconstitution of the Photosystem-I Complex from the P700 and Fx-Containing Reaction Center Core Protein and the Fa/Fb Polypeptide.* Febs Letters, 1988. **240**(1-2): p. 9-14.

132. Zhao, J.D., et al., *Site-Directed Conversion of a Cysteine to Aspartate Leads to the Assembly of a [3fe-4s] Cluster in Psac of Photosystem-I - the Photoreduction of Fa Is Independent of Fb.* Biochemistry, 1992. **31**(22): p. 5093-5099.

133. Li, N., et al., *Psad Is Required for the Stable Binding of Psac to the Photosystem-I Core Protein of Synechococcus-Sp Pcc-6301.* Biochemistry, 1991. **30**(31): p. 7863-7872.

134. Yang, F., et al., *Deletion of the PsaF polypeptide modifies the environment of the redox-active phylloquinone (A(1)). Evidence for unidirectionality of electron transfer in photosystem I.* Journal of Physical Chemistry B, 1998. **102**(42): p. 8288-8299.

135. Warden, J.T. and J.H. Golbeck, *Photosystem-I Charge Separation in the Absence of Center-a and Center-B .2. Electron-Spin-Resonance Spectral Characterization of Center X and Correlation with Optical Signal A2.* Biochimica Et Biophysica Acta, 1986. **849**(1): p. 25-31.

136. van der Est, A., et al., *Removal of PsaF alters forward electron transfer in photosystem I: Evidence for fast reoxidation of Q(K)-A in subunit deletion mutants of Synechococcus sp PCC 7002.* Biochemistry, 2004. **43**(5): p. 1264-1275.

137. Golbeck, J.H., K.G. Parrett, and A.E. McDermott, *Photosystem-I Charge Separation in the Absence of Center-a and Center-B .3. Biochemical-Characterization of a Reaction Center Particle Containing P-700 and Fx.* Biochimica Et Biophysica Acta, 1987. **893**(2): p. 149-160.

138. Golbeck, J.H., *A comparative analysis of the spin state distribution of in vitro and in vivo mutants of PsaC - A biochemical argument for the sequence of electron transfer in*

Photosystem I as F-X -> F-A -> F-B -> ferredoxin/flavodoxin. Photosynthesis Research, 1999. **61**(2): p. 107-144.

139. Kiley, P., et al., *Self-assembling peptide detergents stabilize isolated photosystem I on a dry surface for an extended time.* Plos Biology, 2005. **3**(7): p. 1180-1186.
140. Prince, R.C. and H.S. Kheshgi, *The photobiological production of hydrogen: Potential efficiency and effectiveness as a renewable fuel.* Critical Reviews in Microbiology, 2005. **31**(1): p. 19-31.
141. Fromme, P. and H.T. Witt, *Improved isolation and crystallization of photosystem I for structural analysis.* Biochimica et Biophysica Acta (BBA) - Bioenergetics, 1998. **1365**(1-2): p. 175-184.
142. Incorporated, Y., *YSI model 5300 biological oxygen monitor instruction manual*.
143. Hervás, M., et al., *Laser flash kinetic analysis of Synechocystis PCC 6803 cytochrome c6 and plastocyanin oxidation by Photosystem I.* Biochimica et Biophysica Acta (BBA) - Bioenergetics, 1994. **1184**(2-3): p. 235-241.
144. Sigfridsson, K., et al., *A comparative flash-photolysis study of electron transfer from pea and spinach plastocyanins to spinach Photosystem 1. A reaction involving a rate-limiting conformational change.* Photosynthesis Research, 1996. **50**: p. 11-21.
145. Sigfridsson, K., *Ionic strength and pH dependence of the reaction between plastocyanin and Photosystem I. Evidence of a rate-limiting conformational change.* Photosynthesis Research, 1997. **54**: p. 143–153.
146. Nakamura, Y., et al., *Complete genome structure of the thermophilic cyanobacterium Thermosynechococcus elongatus BP-1*. DNA Res, 2002. **9**(4): p. 123-30.
147. Hervas, M., et al., *Cyanobacterial photosystem I lacks specificity in its interaction with cytochrome c(6) electron donors.* Photosynthesis Research, 2005. **83**(3): p. 329-333.
148. Du, H.B., et al., *The chemistry of selective ring-opening catalysts.* Applied Catalysis a-General, 2005. **294**(1): p. 1-21.
149. Hegedus, L. and T. Mathe, *Hydrogenation of pyrrole derivatives - Part V. Poisoning effect of nitrogen on precious metal on carbon catalysts.* Applied Catalysis a-General, 2002. **226**(1-2): p. 319-322.

150. Irandoust, S. and J. Edvardsson, *Poisoning of Nickel-Based Catalysts in Fat Hydrogenation.* Journal of the American Oil Chemists Society, 1993. **70**(11): p. 1149-1156.
151. Millsaps, J.F., et al., *Nanoscale photosynthesis: photocatalytic production of hydrogen by platinized photosystem I reaction centers.* Photochem Photobiol, 2001. **73**(6): p. 630-5.
152. Grimme, R.A., et al., *Photosystem I/molecular wire/metal nanoparticle bioconjugates for the photocatalytic production of H2.* J Am Chem Soc, 2008. **130**(20): p. 6308-9.
153. Anta, J.A., F. Casanueva, and G. Oskam, *A numerical model for charge transport and recombination in dye-sensitized solar cells.* J Phys Chem B, 2006. **110**(11): p. 5372-8.
154. Ihara, M., et al., *Light-driven hydrogen production by a hybrid complex of a [NiFe]-hydrogenase and the cyanobacterial photosystem I.* Photochem Photobiol, 2006. **82**(3): p. 676-82.
155. Garavito, R.M. and S. Ferguson-Miller, *Detergents as tools in membrane biochemistry.* Journal of Biological Chemistry, 2001. **276**(35): p. 32403-32406.
156. Gohon, Y. and J.L. Popot, *Membrane protein-surfactant complexes.* Current Opinion in Colloid & Interface Science, 2003. **8**(1): p. 15-22.
157. le Maire, M., P. Champeil, and J.V. Moller, *Interaction of membrane proteins and lipids with solubilizing detergents.* Biochimica Et Biophysica Acta-Biomembranes, 2000. **1508**(1-2): p. 86-111.
158. Du, H., et al., *The chemistry of selective ring-opening catalysts.* Applied Catalysis A: General, 2005. **294**(1): p. 1-21.
159. Hegedus, L. and T. Máthé, *Hydrogenation of pyrrole derivatives: Part V. Poisoning effect of nitrogen on precious metal on carbon catalysts.* Applied Catalysis A: General, 2002. **226**(1-2): p. 319-322.
160. Jamil, Z., et al., *Optimization of phototrophic hydrogen production by Rhodopseudomonas palustris PBUM001 via statistical experimental design.* International Journal of Hydrogen Energy, 2009. **34**(17): p. 7502-7512.
161. Chen, C.-Y., et al., *Improved phototrophic H2 production with Rhodopseudomonas palustris WP3-5 using acetate and butyrate as dual carbon substrates.* Bioresource Technology, 2008. **99**(9): p. 3609-3616.

162. Chen, C.-Y., et al., *Enhancing phototrophic hydrogen production of Rhodopseudomonas palustris via statistical experimental design.* International Journal of Hydrogen Energy, 2007. **32**(8): p. 940-949.
163. Mu, Y., G. Wang, and H.Q. Yu, *Response surface methodological analysis on biohydrogen production by enriched anaerobic cultures.* Enzyme and Microbial Technology, 2006. **38**(7): p. 905-913.
164. CÌ§am, M. and K. Aaby, *Optimization of Extraction of Apple Pomace Phenolics with Water by Response Surface Methodology.* Journal of Agricultural and Food Chemistry. **58**(16): p. 9103-9111.
165. Montgomery, D.C., *Design and Analysis of Experiments*. 5th ed. 2001, New York: Wiley. 680.
166. Draper, N.R., and Smith, H., *Applied Regression Analysis*. 3rd ed. 1998, New York: Wiley.
167. Zinatizadeh, A.A.L., et al., *Process modeling and analysis of palm oil mill effluent treatment in an up-flow anaerobic sludge fixed film bioreactor using response surface methodology (RSM).* Water Research, 2006. **40**(17): p. 3193-3208.
168. Kutner, M.H., Nachtsheim, C. J., Neter, J., *Applied Linear Regression Model*. 4th ed. 2004: McGrew-Hill Irwin
169. Ghirardi, M.L., R.K. Togasaki, and M. Seibert, *Oxygen sensitivity of algal H-2-production.* Applied Biochemistry and Biotechnology, 1997. **63-5**: p. 141-151.
170. Fromme, P., W.D. Schubert, and N. Krauss, *Structure of Photosystem-I - Suggestions on the Docking Sites for Plastocyanin, Ferredoxin and the Coordination of P700.* Biochimica Et Biophysica Acta-Bioenergetics, 1994. **1187**(2): p. 99-105.
171. Klukas, O., et al., *Localization of two phylloquinones, Q(K) and Q(K)', in an improved electron density map of photosystem I at 4-angstrom resolution.* Journal of Biological Chemistry, 1999. **274**(11): p. 7361-7367.
172. Xu, Q., et al., *Mutational Analysis of Photosystem-I Polypeptides in Synechocystis Sp Pcc-6803 - Subunit Requirements for Reduction of Nadp(+) Mediated by Ferredoxin and Flavodoxin.* Journal of Biological Chemistry, 1994. **269**(34): p. 21512-21518.

173. Chitnis, P.R. and N. Nelson, *Assembly of 2 Subunits of the Cyanobacterial Photosystem-I on the N-Side of Thylakoid Membranes.* Plant Physiology, 1992. **99**(1): p. 239-246.

174. Cohen, Y., et al., *Stable Assembly of Psae into Cyanobacterial Photosynthetic Membranes Is Dependent on the Presence of Other Accessory Subunits of Photosystem-I.* Plant Molecular Biology, 1993. **23**(4): p. 895-900.

175. Lushy, A., L. Verchovsky, and R. Nechushtai, *The stable assembly of newly synthesized PsaE into the photosystem I complex occurring via the exchange mechanism is facilitated by electrostatic interactions.* Biochemistry, 2002. **41**(37): p. 11192-11199.

176. Minai, L., et al., *The assembly of the PsaD subunit into the membranal photosystem I complex occurs via an exchange mechanism.* Biochemistry, 2001. **40**(43): p. 12754-12760.

177. Setif, P., *Ferredoxin and flavodoxin reduction by photosystem I.* Biochimica Et Biophysica Acta-Bioenergetics, 2001. **1507**(1-3): p. 161-179.

178. Chitnis, P.R., et al., *Structure and targeted mutagenesis of the gene encoding 8-kda subunit of Photosystem I from the cyanobacterium Synechocystis sp PCC-6803.* Journal of Biological Chemistry, 1989. **264**(31): p. 18374-18380.

179. Chitnis, P.R., P.A. Reilly, and N. Nelson, *Insertional Inactivation of the Gene Encoding Subunit-Ii of Photosystem-I from the Cyanobacterium Synechocystis Sp Pcc-6803.* Journal of Biological Chemistry, 1989. **264**(31): p. 18381-18385.

180. Sonoike, K., H. Hatanaka, and S. Katoh, *Small subunits of Photosystem I reaction center complexes from Synechococcus elongatus. II. The psaE gene product has a role to promote interaction between the terminal electron acceptor and ferredoxin.* Biochimica et Biophysica Acta (BBA) - Bioenergetics, 1993. **1141**(1): p. 52-57.

181. Ausubel, F.M., Brent, R., Kingstone, R. E., Moore, D. D., Seidman, J .G., Smith, J. A., and Struhl, K., *Current protocols in molecular biology*. 1996, New York, N. Y.: John Wiley & Sons.

182. Christian, M., M.F. Victor, and F. Bärbel, *C-Terminal Extension of the H₂-Activating Subunit, HoxH, Directs Maturation of the NAD-Reducing Hydrogenase in Alcaligenes Eutrophus*. 1997. p. 441-448.

183. Simon, R., U. Priefer, and A. Puhler, *A Broad Host Range Mobilization System for In Vivo Genetic Engineering: Transposon Mutagenesis in Gram Negative Bacteria.* Nat Biotech, 1983. **1**(9): p. 784-791.
184. Iwai, M., et al., *Improved Genetic Transformation of the Thermophilic Cyanobacterium, Thermosynechococcus elongatus BP-1*. 2004. p. 171-175.
185. Massanz, C., V.M. Fernandezz, and B. Friedrich, *C-Terminal Extension of the H2-Activating Subunit, HoxH, Directs Maturation of the NAD-Reducing Hydrogenase in Alcaligenes Eutrophus.* European Journal of Biochemistry, 1997. **245**(2): p. 441-448.
186. Lenz, O. and B. Friedrich, *A novel multicomponent regulatory system mediates H-2 sensing in Alcaligenes eutrophus.* Proceedings of the National Academy of Sciences of the United States of America, 1998. **95**(21): p. 12474-12479.
187. Lenz, O., et al., *The Alcaligenes-Eutrophus H16 Hoxx Gene Participates in Hydrogenase Regulation.* Journal of Bacteriology, 1994. **176**(14): p. 4385-4393.
188. Friedrich, B., et al., *Nickel Requirement for Active Hydrogenase Formation in Alcaligenes-Eutrophus.* Journal of Bacteriology, 1981. **145**(3): p. 1144-1149.
189. Gay, P., et al., *Positive Selection Procedure for Entrapment of Insertion-Sequence Elements in Gram-Negative Bacteria.* Journal of Bacteriology, 1985. **164**(2): p. 918-921.
190. Saha, S., L. Uma, and G. Subramanian, *An improved method for marine cyanobacterial DNA isolation.* World journal of microbililogy & biotechnology, 2005. **21** (6-7): p. 877-881.
191. Hogrefe, C. and B. Friedrich, *Isolation and characterization of megaplasmid DNA from lithoautotrophic bacteria.* Plasmid, 1984. **12**(3): p. 161-169.
192. Schwarze, A., et al., *Requirements for the construction of a functional hybrid complex between photosystem I and [NiFe]-hydrogenase*. p. AEM.02700-09.
193. Villalobos, A., et al., *Gene Designer: a synthetic biology tool for constructing artificial DNA segments.* BMC bioinformatics, 2006. **7**: p. 285.
194. Miyake, M., H. Kotani, and Y. Asada, *Isolation and Identification of Restriction Endonuclease, Seli from a Cyanobacterium, Synechococcus-Elongatus.* Nucleic Acids Research, 1992. **20**(10): p. 2605-2605.

195. Whitton B. A, P.M., *The ecology of cyanobacteria: their diversity in time and space* 2000, Kluwer Academic Publishers. p. 478.
196. Binder, B.J. and S.W. Chisholm, *Relationship between DNA cycle and growth rate in Synechococcus sp. strain PCC 6301*. 1990. p. 2313-2319.
197. Matsuoka, M., K. Takahama, and T. Ogawa, *Gene replacement in cyanobacteria mediated by a dominant streptomycin-sensitive rps12 gene that allows selection of mutants free from drug resistance markers*. 2001. p. 2077-2087.
198. Gouy, M. and C. Gautier, *Codon Usage in Bacteria - Correlation with Gene Expressivity.* Nucleic Acids Research, 1982. **10**(22): p. 7055-7074.
199. Ikemura, T., *Correlation between the abundance of Escherichia coli transfer RNAs and the occurrence of the respective codons in its protein genes: A proposal for a synonymous codon choice that is optimal for the E. coli translational system.* Journal of Molecular Biology, 1981. **151**(3): p. 389-409.
200. Hayes, C.S., B. Bose, and R.T. Sauer, *Stop codons preceded by rare arginine codons are efficient determinants of SsrA tagging in Escherichia coli.* Proceedings of the National Academy of Sciences of the United States of America, 2002. **99**(6): p. 3440-3445.
201. Kane, J.F., et al., *Novel in-Frame 2 Codon Translational Hop During Synthesis of Bovine Placental-Lactogen in a Recombinant Strain of Escherichia-Coli.* Nucleic Acids Research, 1992. **20**(24): p. 6707-6712.
202. McNulty, D.E., et al., *Mistranslational errors associated with the rare arginine codon CGG in Escherichia coli.* Protein Expression and Purification, 2003. **27**(2): p. 365-374.
203. Lithwick, G. and H. Margalit, *Hierarchy of sequence-dependent features associated with prokaryotic translation.* Genome Research, 2003. **13**(12): p. 2665-2673.
204. Kurland, C. and J. Gallant, *Errors of heterologous protein expression.* Current Opinion in Biotechnology, 1996. **7**(5): p. 489-493.
205. Bernhard, M., et al., *The Alcaligenes eutrophus membrane-bound hydrogenase gene locus encodes functions involved in maturation and electron transport coupling.* Journal of Bacteriology, 1996. **178**(15): p. 4522-4529.

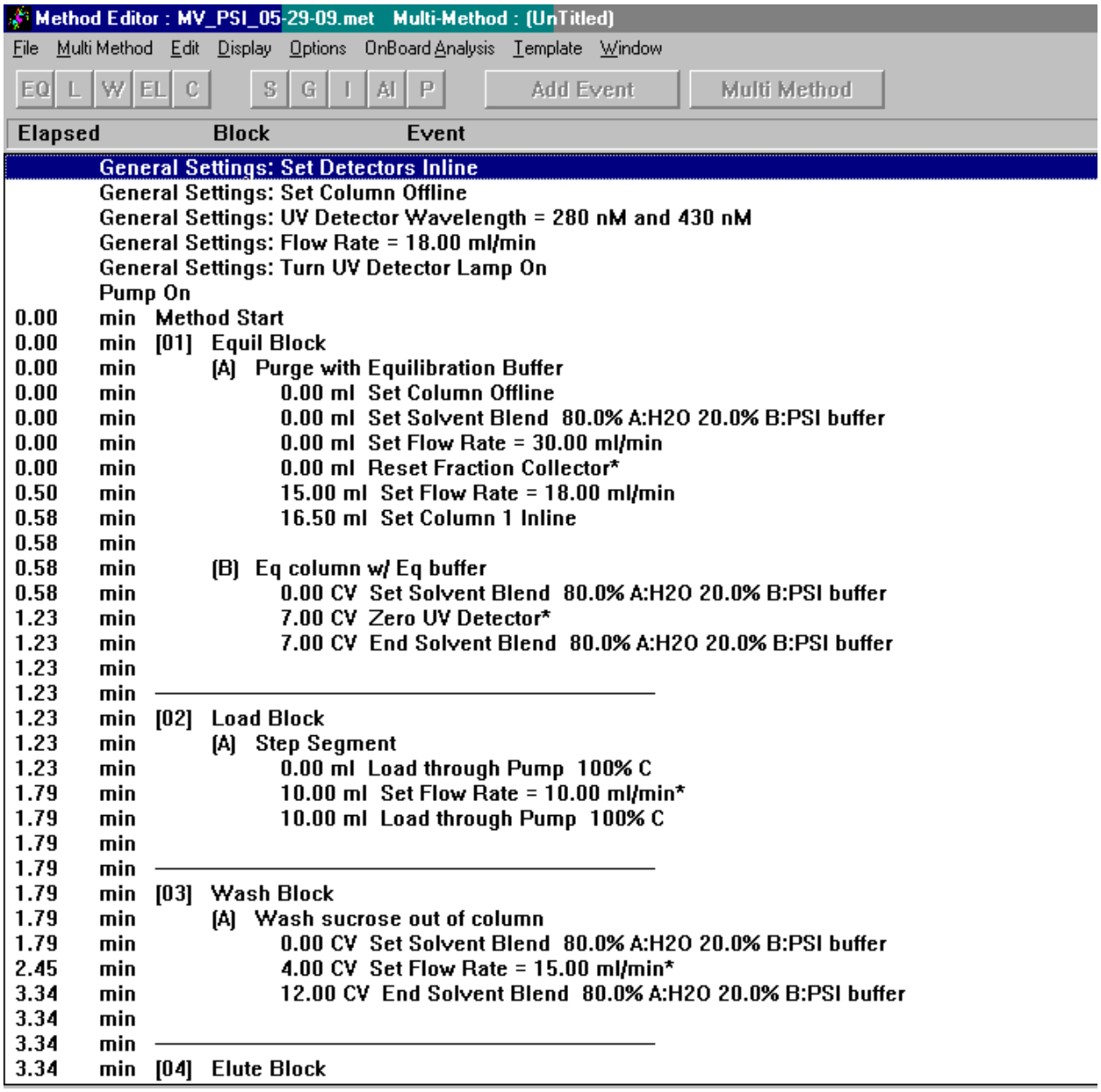
206. Ihara , M., et al., *Light-driven hydrogen production by a hybrid complex of a [NiFe]-hydrogenase and the cyanobacterial Photosystem I.* Photochemistry and Photobiology, 2006. **82**(3): p. 676–682

207. Gross, R., et al., *Two membrane anchors of Wolinella succinogenes hydrogenase and their function in fumarate and polysulfide respiration.* Archives of Microbiology, 1998. **170**(1): p. 50-58.

208. Rousset, M., et al., *[3Fe-4S] to [4Fe-4S] cluster conversion in Desulfovibrio fructosovorans [NiFe] hydrogenase by site-directed mutagenesis.* Proceedings of the National Academy of Sciences of the United States of America, 1998. **95**(20): p. 11625-11630.

APPENDIX

Appendix I – HPLC method for PSI purification



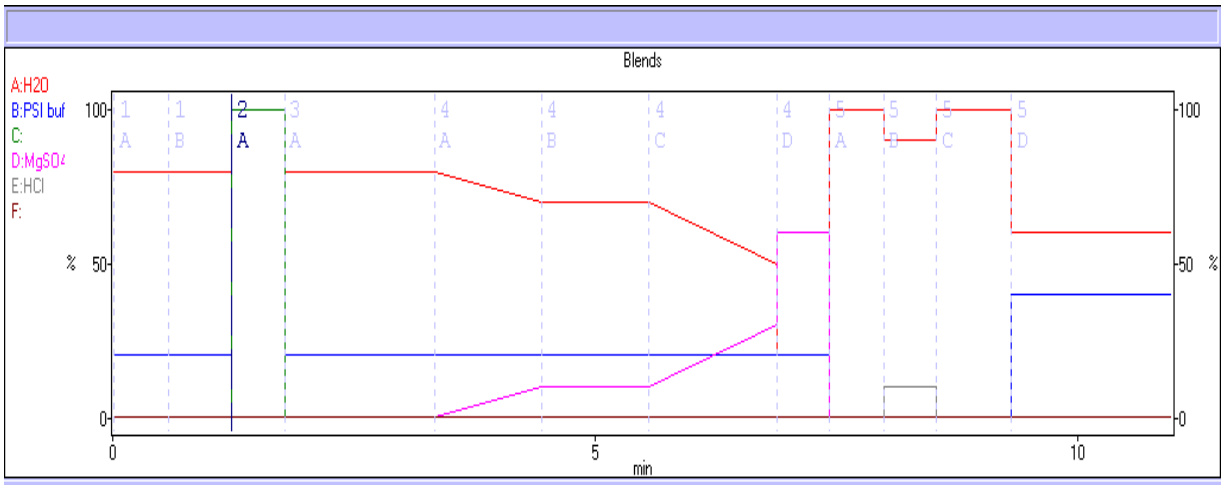
Method Editor : MV_PSI_05-29-09.met Multi-Method : (UnTitled)

File Multi Method Edit Display Options OnBoard Analysis Template Window

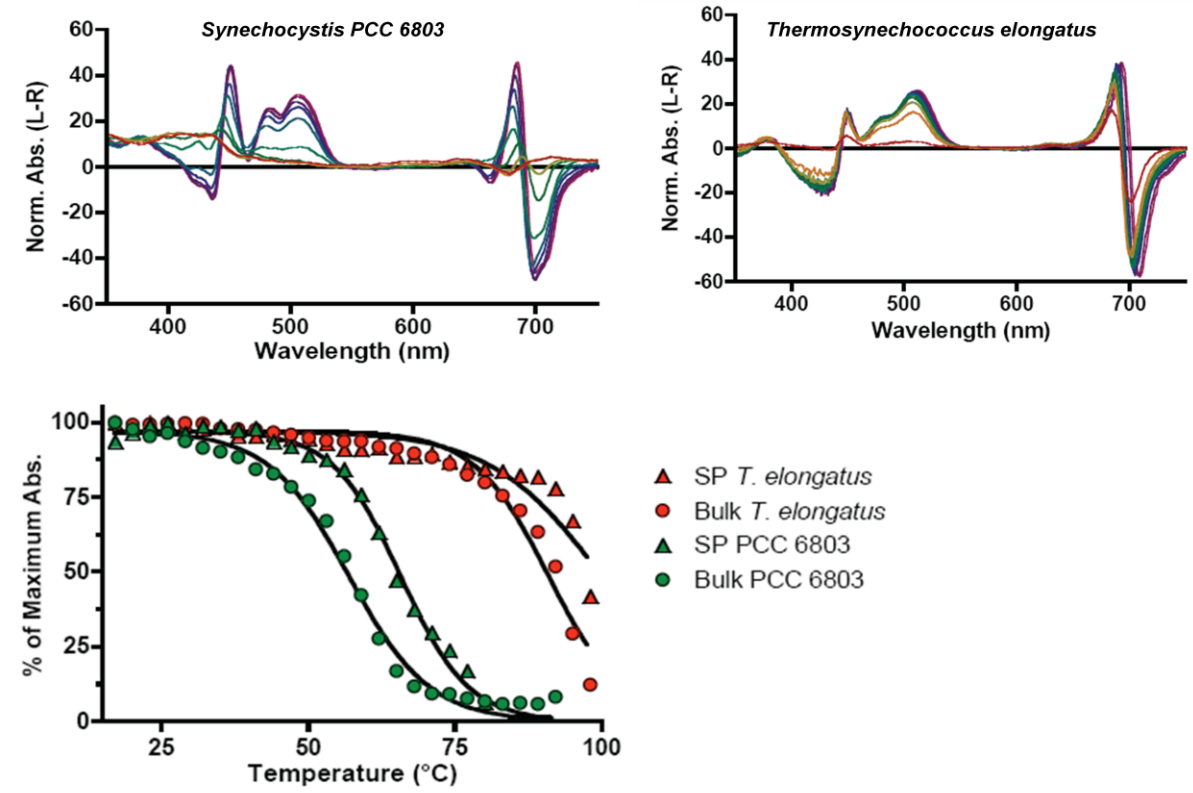
EQ L W EL C S G I AI P Add Event Multi Method

Elapsed		Block	Event
			General Settings: Set Detectors Inline
			General Settings: Set Column Offline
			General Settings: UV Detector Wavelength = 280 nM and 430 nM
			General Settings: Flow Rate = 18.00 ml/min
			General Settings: Turn UV Detector Lamp On
			Pump On
0.00	min		Method Start
0.00	min	[01]	Equil Block
0.00	min		(A) Purge with Equilibration Buffer
0.00	min		0.00 ml Set Column Offline
0.00	min		0.00 ml Set Solvent Blend 80.0% A:H2O 20.0% B:PSI buffer
0.00	min		0.00 ml Set Flow Rate = 30.00 ml/min
0.00	min		0.00 ml Reset Fraction Collector*
0.50	min		15.00 ml Set Flow Rate = 18.00 ml/min
0.58	min		16.50 ml Set Column 1 Inline
0.58	min		
0.58	min		(B) Eq column w/ Eq buffer
0.58	min		0.00 CV Set Solvent Blend 80.0% A:H2O 20.0% B:PSI buffer
1.23	min		7.00 CV Zero UV Detector*
1.23	min		7.00 CV End Solvent Blend 80.0% A:H2O 20.0% B:PSI buffer
1.23	min		
1.23	min		————————————————
1.23	min	[02]	Load Block
1.23	min		(A) Step Segment
1.23	min		0.00 ml Load through Pump 100% C
1.79	min		10.00 ml Set Flow Rate = 10.00 ml/min*
1.79	min		10.00 ml Load through Pump 100% C
1.79	min		
1.79	min		————————————————
1.79	min	[03]	Wash Block
1.79	min		(A) Wash sucrose out of column
1.79	min		0.00 CV Set Solvent Blend 80.0% A:H2O 20.0% B:PSI buffer
2.45	min		4.00 CV Set Flow Rate = 15.00 ml/min*
3.34	min		12.00 CV End Solvent Blend 80.0% A:H2O 20.0% B:PSI buffer
3.34	min		
3.34	min		————————————————
3.34	min	[04]	Elute Block

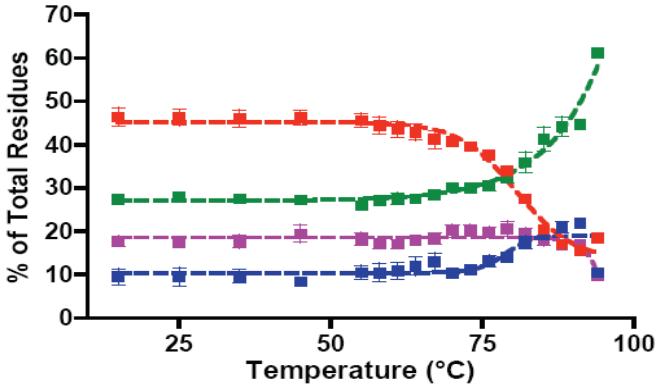
```
3.34    min        (A)  Gradient segment
3.34    min             0.00 CV  Start Gradient  80.0% A:H2O 20.0% B:PSI buffer
4.00    min             6.00 CV  Start Fraction Collection Peak 1.00ml Thr 0.500 Slp  0.200*
4.44    min             10.00 CV  End Gradient  70.0% A:H2O 20.0% B:PSI buffer 10.0% D:MgSO4
4.44    min
4.44    min        (B)  Step Segment
4.44    min             0.00 CV  Set Solvent Blend  70.0% A:H2O 20.0% B:PSI buffer 10.0% D:MgSO4
5.55    min             10.00 CV  End Solvent Blend  70.0% A:H2O 20.0% B:PSI buffer 10.0% D:MgSO4
5.55    min
5.55    min        (C)  Elution gradient
5.55    min             0.00 CV  Start Gradient  70.0% A:H2O 20.0% B:PSI buffer 10.0% D:MgSO4
6.88    min             12.00 CV  End Gradient  50.0% A:H2O 20.0% B:PSI buffer 30.0% D:MgSO4
6.88    min
6.88    min        (D)  Step Segment
6.88    min             0.00 CV  Set Solvent Blend  20.0% A:H2O 20.0% B:PSI buffer 60.0% D:MgSO4
7.44    min             5.00 CV  End Solvent Blend  20.0% A:H2O 20.0% B:PSI buffer 60.0% D:MgSO4
7.44    min
7.44    min  ----------------------------------------
7.44    min  [05]  Clean Block
7.44    min        (A)  Rinse Column with H2O
7.44    min             0.00 CV  Set Solvent Blend  100% A:H2O
7.77    min             3.00 CV  Stop Fraction Collection*
7.78    min             3.10 CV  Reset Fraction Collector*
7.99    min             5.00 CV  End Solvent Blend  100% A:H2O
7.99    min
7.99    min        (B)  Acid wash column
7.99    min             0.00 CV  Set Solvent Blend  90.0% A:H2O 10.0% E:HCl
8.54    min             5.00 CV  End Solvent Blend  90.0% A:H2O 10.0% E:HCl
8.54    min
8.54    min        (C)  Rinse out acid with H2O
8.54    min             0.00 CV  Set Solvent Blend  100% A:H2O
9.32    min             7.00 CV  End Solvent Blend  100% A:H2O
9.32    min
9.32    min        (D)  Restore column pH
9.32    min             0.00 CV  Set Solvent Blend  60.0% A:H2O 40.0% B:PSI buffer
10.98   min             15.00 CV  End Solvent Blend  60.0% A:H2O 40.0% B:PSI buffer
10.98   min         Thresholds [  pH >  5.5, Delay 0.00 CV]
```


Blends
A:H2O
B:PSI buf
C:
D:MgSO4
E:HCl
F:
100
50
0
%
1 A
1 B
2 A
3 A
4 A
4 B
4 C
4 D
5 A
5 B
5 C
5 D
0
5
10
min

Appendix II – Temperature stability of cytochrome c_6 and temperature stability comparism of *Synechocystis PCC6803* and *T. Elongatus (*Circular dichroism spectroscopy)

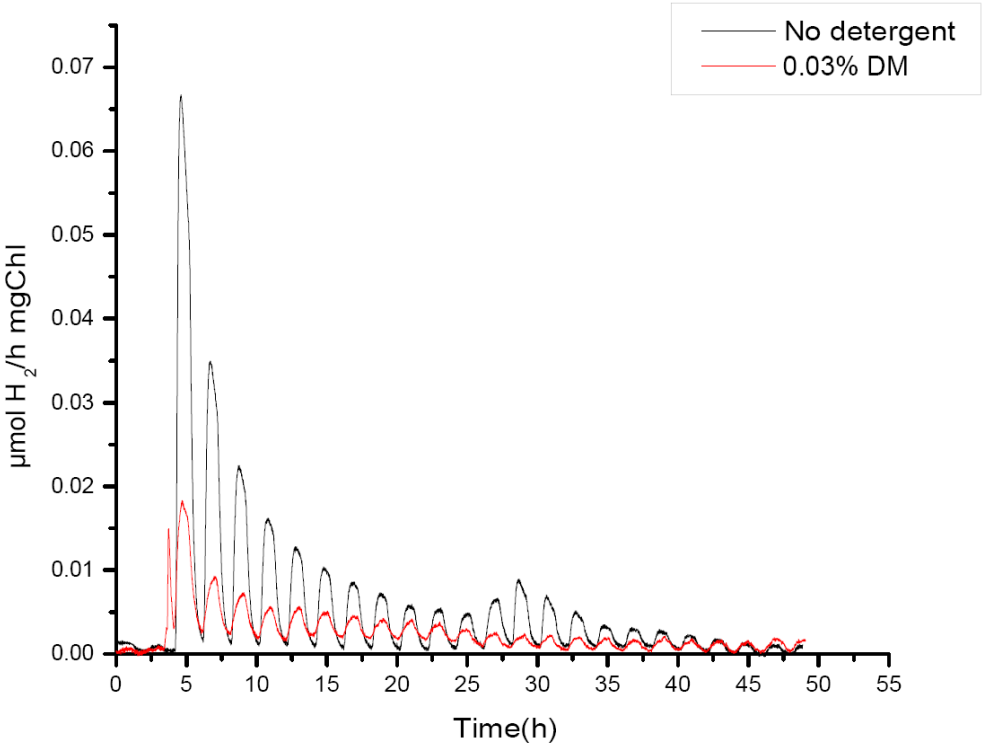


Thermal stability of purified PSI (Prepared by Micheal Vaungh, Barry Bruce Laboratory Univeristy of Tennessee). Top panel contain the visible CD absorbance data for *Synechocysitis* PCC 6803(left) and *Thermosynechococcus elongatus* (right) measured between 15 and 98°C, respectively. Lowest temperature scans are shown in violet and increasing temperatures proceed through blue, green yellow and finally red for the highest temperature scans. The visible CD absorbance for PSI is a function of pigment arrangement/environment and is a sensitive indicator of the functional state of PSI, the fine stucture of these spectra are lost as temperature is increased. The botton panel indicates the normalized maximal absorbance for each of the data sets; green filled symbols indicate data for *Synechocystis* PCC 6803 while the red symbols indicate *T. elongatus.* In both cases, filled circles indicate antenna chlorophyll (positive peak at 515 nm) and the filled triangles absorbance values are the split exciton signal originating from P700 (negative minima at 700 nm).



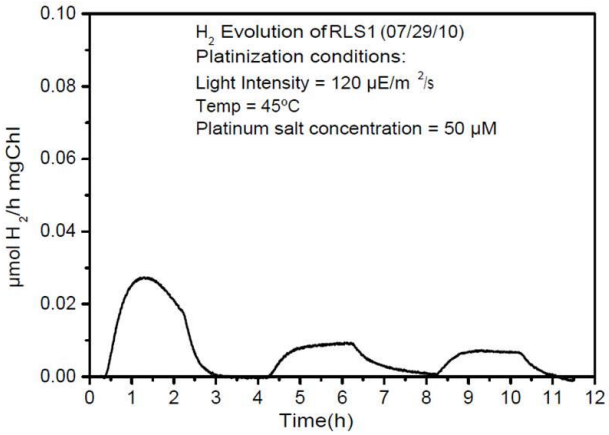
Thermal stability of purified cyt c_6 (Prepared by Micheal Vaungh, Barry Bruce Laboratory Univeristy of Tennessee). The thermal stability of cyt c_6 was also investigated using UV-Vis CD spectroscopy. Using the CDPro software package the data was deconvoluted as indicated in the text and the resulting values are plotted as a function of temperature. Helical content plotted with red circles, unordered with green diamonds, turn with inverse purple triangles, and beta strand with blue squares. Using the helical content for fitting to a sigmoidal Boltzman distribution we estimate the T_m value to be 80.6±1°C.

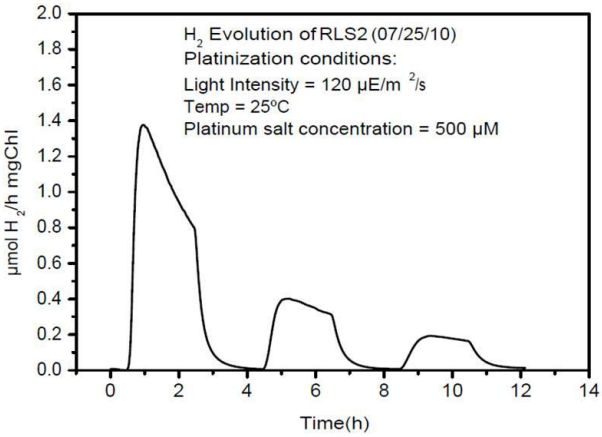
Appendix III – Comparison of hydrogen evolution using no detergent and 0.03% DM in buffer.

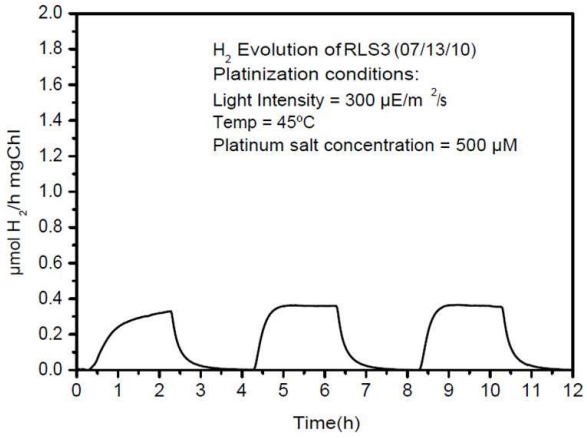


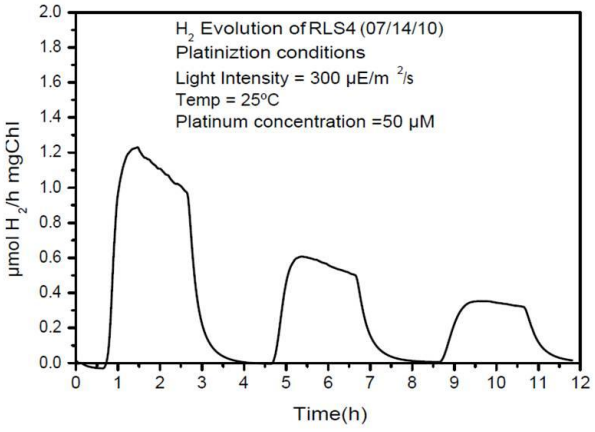
Hydrogen evolution activities of PSI samples using DM and no detergent. Platinized PSI complex (20 µg chl ml^{-1}), 10 mM NaAsc, and 10 molar excess cyt c_6 in 20 mM MES buffer pH 6.4. 0.03% DM and no detergent were used in the buffer during platinization and also during hydrogen evolution activity. White light was used at an intensity of about 400 µE m^{-2} s^{-1}. After about 40 h, the rate of both samples equilibrated to about the same value.

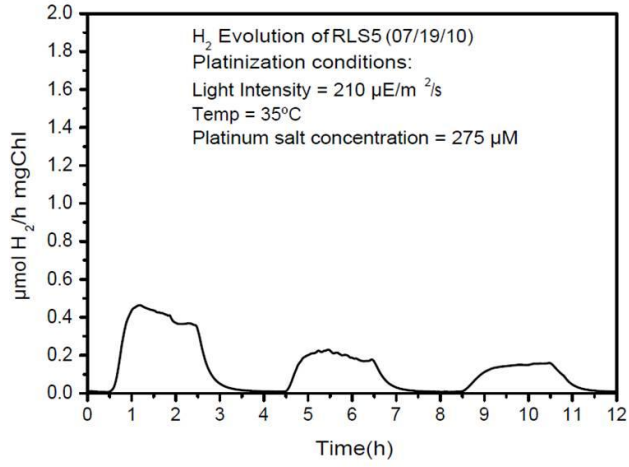
Appendix IV – Raw data for hydrogen evolution used in the design of experiment (DOE).

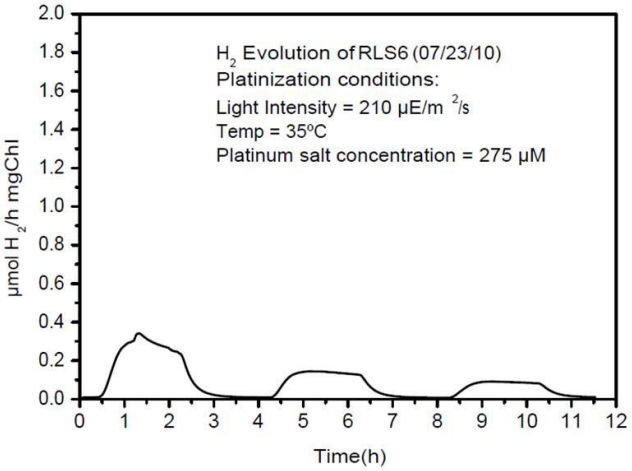


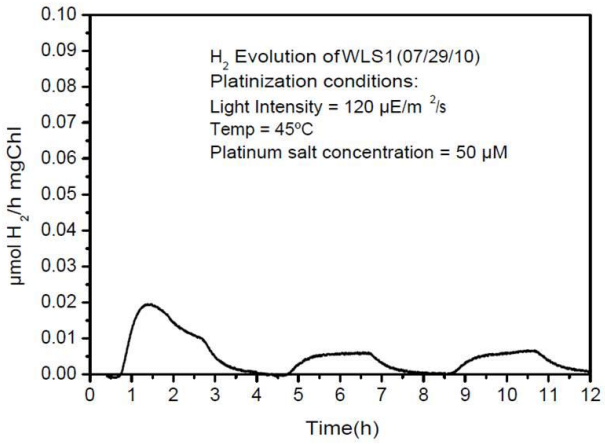


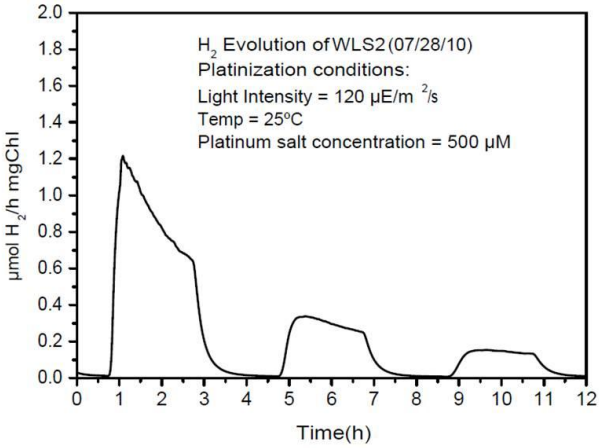


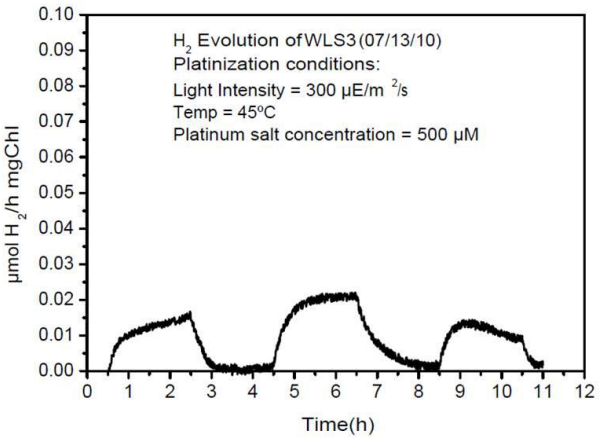


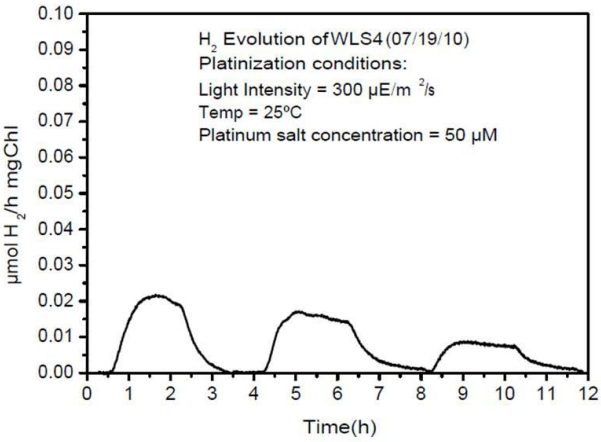


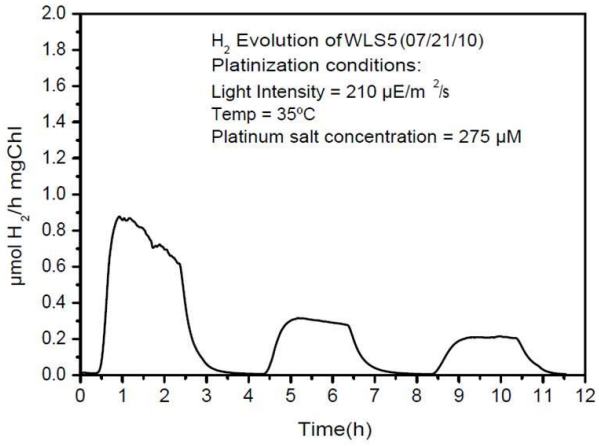


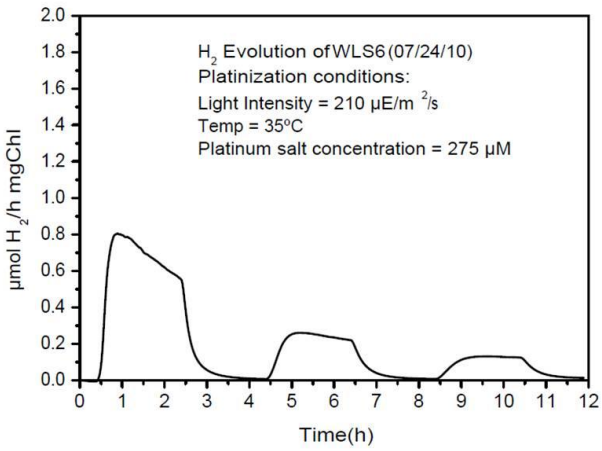

H2 Evolution of WLS1 (07/29/10)
Platinization conditions:
Light Intensity = 120 µE/m 2/s
Temp = 45ºC
Platinum salt concentration = 50 µM
µmol H2/h mgChl
Time(h)

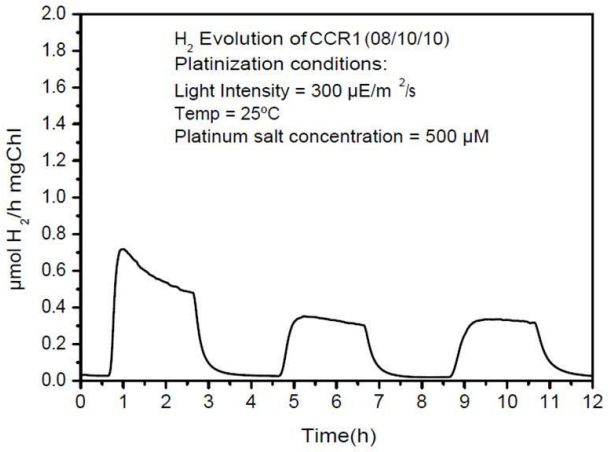

H2 Evolution of WLS2 (07/28/10)
Platinization conditions:
Light Intensity = 120 µE/m 2/s
Temp = 25ºC
Platinum salt concentration = 500 µM
µmol H2/h mgChl
Time(h)

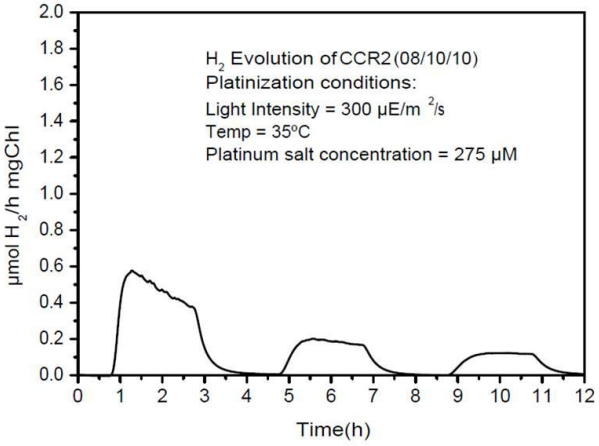

H2 Evolution of WLS3 (07/13/10)
Platinization conditions:
Light Intensity = 300 µE/m 2/s
Temp = 45ºC
Platinum salt concentration = 500 µM
µmol H2/h mgChl
Time(h)

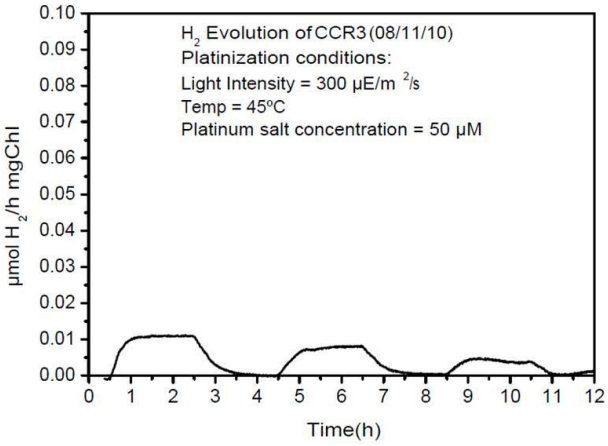

H2 Evolution of WLS4 (07/19/10)
Platinization conditions:
Light Intensity = 300 µE/m 2/s
Temp = 25ºC
Platinum salt concentration = 50 µM
µmol H2/h mgChl
Time(h)

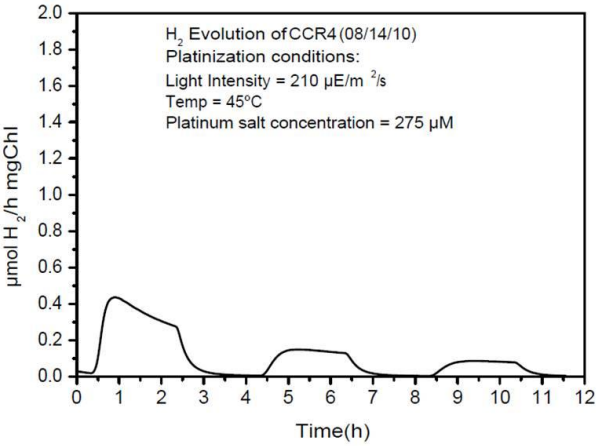

H2 Evolution of WLS5 (07/21/10)
Platinization conditions:
Light Intensity = 210 µE/m 2/s
Temp = 35ºC
Platinum salt concentration = 275 µM
µmol H2/h mgChl
Time(h)

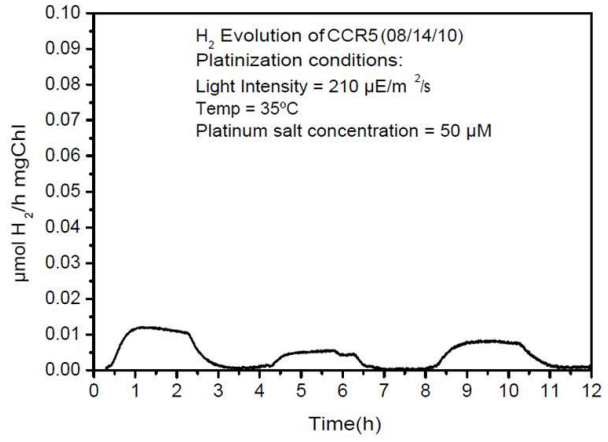

H2 Evolution of WLS6 (07/24/10)
Platinization conditions:
Light Intensity = 210 µE/m 2/s
Temp = 35ºC
Platinum salt concentration = 275 µM
µmol H2/h mgChl
Time(h)

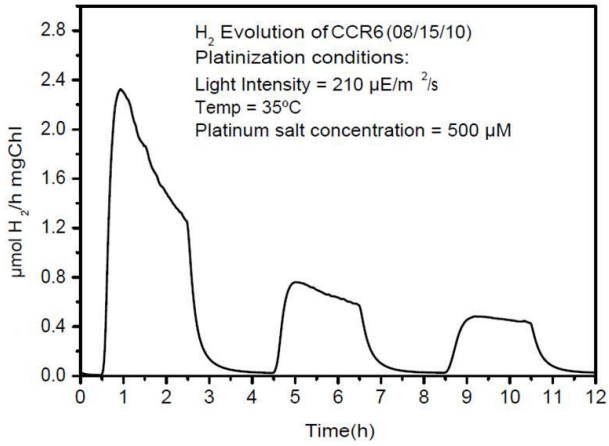

H2 Evolution of CCR1 (08/10/10)
Platinization conditions:
Light Intensity = 300 µE/m 2/s
Temp = 25ºC
Platinum salt concentration = 500 µM
µmol H2/h mgChl
Time(h)

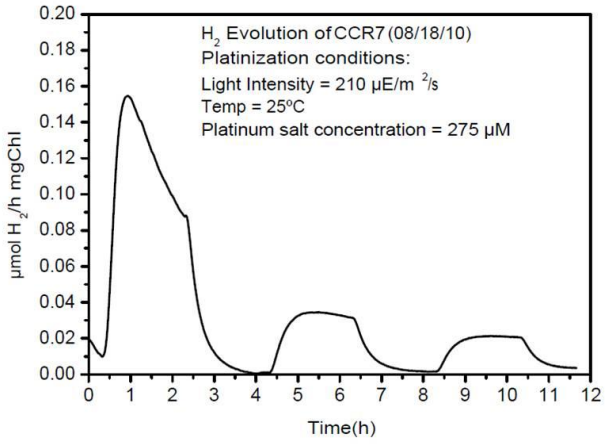

H2 Evolution of CCR2 (08/10/10)
Platinization conditions:
Light Intensity = 300 µE/m 2/s
Temp = 35ºC
Platinum salt concentration = 275 µM
µmol H2/h mgChl
Time(h)

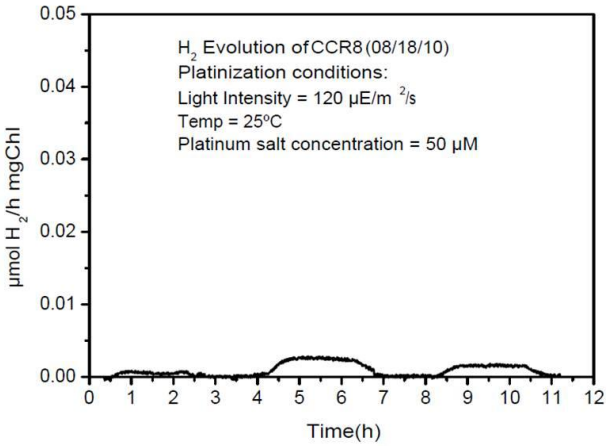

H2 Evolution of CCR3 (08/11/10)
Platinization conditions:
Light Intensity = 300 µE/m 2/s
Temp = 45ºC
Platinum salt concentration = 50 µM
µmol H2/h mgChl
Time(h)

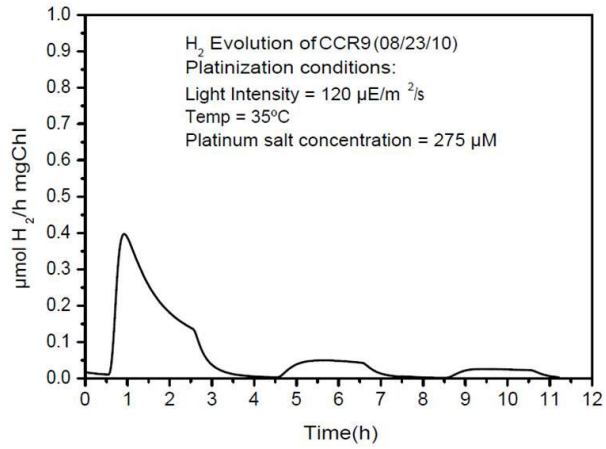

H2 Evolution of CCR4 (08/14/10)
Platinization conditions:
Light Intensity = 210 µE/m 2/s
Temp = 45ºC
Platinum salt concentration = 275 µM
µmol H2/h mgChl
Time(h)

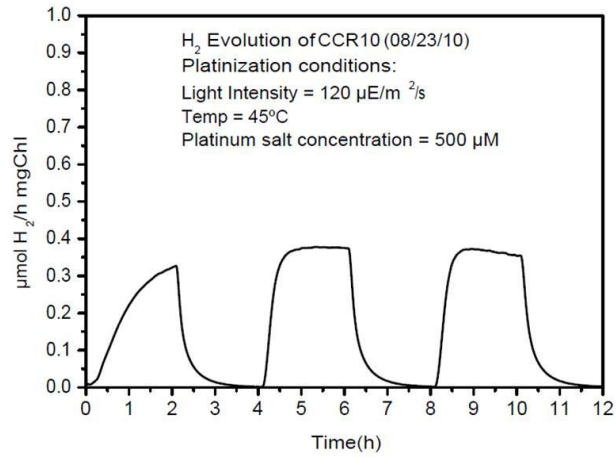

H2 Evolution of CCR5 (08/14/10)
Platinization conditions:
Light Intensity = 210 µE/m 2/s
Temp = 35ºC
Platinum salt concentration = 50 µM
µmol H2/h mgChl
Time(h)


H2 Evolution of CCR6 (08/15/10)
Platinization conditions:
Light Intensity = 210 µE/m 2/s
Temp = 35ºC
Platinum salt concentration = 500 µM
µmol H2/h mgChl
Time(h)


H2 Evolution of CCR7 (08/18/10)
Platinization conditions:
Light Intensity = 210 µE/m 2/s
Temp = 25ºC
Platinum salt concentration = 275 µM
µmol H2/h mgChl
Time(h)


H2 Evolution of CCR8 (08/18/10)
Platinization conditions:
Light Intensity = 120 µE/m 2/s
Temp = 25ºC
Platinum salt concentration = 50 µM
µmol H2/h mgChl
Time(h)


H2 Evolution of CCR9 (08/23/10)
Platinization conditions:
Light Intensity = 120 µE/m 2/s
Temp = 35ºC
Platinum salt concentration = 275 µM
µmol H2/h mgChl
Time(h)


H2 Evolution of CCR10 (08/23/10)
Platinization conditions:
Light Intensity = 120 µE/m 2/s
Temp = 45ºC
Platinum salt concentration = 500 µM
µmol H2/h mgChl
Time(h)

VITA

Ifeyinwa Jane Iwuchukwu was born in Kaduna, Nigeria on June 20, 1979 to Joseph and Bridget Oranugo. She graduated from the Enugu State University of Science and Technology, Nigeria, with First Class Honors in Chemical Engineering, in December, 2000. From January 2002 to December 2002, she worked as an Assistant Program Supervisor at the Nigerian National Petroleum Corporation, Nigeria. In May 2004 she joined the University of Tennessee Space Institute as a Graduate Research Assistant to pursue a Master of Science degree in Chemical Engineering. She is married to Ernest Iwuchukwu and they have a daughter, Oge and a son, Ife. She joined the University of Tennessee, Knoxville, in the fall 2006 to pursue her PhD in Chemical Engineering.